VIBRATIONAL SPECTROSCOPIC STUDIES OF SOME POLYATOMIC MOLECULES

ABSTRACT

OF THE

THESIS

SUBMITTED FOR THE AWARD OF THE DEGREE OF

Doctor of Philosophy

IN

PHYSICS

BY

MOHAMMAD JANE ALAM

UNDER THE SUPERVISION OF

PROF. SHABBIR AHMAD

DEPARTMENT OF PHYSICS
ALIGARH MUSLIM UNIVERSITY
ALIGARH-202 002 (INDIA)

2015

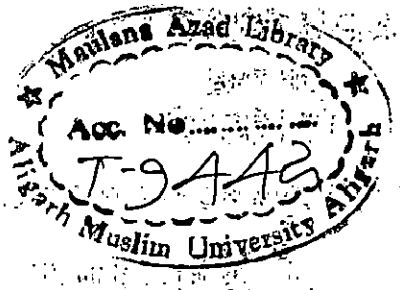
Maulana Azad Library
Acc. No.
T-9445
Aligarh Muslim University Aligarh

Abstract

Vibrational spectroscopy is a powerful and widely used approach in studying the structure, vibrational modes, intramolecular and intermolecular interactions, isomerism, and strength of chemical bonds, etc., with the aid of quantum chemical methods. The harmonic oscillator approach for vibrational studies is useful for medium to large size semi–rigid molecules but is not of sufficient accuracy. Therefore, one has to consider the anharmonic treatment to attain good accuracy in the calculations of vibrational spectra. The PT2 (Barone approach), VSCF and CC–VSCF methods are generally used for anharmonic force field calculations. Such high–level calculations at large basis sets are of high computational cost but these are accurate. It motivates to do first principle–based calculations of the realistic anharmonic potential energy surfaces.

The present thesis mainly deals with the studies of vibrational spectroscopy of polyatomic molecules. It also includes molecular structure and some molecular properties. The molecules for investigations are L–aspartic acid [1], o–, m–, p–iodonitrobenzene [2], 3–methyladenine [3] and allantoin [4]. These are chosen because of their biological, pharmaceutical and industrial importance. In this work, the FTIR and FT–Raman have been recorded and are investigated using quantum chemical calculations. The geometry optimization and harmonic as well as anharmonic frequencies calculations were performed at DFT, MP2 and HF levels with triple zeta basis sets for the molecules in their ground electronic state using Gaussian 09 and GAMESS–US. The correlation plots, RMS error and MAD values reveal good agreement between theories and experiments. In general, the harmonic calculations overestimate the frequencies with respect to experiment. Therefore, IR and Raman spectra have been assigned using anharmonic force field calculations, which need no manual scaling. The frequencies of many modes still show deviations from experiments, which may be due to the limitations of anharmonic methods or intermolecular and intramolecular interactions. In nature, the molecules exist in the form of hydrogen bonded intermolecular complexes. The intermolecular hydrogen bondings stabilize such complexes and they affect the molecular structure, vibrational spectra and properties of the monomer. In order to make good correlation between theoretical results and experimental data, the simulations have been performed on

hydrogen bonded molecular complexes in the harmonic approximation using DFT method. The anharmonic methods fail to define modes having large amplitude of vibrations like hydrogen stretching and soft torsional vibrations. This may be due to use of rectilinear coordinates, large perturbation and strong coupling between modes. In order to study the coupling between pair of modes, the magnitude of mode–mode coupling has been estimated for the ground state using two mode representation of quartic force field (2MR–QFF) potential energy function. The coupling between some important pairs of vibrational modes has been discussed. The vibrational spectra are assigned accurately with the help of PED calculations, animated modes and literature. The non–fundamental bands appeared in the FTIR spectra, are also assigned using anharmonic force field calculations. Moreover, various molecular properties such as atomic charges, chemical reactivity indices, molecular electrostatic potential (MEP), natural bond orbital (NBO), non–linear optical (NLO) properties, thermodynamic properties, HOMO–LUMO analysis, etc., are also presented.

References

[1]. **M. J. Alam**, S. Ahmad, Anharmonic vibrational studies of L–aspartic acid using HF and DFT calculations, Spectrochim. Acta A 96 (2012) 992–1004.

[2]. **M. J. Alam**, S. Ahmad, Molecular structure, anharmonic vibrational analysis and electronic spectra of o–, m–, p–iodonitrobenzene using DFT calculations, J. Mol. Struct. 1059 (2014) 239–254.

[3]. **M. J. Alam**, S. Ahmad, Quantum chemical and spectroscopic investigations of 3–methyladenine, Spectrochim. Acta A 128 (2014) 653–664.

[4]. **M. J. Alam**, S. Ahmad, FTIR, FT–Raman, UV–Visible spectra and quantum chemical calculations of allantoin molecule and its hydrogen bonded dimers, Spectrochim. Acta A 136 (2015) 961–978.

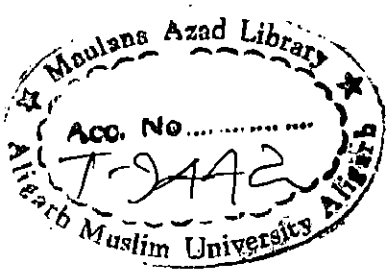

VIBRATIONAL SPECTROSCOPIC STUDIES OF SOME POLYATOMIC MOLECULES

THESIS

SUBMITTED FOR THE AWARD OF THE DEGREE OF

Doctor of Philosophy

IN

PHYSICS

BY

MOHAMMAD JANE ALAM

UNDER THE SUPERVISION OF

PROF. SHABBIR AHMAD

DEPARTMENT OF PHYSICS
ALIGARH MUSLIM UNIVERSITY
ALIGARH-202 002 (INDIA)

2015

Dedicated to

My Parents

CANDIDATE'S DECLARATION

I, **Mohammad Jane Alam**, Department of Physics, certify that the work embodied in this Ph. D. thesis is my own bonafide work carried out by me under the supervision of **Prof. Shabbir Ahmad** at Aligarh Muslim University, Aligarh. The matter embodied in this Ph. D. thesis has not been submitted for the award of any other degree.

I declare that I have faithfully acknowledged, given credit to and referred to the research workers wherever their works have been cited in the text and the body of the thesis. I further certify that I have not willfully lifted up some other's work, para, text, data, result, etc. reported in the journals, books, magazines, reports, dissertations, theses, etc., or available at web-sites and included them in this Ph. D. thesis and cited as my own work.

Date: 09.01.2015

Mohd. Jane Alam.

(Signature of the candidate)

Mohammad Jane Alam

(Name of the candidate)

CERTIFICATE FROM THE SUPERVISOR

This is to certify that the above statement made by the candidate is correct to the best of my knowledge.

Signature of the Supervisor:

Name & Designation: Dr. Shabbir Ahmad (Professor)

Department: Physics

(Signature of the Chairman of the Department with seal)

Chairman
Department of Physics
A.M.U., Aligarh

COURSE/ COMPREHENSIVE EXAMINATION/ PRE-SUBMISSION SEMINAR COMPLETION CERTIFICATE

This is to certify that **Mr. Mohammad Jane Alam**, Department of Physics, has satisfactorily completed the course work/ comprehensive examination and pre-submission seminar requirement which is part of his Ph. D. programme.

Date: 09.01.2015

(Signature of the Chairman of the Department)

Chairman
Department of Physics
A.M.U., Aligarh

COPYRIGHT TRANSFER CERTIFICATE

Title of the Thesis: Vibrational Spectroscopic Studies of Some Polyatomic Molecules

Candidate's Name: Mohammad Jane Alam

COPYRIGHT TRANSFER

The undersigned hereby assigns to the Aligarh Muslim University, Aligarh copyright that may exist in and for the above thesis submitted for the award of the Ph. D. degree.

Mohd. Jane Alam.

Signature of the candidate

Note: However, the author may reproduce or authorize others to reproduce material extracted verbatim from the thesis or derivative of the thesis for author's personal use provide that the source and the University's copyright notice are indicated.

Acknowledgments

All praise to the Almighty Allah, most gracious, most merciful and the creator of the universe, who enabled me to complete this research work successfully.

I would like to express my immense gratitude to my supervisor, *Prof. Shabbir Ahmad*, for his help, valuable suggestions, and excellent guidance during the entire span of my research work.

I am grateful to *Prof. Rahimullah Khan*, Chairman, Department of Physics, A. M. U., Aligarh for providing me all necessary facilities. I am also thankful to him for his encouragement, cooperation and support. I would like to thank *Dr. S. M. Afzal* for his encouragement. A special thank to *Dr. Douglas J. Fox*, Director Gaussian, Inc who is always willing to answer my questions about the Gaussian program. I acknowledge to *Prof. R. Benny Gerber, Prof. Brina Brauer, Dr. Kiyoshi Yagi, Dr. Tapta Kanchan Roy* on their discussions regarding vibrational mode-mode coupling calculations. I express my sincere thanks to *Prof. Mauricio Alcolea Palafox, Prof. Michal H. Jamroz, Prof. William Collier* on their discussions regarding vibrational analysis and PED calculations.

I sincerely thank to all my friends, colleagues and other staff members of the department for their wishes, help, and support.

I am extremely thankful to my parents for their continuous support, endless patience, blessings and encouragement.

UGC, New Delhi and DST-PURSE are gratefully acknowledged for providing me fellowship. FT-Raman recording facility provided by Sophisticated Analytical Instrument Facility (SAIF, IIT Chennai) is gratefully acknowledged. The Department of Physics, A.M.U., Aligarh is duly acknowledged for using FTIR facility.

Mohammad Jane Alam

Contents

List of Publications

❖ ***Papers in peer reviewed journal***

1. **M. J. Alam**, S. Ahmad, "Anharmonic vibrational studies of L–aspartic acid using HF and DFT calculations", Spectrochim. Acta A 96 (2012) 992–1004.
2. **M. J. Alam**, S. Ahmad, "Quantum chemical and spectroscopic investigations of 3–methyladenine", Spectrochim. Acta A 128 (2014) 653–664.
3. **M. J. Alam**, S. Ahmad, "Molecular structure, anharmonic vibrational analysis and electronic spectra of o–, m–, p–iodonitrobenzene using DFT calculations", J. Mol. Struct. 1059 (2014) 239–254.
4. **M. J. Alam**, S. Ahmad, "FTIR, FT–Raman, UV–Vis spectra and quantum chemical calculations of allantoin molecule and its hydrogen bonded dimers", Spectrochim. Acta A 136 (2015) 961–978.
5. H. Khanam, A. Mashrai, N. Siddiqui, M. Ahmad, **M. J. Alam,** S. Ahmad, Shamsuzzaman, "Structural elucidation, density functional calculations and contribution of intermolecular interactions in cholest-4-en-3-one crystals: Insights from X-ray and Hirshfeld surface analysis" J. Mol. Struct., 2015, http://dx.doi.org/10.1016/j.molstruc.2014.12.027.

❖ ***Papers in proceedings***

1. S. Ahmad, S. A. Bhat, **M. J. Alam**, "Spectral analysis of 5–nitrouracil using anharmonic DFT and TD–DFT calculations", Proceedings of the 4th international conference on perspectives in vibrational spectroscopy (ICOPVS–2013) held at Bishop Moore College, Mavelikara, Kerala, India, pp. 62–63, 2013, ISBN: 978–93–82880–54–7.
2. S. A. Bhat, **M. J. Alam**, S. Ahmad, "Anharmonic vibrational and electronic spectra of 6–aminouracil", Proceedings of the 4th international conference on perspectives in vibrational spectroscopy (ICOPVS–2013) held at Bishop Moore College, Mavelikara, Kerala, India, pp. 166–167, 2013, ISBN: 978–93–82880–54–7.
3. **M. J. Alam**, S. A. Bhat, S. Ahmad, V. K. Rastogi, "Anharmonic vibrational studies of 6–aza–thymine using FTIR, laser Raman and DFT calculations",

Proceedings of the 4th international conference on perspectives in vibrational spectroscopy (ICOPVS–2013) held at Bishop Moore College, Mavelikara, Kerala, India, pp. 272–273, 2013, ISBN: 978–93–82880–54–7.

4. **M. J. Alam**, S. A. Bhat, S. Ahmad, "Spectral and quantum chemical investigations of trans–4–hydroxy–L–proline", Proceedings of DAE BRNS symposium on current trends in theoretical chemistry (CTTC–2013) held at BARC Mumbai, India, pp. 91–92, 2013.
5. **M. J. Alam**, S. Ahmad, V. K. Rastogi, "Vibrational spectroscopy of 2, 4, 6–tri–fluoroaniline molecule by HF and DFT simulations using anharmonic 2nd order perturbative approach", Proceedings of the national conference on exploring the frontiers of vibrational spectroscopy (EXFOVIS–2011) held at Women's Christian College, Nagercoil, Tamilnadu, India, pp. 198–204, 2011, ISBN–13:978–81–9085 38–8–0.

❖ ***Papers presented in conferences/ symposia/ workshops***

1. **M. J. Alam**, S. A. Bhat, S. Ahmad, V. K. Rastogi, "Anharmonic vibrational analysis of 5–nitro–6–methyluracil", 5th International Conference on Perspectives in Vibrational Spectroscopy (ICOPVS–2014), July 8–12, 2014, at Mascot Hotel, Trivandrum, Kerala, India.
2. **M. J. Alam**, S. A. Bhat, S. Ahmad, "Spectral and quantum chemical investigations of trans–4–hydroxy–L–proline", DAE–BRNS Symposium on Current Trends in Theoretical Chemistry (CTTC–2013), September 26–28, 2013, at BARC Mumbai, India.
3. S. A. Bhat, **M. J. Alam**, S. Ahmad, "Anharmonic vibrational studies of 6–aza–thymine using FTIR, laser Raman and DFT calculations", DAE–BRNS Symposium on Current Trends in Theoretical Chemistry (CTTC–2013), September 26–28, 2013, at BARC Mumbai, India.
4. S. A. Bhat, **M. J. Alam**, S. Ahmad, "Anharmonic vibrational and electronic spectra of 6–aminouracil", 4th International Conference on Perspectives in Vibrational Spectroscopy (ICOPVS–2013), August 6–9, 2013, at Bishop Moore College, Mavelikara, Kerala, India.
5. S. A. Bhat, **M. J. Alam**, S. Ahmad, "Molecular structure and anharmonic vibrational spectra of L–(–)–xylose using DFT calculations", 3rd DAE–BRNS

Symposium on Atomic, Molecular and Optical Physics–2012, December 14–17, 2012, at IISER Kolkata, India.

6. S. Ahmad, **M. J. Alam**, S. A. Bhat, "FTIR, Raman spectra and anharmonic DFT calculations of 6–amino–1,3–dimethyluracil", 3rd DAE–BRNS Symposium on Atomic, Molecular and Optical Physics–2012, December 14–17, 2012, at IISER Kolkata, India.
7. **M. J. Alam**, S. A. Bhat, S. Ahmad, "Vibrational studies of 5–nitroorotic acid potassium salt monohydrate using FTIR, Raman and anharmonic DFT calculations", 3rd DAE–BRNS Symposium on Atomic, Molecular and Optical Physics–2012, December 14–17, 2012, at IISER Kolkata, India.
8. S. Ahmad, **M. J. Alam**, "Vibrational spectroscopy studies of 5–nitrouracil using FTIR, Laser Raman and anharmonic quantum chemical calculations", ISAMP Topical Conference on Interactions of Laser with Atoms, Molecules & Clusters (TC–2012), January 9–12, 2012, at School of Physics, ACRHEM and TIFR Centre for Interdisciplinary Sciences, Hyderabad, India.
9. **M. J. Alam**, S. Ahmad, "FTIR, Laser Raman Spectroscopy and anharmonic DFT simulations of 6–aminouracil", ISAMP Topical Conference on Interactions of Laser with Atoms, Molecules & Clusters (TC–2012), January 9–12, 2012, at School of Physics, ACRHEM and TIFR Centre for Interdisciplinary Sciences, Hyderabad, India.
10. S. A. Bhat, S. Ahmad, **M. J. Alam**, S. M. Afzal, "*Ab initio* calculations of structures and FTIR spectrum of B_2O_3 glass", 3rd International Conference on Current Developments in Atomic, Molecular, Optical and Nano Physics (CDAMOP–2011), December 14–16, 2011, organized at Department of Physics, University of Delhi, Delhi, India.
11. S. Ahmad, **M. J. Alam**, "Vibrational analysis of active psycho stimulant Caffeine using quantum chemical simulations", 3rd International Conference on Current Developments in Atomic, Molecular, Optical and Nano Physics (CDAMOP–2011), December 14–16, 2011, organized at Department of Physics, University of Delhi, Delhi, India.
12. **M. J. Alam**, S. Ahmad, "Molecular structure and vibrational studies of Allantoin using *ab initio* (HF) and density functional theory (B3LYP) method in the anharmonic approximation", 3rd International Conference on Current

Developments in Atomic, Molecular, Optical and Nano Physics (CDAMOP 2011), December 14–16, 2011, organized at Department of Physics, University of Delhi, Delhi, India.

13. S. Ahmad, **M. J. Alam,** "Vibrational analysis of D–tyrosine based on DFT anharmonic potentials", 2nd DAE/BRNS Symposium on Atomic, Molecular and Optical Physics in Association with ISAMP, February 22–25, 2011, at Department of Physics, Karnatak University, Dharwad, India.
14. **M. J. Alam,** S. Ahmad, "FTIR, Raman spectra and theoretical studies of L–aspartic acid using anharmonic DFT", 2nd DAE/BRNS Symposium on Atomic, Molecular and Optical Physics in Association with ISAMP, February 22–25, 2011, at Department of Physics, Karnatak University, Dharwad, India.
15. S. Ahmad, **M. J. Alam,** "Analysis of vibrational spectra of L–asparagine using FTIR, Raman and anharmonic calculations", Meghnad Saha Memorial International Symposium–cum–Workshop on Laser Induced Breakdown Spectroscopy (MMISLIBS–2010), December 21–23, 2010, at Department of Physics, Allahabad University, Allahabad, India.
16. **M. J. Alam,** S. Ahmad, "FTIR, Raman spectra and anharmonic DFT vibrational studies of L–glutamic acid", Meghnad Saha Memorial International Symposium–cum–Workshop on Laser Induced Breakdown Spectroscopy (MMISLIBS–2010), December 21–23, 2010, at Department of Physics, Allahabad University, Allahabad, India.
17. **M. J. Alam,** S. Ahmad, T. Rasheed, S. M. Afzal, K. Rahimullah, "Anharmonic vibrational spectra of L–alanine", International Conference on Recent Frontiers in Applied Spectroscopy (ICORFAS–2010), September 22–24, 2010, at Department of Physics, Annamalai University, Chidambaram, Tamilnadu, India.

Chapter 1

General introduction

Spectroscopy is the field of study of the interaction between matter and radiations. Molecular spectroscopy deals with mainly absorption, emission and scattering of electromagnetic radiation by molecule. It reveals structural information, dynamics and wide range of properties of the molecule. During the last century, significant and substantial progress has been made in experimental investigations and their theoretical explanations [1–13]. The different regions (e.g. ultraviolet–visible, infrared and microwave) of electromagnetic radiation are used to investigate various molecular processes. Each molecule produces unique spectrum because of its unique set of electronic, vibrational and rotational levels. The analyses of these spectra provide information regarding the quantized energy levels of the molecules and that can be used for qualitative and quantitative chemical analysis as well as for test of quantum chemical calculations.

The various kinds of spectroscopy are used to investigate molecules but the present study is restricted to vibrational spectroscopy which is most important tool in the multidisciplinary areas of sciences. This spectroscopy involves the transitions between quantum states that are evolved due to vibrational motion of the nuclei around their mean position. The accurate measurements of these transitions have become possible due to the advance developments in instrumentations that produce the reliable spectroscopic information by measuring the vibrational spectra of molecules [1–5]. The vibrational spectroscopy provides information like molecular structure, molecular vibrations, isomerism, thermodynamic properties, strength of chemical bonds, intermolecular and intramolecular interactions of molecules in solid, liquid and gas phase [9, 14–17]. It is commonly used for characterisation and

identification of materials, structure elucidation, reaction monitoring and quality control in industries.

Molecule possesses energy due to its translation, rotational and vibrational motions. All nuclei of a molecule vibrate periodically about their equilibrium position. This periodic motion is known as molecular vibration. During molecular vibration, all nuclei of a molecule are in periodic motions with same frequency and same phase but with different amplitudes. Because of the equality of phase and frequency, all nuclei reach their positions of maximum displacement at the same time and pass through their equilibrium positions at the same time. A mode of vibration having all these characteristics is called a normal mode, and its frequency is known as a fundamental frequency of the mode [9]. An *N*–atom non–linear (or linear) molecule has *3N–6* (or *3N–5*) normal modes of vibrations. In general, a normal mode of vibration involves motions of all the atoms of the molecule. There are some conditions in which normal modes are localized in a part of the molecule.

The infrared (IR) and Raman spectroscopy are the two main techniques used to obtain vibrational spectra. The success of vibrational spectroscopy in the field of sciences is due to technical developments, for instance, availability of laser as an excitation source for Raman spectroscopy and the development of interferometers for measuring accurate vibrational spectra. These are the important milestones in the development of vibrational spectroscopy. These techniques involve the interaction of radiation with molecule by different mechanisms (absorption or scattering) which change the vibrational state of molecule. The complete vibrational analysis requires both IR and Raman spectroscopy because they have different selection rules and sensitivity to molecular vibrations. The infrared absorption spectroscopy is a direct absorption process in which the radiation of frequencies equal to those of the normal modes of vibrations of a molecule is absorbed from continuous infrared sources. In Raman spectroscopy, the molecular vibrations are excited by the inelastic scattering of monochromatic radiation by the molecule.

The transitions between the vibrational states are governed by the vibrational selection rules i.e., electric dipole and Raman selection rules [18]. The charge distribution over molecule undergoes a periodic change during the vibrational motion and, therefore, in general, the dipole moment changes periodically. The vibrations,

connected with a change of dipole moment, show absorption in the infrared region and are known as infrared active. The integral

$$R^{v'v''} = \int \psi_v^{'*} \mu \psi_v'' \, d\tau \tag{1.1}$$

where μ is the dipole moment vector; ψ_v', *and* ψ_v'' are the wave functions of the upper (v') and lower (v'') vibrational state respectively; is known as the electric dipole transition moment for a vibrational transition and the intensity of transition is proportional to the square of the magnitude of this integral. The vibration is said to be IR active when at least one of the components of the electric dipole transition moment is non–zero. The symmetry considerations are also important in dipole selection rules. There are symmetry requirements for the integral (Eq. 1.1) to be non–zero. The symmetry requirement for the transition between states, which are non–degenerate, is that the symmetry of the quantity to be integrated is totally symmetric which can be given as:

$$\Gamma(\psi_v') \times \Gamma(\mu) \times \Gamma(\psi_v'') = A \tag{1.2}$$

where A is the totally symmetric species of any point group. The symmetry requirement for the transition between states, of which at least one is degenerate, is that the symmetry species of the quantity to be integrated contains the totally symmetric symmetry species. It can be written as:

$$\Gamma(\psi_v') \times \Gamma(\mu) \times \Gamma(\psi_v'') \supset A \tag{1.3}$$

The vibrational modes, connected with change in polarizability, which arises due to the oscillating electric field of the incident radiation on the molecule, appear in Raman spectrum of a molecule. The intensity of scattered Raman light is proportional to the square of the transition moment,

$$R^{v'v''} = \int \psi_v^{'*} \mu^o \psi_v'' \, d\tau \tag{1.4}$$

The amplitude of dipole moment, $\mu^o = \alpha' Q_k E^o$, where Q_k is the normal coordinate for the vibration k and α' is the derivative of polarizability tensor which has the six different components. The vibration is said to be Raman active when at least one of the six components of the integral, $\int \psi_v^{'*} \mu^o \psi_v'' \, d\tau$, remains non–zero. The symmetry requirement for transitions between non–degenerate vibrational states is that the

product of the symmetry species of the quantities inside the integral must be totally symmetric. This can be written as:

$$\Gamma(\psi_v') \times \Gamma(\alpha_{ij}) \times \Gamma(\psi_v'') = A \quad (1.5)$$

Since, $$\Gamma[(d\alpha_{ij}/dQ_k)Q_k] = \Gamma(\alpha_{ij}) \quad (1.6)$$

The symmetry requirement for the transition between two vibrational states (one of which is degenerate) becomes:

$$\Gamma(\psi_v') \times \Gamma(\alpha_{ij}) \times \Gamma(\psi_v'') \supset A \quad (1.7)$$

The molecules having the center of inversion follow the rule of mutual exclusion. According to this rule, the fundamental vibrations which are active in the Raman spectrum are inactive in the infrared spectrum and vise versa. However, the converse is not always true: there are some vibrations which are inactive in both the IR and Raman spectra [18, 20]. The IR and Raman spectra have many similarities of intensities but also have some differences. The Raman spectrum provides some additional information regarding symmetry of vibrations. The measurement of the depolarization ratio of Raman band gives the degree to which polarization properties of the incident radiation may be changed after scattering.

The molecular vibrations are anharmonic in nature. Therefore, combinations and overtone bands may appear in the vibrational spectrum in addition to the fundamentals. However, these bands are generally weaker than the fundamentals [19, 20]. Vibrational spectra of polyatomic molecules of medium size are generally very complex due to large number of bands. The bands, which appear in vibrational spectra, are characterized by their frequencies, intensities and band shapes, which give the information of energies, polar characters or polarizabilities and environmental effects respectively [16]. The vibrational spectra of the organic polyatomic molecules can be split in two spectral regions for the convenience of its interpretation. These are functional group (higher wavenumber) and fingerprint regions (lower wavenumber) or region of skeletal vibrations. The normal modes corresponding to the skeletal vibrations involve strong coupling between stretching or bending motions of atoms in a chain or ring. The two different molecules may have the same band positions in the functional group region due to a common functional groups but different in the

fingerprint region. The fingerprint region has unique signature for a molecule. The wavenumbers and their intensities of group vibrations are fairly constants from one molecule to another. Many transferable group vibrations occur in functional group region. The appearance of Raman band depends on the magnitude of the change of the amplitude of the induced dipole moment. This change is less sensitive than the change of dipole moment due to the environment of the vibrating group. Therefore, intensities of group vibrations are more accurately transferrable from one molecule to another or from one phase to another in the Raman than the IR spectrum. The group vibrations are termed as symmetric and asymmetric stretching, in–plane and out–of–plane bendings (or deformation), rocking, twisting, scissoring, wagging, torsion, ring breathing, inversion (or umbrella) and Kekule type [18].

Practically, it is very difficult task, almost impossible, to get isolated molecule. In nature, the molecules occur within the intermolecular networks. Therefore, the structure, vibrational frequencies and other properties of the molecule are affected due to influence of intermolecular interactions. Factors such as anharmonic mode–mode coupling interactions [21–23], intramolecular and intermolecular hydrogen bonding [24–26], Fermi resonance and Darling–Dennison resonance [18–20, 27–29] affect the bands of vibrational spectra. The studies of intermolecular and intramolecular hydrogen bonding interactions are important because they stabilize the structure of molecules [30]. Many people have studied the tera–Hertz time domain (THz–TD) spectra (0.1–3.0 THz or 3–100 cm^{-1}) of DNA and amino acids that reveal the signature as vibrational modes of intermolecular and intramolecular hydrogen bond networks [30–32]. It is still not easy to distinguish between intramolecular and intermolecular vibrational modes experimentally since they have similar frequencies. The *ab initio* theoretical models play crucial role in understanding the vibrational spectra under influence of the intramolecular and intermolecular interactions, resonances and mode–mode coupling.

The molecular vibrations are associated to the force constants which can be derive from the fundamental vibrational frequencies. The bond stretching and angle bending type of force constants are associated to a molecule. The bending force constants are more sensitive than stretching one. The force constants for stretching and bending vibrations of groups of atoms are invariant to the neighbouring atoms of

the molecule. Therefore, force constants can be transfer from one molecule to other similar molecule [18].

In 1955, Wilson et al. [9, 33] developed *FG* matrix method for normal coordinate analysis (NCA) [33]. This provides the normal coordinates, force constants, vibrational frequencies and the potential energy distribution of the various modes. These calculations have played a vital role in making assignments of vibrational bands. The NCA method assumes the fore information of the equilibrium molecular geometry, atomic masses and vibrational frequencies. In this method, the secular determinant, $|FG - \lambda I| = 0$, is solved where the *F, G, I* are matrices. The matrix *F* defines the harmonic force constants; *I* is the unit matrix; *G* is invert kinetic energy matrix and λ is related to frequency (ν) of the mode by the expression, $\lambda = 4\pi^2c^2\nu^2$. The *FG* calculations involve the internal coordinates and start with the adhoc assignments of bands of vibrational spectra [34].

In the field of vibrational spectroscopy, the quantum chemical methods play very crucial role for interpreting and assigning the vibrational spectra of medium sized polyatomic molecules. Moreover, based on equilibrium molecular geometry, the quantum chemical methods provide various properties of molecules in their ground and excited states. Improvements in computational power along with quantum chemical programs enable the utilization of *ab initio* quantum mechanical calculations for vibrational analysis. The vibrational analysis of molecules takes into accounts both the vibrational frequencies and intensities to assure reliable assignments of experimentally observed vibrational bands. The *ab initio* quantum chemical methods are based on first principle calculations, which are used to solve Schrödinger equations without reference to experimental parameters except physical constants. These are mathematically rigorous and accurate, but computationally expensive. Among these methods, DFT is very popular because it is more accurate and computationally less expensive. This method comprises variety of gradient–corrected exchange–correlation functionals such as BLYP, B3LYP and B3PW91 that generate reliable theoretical molecular data. HF method is important due to its legacy but the results deviate much from experimental results due to negligence of electron–electron correlations. In post HF methods e.g., multi–configuration self–consistence field (MCSF) and Moller–Plesset perturbation (MP*n*) methods, such correlations have been

included. Currently, high–speed computing systems, numerical algorithms and the quantum chemical methods [35–39] have been efficiently used to solve many chemical and biological problems.

1.1 Motivation

Vibrational spectroscopy technique is an effective and sensitive tool to probe the basic process of life and it has proven itself a valuable contributor in the field of medicine, biochemistry, materials science, analytical chemistry and pharmaceutical science etc [40, 41]. In addition to this experimental technique, the *ab initio* HF, MP2 and DFT methods are used to describe the structural and vibrational properties of medium to large sized molecules. The vibrational spectra of medium to large size organic molecules are very complex and appear with many overlapping fundamental as well as non–fundamental bands. Therefore, the analysis of vibrational spectra becomes very difficult and tedious. The theoretical calculations using *ab initio* approach play key role in assigning the vibrational spectra with good accuracy. The *ab initio* HF method is a fundamental approach but show large deviations from experimental results due to ignorance of electron–electron correlation effects. This has motivated to do the calculations using methods that include these effects. The MP2 and DFT methods include these effects and reproduce the results with great accuracy. The molecules show anharmonicity in nature. Therefore, the combination and overtone bands appear along with fundamentals in vibrational spectra of molecules. The harmonic force field calculations by these methods are useful to interpret vibrational spectra due to its low computational cost but are not of sufficient accuracy. This approach does not include the anharmonic terms in potential energy function that is itself of great interest. Therefore, such calculation does not give the information regarding combination and overtone bands. The harmonic vibrational calculations generally overestimate the frequency with respect to the experimental one. Various scaling procedures are used to compensate discrepancies between theoretical and experimental frequencies. These are useful to assign vibrational spectra but are not based on first principle. The advantages of anharmonic calculations motivate to do simulation of vibrational spectra in the anharmonic approximations within MP2 and DFT framework. These calculations give the reliable and accurate data that help in assigning the fundamentals as well as combination and overtone bands without any

scaling. The vibrational modes are coupled due to anharmonicity and, therefore, affect the vibrational spectrum. The vibrational modes show anharmonicity due to mode–mode coupling along with intrinsic anharmonicity. It has motivated to do mode–mode coupling computation to study the anharmonic nature of vibrational modes. In nature, the molecules are found in hydrogen bond networks. In order to achieve the theoretical results close to solid phase or matrix–isolated data, it is necessary to define structure within intermolecular hydrogen bond network for the calculations. Therefore, present thesis also comprises quantum chemical calculations on intermolecular complexes of associated molecule to investigate the effect of associations.

1.2 Objectives and scope of the present work

The present work aims to study some polyatomic molecules of biological, pharmaceutical and industrial importance (L–aspartic acid, o–, m–, p–iodonitrobenzene, 3–methyladenine and allantoin) using FTIR, Raman spectroscopy and quantum chemical calculations. The objectives of the present thesis include the computation of vibrational spectra in the harmonic and anharmonic approximations, molecular structures and mode–mode coupling strengths. Molecular simulations for the intermolecular complexes of associated molecules have been performed including some molecular properties. The quantum chemical approaches do help in solving various chemical problems. The FTIR and Raman spectroscopy along with efficient algorithm and theoretical models are very effective in analysing the molecules. The present investigations of molecular vibrations provide the site for the new research for understanding the physics of complex biological system. The vibrational spectroscopy has very broad range of application to the biomedical, biochemical, genetic engineering etc. The elucidation of the structure and monitoring of vibrations of the molecules of biological importance using spectroscopy and high–level theoretical calculations, help to understand the various biochemical and biological processes. The researches on molecules are of high demands because these are utilized in pharmaceutical, polymer and chemical industries. The biochemical components of a cell can be observed with the help of their inherent vibrational signatures. Any changes in the structure and biochemical composition due to stress, injury or any disease at cellular level can be understood with the help of vibrational

spectroscopy [40]. It proves to be a potential tool in diagnosing various clinical disorders and can be used to identify the foreign molecular species, bacteria, cancerous cells and metabolites in living cells. This has increased the utility in different field of research due to advance development in FTIR and Raman spectroscopies.

1.3 Thesis overview

The work presented in thesis mainly deals with the studies of vibrational spectroscopy of polyatomic molecules. It also includes molecular structure and properties. The molecules for investigations are L–aspartic acid [42], o–, m–, p–iodonitrobenzene [43], 3–methyladenine [44] and allantoin [45]. These are chosen because of their biological, pharmaceutical and industrial importance. The short summary of each thesis chapter are given as follows.

In the above sections of **Chapter 1**, a brief introduction of the molecular vibrations, vibrational spectroscopy and quantum chemical methods are presented. It includes the importance of vibrational spectroscopy and quantum chemical calculations which are used for investigating the polyatomic molecules. It also comprises the motivation, objectives, scope of the work and the thesis structure.

Chapter 2 is devoted to methodology of vibrational spectroscopy that includes experimental and theoretical methods used for the present work. The instrumentation and advantages of FTIR and Raman spectroscopy techniques have been discussed in this chapter. On the other hand, the brief descriptions on the quantum chemical methods like *ab initio* Hartree–Fock (HF), Moller–Plesset second order perturbation (MP2) method and density functional theory (DFT) along with basis sets are presented. The structures of the calculations are presented in terms of geometry optimization, vibrational frequencies calculations and potential energy distribution calculations. The anharmonic force field calculations that include second order perturbation (PT2), vibrational self–consistent field (VSCF) and correlation corrected VSCF (CC–VSCF) approaches have been discussed. In addition to these, the calculation of mode–mode coupling strengths based on 2–mode coupling representation of the quartic force field (2MR–QFF) approximation as well as estimation of IR and Raman intensities are also described. The theory regarding

molecular properties like molecular electrostatic potential (MEP), thermochemistry, non–linear optical properties, atomic charges, chemical reactivity indices and natural bond orbitals (NBO) have been also included in this chapter.

Chapter 3 mainly deals with the vibrational and quantum chemical studies of L–aspartic acid. The experimental vibrational spectra were fully studied with the aid of quantum chemical calculations. The molecular structure and vibrational spectra were computed using DFT/B3LYP, MP2 and HF calculations in the harmonic as well as anharmonic approximations with triple zeta Pople's and Dunning basis sets. The anharmonic vibrational frequencies were obtained using PT2, VSCF and CC–VSCF approaches. The correlation plots, root mean square (RMS) and mean absolute deviation (MAD) values are obtained that reveal the good agreement between theoretical and experimental data. The vibrational spectra have been assigned accurately using potential energy distribution (PED) values and with the help of animated modes. The non–fundamental bands of the FTIR spectrum have been also assigned with the help of anharmonic computations. To study the anharmonic mode–mode coupling, the coupling integrals have been computed using 2–mode coupling representation of the quartic force field (2MR–QFF) approximation within DFT framework. The simulations on L–aspartic acid dimers (D1 and D2) have been performed at B3LYP/6–311G(d,p) level of theory to investigate the effect of the intermolecular interactions on the structure and vibrational frequencies. The anharmonic vibrational frequencies of monomer and scaled frequencies of dimer, D1, are found close to experimental values. Moreover, various molecular properties such as atomic charges, non–linear optical (NLO) properties, molecular electrostatic potential (MEP) diagram, thermodynamic properties, natural bond orbital (NBO) analysis, etc. are also presented.

Chapter 4 presents the studies on ortho–, meta–, para–iodonitrobenzene using vibrational spectroscopy and quantum chemical calculations. The molecular structure and vibrational spectra were computed using DFT/B3LYP, MP2 and HF methods in the harmonic as well as anharmonic approximations. The basis sets 6–311G(d,p), 6–311++G(d,p) and cc–pVTZ were used on each atoms except iodine in iodonitrobenzenes. The basis sets for the heavy elements beyond the fourth row in the periodic table, are relatively limited. The basis sets 3–21G* and LANL2DZ were

used for iodine atom. To determine the stable conformations of these molecules, the torsional angle T (C–C–N–O) was varied and energy profiles were obtained. The assignments of vibrational modes of isomeric iodonitrobenzenes were done by using potential energy distribution (PED) and vibrational assignments of benzene, nitrobenzene and iodobenzene. The anharmonic vibrational frequencies were obtained using PT2 approach within HF, MP2 and DFT framework. The correlation plots, RMS and MAD values were used to compare between theoretical and experimental data. The combination and overtone bands appeared in the FTIR spectra are also assigned. This chapter demonstrates the comparative studies of o–, m–, p–iodonitrobenzene. Moreover, atomic charges, MEP mapping, HOMO–LUMO, NBO analysis, thermodynamics quantities and other molecular properties are presented.

Chapter 5 describes the experimental and theoretical investigations on 3–methyladenine molecule. This chapter presents complete vibrational analysis using FTIR, FT–Raman and anharmonic force field calculations. The molecular geometry and vibrational spectra of 3–methyladenine in the ground state are computed by using DFT (B3LYP and B3PW91), MP2 and HF methods in the harmonic as well as anharmonic approximations with 6–311G(d,p), 6–311++G(d,p) and cc–pVTZ basis sets. The anharmonic vibrational frequencies were obtained using PT2, VSCF and CC–VSCF approaches. The PT2 approach was used within HF, MP2 and DFT frameworks while VSCF and CC–VSCF algorithms were employed at B3LYP/6–311G(d,p) level of theory. The correlation plots, RMS and MAD values were used to compare between theoretical and experimental data. The vibrational spectra have been assigned accurately using literature and with the help of animated modes. In order to know the coupling between pairs of modes, the magnitude of mode–mode coupling for the ground state has been estimated. The 2MR–QFF potential energy function was used for calculating anharmonic mode–mode coupling strengths. The coupling between some important pairs of vibrational modes has been discussed. The intermolecular hydrogen bonding interactions affect the molecular structure, vibrational spectra and other molecular properties of monomer. Therefore, in order to make good correlation between theoretical results and solid phase experimental data, the simulations have been performed also on dimeric and trimeric structures of 3–methyladenine at DFT/6–311G(d,p) level of theory in the harmonic

approximation. Moreover, atomic charges, HOMO–LUMO analysis, NBO analysis, NLO properties and various other molecular properties have been also presented. The chemical behaviour and the reactivity of the isolated 3–methyladenine were investigated using HOMO (ionization potential) and LUMO (electron affinity) energy eigenvalues calculated at DFT level. These values have been used to compute chemical reactivity descriptors.

Chapter 6 comprises the investigations on the molecular structure and vibrational spectra of allantoin molecule using experiments as well as quantum chemical calculations. FTIR and FT–Raman spectra were recorded and analysed using HF, MP2 and DFT(B3LYP) method along with 6–311G(d,p), 6–311++G(d,p) and cc–pVTZ basis sets. The molecular structure, anharmonic vibrational spectra, natural atomic charges, non–linear optical properties, etc. have been computed for the ground state of allantoin molecule. The anharmonic vibrational frequencies are calculated using PT2 algorithm (Barone method) as well as VSCF and CC–VSCF methods. The PT2 approach was used within HF, MP2 and DFT frameworks while VSCF and CC–VSCF algorithms were employed at B3LYP/6–311G(d,p) level of theory. These methods yield results that are in remarkable agreement with the experiments. The coupling strengths between pairs of modes are also calculated using coupling integral based on 2MR–QFF approximation. The simulations on allantoin dimers have been also performed at B3LYP/6–311++G(d,p) level of theory to investigate the effect of the intermolecular interactions on the molecular structure and vibrational frequencies of the monomer. Vibrational assignments are made with the great accuracy using PED calculations and animated modes. The combination and overtone bands have been also identified in the FTIR spectrum with the help of anharmonic computations. The important global quantities such as electro–negativity, electronic chemical potential, electrophilicity index, chemical hardness and softness based on HOMO, LUMO energy eigenvalues are also computed. NBO analysis has been performed for monomer and dimers of allantoin at B3LYP/6–311++G(d,p) level of theory. The correlation plots, RMS and MAD values were used to compare between theoretical and experimental data.

The final chapter of this thesis, **Chapter 7**, includes the overall conclusion of thesis.

References

[1]. S. G. Stepanian, I. D. Reva, E. D. Radchenko, L. Adamowicz, J. Phys. Chem. A 102 (1998) 4623–4629.

[2]. A. Y. Ivanov, A. M. Plokhotnichenko, V. Izvekov, G. G. Sheina, Y. P. Blagoi, J. Mol. Struct. 408 (1997) 459–462.

[3]. S. Breda, I. Reva, R. Fausto, Vib. Spectrosc. 50 (2009) 57–67.

[4]. S. Breda, I. Reva, R. Fausto, J. Mol. Struct. 887 (2008) 75–86.

[5]. A. Kovacs, A. Y. Ivanov, J. Phys. Chem. B 113 (2009) 2151–2159.

[6]. W. Kiefer, Fresenius' Zeitschrift Für Analytische Chemie 324 (1986) 642–648.

[7]. W.Kiefer, J. Raman Spectrosc. 38 (2007) 1538–1553.

[8]. L. A. Nafie, J. Raman Spectrosc., DOI: 10.1002/jrs.4619, 2014

[9]. E. B. Wilson, Jr., J. C. Decius, P. C. Cross, Molecular Vibrations, McGraw–Hill, New York, 1955.

[10]. H. H. Nielsen, Rev. Mod. Phys. 23 (1951) 90–136.

[11]. K. Yagi, T. Taketsugu, K. Hirao, M. S. Gordon, J. Chem. Phys. 113 (2000) 1005–1017.

[12]. J. O. Jung, R. B. Gerber, J. Chem. Phys. 105 (1996) 10682–10690.

[13]. V. Barone, J. Chem. Phys. 122 (2005) 014108–014118.

[14]. D. A. McQuarrie, J. D. Simon., Physical Chemistry: A Molecular Approach, University Science Books, Sausalito, Ca., 1997.

[15]. D. A. Skoog, F. J. Holler, S. R. Crouch. Principles of Instrumental Analysis, 6th edition, Thomson Higher Education, Belmont, CA., 2007.

[16]. P. Larkin, Infrared and Raman Spectroscopy: Principles and Spectral Interpretation, 1st edition, Elsevier, USA, 2011.

[17]. B. H. Stuart, Infrared Spectroscopy: Fundamentals and Applications, John Wiley & Sons, England, 2004.

[18]. J. M. Hollas, High Resolution Spectroscopy, 2nd edition, John Wiley and Sons, UK, 1998

[19]. G. Herzberg, Molecular Spectra & Molecular Structure: Spectra of Diatomic Molecules, Vol. 1, D. Van Nostrand Company, INC., New York, 1945.

[20]. G. Herzberg, Molecular Spectra & Molecular Structure: Infrared and Raman Spectra of Polyatomic Molecules, Vol. 2, D. Van Nostrand Company, INC., New York, 1945.

[21]. Y. Miller, G. M. Chaban, R. B. Gerber, J. Phys. Chem. A 109 (2005) 6565–6574.

[22]. P. Seidler, T. Kaga, K. Yagi, O. Christiansen, K. Hirao, Chem. Phys. Lett. 483 (2009) 138–142.

[23]. T. Rasheed, S. Ahmad, Vib Spectrosc. 56 (2011) 51–59.

[24]. M. J. Alam, S. Ahmad, Spectrochim. Acta A 136 (2015) 961–978.

[25]. C. Cirak, Y. Sert, F. Ucun, Spectrochim. Acta A 127 (2014) 41–46.

[26]. S. Ortiz, M. A. Palafox, V. K. Rastogi, R. Tomer, Spectrochim. Acta A 97 (2012) 948–962.

[27]. K. V. Berezin, V. V. Nechaev, P. M. El'kin, J. Appl. Spectros 72 (2005) 9–19.

[28]. B. T. Darling, D. M. Dennison, Phys. Rev. 57 (1940) 128–139.

[29]. D. M. Dennison, Rev. Mod. Phys. 12 (1940) 175–321.

[30]. Y. Ueno, R. Rungsawang, I. Tomita, K. Ajito, Chem. Lett. 35 (2006) 1128–1129.

[31]. B. M. Fischer, M. Walther, P. U. Jepsen, Phys. Med. Biol. 47 (2002) 3807–3814.

[32]. K. Yamamoto, M. H. Kabir, K. Tominaga, J. Opt. Soc. Am. B 22 (2005) 2417–2426.
[33]. E. B. Wilson Jr., J. Chem. Phys. 9 (1941) 76–84.
[34]. S. Gunasekaran, Ind. J. Pure Appl. Phys. 43 (2005) 503–508.
[35]. C. J. Cramer, Essentials of Computational Chemistry: Theories and Models, 2nd edition, John Wiley & Sons, Ltd., England, 2004.
[36]. I. N. Levine, Quantum Chemistry, 6th edition, PHI learning private limited, New Delhi, 2010.
[37]. P. Atkins, R. Friedman, Molecular Quantum Mechanics, 4th edition, Oxford University Press Inc., New York, 2005.
[38]. A. M. Sapse, Molecular Orbital Calculations for Biological Systems, Oxford University Press, USA, 1998.
[39]. V. Barone, Computational Strategies for Spectroscopy: from Small Molecules to Nano System, John Wiley & Sons, Inc., Hoboken, 2012.
[40]. B. Singh, R. Gautam, S. Kumar, B. N. V. Kumar, U. Nongthomba, D. Nandi, G. Mukherjee, V. Santosh, K. Somasundaram, S. Umapathy, Current Science 102 (2012) 232–244.
[41]. J. M. Chalmers, P. Griffiths, Handbook of Vibrational Spectroscopy, Vol. 1, Wiley, Chichester, UK, 2001.
[42]. M. J. Alam, S. Ahmad, Spectrochim. Acta A 96 (2012) 992–1004.
[43]. M. J. Alam, S. Ahmad, J. Mol. Struct. 1059 (2014) 239–254.
[44]. M. J. Alam, S. Ahmad, Spectrochim. Acta A 128 (2014) 653–664.
[45]. M. J. Alam, S. Ahmad, Spectrochim. Acta A 136 (2015) 961–978.

Chapter 2

Methodology

In this chapter, the experimental and theoretical methods, which are used to investigate polyatomic molecules, are discussed. Fourier transform infrared (FTIR) and Raman spectroscopic techniques have been used for recording the vibrational spectra of some polyatomic molecules. On the other hand, the *ab initio* Hartree–Fock (HF) theory, density functional theory (DFT) and second order Moller–Plesset perturbation theory (MP2) have been utilized to simulate the molecular structure, vibrational spectra, thermodynamic quantities, electronic and non–linear optical properties, molecular orbitals, natural bond orbitals, etc. The vibrational frequencies and various thermodynamic quantities of polyatomic molecules are obtained in the both harmonic and anharmonic approximations. The calculations of the molecular geometry and vibrational spectra are very crucial because the calculations of many molecular properties need these data.

2.1 Experimental details

Infrared (IR) and Raman spectroscopies are two important techniques of vibrational spectroscopy. These are complementary to each other because of vibrational selection rules. The change in dipole moment during the vibration is necessary for IR absorption whereas Raman activity depends on change in polarizability during the vibration. The complete vibrational studies of molecules require both the techniques. IR and Raman spectroscopy show different sensitivity to functional groups in a molecule. Some vibrational band may appear with different intensities in infrared and Raman spectra.

2.1.1 FTIR spectroscopy and instrumentation

In molecular spectroscopy, FTIR spectrometers are generally used to study the molecular structure as well as the rotational and vibrational spectra of molecules

[1–5]. The FTIR spectroscopy has the advantages of Michelson's interferometer and a mathematical tool i.e. fast Fourier transform. The FTIR spectroscopic technique has almost replaced the conventional IR spectroscopic technique due to its high wavenumber precision, signal to noise ratio and resolution. FTIR spectrometer mainly consists of infrared source, Michelson's interferometer, sample chamber, detector, amplifier, analog–to–digital converter (ADC) and computer processor for performing Fourier transform of the signal. The source produces radiation which passes through the interferometer. The interferometer generates signal (interferogram) that contain all the elements of source. It is passed through sample chamber and is detected by detector. The interferogram is a response of intensity with respect to optical path difference. The spectrum is achieved by the Fourier transform of the interferogram.

Infrared sources

The IR sources emit massive radiation of low energy at certain temperature and are black body radiator. The important IR sources are Globar, Nichrome coils and Nernst Glowers, etc. The most frequently used mid–infrared (MIR) source is Globar which is made of silicon carbide. This is operated at ca. 1300K temperature. To prevent the damages of other components due to heat, the coating of ceramic metal alloy is used. In the FTIR, the signal to noise ratio (SNR) of interferogram can reach up to 100,000 if the full radiant power of Globar source is measured by deutrated triglycine sulfate (DTGS) detector with 16–bit ADC and gain ranging amplifier [1]. For the present case, the Globar source is used in the FTIR spectrometer (Tensor 37 by Bruker). The optics of KBr salt, which is transparent for the spectral region 7500–370 cm^{-1}, is used [6].

Interferometer

The most important component of an FTIR spectrometer is a Michelson's interferometer. It involves the beam splitter and two mirrors in which one is fixed and another is movable. The beamsplitter, which is installed at 45^0 from the position of mirror, splits the incoming IR radiation in to half parts at right angle. The radiations reflect back by movable and fixed mirror then recombine constructively or destructively at beamsplitter. The beam splitter of different materials is used for the different spectral range. The standard germanium coated KBr beam splitter is normally used to study spectrum in the mid IR region 7500–370 cm^{-1}. The movable

mirror introduces optical path difference like 0, λ, 2λ ... for constructive interference pattern [1]. Therefore, if optical path difference, which is twice of the distance moves by movable mirror, is changed smoothly from zero, the intensity of radiation will change. The signal is large at δ=0 since all the waves are in phase. The intense signal at δ=0 is known as the centre burst. The signal is a function of the position of movable mirror i.e. optical path difference, x and is called an interferogram. The interferogram contain information about every IR frequency range of the source. When the interferogram is passed through sample, the transmitted radiations from sample give further an interferogram (length or time domain) which contain the spectrum of the molecule. Detector detects the interferogram. It is digitized before applying fast Fourier transformation by a computer.

Infrared detector

The infrared detector is a type of transducer that changes the IR radiation to electrical signal. There are two types of infrared detectors such as thermal and photon detectors which are used normally in FTIR spectrometers. The pyroelectric detectors, thermal detectors, are operated at room temperature. These detectors induce change in surface charge density due to change in temperature. The most common pyroelectric detector, deuterated triglycine sulfate (DTGS), is used. The deuterated L–alanine doped triglycene sulphate (DLaTGS) detector covers a spectral range from 12000–350 cm^{-1} at room temperature [6]. The other most efficient detectors are the semiconductor detectors that are operated at cryogenic temperature. The conductivity is increased by the absorption of infrared radiations. The increase in conductivity is observed as the increase in current flowing through the detector element. These detectors are better due to their excellent sensitivity and high speed. A liquid N_2 cooled mercury cadmium telluride semiconductor detector is used as infrared detector to accrue better results. For the present case, the DLaTGS detector is used in the FTIR spectrometer (Tensor 37 by Bruker).

The Fourier transform of interferogram

Fourier transform technique is used to recover spectrum (frequency or wavenumber domain) from the interferogram (time or length domain). The resolution is always determined by the maximum displacement of the movable mirror. In this transformation, the intensity, $I(x)$ which is function of optical path difference, x, is

subjected to transform as a whole to give spectrum, $G(\bar{v})$ which is function of the wavenumber $\bar{v}$. The integral used in Fourier transformations is given as follow:

$$F[I(x)] = G(\bar{v}) = \int_{-\infty}^{\infty} I(x)e^{-i2\pi\bar{v}x}dx \tag{2.1}$$

where, the interferogram, $I(x)$ is defined as

$$I(x) = \int_{-\infty}^{\infty} G(\bar{v})e^{i2\pi\bar{v}x}d\bar{v} \tag{2.2}$$

In practical, the x does not go from $-\infty$ to ∞. The maximum distance move by the movable mirror has to be restricted to some distance, say L. Therefore, a function, which is known as apodization function, is multiplied to interferogram. Some important apodization functions are boxcar, triangular, Happ–Genzel and Blackman–Harris functions. Different apodization functions are used for different purposes such as removing side lobes or minimizing smearing of the central absorption peak [1]. Boxcar apodization arises naturally due to finite mirror movement in a Michelson interferometer, and it multiplies collected interferogram data points by unity and is defined to be zero outside the range of mirror travel [7]. The typical experimental arrangement of FTIR spectrometer is shown in Fig. 2.1.

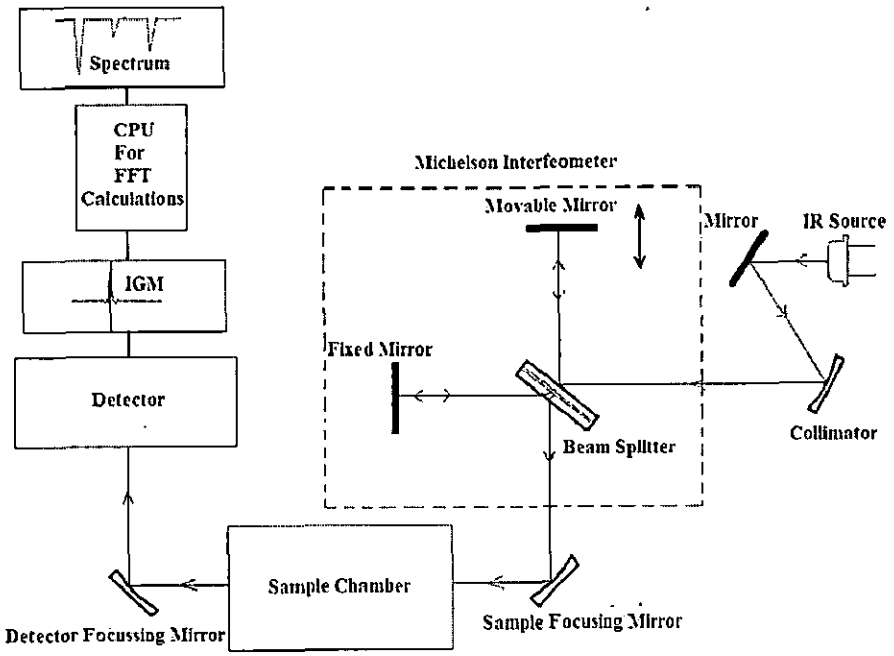

Fig. 2.1 Experimental arrangement of FTIR spectrometer.

Advantages

FTIR spectrometer has some major advantages over the dispersive IR spectrometer [1–4, 8–16]. According to the Fellgett's advantage or multiplex advantage, all elements of IR frequency can be measured simultaneously [17]. In each scan of mirror, the whole spectrum is recorded. Thus, the speed of accruing the spectra of FTIR is much faster than the conventional IR instrument. Second advantage is Jacquinot's advantage or high throughput advantage [18]. The optical throughput through an interferometer is much higher than a conventional dispersive spectrometer, hence, large signal is obtained. In order to increase high signal to noise ratio many scans are performed and averaging is carried out. The third advantage, which is due to He–Ne laser used for internal wavenumber calibration, is known as Connes' advantage [19]. The laser beam provides the fringes due to interference, which is used as reference for the measurement of the position of movable mirror. Due to this, high accuracy in measurement of wavenumber can be achieved.

Sample preparation

The sample preparation in FTIR spectroscopy is very important in order to record a good quality of spectra. There are a number of possible techniques for sample preparation such as attenuated total reflectance (ATR), thin film between two IR transparent plates, preparing a Nujol mull, preparing a solution, KBr pellet, liquid and gas cells. One can choose a technique depending upon the state of sample and application. The KBr pellet technique is preferred for solid samples in terms of the information yield from an IR spectrum because KBr is significantly more IR transparent than most of solvents or Nujol oil. KBr has no absorption in the region 4000 cm^{-1} to 250 cm^{-1} so that a good sample spectrum can be obtained. The disadvantages of this technique include tedious and time–consuming sample preparation and interference of water bands (3960 to 3480 cm^{-1} and 1950 to 1300 cm^{-1} and below 500 cm^{-1}) because of hygroscopic nature of KBr [6]. In KBr pellet technique, the sample is mixed with dry KBr in ratio of 1:200. The grain size must be as fine as possible to minimize the IR scattering on particle surface. The other important factor in sample preparation is absorptivity of the sample that is defined by Lambert–Beer law. According to this law, absorbance (IR band intensity) is directly

proportional to sample concentration, thickness and absorptivity. The proper sample concentration and pellet thickness are used to optimize the absorbance.

2.1.2 Raman spectroscopy and instrumentation

Raman spectroscopy is based upon the observation of inelastic scattering of laser beam from the sample. When photons of laser beam interact with molecules, the most of the photons undergo elastic scattering (Rayleigh scattering) while some are inelastically scattered. The spectroscopy of inelastically scattered radiation gives the Raman spectra. For the vibrational mode to be Raman active, there must be change in molecular polarizability during vibration as well as follow the symmetry requirements [20]. The molecular polarizability comes into picture due to induced dipole moment. The classical and quantum theory of Raman scattering can be found in various textbooks [21–26]. The instrumentation of Raman spectroscopy is usually more complicated than that of IR absorption spectroscopy because Raman signal is weak and sometime fluorescence masks it. Raman spectroscopic technique has some advantages over the IR technique like any size of sample or any portion of sample can be examined and remote measurements are possible through fiber. The Raman spectrometer typically consists of excitation source, sample cell, optical system for sample illumination and collection of scattered light, monochromator or interferometry system and detector [27–29]. The excitation source should be highly monochromatic and very intense to observe the Raman signal, because it is weak. The lasers (Ar ion, Nd:YAG and diode lasers with several hundred mW power) are sources that are ideal for Raman spectroscopy. When the laser light focus on sample, it get scattered in all directions. The two types of observation geometries are used for detecting scattered photons (Fig. 2.2). The observation at 90° to the incident light beam is used often for liquid samples. On the other hand, the scattered light can be observed at 180° geometry (back scattering) that is normally preferred for solid samples. The scattered light is collected through a large condensing lens and then it is directed to a monochromator or an interferometer. A multichannel detector monitors many wavelengths simultaneously, using array of detectors in parallel. However, in FT–Raman, interferometer modulates each wavelength scattered by sample and then send it to a single beam contains all wavelength of interest to single detector.

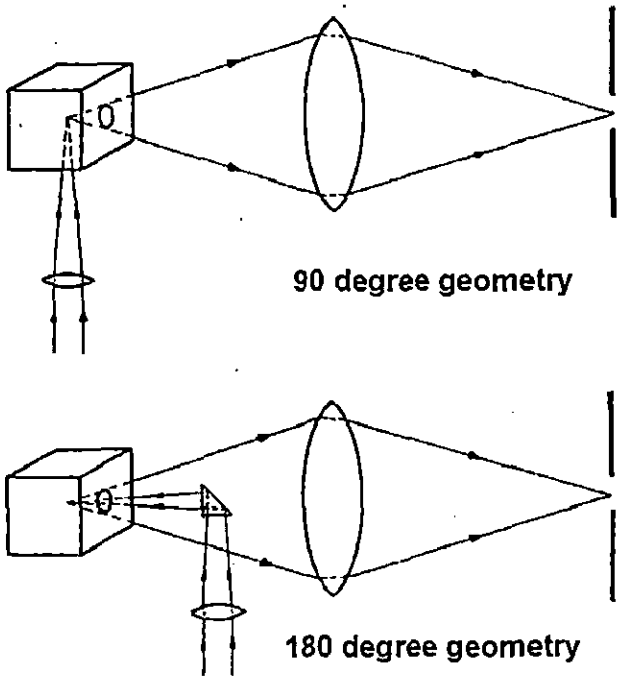

Fig. 2.2 Observation geometries for collecting scattered photons.

In order to eliminate the excitation frequency (Rayleigh line), a notch filter is used within interferomety system before the detector. Each wavelength is modulated and the Fourier transform of the detector output yields a Raman spectrum. A multichannel spectrometer detects Raman signal by array of detectors, while in FT–Raman spectrometer, the scattered light is directed towards a single detector. In IR spectroscopy, the dispersive technique is completely replaced by inteferometric technique. However, in Raman spectroscopy, dispersive spectrometers have some advantages over the FT–Raman spectrometers. The dispersive Raman spectrometers (micro–Raman spectrometers) are more sensitive than FT–Raman spectrometers. The low sensitivity in FT-Raman is due to $1/\lambda^4$ effect with 1064 nm excitation source. The experimental arrangements for dispersive and FT–Raman are shown in Fig. 2.3 and 2.4. Raman spectroscopy technique is a non–destructive and require almost little or no sample preparation. Therefore, this technique is suitable for *in vivo*, *in vitro* and *in situ* analysis.

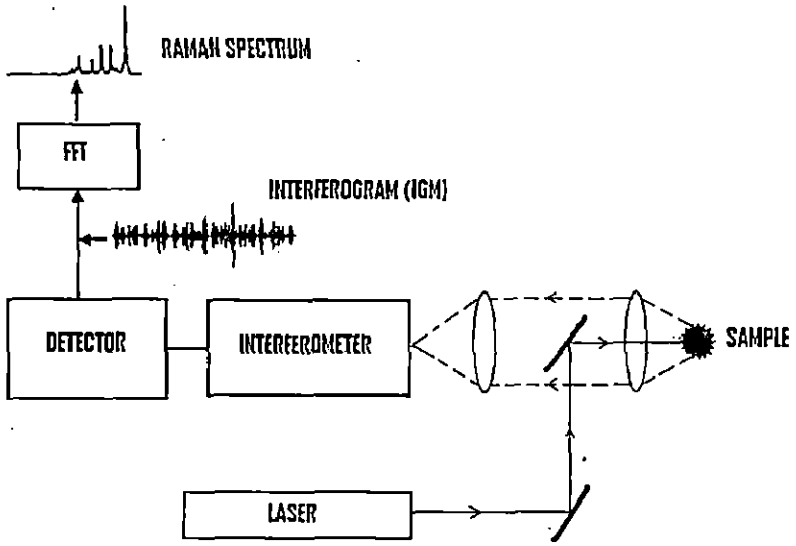

Fig. 2.3 Experimental arrangement for FT–Raman.

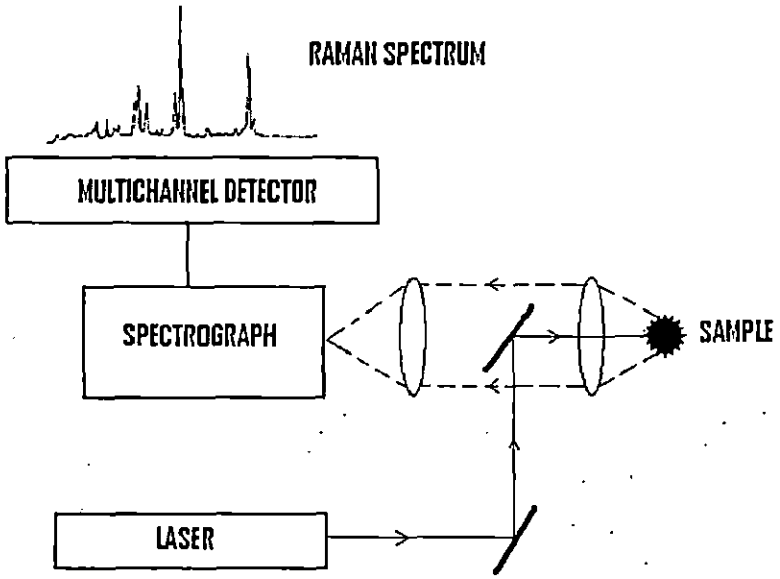

Fig. 2.4 Experimental arrangement for dispersive Raman.

2.2 Quantum chemical calculations

The molecular simulation using the advanced quantum chemical methods is exciting field of research in many disciplines like physics, chemistry, biology, biochemistry, biotechnology, etc. *Ab initio* quantum chemical methods are rigorous and thus accurate but require high computational resources. They do not need any experimental data except the fundamental physical constants. In these methods, the correct Hamiltonian and molecular orbitals satisfy the Schrodinger equation. The

self–consistence field (SCF) minimum energy is calculated by utilizing variational principle. *Ab initio* treatments of polyatomic molecules consist of Hartree–Fock (HF) method, which exclude electron correlation, and post Hartree–Fock methods (MPn, CC, MCSCF and CI), which include electron correlation [30, 31]. These, however, are the most computationally demanding and restrict the size of the molecules. These calculations are based upon the basic laws of quantum mechanics and exploit a variety of mathematical transformation and approximation techniques to solve the fundamental equations [32]. The software packages like Gaussian [33], NWchem [34], MolPro [35], GAMESS–US [36], etc. are available to do quantum chemical calculations for the molecules very efficiently. The density functional theory (DFT) methods attempt to calculate the ground state electron density rather than molecular wave function and calculate the molecular energy functional [37, 38]. The DFT methods take into account the effect of electron correlation by using exchange–correlation functionals. Presently, DFT is most popular and successful approach to compute properties of medium to large sized molecular system because of its high accuracy and relatively low computational cost. These theoretical calculations have gained popularity amongst the scientific community due to the advancement in theoretical models, computer hardwares as well as softwares. In the present thesis, the HF, MP2 and DFT methods have been employed for investigating some polyatomic molecules. The methods, used for the present calculations, are based on both self–consistent field approach (iteration methods) as well as perturbation theory (non–SCF). The brief descriptions of these methods for molecules are given in the following sections.

2.2.1 Hartree–Fock method

The Hartree and Fock have proposed *ab initio* approach (HF method) to solve the Schrödinger equation by invoking variational principle for molecules. The equations are solved using an iteration procedure that gives rise to the term self–consistence field (SCF) method. The approximations, used to solve fundamental equation, are mean field, non–relativistic, Born–Oppenheimer and molecular orbital approximations. According to Born–Oppenheimer approximation, the nuclei of the molecules are treated as stationary and produce a static potential field in which electrons are moving. HF method assumes that the electrons, which are moving in static potential, are not interacting to each other.

Schrödinger equation

The fundamental equation for the motion of electron in potential field (V) can be described by Schrödinger equation:

$$\left\{\frac{-h^2}{8\pi^2 m}\nabla^2 + V\right\}\psi(\vec{r},t) = \frac{ih}{2\pi}\frac{\partial\psi(\vec{r},t)}{\partial t} \tag{2.3}$$

where ψ is the wavefunction associated with electron of mass m and h is Planck's constant. In this case, ψ would be a function of the positions of all electrons in the molecule as well as time. It contains all the information of the system. If V is time independent (stationary electronic state), the Schrödinger equation can be simplified in two parts, one of which depends on the only positions of the particle and other is a function of time only, by using separation of variables technique. Therefore, the Schrödinger equation for the motion of particles in time independent potential can be defined as:

$$H\psi(\vec{r}) = E\psi(\vec{r}) \tag{2.4}$$

where E is the energy of the particle and H denotes the Hamiltonian operator. Eq. 2.4 is valid only for non–relativistic systems and, therefore, this does not describe accurately the core electrons in heavy element.

According to Hartree, the electrons are moving in averaged potential field in molecular system. The notations for the position of the each electron and nucleus are used as $\overrightarrow{r_a}$ and $\overrightarrow{R_A}$ respectively. The complete Hamiltonian for the molecular system can be constructed as [32]:

$$H = T^{elec}(\vec{r}) + T^{nucl}(\vec{R}) + V^{nucl-elec}(\vec{r},\vec{R}) + V^{elec-elec}(\vec{r}) + V^{nucl-nucl}(\vec{R}) \tag{2.5}$$

where, the 1st and 2nd terms are due to kinetic energy of electrons and nuclei respectively, the 3rd, 4th and 5th terms represent all possible interactions (potential energy) between charged particles. For an electron with charge $-e$ and nucleus with charge Ze, where Z is the atomic number of the atom, the coulombic interactions between charged particles are represented by following expression [32]:

$$V = \frac{1}{4\pi\varepsilon_0}\left[-\sum_{a}^{elec}\sum_{A}^{nucl}\left(\frac{Z_I e^2}{\Delta r_{aA}}\right) + \sum_{a}^{elec}\sum_{a'<a}^{elec}\left(\frac{e^2}{\Delta r_{aa'}}\right) + \sum_{A}^{nucl}\sum_{A'<A}^{nucl}\left(\frac{Z_A Z_{A'} e^2}{\Delta R_{AA'}}\right)\right] \tag{2.6}$$

where, the 1st term corresponds to electron–nuclear attraction, the 2nd is due to electron–electron repulsion, and 3rd one is because of nuclear–nuclear repulsion. The first approximation, given by Born–Oppenheimer, is used to solve Schrödinger equation that separates nuclear and electronic motions. By invoking this approximation, one can consider the nuclei as fixed in position and can solve the Schrödinger equation for the electrons in the static electric potential arising from the nuclei in that particular arrangement. The Born–Oppenheimer approximation is reliable for ground electronic states, but it is less reliable for excited states [39]. The electronic Hamiltonian (in a. u.) can be constructed by ignoring the kinetic energy term for the nuclei [32]:

$$H^{elec} = -\frac{1}{2}\sum_{a}^{elec}\nabla_a^2 - \sum_{a}^{elec}\sum_{A}^{nucl}\frac{Z_A}{|\vec{R}_A - \vec{r}_a|} + \sum_{a}^{elec}\sum_{a'<a}^{elec}\frac{1}{|\vec{r}_a - \vec{r}_{a'}|} + \sum_{A}^{nucl}\sum_{A'<A}^{nucl}\frac{Z_A Z_{A'}}{|\vec{R}_A - \vec{R}_{A'}|} \quad (2.7)$$

Thus, Schrödinger equation describing the motion of electrons in the field of fixed nuclei has form:

$$H^{elec}\psi^{elec}(\vec{r},\vec{R}) = U(\vec{R})\psi^{elec}(\vec{r},\vec{R}) \quad (2.8)$$

This equation for electronic wavefunction provides the effective nuclear potential $U(\vec{R})$ which explains the potential energy surface for molecular system (section 2.2.5). Thus, the nuclear Hamiltonian is defined as:

$$H^{nucl} = T^{nucl} + U(\vec{R}) \quad (2.9)$$

The Schrödinger equation with this nuclear Hamiltonian describes the nuclear motion in molecular system. The solution of nuclear Schrödinger equation is used in predicting vibrational spectra [40] (section 2.2.5). The wavefunction must be normalized and satisfy the antisymmetry condition. Indeed, the main problem to solve time independent Schrödinger equation is the presence of interelectronic repulsion (3rd term in Eq. 2.7). This term has been neglected in HF approach but is taken into account in post HF methods.

Molecular orbitals

The molecular orbital (MO), another approximation, is used to define the wave nature of electron in molecule. In HF approach, linear combination of atomic orbitals (LCAO) approximation is utilized to construct the molecular orbitals. According to LCAO–MOs theory, MO can be written as linear combination of atomic orbitals (AOs). The HF approach uses the molecular orbitals (MOs) as wavefunction in Schrodinger equation. The wave function for the MO consists of both orbital and spin functions which describe the electrons in terms of spin up $\alpha(a)$ or spin down $\beta(a)$ for a^{th} electron. It is require that total wave function must be normalized and antisymmetric. The HF method is further characterized in restricted (closed shell) and unrestricted (open shell) HF method because of paired or unpaired electrons respectively in the outer MO. The present discussion is limited to the case of restricted HF (RHF) method. MOs can be written as linear combinations of pre–defined set of one–electron functions known as basis functions or basis set (section 2.2.2). These basis functions are usually centred on the atomic nuclei and so resemblance to AOs. The wave function describing each molecular orbital can be expressed as follows:

$$\psi_i = \sum_{\mu=1}^{N} c_{\mu i}\phi_\mu \tag{2.10}$$

where the coefficients $c_{\mu i}$ are known as the molecular orbital expansion coefficients and N is the number of MOs. The function ϕ_μ refers to a trial basis function and thus ψ_i represents to a trial MO. The ϕ_μ are also chosen to be normalized. The closed shell molecular wavefunction ($\Psi(\vec{r})$), which define $n/2$ molecular orbitals ($\psi_i(\vec{r})$) for a system with n electrons in pairs of opposite spin, can be expressed by Slater determinant [32]:

$$\Psi(\vec{r}) = \frac{1}{\sqrt{n!}}\begin{vmatrix} \psi_1\alpha(1) & \psi_1\beta(1) & \psi_2\alpha(1) & \psi_2\beta(1) & \cdots & \psi_{n/2}\alpha(1) & \psi_{n/2}\beta(1) \\ \psi_1\alpha(2) & \psi_1\beta(2) & \psi_2\alpha(2) & \psi_2\beta(2) & \cdots & \psi_{n/2}\alpha(2) & \psi_{n/2}\beta(2) \\ \vdots & \vdots & & & \vdots & \vdots & \vdots \\ \psi_1\alpha(n) & \psi_1\beta(n) & \psi_2\alpha(n) & \psi_2\beta(n) & \cdots & \psi_{n/2}\alpha(n) & \psi_{n/2}\beta(n) \end{vmatrix} \tag{2.11}$$

where each row represents all possible assignments of electron n to all orbital–spin combinations. This determinant contains all of the possible orbitals for all of the

electrons in the molecular system to form the antisymmetric wavefunction. The interchange of two rows of determinant results in the interchange of two corresponding electrons with effect of change of sign. Thus, the full wavefunction, used in HF method, is expressed as a Slater determinant constructed from the individual occupied MOs.

The variational principle and Roothan–Hall equations

The variational principle is employed to find the lowest energy eigenstate (ground states) and corresponding energy in quantum mechanics. This principle is utilized in Hartree–Fock methods for solving the set of molecular orbital expansion coefficients, $c_{\mu i}$. Thus, one can use the iteration procedure for finding the set of coefficients that minimize the energy of the resultant wavefunction. This suggests a way for obtaining the true wavefunction ψ (spin–orbital function) describing the molecular system. According to this principle, the ground state of any antisymmetric normalized wavefunction of the electronic coordinates is ψ^{trial}, then the expectation value for the energy corresponding to ψ^{trial} will always be greater than the energy for the exact wavefunction ψ.

$$\delta E = \int \psi^{*\,trial}\, H\, \psi^{trial}\, d\tau - \int \psi^{*} H \psi\, d\tau \geq 0 \qquad (2.12)$$

This condition is termed as variational principle. Thus, the trial wavefunction can be optimized using standard techniques [42, 43] until the system energy is minimized. The main motive is the calculation of the electronic wavefunction and the electronic energy.

Roothaan and Hall have introduced the set of basis functions for defining the spinorbitals and transformed the Hartree–Fock equations [39–41]. They derived the following equations using variational principle which describe the molecular orbital expansion coefficients, $c_{\nu i}$.

$$\sum_{\nu=1}^{N} \left(F_{\mu\nu} - \varepsilon_i S_{\mu\nu}\right) c_{\nu i} = 0 \qquad \mu = 1, 2, \ldots, N \qquad (2.13)$$

This equation may be expressed as in matrix form:

$$FC = SC\varepsilon \qquad (2.14)$$

where the matrix S is termed as overlap matrix which represents the overlap between the orbitals and ε is a diagonal matrix of orbital energies. Each element ε_i of diagonal matrix is the one electron orbital energy of molecular orbital ψ_i. The matrix F is known as the Fock matrix that represents the average effects of the field due to all the electrons on each orbital [32]. The C is the matrix of MO expansion coefficients. The elements of Fock matrix for a closed shell molecular system are:

$$F_{\mu\nu} = H_{\mu\nu}^{core} + \sum_{\lambda=1}^{N}\sum_{\sigma=1}^{N} P_{\lambda\sigma}\left[(\mu\nu|\lambda\sigma) - \frac{1}{2}(\mu\lambda|\nu\sigma)\right] \tag{2.15}$$

where $H_{\mu\nu}^{core}$ are the elements of matrix representing the energy of a single electron in the field of the bare nuclei and $P_{\lambda\sigma}$ is the density matrix, defined as:

$$P_{\lambda\sigma} = 2\sum_{i=1}^{occ.} c_{\lambda i}^{*} c_{\sigma i} \tag{2.16}$$

The summation run over the occupied orbitals only and the factor of two is due to fact that each occupied orbital holds two electrons. The elements of single electron energy matrix $H_{\mu\nu}^{core}$ are evaluated once and remain unchanged during iteration [39]. The Fock matrix, density matrix and orbital energy matrix depend on the MO expansion coefficients. The Eq. 2.14 is not linear and, therefore, must be solved iteratively (by SCF procedure). The wavefunction for MO is obtained by simply adjusting the coefficients of AO until the total energy of molecular system cannot be lowered further. An initial set of coefficients are guessed and are used to construct the elements, $P_{\lambda\sigma}$, of the density matrix. The initial Fock matrix is evaluated and used in the secular equations (Eq. 2.13) to derive a new set of coefficients which are used in the construction of a new Fock matrix and the procedure is repeated. The calculation is carried out until the difference between the old and new sets of coefficient is less than or equal to a user defined convergence criterion. The solution produces a set of orbitals, both occupied and unoccupied (virtual). The total number of orbitals is equal to the number of basis functions used. The term $(\mu\nu|\lambda\sigma)$ signifies the two–electron repulsion integrals. In such calculations, the main challenging work is to evaluate the two–electron integrals. The number of two–electron integrals depends on the number of basis functions and size of the molecule.

2.2.2 Basis set

As in previous discussion (section 2.2.1), the molecule may be represented by MOs. The mathematical functions that characterize the AOs are known as basis functions. Thus, one can approximate the MOs using basis set (set of basis functions). There are two kinds of atomic orbital functions which are used in molecular orbital calculations [32, 39–41, 44]. The first is the Slater type orbital (STO) developed by Slater and second is the Gaussian type orbital (GTO) proposed by S. F. Boys. STO functions are not suitable for fast calculations of two–electron integrals while they are good approximation for the AOs. That is why the GTOs were introduced. The shape of the STO function can be approximated by summing up a number of GTOs with different exponents and coefficients. The function obtain by the linear combinations of GTOs to form an STO is called contracted Gaussian type orbitals. The general expression of GTO is expressed in Cartesian variables as:

$$g(r) = N' e^{-\alpha r^2} x^a y^b z^c \tag{2.17}$$

where N' is a normalization constant, α is called exponent, x, y, z are Cartesian coordinates and a, b, c are simply integral exponents at Cartesian coordinates which decides the orbital type. For example, for orbital p_x; $a=1$, $b=c=0$ and for d_{xy} orbital; $a=b=1$, $c=0$. The difference between the STO and GTO is only in the power of 'r'.

The contracted Gaussian type orbital (CGTO) is defined as:

$$\phi^{CGTO}(r) = N' \sum_{i=1}^{n} c_i e^{-\alpha_i r^2} x^a y^b z^c \tag{2.18}$$

where c_i is the contraction coefficient. In quantum chemical computations, the size of a molecule is defined by the number of basis functions rather than by the number of atoms. Finally, the expression for the MOs (normalized) has form:

$$\psi_i = \sum_{\mu} c_{\mu i} \phi_\mu = \sum_{\mu} c_{\mu i} \left(\sum_{j} d_{\mu j} \phi_j^{CGTO} \right) \tag{2.19}$$

where the summation run over the number of MOs and $d_{\mu j}$'s are fixed constants within a basis set [32]. The number of two electron integrals in calculations increase as fourth power of the number of basis functions. Therefore, there must be balance in

basis set, molecular size and computational requirements for computationally attractive calculations. The choice of basis set is such that it must be useful in a chemical sense also [41]. The STOs are more accurate but take longer time while GTOs, relatively less accurate but are much faster to calculate. Thus, to compensate this, many equations of Gaussian type are used to form accurate orbital. The nature of GTO, STO and STO–3G functions [39] are shown for *s*–type orbital with same zeta exponent (=1.0) in Fig. 2.5.

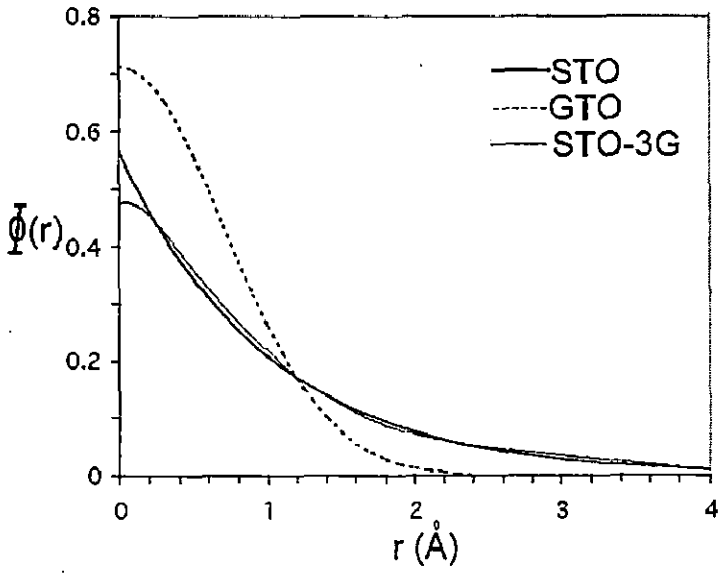

Fig. 2.5 Comparison of the shape of STO, GTO and STO–3G.

The basis sets are the integral part of the methods that are used for quantum chemical calculations. These are characterized in two general categories; minimal basis sets and extended basis sets.

A minimal basis set describes the each inner shell and valence AO by employing minimum basis functions for the individual atom in a molecule. Such type of basis sets can be represented in form of STO–*n*G where *n* denotes the number of primitive GTOs used to approximate one STO for each type AO.

The extended basis sets are characterized as; (1) double, triple, quadruple and higher zeta basis sets (2) split valence (3) polarized sets (4) diffuse sets.

The double zeta basis set defines each type AO by using two basis functions for the individual atoms that comprise molecule. The triple zeta basis set further increases the size of the basis set in order to get closer to the exact electronic SCF energy. In

this case, the triple zeta basis set employs three basis functions for each AO in the atoms within the molecule. This provide more accurate picture of each orbital. There are also available quadruple zeta and higher zeta basis sets. The valence shell electrons play active role and are more affected than core electrons in chemical environment. Therefore, the core electrons are often treated with a minimal basis set while the valence electrons are treated with a larger basis set (double zeta, triple zeta or higher). This is known as a split valence basis set. The split basis sets are denoted by N–M1G or N–M11G, where N and M are integers. The basis set, N–M1G, is a split valence double zeta basis set while the N–M11G is a split valence triple zeta basis set [45]. In the Pople's notations, the 'G' indicates the consideration of gaussian primitives. The 'N' and 'M' represents the number of gaussian primitives used to construct the core orbital and valence orbitals basis functions respectively.

As atoms are held together in the molecules, therefore, charge distribution causes a polarization effect that distorts the shape of atomic orbitals. The polarized basis functions approximate the orbital by adding effect of polarization due to other orbital in the original orbital. Polarized basis functions are denoted by single and double asterisk (* and **) or (*d, p*). One asterisk * or *(d)* denotes that polarization has been taken into account in the non–hydrogen atoms and double asterisk ** or *(d, p)* represents that polarization has taken into account to hydrogen atoms in addition to the non–hydrogen atoms. Diffuse basis functions are used to represent broad electron distributions over the atoms in the molecules. The electron density spread over a large region for an atom in an anion or an excited state, Rydberg states and for lone pair electrons. In these cases, diffuse basis functions are preferred to use. The low value of orbital exponent shows large extent of the diffuse basis function that means the electron is held far away from the nucleus. Diffuse basis functions are represented by the notations '+' and '++'. The '+' represents the *sp*–type diffuse basis functions is added to non–hydrogen atoms and '++' shows the consideration of one set of *sp*– and *s*–type diffuse functions to non–hydrogen and hydrogen atoms respectively.

Moreover, the Dunning and co–workers have proposed the other important basis sets that are of correlation consistent. The Dunning' s basis sets cc–pVDZ, cc–pVTZ, cc–pVQZ, cc–pV5Z and cc–pV6Z are double, triple, quadruple, quintuple–zeta and sextuple–zeta, respectively [46, 47]. The basis sets for the heavy elements beyond the fourth row in the periodic table, are relatively limited. In most of the quantum

mechanical programs, the basis sets available for iodine atom are Midi!, STO–3G, and 3–21G* without using effective core potential (ECP) [48]. For such heavy atoms (beyond the fourth row in the periodic table), ECPs are necessary to use. ECP replaces the core electrons of molecular system by an effective potential and considers only the valence electrons explicitly. This leads to considerable reduction in computational cost and allows for an efficient treatment of relativistic effects. The basis set LANL2DZ (Los Alamos National Laboratory ECP together with valence double zeta basis function) is most widely used for the heavy atoms such as transition metals [49–51].

2.2.3 Moller–Plesset perturbation theory

The Hartree and Fock SCF method ignores the electron correlation although this is critically important for accurate electronic structure calculations. In post HF methods, a great effort has been taken for the development in electron correlation methods. These methods are configuration interaction (CI), n^{th} order Moller–Plesset perturbation (MPn) and quadratic configuration interaction (QCI). The Moller–Plesset perturbation theory. a non–SCF method, provides a systematic approach to finding the correlation energy. In this method, the total Hamiltonian is partitioned into two parts:

$$H = H_0 + \lambda H' \tag{2.20}$$

where the 1st term is unperturbed Hamiltonian that is solvable exactly; the 2nd term is very small perturbation applied to H_0 and λ is a dimensional less parameter. The eigenvalue and the eigenfunction of the total Hamiltonian can be expressed as a power series in terms of HF wavefunction and energy:

$$E = E^{(0)} + \lambda E^{(1)} + \lambda^2 E^{(2)} + \lambda^3 E^{(3)} + \cdots \tag{2.21}$$

$$\psi = \psi^{(0)} + \lambda\psi^{(1)} + \lambda^2\psi^{(2)} + \lambda^3\psi^{(3)} + \cdots \tag{2.22}$$

Substituting these expressions in to the Schrödinger equation and collecting terms in λ^n and the following equations for the n^{th} order MP energy are obtained.

$$E^{(0)} = \int \ldots \int \psi^{(0)} H_0 \psi^{(0)} d\tau_1 d\tau_2 \ldots d\tau_n \tag{2.23}$$

$$E^{(1)} = \int \ldots \int \psi^{(0)} H' \psi^{(0)} d\tau_1 d\tau_2 \ldots d\tau_n \tag{2.24}$$

$$E^{(2)} = \int \dots \int \psi^{(0)} H' \psi^{(1)} d\tau_1 d\tau_2 \dots d\tau_n \tag{2.25}$$

$$\vdots$$

$$\vdots$$

The Moller–Plesset theory upto second order energy correction is designated as MP2 method [32, 39–41, 52]. The Hartree–Fock energy is the sum of the zero and 1st order MP energies:

$$E^{HF} = \int \dots \int \psi^{(0)} (H_0 + H') \psi^{(0)} d\tau_1 d\tau_2 \dots d\tau_n = E^{(0)} + E^{(1)} \tag{2.26}$$

The correlation energy can be defined as:

$$E^{corr.} = E^{(2)} + E^{(3)} + E^{(4)} \tag{2.27}$$

The 1st term may be expended as [39, 52]:

$$E^{(2)} = \frac{1}{4} \sum_{a,b}^{occ.} \sum_{p,q}^{vir.} \frac{(ab||pq)(pq||ab)}{(\varepsilon_a + \varepsilon_b) - (\varepsilon_p + \varepsilon_q)} \tag{2.28}$$

where ε_a and ε_b are energies of occupied molecular orbitals while ε_p and ε_q are energies of virtual molecular orbitals, and integrals $(ab||pq)$ over occupied (a, b) and virtual (p, q) molecular orbitals, which describe the changes in electron–electron interactions as a result of electron promotion, are given as:

$$(ab||pq) = j_o \int \phi_a^*(1) \phi_b^*(2) \frac{1}{r_{12}} \phi_p(1) \phi_q(2) dx_1 dx_2$$
$$- j_o \int \phi_a^*(1) \phi_b^*(2) \frac{1}{r_{12}} \phi_q(1) \phi_p(2) dx_1 dx_2 \tag{2.29}$$

where, ϕ_a and ϕ_b are occupied spinorbitals while the ϕ_p and ϕ_q are the virtual (unoccupied) spinorbitals.

2.2.4 Density functional theory

The density functional theory (DFT) is derived from the Thomas–Fermi–Dirac model and the fundamental work of Slater in the field of quantum chemistry. The DFT has come into existence in 1964 with the paper entitled "Inhomogeneous Electron Gas" by Hohenberg and Kohn [37]. In 1998, W. Kohn and John A. Pople got the Nobel Prize

for the development of the DFT and computational methods in the field of quantum chemistry. This is considered most successful and capable alternative to the traditional *ab initio* quantum chemical methods. It can be applied to medium to large molecular species such as organometallic, inorganic, organic compounds, bio–molecules, etc. Nowadays, it is used routinely in computing molecular energy, structure, spectroscopic quantities and other molecular properties. The molecular wavefunctions involve large number of variables but do not have direct physical significance [40]. This method requires the electron density rather than wavefunction. The other reasons behind its popularity are that the DFT takes in to account the electron correlation effects and demands less computational cost [39]. The DFT also provides some important chemical concepts e.g. reactivity descriptors. The ground state molecular energy and other molecular properties can be uniquely determined by the ground state electron density, $\rho_o(\vec{r})$, for the many electron molecular system with a non–degenerate ground state. The DFT methods are based on the two Hohenberg–Kohn (HK) theorems [37, 53]. They have considered the enclosed arbitrary electrons moving under the influence of an external potential, $v_s(\vec{r})$, and the mutual coulomb repulsion [37]. For the sake of simplicity, the ground state is considered as the non–degenerate. The first theorem states that the ground state electron density of a molecule determines the Hamiltonian and all properties can be obtain from it. In second theorem, a trial electron density must give energy greater than or equal to the true energy.

The Hoehenberg and Kohn theorems do not provide the way to obtain true energy functional from true electron density. Therefore, Kohn and Sham (KS) have given a practical approach to obtain ρ_o and the functional E_o using ρ_o [38]. In solving KS equation [40], the KS orbitals θ_i^{KS} are usually expanded in terms of basis functions, ϕ_μ as:

$$\theta_i^{KS} = \sum_{\mu=1}^{N} c_{\mu i}\phi_\mu \qquad (2.30)$$

where the coefficients $c_{\mu i}$ are known as the molecular orbital expansion coefficients and N is the number of MOs. The function, ϕ_μ refers to an arbitrary (trial) basis set in the same way that θ_i^{KS} refers to a trial MO. These are also chosen to be normalized. The role of basis set is crucial in DFT calculations. The double and triple zeta basis

sets with polarization functions are good enough to provide reliable results in DFT calculations for organic molecules. Some workers recommend the use of diffuse functions with these basis sets on non–hydrogen atoms in DFT calculations [54]. The use of the diffuse functions on uncharged organic molecules produce less accurate results and computations take longer time [55]. The Pople's basis set generally gives better results than correlation–consistence basis set of same size in DFT calculations [40, 56]. Although, KS DFT method gives good results for the medium to large molecular systems but has some drawbacks also because of the approximate functional [40]. Kohn–Sham (KS) method approximates electronic energy functional as:

$$E[\rho] = E_K[\rho] + E_V[\rho] + E_J[\rho] + E_{xc}[\rho] \qquad (2.31)$$

where the square bracket denotes the functional (function of function). The first term, E_K, is due to the kinetic energy of electrons, the second term, E_V, consists the terms that define the potential energy due to the nuclear–electron attraction and nuclear–nuclear repulsion, third one, E_J, describes the electron–electron repulsion, and the last term, E_{xc}, is the exchange–correlation term. The exchange energy arises due to the antisymmetry of the wavefunction while correlation effects are because of the dynamic correlation in the motion of individual electrons [32]. This exchange–correlation functionals can be divided into different classes: local spin density functionals (LDA/LSDA), gradient corrected funcionals (GGA), meta–GGA functionals and hybrid functionals. The LDA/LSDA assume the uniform electron density of the system that varies slowly. The generalized gradient approximation (GGA) accounts the non–uniformity of the electron density.

Some commonly used GGA exchange functionals are Perdew and Wang's (PW86, PW91) [57, 58] and Becke's (B88) [59]. The most popular GGA correlation functionals include those of Perdew (P86), Perdew and Wang (PW91) and Lee, Yang and Parr (LYP) [60]. The further improvement in the GGA functionals can be obtained by including second derivatives of ρ and/or Kohn–Sham kinetic energy density term. Such functionals are known as meta–GGA functionals. There are many mGGA functional like tHCTH, TPSS, VSXC and M06L [41].

The hybrid exchange–correlation functionals are most widely used for the organic molecules due to its accuracy. For example, Becke's three exchange [61] and

Lee–Yang–Parr correlation functionals [60] (B3LYP) are most popular because of its accuracy for a large range of organic compounds. The B3LYP exchange and correlation functional is defined as [40]:

$$E_{xc}^{B3LYP} = (1 - a_0 - a_x)E_x^{LSDA} + a_0 E_x^{exact} + a_x E_x^{B88}$$
$$+(1 - a_c)E_c^{VWN} + a_c E_c^{LYP} \quad (2.32)$$

where E_x^{exact} uses the Hartree–Fock theory and a's are the constants (empirical parameters). Another important hybrid functional is B3PW91 [57, 58, 61] which replaces E_c^{LYP} in Eq. 2.32 with E_c^{PW91}. Many different approximate exchange–correlation functionals are available for DFT calculations e.g. gradient corrected ones (GGAs) such as Becke–Lee–Yang–Parr (BLYP) [59, 60], Perdew–Burke–Enzerhof (PBE) [62] and hybrid functionals such as Becke3–Lee–Yang–Parr (B3LYP) [60, 61]. Moreover, an active research work is going on for improvements in the exchange–correlation functional [57–61]. At present, B3LYP functional is the most widely used exchange–correlation functional within DFT calculations on molecules.

2.2.5 Potential energy surface

A potential energy surface (PES) can be defined by mathematically or graphically by relationship between the potential energy of a molecule and its geometry [40]. It is a hyper–surface of potential energy against the geometric coordinates of the nuclei. The first step for the molecular simulation is to construct of the PES and to locate minimum on it. The PES helps in understanding molecular structure conformation and all molecular properties based on it. The nature of various chemical reactions can also be understood by assessment of the reaction PES. The Born–Oppenheimer approximation makes possible the construction of PES and it simplifies the application of the Schrödinger equation to molecules [63]. Using this approximation, the Schrödinger equation for electronic motions has form given in Eq. 2.8. There are $3N-6$ independent nuclear coordinates R_1, R_2, ..., R_{3N-6} that define a non linear molecular geometry having N nuclei. The molecular electronic energy U is a function of these coordinates. The function U is a potential energy in Schrodinger equation for the nuclear motion. The $3N-6$ coordinates correspond to vibrational motion while the other three translational and three rotational degree of freedom leave U unchanged.

The stable geometry of a molecule can be obtained by minimizing energy U (locating minimum on PES) by using various optimization techniques [42, 43]. The aim of geometry optimization procedures is to achieve nuclear arrangement in molecular system which makes it most stable (minimum energy). The optimization techniques minimize the value of U with respect to each of $3N-6$ variables in searching of minimum on PES. For the large sized molecules, many minima (local minima) are possible on its PES. For this case, finding the true global minimum (minimum among the all-local minima) equilibrium geometry is almost unattainable. The all other molecular properties are based on the molecular geometry. This is why searching the accurate molecular geometry on PES is very important task.

Geometry optimization

Geometry optimization or locating molecular geometry at minimum on PES is the primary task in studying molecules using computational techniques. In order to study molecular properties, an accurate description of the molecular geometry on PES is required. The procedure for locating stationary points (minima or maxima) on the PES for calculating molecular geometry and energy is called geometry optimization. Geometry optimizations require an input guessed structure that is supposed to be close to actual structure. Submitting this structure to a computer algorithm that systematically alters the geometry parameters (bond lengths, bond angles and dihedral angles) until it has found a stationary point. Locating a local minimum on PES is often called an energy minimization [40]. The stable geometry of a molecule is used to determine many of its chemical properties. The efficient algorithm for geometry optimization requires repeated calculation of both U and its partial derivatives (gradients). At a local minimum, the gradient has to be zero i.e. each of the $3N-6$ first partial derivatives of U must be zero. Any point on the PES where the gradient is zero is called stationary point:

$$\frac{\partial U(R)}{\partial R_i} = 0 \tag{2.33}$$

A stationary point on a PES may be a saddle point, minimum or maximum. Thus, for deciding about minimum, maximum or saddle point on PES, the second derivatives of U with respect to $3N-6$ nuclear coordinates are necessary. Therefore, energy minimization techniques also calculate the second derivatives of U with respect to

3N−6 nuclear coordinates. The set of these derivatives arranged in square format called the Hessian or the force constant matrix:

$$H_{ij} = \frac{\partial^2 U(R)}{\partial R_i \partial R_j} \tag{2.34}$$

The geometry optimization starts from the guess of equilibrium structure obtained from X−ray, electron and neutron diffraction experiments if available. The guessed structure is based on typical values for bond lengths, bond angles and dihedral angles. After guessing the geometry, one can choose basis set and use SCF MO method to approximately solve the electronic Schrödinger equation to find U and its 1st as well as 2nd derivatives with respect to the nuclear coordinates. Using these calculated values, the program changes the *3N−6* nuclear coordinates to a new set likely to be closer to the initial set and the new values of U and its derivatives are calculated at this new structure. Using the results of the new calculation, a further improved set of nuclear coordinates is calculated. These SCF calculations repeated until the gradient U reaches to convergence criterion, indicating the stationary point. For ensuring whether the calculated molecular geometry is at minimum or not on PES, vibrational frequency (Hessian) calculations are performed at that geometry. For a true minimum, all the calculated frequencies must be real. For a transition state (1st order saddle point) the gradient is zero while the Hessian has one negative value. In the present work, Berny algorithm [42, 43] implemented in Gaussian software [64] and quadratic approximation in GAMESS−US program [65], were employed for optimizing the geometry of molecules. At the beginning of the optimization procedure, a suitable estimate of the second derivative matrix (Hessian matrix) is required. This algorithm uses the force acting on the atoms of molecule together with the Hessian matrix and optimizes the structure towards the next local minimum on the PES. It builds an approximate Hessian at the beginning of the optimization procedure by using guessed structure (given by user), and then uses the energies and first derivatives calculated along the optimization pathway to update this approximate Hessian matrix. The achievement of optimization procedure depends on the how well is the guessed structure. The optimization algorithm takes lesser time for the guessed geometry that is close to actual. According to Berny algorithm, a single optimization step can be divided in to three parts: (1) Corrections to estimated second derivative matrix, (2) Searching for a minimum along the line between the recent and previous point, and

(3) Estimating the location of the stationary point in the N–dimensional space by using the gradient and the approximate second derivative matrix. Finally, convergence is tested against criteria for the maximum force component, root–mean square force, maximum step component, and root–mean–square step. The step is the change between the most recent point and the next to be computed [66].

Vibrational frequency calculations

An equilibrium or stable molecular structure is characterized by possessing all positive values in Hessian matrix. The harmonic vibrational frequencies of an optimized structure are computed by evaluation of the matrix that contains second derivative energy (Hessian or force constant matrix) analytically or numerically. It is necessary to consider the vibrational zero point energy (ZPE) of the molecular for calculating accurate energy differences. The ZPE requires the molecular vibrational frequencies. Theoretical computation of vibrational frequencies assists in studying vibrational spectra of polyatomic molecules. Calculation of vibrational frequencies on optimized geometry using quantum chemical packages provides also thermochemistry and other properties of the molecule. The harmonic vibrational frequencies of a molecule are calculated by solving following set of *3N* linear equations in *3N* unknowns [40]:

$$\sum_{j=1}^{3N}(F_{ij} - \delta_{ij}\lambda_k)l_{jk} = 0, \qquad i = 1, 2, 3, \ldots, 3N \tag{2.35}$$

where F_{ij} is the mass weighted force constant (mass weighted Hessian) matrix elements, as defined by:

$$F_{ij} \equiv \frac{1}{(m_i m_j)^2}\left(\frac{\partial^2 U}{\partial X_i X_j}\right) \tag{2.36}$$

In Eq. 2.35, δ_{ij} is the Kronecker delta, and λ_k and the l_{jk} are unknown parameters. In order to have a non–trivial solution, the coefficient determinant must vanish,

$$\left|F_{ij} - \delta_{ij}\lambda_k\right| = 0 \tag{2.37}$$

This determinant (secular equation) of order *3N* can be expended in polynomial form whose highest power of λ_k is λ_k^{3N}. The secular equation will give *3N* roots for λ_k.

The vibrational harmonic frequencies are obtained from relation, $\nu_k = \lambda_k^{1/2}/2\pi$. For the non–linear molecule, six of the λ_k values will be zero, yielding six frequencies with zero value which correspond to the three translational and rotational degrees of freedom of the molecule. The remaining *3N–6* vibrational degrees of freedom are the normal modes of vibrations. Frequency calculation must be carried out after the geometry optimization using the same method and basis set [40]. Harmonic vibrational frequencies generally overestimate the experimental frequencies because of anharmonicity and other factors. Therefore, various empirical scaling procedures are used in assigning the vibrational spectra [67–72]. These procedures do not consider the anharmonic terms in potential which is crucial to define anharmonic vibrations. Besides scaling procedures, a great effort has been taken for the calculations of anharmonic frequencies [73–81].

Potential energy distribution

Generally, the vibrational modes of molecule are assigned with help of potential energy distribution (PED) analysis and visualization of atomic displacement. The PED values show the distribution of vibrational potential energy in each internal or symmetry coordinate. These are of great interest for assigning the vibrational frequencies of molecules. The vibrational potential energy, V [82, 83] for the molecule, can be defined in terms of internal coordinate R, by following expression:

$$V = \frac{1}{2}\sum_{i,j} F_{ij} R_i R_j \tag{2.38}$$

where, R_i, R_j are internal coordinates and F_{ij} are elements of the force constant matrix. One can define the transformation matrix, L that express transformation between internal or symmetry coordinates and normal coordinates (Q), by following expression:

$$R = LQ \tag{2.39}$$

Thus, the potential energy term can be rewritten as:

$$V = \frac{1}{2}\sum_{k} Q_k^2 \sum_{i}\sum_{j} L_{jk} L_{ik} F_{ij} \tag{2.40}$$

For each normal coordinate, one can compute the matrix elements $L_{jk}L_{ik}F_{ij}$ with the help of known force constant matrix. Thus, a single symmetric potential energy distribution matrix can be obtained whose elements are given by:

$$[PED]_{kj}^{\lambda} = \sum_{i} \frac{L_{jk}L_{ik}F_{ij}}{\lambda_k} \qquad (2.41)$$

where $\lambda_k = 4\pi^2c^2\tilde{\nu}_k^2$ are the calculated eigenvalues which prefer to use in normalization of the matrix. The elements of PED matrix represent the percent potential energy distribution (its rows and coloumns add up to 100%). The PED values for each normal coordinate show the same order, so they are comparable. PED gives the contribution of the diagonal matrix elements F_{ii}. The off diagonal terms F_{ij} are responsible for the anharmonicity associated with vibrational modes which have significant values for some anharmonic modes of large amplitude of vibrations. Some molecules, which consist of freely rotating methyl, ethyl etc. groups, pucker modes in five or four membered rings, etc., give several anharmonic modes. The anharmonicity will wreak havoc on PED distributions, and the PEDs are not reliable for such modes. Visualizing the mode by arrows and animation is best option to characterize these types of modes.

2.2.6 Anharmonic force field

Vibrational spectroscopy is a powerful technique for characterizing the vibrational modes medium to large size molecules. Development in quantum chemical methods has provided an invaluable support to the vibrational spectroscopy. The vibrational studies in the harmonic approximation are sometime important in the case of medium to large sized molecules but these are often not of sufficient accuracy. The vibrational modes of polyatomic molecules are anharmonic in nature. For the reliable vibrational assignments, it is necessary to carry out the anharmonic force field calculations. The deviation of calculated values from the experimental ones is due to both limitations of the quantum chemical model and neglect of anharmonicity. Many molecules are very floppy and are subjected to strong anharmonic effects. Thus, it is interesting to employ effective approaches for anharmonic calculations that can provide significant improvements. The successful approaches are vibrational self–consistent field (VSCF) method, correlation corrected vibrational self–consistent field (CC–VSCF)

method and Barone's second order perturbation theory (PT2) which are used for anharmonic force field calculations [73–81]. The PT2 approach is very effective for the study of medium size semi–rigid molecules [84]. Barone [81] had implemented an efficient method, PT2, for building anharmonic force constants. In this approach, the third and fourth derivatives are calculated by finite difference approach. The VSCF and CC–VSCF methods correct well the frequencies of vibrational modes for the molecules having floppy vibrations [84].

Second order perturbative approach

The calculation of anharmonic vibrational frequencies of a polyatomic molecule using second order perturbation theory is based on the expansion of the potential energy surfaces in terms of normal coordinate. The potential energy function in the vicinity of minima, can be expressed in terms of Taylor series which is truncated to yield forth order polynomial [85]:

$$V = \frac{1}{2}\sum_{i} \omega_i Q_i^2 + \frac{1}{6}\sum_{ijk} \Phi_{ijk} Q_i Q_j Q_k + \frac{1}{24}\sum_{ijkl} \Phi_{ijkl} Q_i Q_j Q_k Q_l + \cdots \qquad (2.42)$$

where ω_i represent the harmonic frequencies (cm^{-1}); Q is the normal coordinate with unrestricted index *ijkl*.... The third and fourth energy derivatives, Φ_{ijk} and Φ_{ijkl} respectively, can be computed by using numerical differentiations of analytical Hessian matrices (second order energy derivatives) at small increment δQ [81]. The second derivatives are obtained analytically while third and forth order terms are calculated by using finite differences.

The vibrational energy levels (in cm^{-1}) of an asymmetric top molecule characterized by a set of quantum numbers (v) can be expressed as [86]:

$$E_{vib} = x_0 + \sum_{i} \omega_i \left(v_i + \frac{1}{2}\right) + \sum_{i} x_{ii} \left(v_i + \frac{1}{2}\right)^2 + \sum_{i}\sum_{j<i} x_{ij} \left(v_i + \frac{1}{2}\right)\left(v_j + \frac{1}{2}\right) \qquad (2.43)$$

where, ω_i is the harmonic frequency of the i^{th} normal mode of vibration and x_{ij}, a square matrix of real anharmonic constants. The constant, x_{ii} characterizes anharmonicity of the given vibration; x_{ij} characterizes coupling between different

normal modes resulting from anharmonicity and are determined from cubic and quartic force constants. The x_0 is usually negligible.

The fundamental vibrational frequencies (ν_i), overtones $(2\nu_i)$, combination bands $(\nu_i\,\nu_j)$ and zero point energy (ZPE) [81] can be evaluated by using following relations:

$$\nu_i = \omega_i + 2x_{ii} + \frac{1}{2}\sum_{j\neq i} x_{ij} \tag{2.44}$$

$$[2\nu_i] = 2\omega_i + 6x_{ii} + \sum_{j\neq i} x_{ij} = 2\nu_i + 2x_{ii} \tag{2.45}$$

$$[\nu_i\,\nu_j] = \omega_i + \omega_j + 2x_{ii} + 2x_{jj} + 2x_{ij} + \frac{1}{2}\sum_{l\neq i,j}(x_{il} + x_{jl}) = \nu_i + \nu_j + x_{ij} \tag{2.46}$$

$$ZPE = x_0 + \frac{1}{2}\sum_i \left(\omega_i + \frac{1}{2}x_{ii} + \sum_{j>i}\frac{1}{2}x_{ij}\right) \tag{2.47}$$

This can be rewritten as:

$$ZPE = \frac{1}{2}(ZPE_H + ZPE_F) + x_0 - \frac{1}{4}\sum_i x_{ii} \tag{2.48}$$

where

$$ZPE_H = \frac{1}{2}\sum_i \omega_i \tag{2.49}$$

$$ZPE_F = \frac{1}{2}\sum_i \nu_i \tag{2.50}$$

The PT2 method is an important tool for calculations of anharmonic force fields but in some cases this method fails. For the highly anharmonic vibrations, the perturbation is expected to be large that may breakdown this method [84]. This method includes anharmonic effects resulting from small displacement with respect to equilibrium geometry. Other reason is due to choice of coordinates. The rectilinear coordinates fail to define the large amplitude of vibration. Thus, the PT2 method is a good choice for the calculations on semi–rigid organic molecules. This method does

not provide appropriate results for highly anharmonic and floppy molecules like amino acids, peptides and proteins. The VSCF/CC–VSCF methods are quite efficient up to some extent for molecules having floppy vibrations. The CC–VSCF method is a form of VSCF corrected by second order perturbation theory. The PES within VSCF/CC–VSCF approaches is constructed by using full anharmonic potential and quartic force field potential.

Vibrational self–consistent field approach

In the present work, the VSCF and CC–VSCF approaches were also employed to compute anharmonic frequencies of polyatomic molecules. The VSCF method is another effective approach to study anharmonic vibrational system. The Bowmen, Carter and Gerber [73, 76–78] have contributed in the development of VSCF method. In VSCF approach, the normal–mode analysis of equilibrium geometry is performed first which gives the harmonic frequencies and normal modes. Within this normal coordinate system, the vibrational Schrödinger equation is solved using the VSCF approximation. In VSCF method, each vibrational mode is described as moving in an effective field due to the rest of the vibrational motions. The product of single–mode wavefunctions corresponding to the different normal modes defines the full vibrational wavefunction in this approximation. For each single mode wavefunction, a mean field potential that shows the average effects of the other modes is employed. Analytical procedures are not available for such calculations. Therefore, the equations are solved numerically until convergence is reached. Anharmonic effects are treated including coupling between different modes. This approximation provides a grid of points in normal–mode coordinates at which potential energy is calculated. Basic VSCF method provides improvement over the harmonic approximation. For the higher accuracy, second order perturbation theory is used for considering the correlation effects between normal modes. This method is known as CC–VSCF method which is also called PT2–VSCF [77, 78]. The VSCF method uses the separability approximation. For the strong mode–mode coupling, the separability approximation may breakdown due to correlation effect between the vibrational modes. Therefore, the vibrational frequencies for such modes having large coupling show the large deviation.

The VSCF method is analogy of the Hartree SCF method. The Schrödinger equation in terms of weighted normal coordinates $Q_1, Q_2 \ldots., Q_N$ can be written as [84, 87–89]:

$$\left[-\frac{1}{2}\sum_{i=1}^{N}\frac{\partial^2}{\partial Q_i^2} + V(Q_1, \ldots., Q_N)\right]\psi_i^{(n)}(Q_1, \ldots., Q_N) = E_n\psi_i^{(n)}(Q_1, \ldots., Q_N) \qquad (2.51)$$

where, $V(Q_1, \ldots., Q_N)$ is the potential energy function, N denotes vibrational degree of freedom and n shows the state number. In VSCF approximation, the total wavefunction, ψ, can be written as the product of single mode wavefunction, $\psi_i^{(n)}$. The trial wavefunction for the N mode is approximated as:

$$\psi(Q_1, \ldots., Q_N) = \prod_{i=1}^{N}\psi_i^{(n)}(Q_i) \qquad (2.52)$$

The mean field and wavefunctions of the modes are obtained by using SCF approach. The VSCF method provides the N–dimensional Schrodinger equation for the N–mode system [87–90] that leads to N single mode VSCF equation having the form:

$$\left[-\frac{1}{2}\frac{\partial^2}{\partial Q_i^2} + \overline{V_i^{(n)}}(Q_i)\right]\psi_i^{(n)} = \varepsilon_i^{(n)}\psi_i^{(n)}(Q_i) \qquad (2.53)$$

where, $\overline{V_i^{(n)}}(Q_i)$ is the effective potential for mode i corresponding to Q_i which is given by the equation:

$$\overline{V_i^{(n)}}(Q_i) = \langle\prod_{j\neq i}^{N}\psi_j^{(n)}(Q_j)|V(Q_1, \ldots., Q_N)|\prod_{j\neq i}^{N}\psi_j^{(n)}(Q_j)\rangle \qquad (2.54)$$

The Eq. 2.53 and 2.54 are solved self consistently for obtaining single mode wave functions, effective potentials and energies. For VSCF and CC–VSCF approximations, the potential of the system $V(Q_1, \ldots., Q_N)$ introduced by Gerber and Jung [91] is represented by the sum of separable single–mode and pair coupling terms, neglecting triple and higher mode–mode interactions (pair–wise approximation):

$$V(Q_1, \ldots, Q_N) = \sum_{j}^{N} V_j^{diag}(Q_j) + \sum_{i} \sum_{i<j} W_{ij}^{coup}(Q_i, Q_j) \qquad (2.55)$$

The first term is diagonal term that represents the harmonic potential and the intrinsic anharmonicity of the potential function along the normal coordinate Q_j, and the second term shows the contribution to the potential of the mode–mode coupling.

The total energy under VSCF approximation can be written as:

$$E_n^{VSCF} = \sum_{j=1}^{N} \varepsilon_j^{(n)} - (N-1) \langle \prod_{j=1}^{N} \psi_j^{(n)}(Q_j) | V(Q_1, \ldots, Q_N) | \prod_{j=1}^{N} \psi_j^{(n)}(Q_j) \rangle \qquad (2.56)$$

In this equation, first term is sum of all individual mode energies and the rest term accounts for the double counting of the interactions in the energy calculation. In the CC–VSCF approximations, the VSCF approximation is corrected for correlation effects between different vibrational modes using second order perturbation theory. The total energy for the CC–VSCF approximation is then given by:

$$E_n^{CC-VSCF} = E_n^{VSCF} + \sum_{m \neq n} \frac{\left| \langle \prod_{j=1}^{N} \psi_j^{(n)}(Q_j) | \Delta V | \prod_{j=1}^{N} \psi_j^{(m)}(Q_j) \rangle \right|^2}{E_n^{(0)} - E_m^{(0)}} \qquad (2.57)$$

where,

$$\Delta V = V(Q_1, \ldots, Q_N) - \sum_{i=1}^{N} \overline{V_i^{(n)}}(Q_i) \qquad (2.58)$$

All the correlation effects are included in ΔV which is the difference between the correct Hamiltonian and VSCF one. For the CC–VSCF approach, the difference between true Hamiltonian of the system and VSCF Hamiltonian must be small which is treated as the perturbation. The VSCF/CC–VSCF computations demand the high computational cost for medium to large size molecules because above equations involved multidimensional integrals which must be computed numerically.

Quartic force field potential and anharmonic mode–mode coupling strength

The most important task of quantum chemical calculations is to acquire accurate potential energy surface (PES) which governs the dynamics of nuclear motions. Yagi and coworkers [92, 93] introduced a quartic force field (QFF) approximation to

represent PES that includes anharmonic effects. In the QFF representations, the PES around the equilibrium geometry of molecule can be approximated using Taylor series expansion as (similar to Eq. 2.42):

$$U(Q_i) = U_0 + \frac{1}{2}\sum_{i}^{f} h_i Q_i^2 + \frac{1}{6}\sum_{ijk}^{f} t_{ijk}\, Q_i\, Q_j\, Q_k + \frac{1}{24}\sum_{ijkl}^{f} u_{ijkl}\, Q_i\, Q_j\, Q_k\, Q_l \quad (2.59)$$

where U_0, h_i, t_{ijk} and u_{ijkl} represent the potential energy and its second, third and fourth order derivatives with respect to normal coordinates; $f = 3N - 6\ or\ 5$, where N is the number of atoms in a molecule. The approximate PES, which includes up to n coordinate couplings, is referred to as U_{QFF}^{n}. In form of n–mode coupling representation (nMR–QFF), the PES can be defined by:

$$U(Q_i) = U_{QFF}^{1} + U_{QFF}^{2} + U_{QFF}^{3} + \cdots \quad (2.60)$$

where

$$U_{QFF}^{1} = U_0 + \sum_{i}^{f}\left[\frac{1}{2}h_i Q_i^2 + \frac{1}{6}t_{iii}Q_i^3 + \frac{1}{24}u_{iiii}Q_i^4\right] \quad (2.61)$$

$$U_{QFF}^{2} = U_{QFF}^{1} + \sum_{i\neq j}^{f}\left[\frac{1}{2}t_{ijj}Q_i\, Q_j^2 + \frac{1}{6}u_{ijjj}Q_i\, Q_j^3\right] + \frac{1}{4}\sum_{i<j}^{f} u_{iijj}\, Q_i^2 Q_j^2 \quad (2.62)$$

$$U_{QFF}^{3} = U_{QFF}^{2} + \sum_{i<j<k}^{f} t_{ijk}Q_i\, Q_j\, Q_k + \frac{1}{2}\sum_{i\neq j<k}^{f} u_{iijk}Q_i^2\, Q_j\, Q_k \quad (2.63)$$

where U_{QFF}^{n} denotes a reduced QFF including up to n coordinate couplings. This type of representation of PES under QFF is known as n–mode coupling representation. The third and fourth energy derivatives in above equations can be obtain through numerical differentiations. The existing VSCF code implemented in GAMESS–US [65] can treat two mode couplings (2MR–QFF). The number of grid points involved to determine all the coefficients in the 2MR–QFF are:

$$N_{QFF}^{2} = 1 + 6f + \frac{12(f(f-1))}{2} \quad (2.64)$$

The coefficients, t_{ijj}, u_{ijjj} and u_{iijj} occured in 2MR–QFF can be computed by numerical differentiations [92].

The QFF can be utilized with both VSCF and CC–VSCF methods as implemented in GAMESS–US package. The direct VSCF includes the full PES that increases the computational cost. The number of quadrature points for VSCF calculations with a 2MR–PES is given by:

$$N_{grid}^{2} = 1 + Mf + M^{2}\frac{f(f-1)}{2} \tag{2.65}$$

where M is number (12 for 2MR–PES) of grid points along each normal coordinate. Thus, 2MR–QFF can be constructed with less computational effort than the direct VSCF calculations. The QFF approximation method is slightly less accurate but remarkably reduces the computational effort.

The mode coupling strength (MCS) can be computed by invoking Rayleigh–Schrödinger perturbation theory based on a zeroth order state. The 1st and 2nd order corrections to the energy for a state $|n\rangle$ can be obtained by following equations:

$$E_{n}^{(1)} = \langle n|H'|n\rangle \tag{2.66}$$

$$E_{n}^{(2)} = \sum_{k\neq n}\frac{|\langle k|H'|n\rangle|^{2}}{E_{n}^{(0)} - E_{k}^{(0)}} \tag{2.67}$$

where $E_{n}^{(0)}$ is zeroth order energy for the state $|n\rangle$ that can be defined by:

$$E_{n}^{(0)} = \sum_{i}\left(n_{i} + \frac{1}{2}\right)\omega_{i} \tag{2.68}$$

and H' is small perturbation which represents the anharmonicity in full PES:

$$V(Q) = \frac{1}{2}\sum_{i}\omega_{i}^{2}\,Q_{i}^{2} + H' \tag{2.69}$$

which implies that $H' = V(Q) - \frac{1}{2}\sum_{i}\omega_{i}^{2}\,Q_{i}^{2}$

$$= \sum_{i}\left(V_{i} - \frac{1}{2}\sum_{i}\omega_{i}^{2}\,Q_{i}^{2}\right) + \sum_{i>j}V_{ij} + \sum_{i>j>k}V_{ijk} + \cdots \tag{2.70}$$

For reliable estimate of the mode coupling strengths (MCSs), we may express the two mode coupling terms in a QFF, a 4th order polynomial, is given as:

$$V_{ij}^{QFF}(Q_i, Q_j) = c_{ijj}Q_iQ_j^2 + c_{iij}Q_i^2Q_j + c_{iijj}Q_i^2Q_j^2 + c_{ijjj}Q_iQ_j^3 + c_{iiij}Q_i^3Q_j \quad (2.71)$$

The coefficients in above expression can be computed efficiently by numerical differentiations of an analytical Hessian available. Thus, the MCS based on QFF coefficients are attractive since they can potentially be used to detect the strong coupling and the unimportant part of PES is neglected. Using the Eq. 2.71 of the PES, we may estimate the contribution of each mode coupling term to the energy in Eq. 2.66. For the first–order correction, only the two–mode part of the PES survives through the $Q_i^2Q_j^2$ term. We obtain for the ground state:

$$\eta_{ij} = \eta_{iijj}^{(1)} = c_{iijj}\langle 0|Q_i^2Q_j^2|0\rangle = c_{iijj}\left(\frac{\hbar}{2\omega_i}\right)\left(\frac{\hbar}{2\omega_j}\right) \quad (2.72)$$

This expression gives the mode–mode coupling strength based on 2MR–QFF for ground state in which second order correction is ignored [94].

IR and Raman intensities

The theoretical IR and Raman intensities along with vibrational frequencies play important role in assignments of FTIR and Raman spectra. The quantity, molar absorptivity (ε), which measures how strongly a chemical species absorb the light at given wavelength, is used to define IR intensity. It is defined as [95]:

$$\varepsilon(\tilde{\nu}) = \frac{1}{cl}log_{10}\left(\frac{I_0(\tilde{\nu})}{I\ (\tilde{\nu})}\right) = \frac{A(\tilde{\nu})}{cl} \quad (2.73)$$

where, c is the concentration (mol/L), l is the optical path length (cm), I_0 and I are the intensities of the incident and transmitted radiation, respectively, and $A(\tilde{\nu})$ is the absorbance at the wavenumber $\tilde{\nu}$ (cm^{-1}). For the i^{th} fundamental vibrational band of molecule, the integrated absorbance is defined as [96]:

$$\mathcal{A}_i = \int \varepsilon(\tilde{\nu})\, d\tilde{\nu} = \frac{1}{cl}\int A(\tilde{\nu})\, d\tilde{\nu} \quad (2.74)$$

In IR spectroscopy, the unit of intensity is 1000 m mol^{-1} = km mol^{-1}.

The $\mathcal{A}_i$ can be approximated under electric and mechanical harmonicity as:

$$\mathcal{A}_i = \frac{\pi N_A g_k}{3000\, c^2 \times 2.302581} \left|\frac{\partial \mu}{\partial Q_i}\right|^2 \tag{2.75}$$

where N_A is the Avogadro's number (mol^{-1}), c is the speed of light (cm s^{-1}), g_k is the degeneracy, and $\frac{\partial \mu}{\partial Q_i}$ is the dipole moment derivative with respect to i^{th} normal coordinate. For the i^{th} normal coordinate, the derivative of the j^{th} component of the dipole moment vector of a system of fixed charge is given by:

$$\frac{\partial \mu_j}{\partial Q_i} = \frac{\partial}{\partial Q_i}\left(\frac{\partial E}{\partial \xi_j}\right) = \frac{\partial}{\partial \xi_j}\left(\frac{\partial E}{\partial Q_i}\right) \tag{2.76}$$

where E is the energy of the system in a constant electric field ξ, sufficiently weak to polarize. The quantities $\left(\frac{\partial E}{\partial Q_i}\right)$ are the components of energy gradient that are needed for the computation of $\frac{\partial \mu_j}{\partial Q_i}$ and infrared intensities form Eq. 2.75. The geometry optimization and frequency calculation provide the quantities $\left(\frac{\partial E}{\partial Q_i}\right)$.

Anharmonic IR intensities are also calculated by using dipole moments estimated during VSCF and CC–VSCF anharmonic computations with the help of GAMESS–US program. For the fundamental and overtone excitations, the IR intensity is defined by:

$$I_i = \frac{8\pi^3 N_A}{3hc}\omega_i \left|\left\langle \psi_i^{(0)}(Q_i)\middle|\vec{\mu}(Q_i)\middle|\psi_i^{(n)}(Q_i)\right\rangle\right|^2 \tag{2.77}$$

where $\vec{\mu}$ denotes dipole moment vector, ω_i is the vibrational frequency calculated by CC–VSCF for normal mode i, $\psi_i^{(0)}$ and $\psi_i^{(n)}$ are the VSCF wavefunction for the ground and n^{th} excited vibrational states [84].

The calculation of Raman activities utilizes the Placzek's polarizability theory [97, 98]. The calculations are restricted to harmonic approximation and only linear term is considered in series expansion of the polarizability tensor components with respect to normal coordinate. The incident light is considered as plane polarized light and observations made in the direction perpendicular the electric field and to direction

of propagation [99]. The Raman scattering activity (S_i) and depolarization ratio (ρ_i) associated with the normal coordinate Q_i are defined by the following equations:

$$S_i = g_i[45\,(\alpha_i')^2 + 7\,(\gamma_i')^2] \quad \left(\frac{\text{Å}^4}{amu}\right) \tag{2.78}$$

$$\rho_i = \frac{3\,(\gamma_i')^2}{45\,(\alpha_i')^2 + 4\,(\gamma_i')^2} \tag{2.79}$$

where g_i is the degeneracy of the normal mode; α_i' and γ_i' are, respectively, the derivatives of the trace and of the anisotropy of the polarizability tensor,

$$(\alpha_i')^2 = \frac{1}{9}\sum_m \left(\frac{\partial \alpha_{mm}}{\partial Q_i}\right)^2 ; m = x, y, z \tag{2.80}$$

$$(\gamma_i')^2 = \frac{1}{2}\sum_{mn}\left[3\left(\frac{\partial \alpha_{mm}}{\partial Q_i}\right)^2 - \left(\frac{\partial \alpha_{mm}}{\partial Q_i}\frac{\partial \alpha_{mn}}{\partial Q_i}\right)\right] \tag{2.81}$$

The absolute differential Raman scattering cross section (in m^2/sr) is given by [97, 100]:

$$\frac{\partial \sigma_i}{\partial \Omega} = \frac{(2\pi)^4}{45}(\nu_0 - \nu_i)^4 \frac{h}{8\pi^2 c \nu_i B_i} S_i \tag{2.82}$$

where σ_i is the scattering cross section while Ω represents the solid angle of light collection. The factor B_i arises due to temperature, which accounts for the intensity contribution of excited vibrational states, and is represented by the Boltzmann distribution:

$$B_i = 1 - e^{\left(-h\nu_i c/kT\right)} \tag{2.83}$$

In Eq. 2.82, ν_0 is the frequency of laser excitation line; ν_i is the frequency of i^{th} normal mode, and constants have their usual meanings. It is noted that the Gaussian program computes the Raman activity S_i not Raman intensities. Therefore, theoretical Raman intensity that simulates the experimental Raman spectrum can be obtained using Eq 2.82.

2.2.7 Other molecular properties

Quantum chemical methods have proven important tools for studying various molecular properties based on optimized geometry. In present thesis, in addition to molecular structure and vibrational spectra, many molecular properties such as chemical reactivity descriptors based on HOMO and LUMO energy eigenvalues, dipole moments, non–linear optical properties (NLO), atomic charges, thermochemistry, molecular electrostatic potential, NBO analysis, etc., have been also presented. The brief accounts of these calculations are discussed in this section.

Molecular electrostatic potential

The molecules can be considered as a compilation of point–charge nuclei and electronic charge spread out into a continuous distribution. The electrostatic potential $V(\vec{r})$ is formed in the space over a molecule by its nuclei and electrons [101, 102]. This can be computed by following relation at any point $\vec{r}$:

$$V(\vec{r}) = \sum_A \frac{Z_A}{|\vec{R}_A - \vec{r}|} - \int \frac{\rho(\vec{r'})d\vec{r'}}{|\vec{r'} - \vec{r}|} \qquad (2.84)$$

where Z_A is the charge on nucleus A, located at $\vec{R}_A$ and $\vec{r'}$ is the dummy integration varaible. The electron density function is $\rho(\vec{r'})$. The 1st and 2nd terms represent the contribution to the potential due to nuclei and electrons, respectively. The potential $V(\vec{r})$ created by the static charge distribution of the molecule is also defined as interaction energy of this static charge distribution with a proton located at the point $\vec{r}$. The $\rho(r)$ is considered as the unperturbed ground state density. Therefore, the polarization effect on molecule's electronic density due to proton is not taken into account. The electrostatic potential is a real physical quantity that plays an important role for elucidating and predicting the reactive behaviour of molecules. This helps to know charge related properties of the molecules [103]. One can determined this quantity experimentally by diffraction methods as well as computationally [101]. This quantity can be visualized by the molecular electrostatic potential (MEP) mapping. The MEP map is a plot of electrostatic potential mapped on to the total electron density surface. The MEP is commonly shown by contour map with curves in a particular plane through the molecule or by a three dimensional surface. MEP represents the size of the molecule and electrostatic potential in terms of colour

coding. The surfaces with blue, green and red colours indicate the positive, zero and negative values of the potential respectively. The red colour surfaces with negative MEP are due to high electron density, indicating a strong attraction between the proton and points on the molecular surface. The blue colour surfaces correspond to areas of low electron density. MEP plays an efficient role in understanding and predicting the chemical interactions. An electrophilic (electron–loving) species will preferentially attack a molecule at sites where the MEP is most negative. Similarly, the neucleophile (proton–loving) species will attack at sites where the MEP is most positive. MEPs provide insight into molecular recognition processes such as enzyme–substrate and drug receptor interactions [40]. Furthermore, MEP is largely responsible for the binding of the substrate at the active site of a receptor. The MEP is very helpful in understanding the sites for electrophilic and nucleophilic attacks for the study of biological recognition processes. The sign of electrostatic potential in any particular region around a molecule, which depends upon whether the effects of the nuclei or electrons are dominant, is a key to assessing its reactivity there. This also provides information for understanding the intermolecular interactions, shape, size, charge density and delocalization of the molecules.

Thermochemistry

The quantum chemical methods play crucial role in statistical thermodynamic calculations. These calculations assume the non–interacting particles and, hence, apply to ideal gas. Geometry optimization and frequency calculations of the molecules generate all the data needed to compute the partition function of a molecule which is used to determine the thermodynamic variables of the system. In order to attain reliable thermodynamic properties within the error limit arises due to non ideal gas, one need to do accurate electronic structure calculations. The translational, electronic, vibrational and rotational motions of the molecules contribute to their thermodynamic properties. In this section, the overview of calculation of thermodynamic quantities like thermal energy, entropy, enthalpy and heat capacities from the partition function are presented [104]. The entropy (S) in terms of partition function (Z) is expressed as [105]:

$$S = Nk_B + Nk_B \ln\left(\frac{Z(V,T)}{N}\right) + Nk_BT\left(\frac{\partial \ln Z}{\partial T}\right)_V \qquad (2.85)$$

here, the molar values are given. Therefore, dividing the Eq. 2.85 by $n = \frac{N}{N_A}$ where N_A is Avogadro number, and substituting, $N_A k_B = R$, the entropy is

$$S = R\ln(Z(V,T)e) + RT\left(\frac{\partial \ln Z}{\partial T}\right)_V \tag{2.86}$$

The thermal energy can be obtained from partition function using the relation:

$$E = Nk_BT^2\left(\frac{\partial \ln Z}{\partial T}\right)_V \tag{2.87}$$

This thermal energy is used to obtain the heat capacity:

$$C_V = \left(\frac{\partial E}{\partial T}\right)_{N,V} \tag{2.88}$$

These equations are used to compute the thermodynamic quantities with the help of Gaussian program.

The entropy, thermal energy and heat capacity due to contribution of translational, electronic, rotational and vibrational motions can be obtained by using above equations and the partition function due to these motions. The partition functions due to translational, electronic, rotational and vibrational motions are given as follows.

The partition function due to translation motion is defined as:

$$Z_t = \left(\frac{2\pi m k_B T}{h^2}\right)^{\frac{3}{2}} V \tag{2.89}$$

For an ideal gas, $PV = nRT = \left(\frac{n}{N_A}\right) N_A k_B T$ and, $V = \frac{k_B T}{P}$. Therefore,

$$Z_t = \left(\frac{2\pi m k_B T}{h^2}\right)^{\frac{3}{2}} \frac{k_B T}{P} \tag{2.90}$$

The partition function due to contribution of electronic motion is expressed as:

$$Z_e = \omega_0 e^{-\frac{\varepsilon_0}{k_B T}} + \omega_1 e^{-\frac{\varepsilon_1}{k_B T}} + \omega_2 e^{-\frac{\varepsilon_2}{k_B T}} + \cdots \tag{2.91}$$

where ω is the degeneracy of the energy level, ε_n. It is assumed that, the first electronic excitation energy is much greater than the $k_B T$. The first and higher excited

states are supposed to be inaccessible at any temperature. Further, the ground state energy is set to zero. These approximations give the electronic partition function; $Z_e = \omega_0$.

The partition function due to rotational motion is defined differently for linear and non–linear polyatomic molecules. For the general case, the rotational partition function for non–linear polyatomic molecules is defined as:

$$Z_r = \frac{\pi^{\frac{1}{2}}}{\sigma_r}\left(\frac{T^{\frac{3}{2}}}{(\Theta_{r,x}\Theta_{r,y}\Theta_{r,z})^{\frac{1}{2}}}\right) \tag{2.92}$$

where $\Theta_r = \frac{h^2}{8\pi^2 I k_B}$, I is the moment of inertia.

The product of partition function due to vibrational motion of each vibrational mode, M defines the total partition function due to vibrational motions. Each of the $3N-6$ vibrational modes for non–linear polyatomic molecules has a characteristic vibrational temperature, $\theta_{v,M} = {h\nu_M}/{k_B}$. One can choose the zero reference point to be bottom of the well, and, then, the vibrational partition function for overall vibrational modes can be defined as:

$$Z_v = \prod_M \frac{e^{-\frac{\theta_{v,M}}{2T}}}{1 - e^{-\frac{\theta_{v,M}}{2T}}} \tag{2.93}$$

With the partition functions due to contribution of translational, electronic, rotational vibrational motions, one can easily obtain the thermodynamic quantities entropy, thermal energy and heat capacity from Eq. 2.85–2.88. The expressions of these thermodynamic quantities evaluated by using translational, electronic, rotational and vibrational partition functions are given as follows.

Translational, electronic, rotational and vibrational entropy are as follow:

$$S_t = R\left(\ln Z_t + {5}/{2}\right),\quad S_e = R\ln Z_e,\quad S_r = R\left(\ln Z_r + {3}/{2}\right),$$

$$S_v = R\sum_M \left(\frac{{\theta_{v,M}}/{T}}{e^{{\theta_{v,M}}/{T}} - 1} - \ln\left(1 - e^{-{\theta_{v,M}}/{T}}\right)\right) \tag{2.94}$$

Translational, electronic, rotational and vibrational thermal energy are given by:

$$E_t = E_r = \frac{3RT}{2},\ E_e = 0,\ E_v = R\sum_M \Theta_{v,M}\left(\frac{1}{2} + \frac{1}{e^{\Theta_{v,M}/T} - 1}\right) \quad (2.95)$$

Translational, electronic, rotational and vibrational heat capacities at constant volume are given by following expression:

$$C_t = C_r = \frac{3R}{2},\ C_e = 0,\ C_v = R\sum_M e^{\Theta_{v,M}/T}\left(\frac{\Theta_{v,M}/T}{e^{-\Theta_{v,M}/T} - 1}\right)^2 \quad (2.96)$$

Non–linear optical properties

The quantum chemical computations play crucial role in designing the system of non–linear optical response. This is a topic of active research because of their potential applications in a number of advanced optoelectronic devices. The molecules exhibiting large hyperpolarizibilty values have a strong NLO potential. These values can be calculated using quantum chemical methods. The organic molecules with aromatic systems in conjugated positions, leading to charge transfer in systems, show high potential nonlinearities. The high NLO response is caused by high degree of electron delocalization in π conjugated organic molecules. The larger NLO potential arises due to π electron cloud movement from donor to acceptor groups [106]. The conjugated π electron system with appropriate electron donor and acceptor groups can enhance the asymmetric electronic distribution thus leading to an increased optical non–linearity. The dipole moment and polarizability tensor are important molecular properties for providing information about a distribution of charge within a molecule. The isotropic polarizability is a measure of electronic distribution in a molecule, caused by an external electric field. The magnitudes of molecular polarizability and hyperpolarizability coefficients are found to increase linearly with an increase in conjugation length between the donor and the acceptor [107]. The energy of a system shows non–linearity in the presence of weak homogeneous external electric field. Therefore, the energy (E) in the external eclectic field (F) can be expanded in terms of Taylor series:

$$E = E^0 - \mu_i F_i - \frac{1}{2!}\alpha_{ij}F_iF_j - \frac{1}{3!}\beta_{ijk}F_iF_jF_k + \cdots \quad (2.97)$$

where E^0 is the energy of unperturbed system, μ_i, α_{ij} and β_{ijk} are the components of dipole moment, polarizability and first order hyperpolarizability respectively. The molecular polarizability is the 2nd rank tensor by which the induced dipole moment of a molecule is related to the external electric field. This measures the ability of molecule to respond to an electric field [39]. First order hyperpolarizability is a third rank tensor that can be defined by a 3×3×3 matrix (3D matrix). The 27 components of this matrix can be reduced to 10 components due to the Kleinman symmetry [108]. The total static dipole moment μ, the mean polarizability α_0, the anisotropy of the polarizability $\Delta\alpha$ and the mean first hyperpolarizability β_0, using the Cartesian coordinates x, y and z are defined as (in a.u.):

$$\mu = \left(\mu_x^2 + \mu_y^2 + \mu_z^2\right)^{1/2} \tag{2.98}$$

$$\alpha_0 = \frac{\alpha_{xx} + \alpha_{yy} + \alpha_{zz}}{3} \tag{2.99}$$

$$\Delta\alpha = \frac{1}{\sqrt{2}}\left[\left(\alpha_{xx} - \alpha_{yy}\right)^2 + \left(\alpha_{yy} - \alpha_{zz}\right)^2 + \left(\alpha_{zz} - \alpha_{xx}\right)^2 + 6\alpha_{xx}^2\right]^{1/2} \tag{2.100}$$

$$\beta_0 = \left(\beta_x^2 + \beta_y^2 + \beta_z^2\right)^{1/2} \tag{2.101}$$

where

$$\beta_x = \beta_{xxx} + \beta_{xyy} + \beta_{xzz} \tag{2.102}$$

$$\beta_y = \beta_{yyy} + \beta_{xxy} + \beta_{yzz} \tag{2.103}$$

$$\beta_z = \beta_{zzz} + \beta_{xxz} + \beta_{yyz} \tag{2.104}$$

The high values of dipole moment, polarizability and hyperpolarizability of molecule reveals its high NLO potential.

Chemical reactivity descriptors

Parr and Yang have developed a powerful framework to understand chemical reactivity within the density functional theory [109–114]. Chemical reactivity descriptors of the molecule help to understand the way the molecules react with other molecular species. The energy eigenvalues of frontier molecular orbitals (HOMO and LUMO) can be considered as a simple tool to deal chemical reactivity. In this thesis, the global chemical reactivity descriptors have been obtained based on frontier molecular orbitals. The global chemical reactivity descriptors such as softness,

hardness, electrophilicity index are used to explorer reactive sites. A detailed description on these descriptors can be found elsewhere [109–114] and only the relevant expressions used for the computation of these quantities are given here. According to Koopman's theorem, the ionization potential (I) and electron affinity (A) can be expressed in terms of the frontier orbital energy eigenvalues as [115, 116]:

$$I = -\varepsilon_{HOMO} \tag{2.105}$$

$$A = -\varepsilon_{LUMO} \tag{2.106}$$

The HOMO and LUMO energy eigenvalues help to predict whether the chemical reactions are electrophilic or nucleophilic. The expression for absolute electronegativity (χ), chemical potential (μ), chemical hardness (η), chemical softness (S) and electrophilicity (ω) are given as:

$$\mu = \frac{1}{2}(I + A) = -\chi \tag{2.107}$$

$$\eta = \frac{1}{2}(I - A) \tag{2.108}$$

$$S = \frac{1}{2\eta} \tag{2.109}$$

$$\omega = \frac{\mu^2}{2\eta} \tag{2.110}$$

The χ value determines whether the molecule is Lewis acid or base. The large values of χ characterize acids and small values are found for bases. When the molecule interacts to other molecular species, electrons transfer from low χ value to high χ value (electrons flow from high chemical potential to low chemical potential) [110–114]. The global hardness can be treated as the resistance of a chemical species to charge transfer. The global softness is inversely proportional to global hardness. A molecule having higher S value (low η value) is more reactive than a molecule having smaller S value (high η value). In general, it can be said that the hard molecules, which have large HOMO–LUMO gap, imply high stability and soft molecules, have a small HOMO–LUMO gap, show low stability. Therefore, the large or small energy gap reflects respectively the low or high reactivity. The other chemical reactivity descriptor is the electrophilicity index which characterizes the electrophilic power of

the molecule. It is clear from Eq. 2.110 that the good electrophile will be described by a high electronegativity and low value of chemical hardness. Thus, DFT based chemical reactivity descriptors can be used for a quantitative prediction of relative stability and chemical reactivity of the molecules.

Natural bond orbital analysis

Natural Bond Orbital (NBO) analysis is an important technique for studying hybridization, natural charges, donor–acceptor interactions, covalancy effects and charge transfer in polyatomic molecules [117–120]. NBOs are localized centre orbitals that explain the Lewis like molecular bonding patterns of electron pairs or individual electrons in the open shell case. This is based on a method, which transforms the wavefunctions in to localized forms which correspond to the one–centre (lone pair) and two centres Lewis picture. A many electron molecular wavefunction is analysed in terms of localized electron pair bonding units. The NBOs are calculated as local block eigenfunctions of the one electron density matrix having optimal convergence properties for describing the electron density. The following sequence shows the transformations from input basis sets to various localized basis sets. The program determines natural atomic orbitals (NAOs), natural hybrid orbitals (NHOs), natural bond orbitals (NBOs) and natural localized molecular orbitals (NLMOs) [121, 122]. Each natural localized set forms a complete orthonormal set of one–electron functions for expanding the delocalized molecular orbitals. These are used to perform natural population analysis, NBO energetic analysis and localized analysis of wavefunction properties.

The NBO for a localized bond σ_{pq} between atoms p and q is formed from orthonormal hybrids (NHOs) h_p, h_q using the relation $\sigma_{pq} = c_p h_p + c_q h_q$ where c_p and c_q are polarization coefficients. Larger polarization coefficient corresponds to higher electron density (%) of NBO as well as electronegativity. The filled NBOs, σ_{pq} of the natural Lewis structure are used to describe covalancy effects in molecules. The general transformations to NBOs also form unoccupied orbitals which may be used to describe the non–covalancy effects. These are known as antibonds, σ^*_{pq}, defined as $\sigma^*_{pq} = c_p h_p - c_q h_q$ which is a non–Lewis orbital. It plays the primary role in delocalization from the ideal Lewis structure.

The NBOs calculations also perform energetic analysis of NBO interactions based on the one electron effective energy operator $\hat{F}$ i.e. Fock matrix. All the possible interactions between filled (donor) NBOs and empty (acceptor) NBOs with their interaction energy are estimated by second order perturbation theory. The two electron stabilization energy $E^{(2)}$ associated with delocalization $i \rightarrow j$ for each donor NBO (i) and acceptor NBO (j) is computed by second order perturbation theory using relation,

$$E^{(2)} = \Delta E_{ij} = \frac{q_i F(i,j)^2}{(\epsilon_j - \epsilon_i)} \qquad (2.111)$$

where, q_i is the donor orbital occupancy; $\epsilon_i = < i|\hat{F}|i >$ and $\epsilon_j = < j|\hat{F}|j >$ are diagonal elements and $F(i,j) = < i|\hat{F}|j >$ are the off diagonal elements of NBO Fock matrix. This equation describes the donor–acceptor interactions in the NBO analysis. These interactions lead to loss of occupancy from localized NBOs in to the empty non–Lewis structure. These are referred as delocalization correction to zero order natural Lewis structure. The larger the $E^{(2)}$ value, the more intensive is the interaction between electron donors and electron acceptors.

There are many population analysis methods to obtain atomic charges using quantum chemical calculations. These methods include mainly Mullikan population analysis, Lowdin population analysis, NBO analysis, atom in molecule (AIM) potential. The Mullikan population analysis is based on the LCAO–MO theory [103, 123]. The NBO analysis calculates atomic charges, by summing occupancy of natural AOs [117–120]. NBO analysis is a very popular population analysis method. In this analysis, natural AOs, which are the effective orbitals of an atom in molecular environment, are determined. These are also the maximum occupancy orbitals. NBOs are localised few–center MOs that reveal Lewis like bonding structures. NBO analysis is computationally more expensive than any other population analysis method and predicts larger charges than others predict.

References

[1]. P. R. Griffiths, J. A. De Haseth, Fourier Transform Infrared Spectrometry, John Wiley & Sons, New York, 1986.

[2]. R. J. Bell, Introductory Fourier Transform Spectroscopy, Academic press, New York, 1972.

[3]. B. C. Smith, Fundamentals of Fourier Transform Infrared Spectroscopy, CRC Press, New York, 1995.

[4]. J. Kauppinen, J. Partanen, Fourier Transforms in Spectroscopy, 1st edition, Wiley–VCH, New York, 2001.

[5]. B. Schrader, Infrared & Raman Spectroscopy, VCH publishers, Inc., New York, 1995.

[6]. Tensor 37 (Bruker) FTIR manual.

[7]. R. S. Bretzlaff et, T. B. Bahder, Rev. Phys. Appl. (Paris) 21 (1986) 833–844.

[8]. B. H. Stuart, Infrared Spectroscopy: Fundamentals and Applications, John Wiley & Sons, England, 2004.

[9]. S. Wartewig, IR and Raman Spectroscopy: Fundamental Processing, Wiley & Sons, Viernheim, 2003.

[10]. J. R. Ferraro, L. J. Basile, Fourier Transform IR Spectroscopy Application to Chemical Systems, Vol. 1, Academic Press, INC, New York, 1978.

[11]. J. R. Ferraro, L. J. Basile, Fourier Transform IR Spectroscopy Application to Chemical Systems, Vol. 2, Academic Press, INC, New York, 1979.

[12]. J. R. Ferraro, L. J. Basile, Fourier Transform IR Spectroscopy Application to Chemical Systems, Vol. 3, Academic Press, INC, New York, 1982.

[13]. J. R. Ferraro, L. J. Basile, Fourier Transform IR Spectroscopy Application to Chemical Systems, Vol. 4, Academic Press, INC, New York, 1985.

[14]. D. Oepts, Fourier Transform Spectroscopy in Methods of Experimental Physics, Vol. 13, Part B, Edited by D. Williams, Academic press, New York, 1976.

[15]. H. W. Schnopper, R. I. Thompson, Fourier Spectrometers, in Methods of Experimental Physics, Vol. 12, Part A, Edited by N. Carleton, Academic press, New York, 1974.

[16]. H. Sakai, High Resolution Power Fourier Spectroscopy in Spectrometric Techniques, Vol. 1, Edited by G. A. Vanarse, Academic press, New York, 1977.

[17]. P. B. Fellgett, J. Opt. Soc. Am. 39 (1949) 970–976.

[18]. P. Jacquinot, J. Opt. Soc. Am. 44 (1954) 761–765.

[19]. J. Connes, P. Connes, J. Opt. Soc. Am. 56 (1966) 896–910.

[20]. J. M. Hollas, High Resolution Spectroscopy, 2nd edition, John Wiley and Sons, UK, 1998.

[21]. P. Vandenabeele, Practical Raman Spectroscopy: An introduction, Wiley UK, 2013.

[22]. D. A. Long, The Raman Effect, John Wiley & Sons Ltd., Chichester, 2002.

[23]. E. Smith, G. Dent, Modern Raman Spectroscopy: A practical approach, John Wiley & Sons Ltd., Chichester, 2005.

[24]. G. Herzberg, Molecular Spectra & Molecular Structure, Vol. 2, Von Nostrand Reinhold Company, New York, 1945.

[25]. C. N. Benwell, Fundamentals of Molecular Spectroscopy, 4th edition, Tata McGraw–Hill, UK, 1995.

[26]. G. Aruldhas, Molecular Structure and Spectroscopy, 2nd edition, PHI learning private limited, New Delhi, 2008.
[27]. P. Hendra, C. Jones, G. Warnes, Fourier Transform Raman Spectroscopy: Instrumentation and Chemical Applications, Ellis Horwood Ltd, 1991.
[28]. D. B. Chase, J. F. Rabolt, Fourier Transform Raman Spectroscopy: From Concept to Experiment, Academic Press, 1994.
[29]. J. J. Laserna, Modern Techniques in Raman Spectroscopy, Wiley, 1996.
[30]. C. Moller, M. S. Plesset, Phys. Rev. 46 (1934) 618–622.
[31]. J. A. Pople, M. H. Gordon, K. Raghavachari, J. Chem. Phys. 87 (1987) 5968–5975.
[32]. J. B. Foresman, A. Frisch, Exploring Chemistry with Electronic Structure Methods, 2nd edition, Gaussian, Inc, Pittsburgh, 1996.
[33]. http://www.gaussian.com
[34]. http://www.nwchem-sw.org/index.php/Main_Page
[35]. http://www.molpro.net/
[36]. http://www.msg.ameslab.gov/gamess/
[37]. P. Hohenberg, W. Kohn, Phys. Rev. B 136 (1964) 864–871.
[38]. W. Kohn, L. J. Sham, Phys. Rev. A 140 (1965) 1133–1138.
[39]. P. Atkins, R. Friedman, Molecular Quantum Mechanics, 4th edition, Oxford University Press Inc., New York, 2005.
[40]. I. N. Levine, Quantum Chemistry, 6th edition, PHI Learning Private Ltd., New Delhi, 2010.
[41]. C. J. Cramer, Essentials of Computational Chemistry: Theories and Models, 2nd edition, John Wiley & Sons, Ltd., England, 2004.
[42]. H. B. Schlegel, J. Comp. Chem. 3 (1982) 214–218.
[43]. H. B. Schlegel, Theor. Chem. Acc. 66 (1984) 333–340.
[44]. http://www.ccl.net/cca/documents/basis-sets/basis.html.
[45]. R. Krishnan, J. S. Binkley, R. Seeger, J. A. Pople, J. Chem Phys. 72 (1980) 650–654.
[46]. T. H. Dunning, Jr., J. Chem. Phys. 90 (1989) 1007–1023.
[47]. D. E. Woon, T. H. Dunning Jr., J. Chem. Phys. 98 (1993) 1358–1371.
[48]. C. K. Kim, S. H. Yoon, J. Won, C. Kyung Kim, Bull. Korean Chem. Soc. 27 (2006) 1219–1221.
[49]. T. H. Dunning Jr., P. J. Hay, Modern Theoretical Chemistry, Vol. 3, Plenum, New York, 1977.
[50]. P. J. Hay, W. R. Wadt, J. Chem. Phys. 82 (1985) 270–283.
[51]. C. E. Check, T. O. Faust, J. M. Bailey, B. J. Wright, T. M. Gilbert, L. S. Sunderlin, J. Phys. Chem. A 105 (2001) 8111–8116.
[52]. W. J. Hehre, A Guide to Molecular Mechanics and Quantum Chemical Calculations, Wavefunction Inc, Irvine, 2003.
[53]. W. Kohn, Rev. Mod. Phys. 71 (1999) 1253–1266.
[54]. B. J. Lynch, Y. Zhao, D. G. Truhlar, J. Phys. Chem. A 107 (2003) 1384–1388.
[55]. S. Grimme, M. Steinmetz, M. Korth, J. Org. Chem. 72 (2007) 2118–2126.
[56]. A. D. Boese, J. M. L. Martin, N. C. Handy, J. Chem. Phys. 119 (2003) 3005–3014.
[57]. J. P. Perdew, J. A. Chevary, S. H. Vosko, K. A. Jackson, M. R. Pederson, D. J. Singh, C. Fiolhais, Phys. Rev. B 46 (1992) 6671–6687.
[58]. J. P. Perdew, W. Yue, Phys. Rev. B 33 (1986) 8800–8802.
[59]. A. D. Becke, Phys. Rev. A 38 (1988) 3098–3100.
[60]. C. Lee, W. Yang, R. G. Parr, Phys. Rev. B 37 (1988) 785–789.

[61]. A. D. Becke, J. Chem. Phys. 98 (1993) 5648–5652.
[62]. J. P. Perdew, K. Burke, M. Ernzerhof, Phys. Rev. Lett. 77 (1996) 3865–3868.
[63]. E. G. Lewars, Computational Chemistry: Introduction to the Theory and Applications of Molecular and Quantum Mechanics, 2nd edition, Springer Science, New York, 2011.
[64]. M. J. Frisch et al., Gaussian 09, Revision D.01, Gaussian, Inc., Wallingford CT, 2009.
[65]. M. W. Schmidt, K. K. Baldridge, J. A. Boatz, S. T. Elbert, M. S. Gordon, J. H. Jensen, S. Koseki, N. Matsunaga, K. A. Nguyen, S. J. Su, T. L. Windus, M. Dupuis, J. A. Montgomery, J. Comput. Chem. 14 (1993) 1347–1363.
[66]. http://www.gaussian.com/g_tech/g_ur/k_opt.htm
[67]. G. Forgarasi, P. Pulay, Vibrational Spectra and Structure, Vol. 14, Edited by J. R. Durig, Elsevier, Amsterdam, 1985.
[68]. P. Pulay, Applications of Molecular Electronic Structure Theory, Vol. 4, Edited by H. F. Schaefer III, Plenum, New York, 1997.
[69]. P. Pulay, G. Forgarasi, F. Pong, J. E. Boggs, J. Am. Chem. Soc. 101 (1979) 2550–2560.
[70]. P. Pulay, G. Fogarasi, G. Pongor, J. E. Boggs, A. Vargha, J. Am. Chem. Soc. 105 (1983) 7037–7047.
[71]. G. Rauhut, P. Pulay, J. Phys. Chem. 99 (1995) 3093–3100.
[72]. M. A. Palafox, J. Talaya, A. G. Martinez, G. Tardajos, H. Kumar, J. K. Vats, V. K. Rastogi, Spectrosc. Lett. 43 (2010) 51–59.
[73]. J. M. Bowman, J. Chem. Phys. 68 (1978) 608–610.
[74]. G. D. Carney, L. L. Sprandel, C. W. Kern, Adv. Chem. Phys. 37 (1978) 305–379.
[75]. M. Cohen, S. Greita, R. D. McEarchran, Chem. Phys. Lett. 60 (1979) 445–450.
[76]. R. B. Gerber, M. A. Ratner, Chem. Phys. Lett. 68 (1979) 195–198.
[77]. L. Pele, B. Brauer, R. B. Gerber, Theor. Chem. Acc. 117 (2007) 69–72.
[78]. L. Pele, R. B. Gerber, J. Chem. Phys. 128 (2008) 165105–165115.
[79]. V. Barone, J. Bloino, C. A. Guido, F. Lipparini, Chem. Phys. Lett. 496 (2010) 157–161.
[80]. V. Barone, Chem. Phys. Lett. 383 (2004) 528–532.
[81]. V. Barone, J. Chem. Phys. 122 (2005) 014108–014118.
[82]. K. Chaitanya, C. Santhamma, K. V. Prasad, V. Veeraiah, J. At. Mol. Sci. 3 (2012) 1–22.
[83]. E. B. Wilson, Jr., J. C. Decius, P. C. Cross, Molecular Vibrations, McGraw–Hill, New York, 1955.
[84]. T. K. Roy, R. B. Gerber, Phys. Chem. Chem. Phys. 15 (2013) 9468–9492.
[85]. A. Miani, E. Cane, P. Palmieri, A. Trombetti, N. C. Handy, J. Chem. Phys. 112 (2000) 248–259.
[86]. G. I. Csonka, A. Ruzsinszky, J. P. Perdew, J. Phys. Chem. A 109 (2005) 6779–6789.
[87]. J. M. Bowman, Acc. Chem. Res. 19 (1986) 202–208.
[88]. R. Gerber, M. A. Ratner, Adv. Chem. Phys. 70 (1988) 97–132.
[89]. T. Rasheed, S. Ahmad, Vib. Spectrosc. 56 (2011) 51–59.
[90]. T. Rasheed, S. Ahmad, Spectrochim. Acta A 77 (2010) 446–456.
[91]. J. O. Jung, R. B. Gerber, J. Chem. Phys. 105 (1996) 10332–10348.
[92]. K. Yagi, K. Hirao, T. Taketsugu, M. W. Schmidt, M. S. Gordon, J. Chem. Phys. 121 (2004) 1383–1389.

[93]. K. Yagi, T. Taketsugu, K. Hirao, M. S. Gordon, J. Chem. Phys. 113 (2000) 1005–1017.
[94]. P. Seidler, T. Kaga, K. Yagi, O. Christiansen, K. Hiraro, Chem. Phys. Lett. 483 (2009) 138–142.
[95]. International Union of Pure and Applied Chemistry (IUPAC), Glossary of terms used in Photochemistry, 3rd edition, 2004.
[96]. B. A. Hess, Jr., L. J. Schaad, Chem. Rev. 86 (1986) 709–730.
[97]. G. Placzek, Handbuch der Radiologie, Akademische Verlagsgesellschaft, Leipzig, Vol. 2, Edited by E. Marx, California, 1934.
[98]. P. L. Polavarapu, J. Phys. Chem. 94 (1990) 8106–8112.
[99]. D. Michalska, R. Wysokinski, Chem. Phys. Lett. 403 (2005) 211–217.
[100]. L. Goodman, A. G. Ozkabak, S. N. Thakur, J. Phys. Chem. 95 (1991) 9044–9058.
[101]. A. M. Sapse, Molecular Orbital Calculations for Biological Systems, Oxford University Press, USA, 1998.
[102]. J. S. Murray, K. Sen, Molecular Electrostatic Potential: Concepts and Applications, Elsevier, Netherlands, 1996.
[103]. I. G. Csizmadia, Theory and Practice of MO Calculations on Organic Molecules, Elsevier, Amsterdam, 1976.
[104]. http://www.gaussian.com/g_whitepap/thermo.htm
[105]. D. A. McQuarrie, Statistical Thermodynamics, Harper and Row, New York, 1973.
[106]. http://www.sigmaaldrich.com/materials-science/organic-electronics/photonic-optical-materials/tutorial/nlo-materials.html
[107]. P. C. Jha, A. Krishnan, P. K. Das, S. Ramashesha, J. Chem. Phys. 117 (2002) 2873–2881.
[108]. D. A. Kleinman, Phys. Rev. 126 (1962) 1977–1979.
[109]. R. G. Pearson, J. Am. Chem. Soc. 85 (1963) 3533–3539.
[110]. R. G. Parr, R. G. Pearson, J. Am. Chem. Soc. 105 (1983) 7512–7516.
[111]. R. G. Parr, R. A. Donnelly, M. Levy, W. E. Palke, J. Chem. Phys. 68 (1978) 3801–3807.
[112]. R. G. Pearson, J. Am. Chem. Soc. 107 (1985) 6801–6806.
[113]. R. G. Parr, W. Yang, Density Functional Theory of Atoms and Molecules, Oxford University Press, Oxford, 1989.
[114]. R. G. Parr, W. Yang, J. Am. Chem. Soc. 106 (1984) 4049–4050.
[115]. T. Koopmans, Physica 1 (1934) 104–110.
[116]. R. G. Pearson, Proc. Natl. Acad. Sci. 83 (1986) 8440–8441.
[117]. J. P. Foster, F. Weinhold, J. Am. Chem. Soc. 102 (1980) 7211–7218.
[118]. A. E. Reed, F. Weinhold, J. Chem. Phys. 78 (1983) 4066–4073.
[119]. A. E. Reed, R. B. Weinstock, F. Weinhold, J. Chem. Phys. 83 (1985) 735–746.
[120]. A. E. Reed, F. Weinhold, J. Chem. Phys. 83 (1985) 1736–1740.
[121]. A. E. Reed, L. A. Curtiss, F. Weinhold, Chem. Rev. 88 (1988) 899–926.
[122]. F. Weinhold, C. R. Landis, Chemistry Education: Research and Practice in Europe 2 (2001) 91–104.
[123]. R. S. Mulliken, J. Chem. Phys. 23 (1955) 1833–1840.

Chapter 3

Structural and vibrational studies of L–aspartic acid based on monomer and dimer calculations

3.1 *Introduction*

Amino acids are the building block of the peptides and proteins, which have numerous biological importances. Aspartic acid is one of the 20 natural amino acids. In nature, it is found in L –, D – and LD – form [1]. This molecule has a zwitterionic structure in solution or solid phase but it has non–zwitterionic form in gaseous phase. It has a special importance among the amino acids due to its property to racemize from L– to D–form, which can be used to determine age of living and nonliving systems [2, 3]. Its polymer form is an eco–friendly and biodegradable product that can be widely used in pharmacy, cosmetics and agriculture [4]. It is found that, the first aspartic acid of a calcium–binding epidermal growth factor (cbEGF) domain in FBN–1 gene is important for the function of fibrillin–1 [5]. Due to such enormous importance and being a unit of protein, the L–aspartic acid has been chosen for the studies of its molecular structure, vibrational spectra and various molecular properties.

Molecular geometries of zwitterionic, neutral and anions forms of aspartic acid were calculated at the HF/6–31 + G* level of theory [6]. The different conformers of aspartic acid were identified in the supersonic expansion through the analysis of the rotational spectrum by Fourier transform microwave spectroscopy [7] and these were also computed in liquid and gas phase using DFT method [8, 9]. Navarrete et al. [10, 11] have proposed general assignments for fundamental vibrations of L–aspartic acid and its isotopic derivatives by using MNDO scaled semiempirical force field calculations and vibrational (FTIR and Raman) spectra. The SERS and normal Raman spectra of aspartic acid as well as FTIR and Raman spectra of its dipeptide were studied [12]. Mohamed et al. [13] have reported theoretical and experimental vibrational spectra as well as their assignments for some amino acids. The electron

density and related properties of D, L–aspartic acid at 20K have been computed by using X–ray diffraction technique [14]. Derissen et al. [15] determined the crystal structure of L–aspartic acid using X–ray diffraction technique. Many workers [16–19] have reported various thermodynamic properties of L–aspartic acid in different media. For polyatomic molecules, geometry optimizations and vibrational studies are the most important jobs in computational chemistry. The harmonic frequencies usually overestimate from the observed frequencies due to various approximations in quantum chemical methods [20] as well as phase chosen for the calculations. Therefore, the scaling procedures [21–25] are used to obtain better agreement with experimental data. High frequencies modes due to C–H, N–H and O–H stretching vibrations usually show large deviations from experiment due to large anharmonicity associated to these vibrations. Thus, it is crucial to consider the anharmonic nature while computing potential energy surface (PES). The vibrational calculations at the anharmonic level are of high computational cost but provide results in close agreement to the experimental data. This can be used for assignment of modes without any manual scaling. Many workers have performed vibrational analysis of small and large size molecules in the harmonic approximation and they have used various scaling procedures for compensating discrepancies but in order to get reliable results without any scaling, a great effort has been also made to carry out anharmonic computations [26–41]. Recently, anharmonic vibrational frequencies of chlorotrifluoroethene, monofluoroaniline isomers, benzene, uracil, butane, diaminomaleonitrile, dichloromethylsilyl cyclopropene, sulfanilamide conformers, L–aspartic acid, iodonitrobenzenes, 3–methyladenine and allantoin molecules have been reported [42–55].

In this chapter, the molecular structure and vibrational spectra of L–aspartic acid in the ground state have been obtained using the *ab initio* HF, MP2 and DFT (B3LYP) methods with 6–311G(d,p), 6–311++G(d,p) and cc–pVTZ basis sets. The Barone's PT2 as well as VSCF and CC–VSCF methods were employed for anharmonic calculations on present molecule in monomeric form. The VSCF and CC–VSCF approaches based on quartic force field (QFF) potential function have been utilized to compute anharmonic vibrational spectra at B3LYP/6–311G(d,p) level of theory, which are quite efficient for floppy molecules but demands high computational cost. The vibrational modes, in general, couple to other modes due to anharmonicity. In order to understand the coupling behaviour between pairs of modes

for isolated molecule, the mode–mode coupling strength (CS) based on two mode coupling representation of the quartic force field (2MR–QFF) for the ground state are computed [56] at B3LYP/6–311G(d,p) level of theory and are discussed in the relevant sections. The experiments are not done on molecule in isolated monomeric form while theoretical calculations are performed on isolated molecule in present work. Therefore, the discrepancies between theory and experiment will always be there. In nature, the molecules exist in form of intermolecular complexes in solid and liquid phases. In gaseous or matrix form, there may be possibility to form hydrogen–bonded dimer, trimer and so on. The intermolecular hydrogen bonds stabilize such intermolecular complexes and it affects the molecular structure, vibrational spectra and other molecular properties of isolated molecule. Therefore, in order to make good correlation between theoretical results and solid phase experimental data, the simulations have been performed also on dimeric structures of L–aspartic acid using harmonic force field calculations within DFT/B3LYP approach with 6–311G(d,p) and 6–311++G(d,p) basis sets. The DFT calculations with these basis sets for dimer in the anharmonic approximation are of very high computational cost, therefore, anharmonicity was ignored. Various molecular properties like atomic charges, thermodynamic parameters, NLO properties, chemical reactivity descriptors, MEP mapping, HOMO–LUMO and NBO analysis have been also presented. The NBO analysis was carried out at B3LYP/6–311G(d,p) level of theory for studying charge delocalization within the molecule and hydrogen bonded intramolecular and intermolecular interactions. Literature survey reveals that only harmonic force filed calculations have been reported so far for the L–aspartic acid. Therefore, anharmonic force field calculations have been taken into account for isolated molecule in the present investigations. The dimeric simulations on L–aspartic acid have not been reported so far. To the best of our knowledge, anharmonic frequencies, dimeric parameters, MEP mapping, chemical reactivity descriptors, HOMO–LUMO and NBO analysis of L–aspartic acid have been presented first time. The present studies encourage to use anharmonic method within the DFT framework for medium size polyatomic molecules. DFT method is more popular due to its great accuracy in reproducing the experimental results and low computational cost.

3.2 Experimental details

L–aspartic acid was obtained from Sigma–Aldrich chemical company with stated purity greater than 98% in the solid form and it was used for spectral measurements without any further purification. FTIR spectra of this compound were recorded at room temperature on Tensor 37 spectrometer (Bruker) within the spectral region of 370–5000 cm^{-1} with a spectral resolution of 1 cm^{-1}. To increase the signal–to–noise ratio, a minimum of 32 scans were accumulated. The spectrum was recorded by using KBr pellet technique.

3.3 Computational details

The quantum chemical calculations were carried out using Gaussian 09 [57] and GAMESS–US packages [58]. The optimized molecular structures in the ground state were computed by performing *ab initio* HF, MP2 and DFT (B3LYP) calculations with 6–311G(d,p), 6–311++G(d,p) and cc–pVTZ basis sets using Berny optimization algorithm (section 2.2.5) under the tight convergence criteria. Subsequently, harmonic and anharmonic vibrational frequencies along with infrared intensities and Raman activities were calculated. For the present case, the anharmonic force field calculations with large basis set (cc–pVTZ) in MP2 framework are of very high computational cost and less accurate than DFT method at same basis set. Therefore, the 6–311G(d,p) and 6–311++G(d,p) basis sets have been adopted for the MP2 anharmonic computations. Gaussian program does not calculate Raman intensities (section 2.2.7). Therefore, it was computed with the help of RAINT program [59]. All the real values of frequency confirm that the optimized geometry corresponds to a right energy minimum. In the B3LYP level of theory, Becke's three parameter (B3) [60] was used for exchange interactions and Li–Yang–Parr (LYP) [61] functional was adopted to consider electron correlations. Anharmonic corrections in vibrational frequencies were computed using Barone's PT2 method with Gaussian 09 package [57] as well as VSCF and CC–VSCF methods (section 2.2.6) implemented into GAMESS–US package [58]. The Barone's PT2 method [26] was used within the HF, MP2 and DFT framework while VSCF and CC–VSCF approaches [37–41] were utilized only at B3LYP/6–311G(d,p) level of theory. The vibrational modes are in general coupled with other modes due to anharmonicity and, therefore, vibrational energy flows between different modes [62]. The anharmonic mode–mode coupling

affects the vibrational frequencies and the modes of large anharmonicity show larger mode–mode coupling strengths. In order to know the strength of the coupling between pair of modes, the magnitudes of mode–mode coupling strength (section 2.2.6) for the ground state have been estimated at B3LYP/6–311G(d,p) level of theory. The 2MR–QFF potential energy function was used for calculating mode–mode coupling strengths [56, 63]. The contribution of intrinsic and mode–mode coupling anharmonicities were also presented for each mode using VSCF approach within DFT method [62, 64]. The crystal structure of L–aspartic acid shows the intermolecular hydrogen bonds, H–N–H···O and O–H···O [15]. The optimized structural parameters and vibrational spectra of the hydrogen bonded dimers of L–aspartic acid (D1 and D2) have been also calculated at B3LYP/6–311G(d,p) and B3LYP/6–311++G(d,p) levels of theory in the harmonic approximation. The theoretical vibrational frequencies are, in general, overestimated from the corresponding experimental data because of many reasons like absence of anharmonicity, basis set deficiencies, other approximations etc. Therefore, it is customary to scale down the calculated harmonic vibrational frequencies to make good correlation between theory and experiment. In the case of calculated harmonic frequencies of present monomer and dimers, a uniform scaling factor (0.967) was used [65, 66]. Vibrational assignments were made with a high degree of accuracy by using potential energy distribution (PED) values and visual inspection by GaussView 5. The PED calculations were done using VEDA4 program [67]. The PED values give the percentage of contributions of vibrational coordinates in a mode (section 2.2.5). The NBO analysis was performed for monomeric and dimeric structures of L–aspartic acid and natural atomic charges were calculated at B3LYP/6–311G(d,p) level of theory by using the NBO 3.1 program [68] implemented in Gaussian 09. For the plots of simulated IR and Raman spectra, pure Lorentzian band shapes were used with full width at half maxima (FWHM) of 5 cm^{-1} [69]. For the comparison between experimental and theoretical results, root mean square (RMS) and mean absolute deviation (MAD) values have been computed using the following expression:

$$RMS = \sqrt{\frac{1}{N-1}\sum_{i}^{N}(Y_i^{Calc.} - X_i^{Exp.})^2} \qquad (3.1)$$

$$MAD = \frac{1}{N}\sum_{i}^{N}\left|Y_i^{Calc.} - X_i^{Exp.}\right| \quad (3.2)$$

The chemical behaviour and the reactivity of the isolated L–aspartic acid molecule were investigated using HOMO (ionization potential) and LUMO (electron affinity) energy eigenvalues calculated at DFT level. These values have been used to compute chemical reactivity descriptors such as chemical potential (μ), electronegativity (χ), chemical hardness (η), chemical softness (S) and electrophilicity index (ω). These so called global quantities describe the reactivity of the molecule [70–77]. The theory regarding global indices is discussed in section 2.2.7.

3.4 Results and discussion

3.4.1 Molecular geometry

Isolated form

The optimized molecular structure of L–aspartic acid monomer along with numbering of atoms is shown in Fig. 3.1. The minimum self–consistent field (SCF) energy values of the optimized molecular structures at different levels of theory are presented in Table 3.1. The most optimized geometrical parameters (bond lengths and bond angles) are tabulated in Table 3.2 and 3.3. In this work, the calculated optimized geometrical parameters were compared with the X–ray diffraction data [10, 15] and are found in a reasonable agreement. Hydrogen bonding (intramolecular) between N9 and H16 is also predicted (section 3.4.3). It is found that the calculated bond lengths are close to the experimental data but most of the bond angles are slightly deviated from the experiment. These deviations may arise due to the fact that the theoretical calculations are done for single isolated molecule in gaseous phase and the experimental values are taken from the measurement in solid phase. The bond angle, C6–N9–H14, shows the large deviation of ca. 9°. This is because the experimental geometry belongs to zwitterionic form and has NH_3 group while in gas phase L–aspartic molecule has non–zwitterionic form (H atom of NH_3 group is transferred to O atom to form O–H group). The RMS error and MAD values between theoretical and experimental structural parameters were also calculated and are given in Table 3.2 and 3.3.

Dimer form

In fact, the molecules in solid phase exist with intermolecular hydrogen bonding interactions. Among other properties, the molecular structure and vibrational spectra of molecules strongly depend on intermolecular interactions. In the present work, the discrepancies between theoretical and measured values of structural parameters have been noticed. These discrepancies seem to be arisen due to interactions in the solid. In order to obtain good agreement with solid phase experimental data, it is necessary to do simulation on intermolecular complexes of associated molecule. The simulation of intermolecular hydrogen bonded dimer may improve these discrepancies. The molecular structure of the L–aspartic acid in crystal shows the intermolecular interactions by hydrogen bonds, O···H–N–H and O···H–O [14, 15]. Therefore, the simulations have been carried out on two possible intermolecular complexes of L–aspartic acid in gaseous phase stabilized by hydrogen bonding. In this work, optimized structures of L–aspartic acid dimers, D1 and D2, were obtained in the ground state at B3LYP/6–311G(d,p) and B3LYP/6–311++G(d,p) levels of theory. The hydrogen–bonded dimers possess a form that has a centre of symmetry (C_2 point group). The optimized geometries of the dimers with intermolecular hydrogen bond descriptions (O···H–N–H and O···H–O) are given in Fig. 3.2. The lengths of intermolecular hydrogen bonds are found same in each dimers. The calculated structural parameters for the hydrogen–bonded dimers are compared with the monomer as well as solid phase data and are presented in Table 3.2 and 3.3. These tables also show the RMS and MAD values for the structural parameters of the monomer and dimers at different theories. The comparative graphs between experimental (XRD) and theoretical bond lengths and bond angles at different levels of theory are shown in Fig. 3.3 and 3.4. By comparing the monomer and dimer structures in the gas phase, it has been noticed that the intermolecular hydrogen bonds affect the molecular structure of the monomer. According to RMS and MAD values, the bond lengths for L–aspartic molecule in dimers are in good correlation with solid phase experimental data. The minimum SCF energies for the monomer, dimer D1 and dimer D2 are found, respectively, −512.48641101, −1024.99846547 and −1024.98528322 a. u. at B3LYP/6–311++G(d,p) level of theory. The formation of intermolecular of non–covalent bonding between oxygen and hydrogen atoms makes the present dimeric structures stable. The dimer D1 is more stable. The calculated

bond lengths of dimers are found close to monomer but bond angles slightly differ from monomer. In dimer D1, the calculated bond angles, H11–C7–H12 and O3–C8–C7, at B3LYP/6–311++G(d,p) level, are shortened by ca. 1.6 ° and 3.8° respectively while angles C8–O4–H10, C6–C7–C8, O3–C8–O4 and O4–C8–C7 are increased by ca. 3.2 °, 1.7 °, 1.2 ° and 2.6 °, respectively, upon dimerization. The predicted values of these bond angles show excellent agreement with solid phase XRD data [10, 15]. In dimer D2, no noticeable changes are predicted upon dimerization. Therefore, the presence of dimer D1, that forms stabilized intermolecular hydrogen bonds (O···H–O), is expected in the crystal of L–aspartic acid. It also appears from the experimental molecular structure of the L–aspartic acid in crystal [15]. For the present case, the supermolecular approach [77–79] was used to calculate the interaction energy of pair of interacting molecules. The computed interaction energy ($E_{int} = E_{AB} - E_A - E_B$) of the formation of hydrogen bonded dimers, D1 and D2, are −16.091 and −7.819 kcal/mole, respectively, at B3LYP/6–311++G(d,p) level of theory. Thus, the value of hydrogen bonding interaction energy predicted for D1 is much lower as compared to that obtained for D2 which explains the formation and the stability of the dimer D1 [80]. The electronic energy of rigid monomer is only considered and the energy associated with the deformation of the monomer did not used. The minimum electronic energy of dimers are found more than two times of the energy of monomer because of high stabilization of hydrogen bonded complex. The predicted dipole moment for the monomer, dimer D1 and dimer D2 are 4.572, 5.687 and 9.104 Debye respectively at B3LYP/6–311++G(d,p) level of theory. The high dipole moment values could be contributing to favour the formation of intermolecular complexes [81].

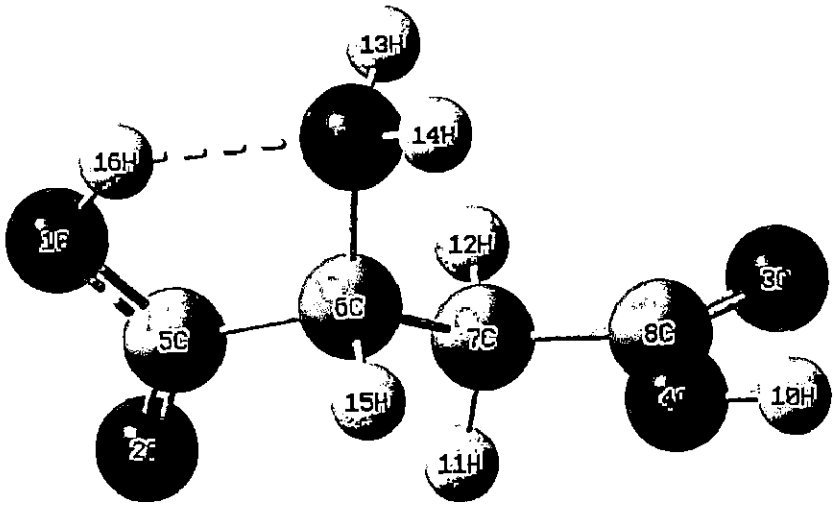

Fig. 3.1 Optimized molecular geometry of L–aspartic acid in monomer form with numbering scheme.

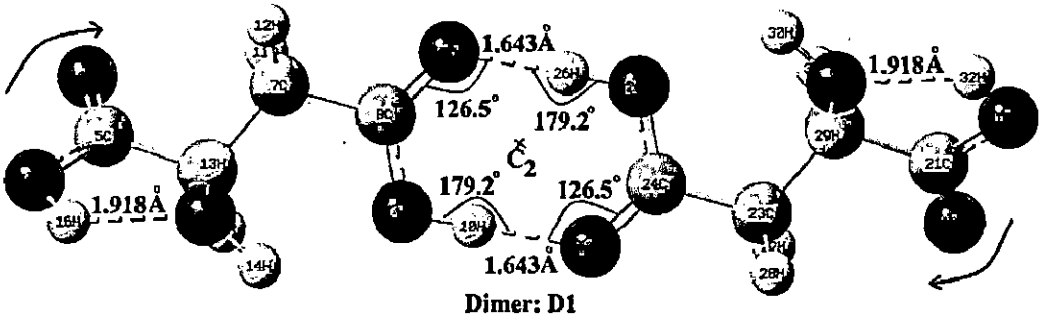

Dimer: D1

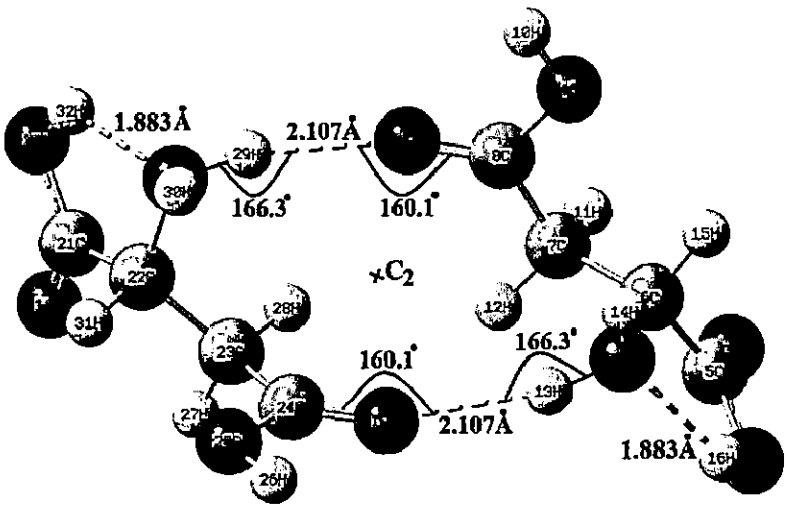

Dimer: D2

Fig. 3.2 Optimized molecular structures of L–aspartic acid in dimer form (D1 and D2).

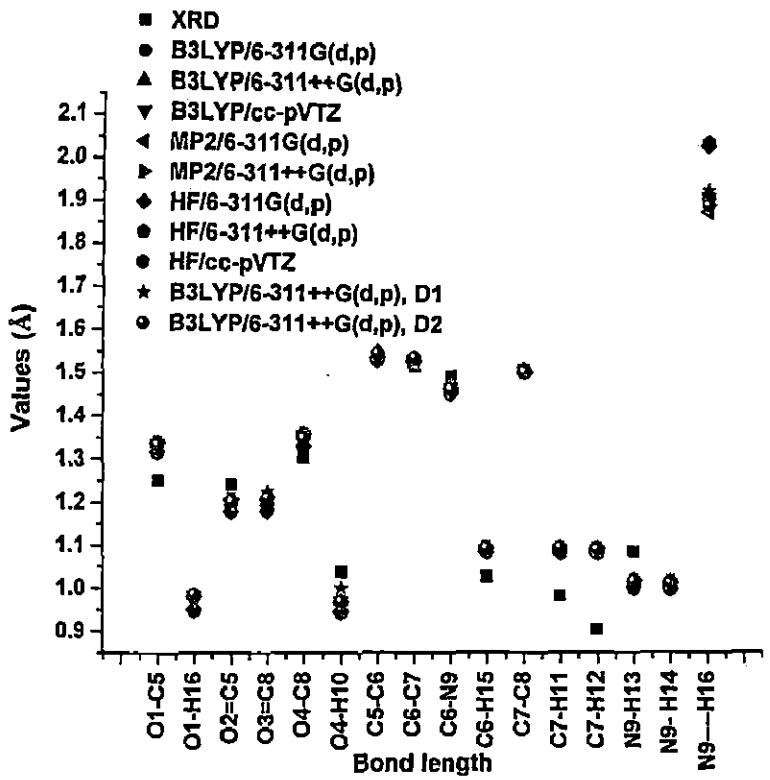

Fig. 3.3 Comparison of computed bond lengths with experimental (XRD) data.

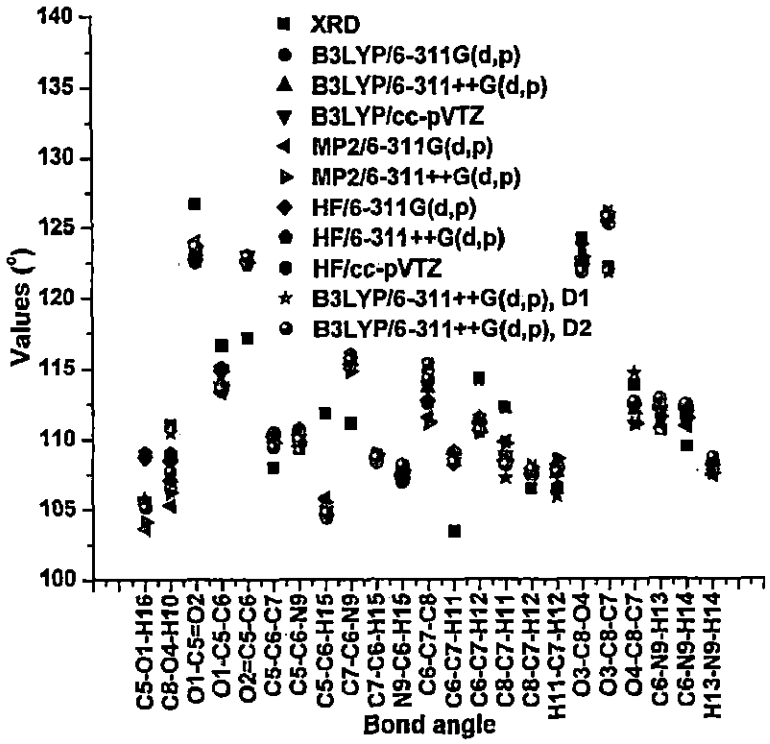

Fig. 3.4 Comparison of computed bond angles with experimental (XRD) data.

Table 3.1 Calculated minimum SCF energies (a. u.) for the monomer and dimers of L-aspartic acid at different levels of theory.

Basis Sets	Monomer				D1	D2
	B3LYP	PCM-B3LYP	MP2	HF	B3LYP	B3LYP
6-311G(d,p)	-512.46920129	-512.48590719	-511.15413294	-509.62823730	-1024.96905998	-1024.95405573
6-311++G(d,p)	-512.48641101	-512.50476955	-511.18017537	-509.64015369	-1024.99846547	-1024.98528322
cc-pVTZ	-512.52169271	-512.53841892	--	-509.68632960	--	--

parison of bond lengths obtained from quantum chemical calculations for the monomer and dimers of L-aspartic acid with experiment (XRD).

Bond length (Å)	XRD[a]	Monomer								D1		D2	
		B3LYP			MP2		HF			B3LYP		B3LYP	
		6-311 G(d,p)	6-311++ G(d,p)	cc-pVTZ	6-311 G(d,p)	6-311++ G(d,p)	6-311 G(d,p)	6-311++ G(d,p)	cc-pVTZ	6-311 G(d,p)	6-311++ G(d,p)	6-311 G(d,p)	6-311++ G(d,p)
O1-C5	1.252	1.338	1.338	1.337	1.339	1.340	1.317	1.316	1.315	1.338	1.338	1.335	1.335
O1-H16		0.982	0.982	0.982	0.980	0.981	0.949	0.949	0.949	0.982	0.982	0.985	0.985
O2=C5	1.242	1.202	1.202	1.201	1.207	1.208	1.179	1.180	1.179	1.202	1.203	1.203	1.203
O3=C8	1.202	1.202	1.204	1.203	1.208	1.210	1.181	1.182	1.181	1.225	1.225	1.210	1.211
O4-C8	1.306	1.360	1.359	1.358	1.359	1.360	1.332	1.331	1.330	1.321	1.323	1.351	1.351
O4-H10	1.039	0.969	0.969	0.969	0.968	0.969	0.946	0.946	0.946	1.003	1.001	0.969	0.969
C5-C6	1.542	1.545	1.548	1.543	1.539	1.540	1.532	1.534	1.532	1.545	1.546	1.548	1.549
C6-C7	1.518	1.533	1.537	1.533	1.529	1.532	1.531	1.532	1.530	1.531	1.532	1.536	1.539
C6-N9	1.495	1.471	1.470	1.468	1.468	1.467	1.456	1.456	1.454	1.470	1.470	1.469	1.466
C6-H15	1.028	1.094	1.094	1.091	1.095	1.095	1.085	1.085	1.083	1.094	1.094	1.094	1.094
C7-C8	1.512	1.511	1.511	1.507	1.507	1.506	1.506	1.506	1.505	1.510	1.509	1.506	1.506
C7-H11	0.982	1.094	1.094	1.091	1.094	1.094	1.083	1.083	1.081	1.094	1.095	1.095	1.095
C7-H12	0.904	1.092	1.092	1.089	1.093	1.093	1.083	1.083	1.081	1.094	1.093	1.090	1.091
N9-H13	1.085	1.016	1.016	1.013	1.017	1.017	1.001	1.001	0.999	1.016	1.016	1.018	1.018
N9-H14	1.010	1.013	1.013	1.011	1.014	1.014	0.998	0.998	0.996	1.013	1.013	1.012	1.012
N9···H16		1.913	1.924	1.918	1.883	1.900	2.037	2.046	2.043	1.918	1.933	1.883	1.899
RMS		0.073	0.073	0.072	0.073	0.073	0.072	0.072	0.071	0.071	0.071	0.072	0.073
MAD		0.052	0.053	0.052	0.053	0.053	0.055	0.055	0.055	0.049	0.049	0.053	0.053

[a]Ref [10, 15]

arison of bond angles obtained from quantum chemical calculations for the monomer and dimers of L-aspartic acid with experiment (XRD).

Bond angle (°)	XRD[a]	Monomer								D1		D2	
		B3LYP			MP2		HF			B3LYP		B3LYP	
		6-311 G(d,p)	6-311++ G(d,p)	cc-pVTZ	6-311 G(d,p)	6-311++ G(d,p)	6-311 G(d,p)	6-311++ G(d,p)	cc-pVTZ	6-311G (d,p)	6-311++ G(d,p)	6-311G (d,p)	6-311++ G(d,p)
:5-O1-H16		105.2	105.6	105.4	103.6	104.1	108.7	109.0	108.8	105.3	105.7	104.6	105.1
:8-O4-H10	111.0	106.5	107.3	106.8	105.3	106.2	108.5	109.0	108.7	110.4	110.5	107.1	107.7
O1-C5=O2	126.7	123.5	123.3	123.3	124.0	123.7	122.7	122.6	122.5	123.5	123.2	123.9	123.6
O1-C5-C6	116.6	113.4	113.8	113.7	113.3	113.8	114.8	115.0	115.0	113.4	113.8	113.2	113.5
O2=C5-C6	117.1	123.0	122.9	123.0	122.7	122.5	122.5	122.4	122.5	123.1	123.0	122.9	122.9
C5-C6-C7	108.0	110.5	110.1	110.2	110.2	109.7	110.2	110.0	110.0	110.5	110.3	109.6	109.4
C5-C6-N9	109.3	109.5	109.8	110.0	109.5	109.8	110.3	110.5	110.7	109.4	109.8	109.6	109.9
C5-C6-H15	111.8	105.0	104.9	104.9	105.7	105.5	104.6	104.4	104.4	104.9	104.7	104.9	104.7
C7-C6-N9	111.1	116.0	115.5	115.5	115.0	114.8	115.3	115.2	115.1	116.4	116.0	115.6	115.6
C7-C6-H15	108.8	108.3	108.6	108.5	108.6	108.9	108.7	108.8	108.7	108.4	108.5	108.6	108.6
N9-C6-H15	107.8	106.9	107.4	107.3	107.4	107.8	107.2	107.3	107.3	106.6	106.9	107.9	108.1
C6-C7-C8	115.3	114.8	113.6	113.7	111.5	111.2	112.7	112.7	112.5	115.7	115.3	114.6	114.2
C6-C7-H11	103.4	108.3	108.4	108.3	108.9	108.9	109.1	109.1	109.1	109	108.8	108.1	108.3
C6-C7-H12	114.2	111.4	110.9	110.9	110.6	110.5	111.1	111.0	110.8	111.3	111.5	110.5	110.6
C8-C7-H11	112.2	108.1	108.6	108.8	109.8	109.7	108.4	108.3	108.6	107.5	107.2	108.1	108.1
C8-C7-H12	106.4	107.3	107.6	107.5	107.9	108.0	107.5	107.6	107.5	107.4	107.6	107.6	107.8
H11-C7-H12	106.4	106.5	107.5	107.5	108.2	108.5	107.9	108.0	108.1	105.3	105.9	107.7	107.6
O3-C8-O4	124.1	122.3	122.4	122.4	122.8	122.9	122.3	122.3	122.3	123.8	123.6	121.7	121.8
O3-C8-C7	122.1	125.4	125.6	125.5	126.0	126.0	125.3	125.3	125.2	121.4	121.8	125.4	125.6
O4-C8-C7	113.8	112.3	112.0	112.1	111.2	111.1	112.4	112.4	112.5	114.8	114.6	112.9	112.6
C6-N9-H13	110.6	111.5	112.2	111.8	110.7	111.5	112.2	112.6	112.3	111.3	112.0	111.6	112.8
C6-N9-H14	102.8	111.4	112.3	112.0	110.9	111.4	112.0	112.2	112.1	110.8	111.6	111.8	112.4
H13-N9-H14		107.9	108.0	107.8	107.4	107.5	108.1	108.2	108.1	107.8	108.0	108.4	108.6
RMS		3.742	3.806	3.779	3.765	3.769	3.778	3.812	3.808	3.590	3.648	3.745	3.850
MAD		2.952	3.057	3.048	3.091	3.100	3.048	3.057	3.067	2.657	2.633	2.943	3.071

[10, 15]

3.4.2 Vibrational analysis

L–aspartic acid has 16 atoms. Being a nonlinear molecule, it has 42 normal modes of vibration. It is a chiral molecule and belongs to lowest symmetry C_1 point group. Therefore, all the fundamental vibrations are expected to be active in both IR and Raman spectra. The experimental vibrational spectra (FTIR and Raman), calculated fundamental harmonic frequencies, anharmonic frequencies, IR intensities, Raman intensities and vibrational assignments along with PED values at DFT (B3LYP) level are presented in Table 3.4. The calculated vibrational frequencies along with intensities at MP2 and HF levels are given in Table 3.5. The simulated and experimental vibrational spectra of L–aspartic acid at DFT (B3LYP) level are shown in Fig. 3.5. In solid phase, it is expected that the hydrogen atom in NH_2 and OH groups of L–aspartic acid form dimers by strong hydrogen bonding interaction with oxygen atom. The affect of intermolecular interactions on vibrational modes of monomer is discussed. The calculations of vibrational frequencies for dimeric structures of L–aspartic acid provide significant changes in many vibrational modes of monomer. The theoretical vibrational frequencies of dimers at B3LYP/6–311G(d,p) and B3LYP/6–311++G(d,p) levels of theory are presented in Table 3.6. It is interesting to note that the harmonic scaled frequencies of many vibrational modes of dimer, D1, are found more close to solid phase FTIR data. The low values of the RMS and MAD (Table 3.6) are found for the calculated vibrational frequencies of dimer D1 that show the good agreement with solid phase vibrational spectra. In general, the region 2800–1800 cm^{-1} of FTIR shows overtone, Fermi resonances and combination bands [82]. In the present FTIR spectrum, combination and overtone bands have been assigned with the help of calculated combination and overtone wavenumbers at different levels of theory. These bands are presented in Table 3.7. The different regions of experimental FTIR spectra of L–aspartic acid that comprise the combination and overtone bands are shown in Fig. 3.6. These experimental bands are found in well agreement with the theoretical anharmonic frequencies. To make comparison with experiment, linear correlation plots between theoretical (harmonic and anharmonic) and the experimental (IR) frequencies are presented in Fig. 3.7 and 3.8. The mode–mode coupling strength values larger than ca. 25 cm^{-1} are presented graphically in Fig. 3.9. The mode–mode coupling strengths greater than ca. 100 cm^{-1} are predicted for mode pairs (2, 28), (3, 27), (1, 37), (4, 37),

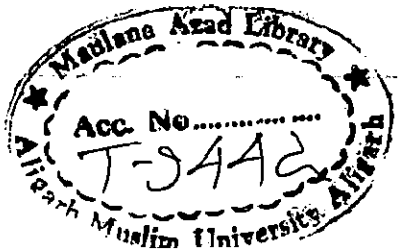

(36, 37), (5, 6), (1, 4) and (1, 36). The mode pairs that involve large amplitude of vibrations (large anharmonicity) show high mode–mode coupling strengths. The 3D graphical representation of mode–mode pair coupling strengths for L–aspartic acid calculated at B3LYP/6–311G(d,p) level in the 2–mode coupling representations of the quartic force field (2MR–QFF) is shown in Fig. 3.10. This indicates that most of the normal mode pairs have very low coupling strengths except some pairs, which show the medium to high coupling strengths. The frequencies (harmonic, diagonal, VSCF and CC–VSCF), anharmonic intensity, contribution of intrinsic anharmonicity to a mode ($\Delta E_{diag.}$) and contribution of anharmonic coupling between pair of modes ($\Delta E_{coupl.}$) are calculated [62, 64] at B3LYP/6–311G(d,p) level of theory using GAMESS–US code and are given in Table 3.8. It is clear from Table 3.8 that the absolute values of $\Delta E_{coupl.}$ are larger than the absolute values of $\Delta E_{diag.}$ for most of the modes. Therefore, the contribution of anharmonic mode–mode coupling is larger than the intrinsic anharmonicity for the present molecule.

L–aspartic acid consists of one amino (NH_2), two carboxylic (COOH) and one methyl (CH_2) groups. In addition to skeletal vibrations, the vibrational modes of the molecule are classified into these group vibrations. The vibrations related to each characteristic group of the molecule are discussed.

NH_2 vibrations

The NH_2 group gives rise to six possible internal modes of vibrations like asymmetric and symmetric stretching, scissoring, rocking, wagging and twisting motions. In solid phase IR spectra, the bands due to NH_2 stretching vibrations usually occur in the region 3450–3160 cm^{-1} [83, 84]. In this work, the bands predicted at anharmonic frequency 3414 and 3351 cm^{-1} at PT2–B3LYP/cc–pVTZ level of theory are assigned to asymmetric (mode 2, 99% PED) and symmetric (mode 3, 73% PED) stretching vibrations respectively. The vibrational bands of NH_2 stretching motions were not observed in the FTIR spectrum due to appearance of broad absorption in this region, which may be associated to hydrogen bonding. The O–H stretching vibration of carboxylic group occurs in the same wavenumber region as that of the NH_2 stretching vibrations [85]. The NH_2 symmetric stretching vibration is found mixed with O1–H16 stretching vibration (22% PED) in mode 4. Mohamed et al [13] observed and predicted NH_2 asymmetric stretching vibrations at frequency 3099 and 3310 cm^{-1} in L–alanine, at 3436 and 3187 cm^{-1} in L–phenylalaline, at 3141and3189 cm^{-1} in

L–aspartic acid and at 3020 and 3130 cm^{-1} in L–glutamic acid respectively. The band due to NH_2 symmetric stretching vibration is observed at 3011 cm^{-1} in L–aspartic acid [13]. These vibrations show large anharmonicities due to large amplitudes of vibrations and, hence, large deviations between calculated harmonic and experimental (IR) frequencies of these vibrations are found. These stretching modes have shown very strong coupling (CS: >250 cm^{-1}) with mode 27 and 28 which have also caused deviations. The anharmonic methods have corrected these up to some extent. In dimers, the calculated vibrational frequencies of NH_2 group vibrations are found lower than those of monomer. The IR band due to NH_2 scissoring vibration shows their presence in the region 1650–1580 cm^{-1} [84]. The vibrational band, appeared in the FTIR spectrum at 1561 cm^{-1} with weak intensity, is assigned to NH_2 scissoring motion with high PED value (77%). This vibration is also observed in some amino acids at lower wavenumber than expected [13]. The experimental wavenumber for this vibration shows deviation from the said region may be due to intermolecular or intramolecular interactions. The corresponding theoretical anharmonic frequency is 1582 cm^{-1} at PT2–B3LYP/6–311G(d,p) level of theory. This vibration is predicted at higher wavenumber (1608 cm^{-1}) at B3LYP/6–311++G(d,p) level in dimers than that of monomer. This vibration (mode 10) is coupled to O–H stretching vibration with CS <75 cm^{-1}. The NH_2 rocking vibration normally shows its presence in the region 1150–900 cm^{-1} while the wagging vibration appears in the region 850–500 cm^{-1} [86, 87]. In this work, rocking vibration mixed with other vibrations is identified in mode 13, 16, 19 and 21. The wagging vibration is predicted in mode 25 and 27, with mixing of other vibrations. The NH_2 twisting vibration is assigned to mode 37 (72% PED). The shift in experimental value from literature is probably associated to intramolecular hydrogen bonding O1–H16···N9, which is supported by atomic charge calculation (section 3.4.6). A large negative charge on the N9 (–0.8796) and positive charge on H16 (0.4897) support the existence of this bonding (section 3.4.6). NBO analysis (section 3.4.3) also supports the formation of the hydrogen bonding. The strong absorption bands in FTIR at 899 and 777 cm^{-1} are assigned to modes 23 and 27 respectively that contain 17% and 25% PED contributions, respectively, from NH_2 deformation. These modes are also observed in Raman spectrum. The calculated anharmonic frequencies at B3LYP level are in good agreement with experimental values. In dimers, D1 and D2, the vibrational frequencies of NH_2 group vibrations have changed noticeable from those of monomer (Table 3.6).

CH_2 group and C–H vibrations

The CH stretching vibrations in CH_2 group usually appear in the region 3000–2850 cm^{-1} [83, 84]. Many shoulders of the intense broad band are appeared in this spectral region of the FTIR spectrum. The shoulders at 2995 and 2957 cm^{-1} are assigned to CH_2 asymmetric and symmetric stretching vibrations respectively. They are also identified in the Raman spectrum with very strong intensity [10]. The shoulder at 2982 cm^{-1} is assigned to C6–H15 stretching vibration. In dimer D1, the CH asymmetric stretching vibration is predicted at 2980 cm^{-1} (B3LYP/6–311++G(d,p)) which is close to solid phase FTIR data but in dimer D2, the calculated vibrational frequencies for this vibration show large deviations at different levels of theory. The CH symmetric stretching vibration is calculated at 2950 and 2957 cm^{-1} (B3LYP/6–311++G(d,p)), respectively, in D1 and D2 dimers that are in excellent agreement with FTIR data. CH_2 deformation vibrations appear in the region 1470–1400 cm^{-1} with medium to strong intensity [84]. The band appeared at 1422 cm^{-1} in the FTIR and Raman spectra is assigned to scissoring vibration of CH_2 group. This vibration is pure as confirmed from PED value and is associated to mode 11. The corresponding calculated anharmonic frequency at PT2–B3LYP/6–311G(d,p) level of theory is 1424 cm^{-1}. The strong band due to CH_2 wagging vibration is appeared at 1336 cm^{-1} in the FTIR and Raman spectra. This vibration has shown major contribution (42% PED) in mode 14, which is correlated with the predicted anharmonic frequency, 1336 cm^{-1}, at PT2–B3LYP/cc–pVTZ level of theory. The C–H15 deformation vibrations are identified with significant PED values in the mode 14 to 21. The CH_2 group vibrations for L–aspartic acid are found in accordance with literature [13].

COOH vibrations

The C=O stretching vibration in COOH group shows very strong absorption near 1700 cm^{-1} [10]. The two strong bands at 1691 and 1611 cm^{-1} in FTIR spectrum are appeared due to C=O stretching vibrations. The corresponding anharmonic frequencies are 1812 and 1796 cm^{-1} with IR intensities, 290.6 and 329.6 km/mole, respectively as predicted at PT2–B3LYP/cc–pVTZ level of theory. Navarrete et al. [10] reported these vibrations at 1691 and 1612 cm^{-1} for aspartic acid. The C=O stretching vibrations are observed at 1607, 1596 and 1617 cm^{-1} in the vibrational

spectra of alanine, glycine and glutamic amino acids, respectively [10]. A large discrepancy is observed between calculated and experimental frequencies of this vibration. This may be due to large negative charge on O atom that forms intermolecular and intramolecular interactions in solid phase. The stretching frequency of this group depends much on its environment and shifts due to intermolecular or intramolecular interactions [84]. In the higher frequency region above 1600 cm^{-1}, it is found that the anharmonic frequencies of modes such as O–H and C=O stretching vibrations show large deviations (more than 100 cm^{-1}). The anharmonic corrections are not much useful for these modes because these are very sensitive to the intramolecular interactions in solid phase [88]. The mode corresponding to O–H stretching vibrations have shown large coupling strength with 36 and 37 modes while C=O stretching modes show low value of coupling strength to others. The contribution of anharmonicity due to mode–mode coupling is found larger than intrinsic anharmonicity for O–H stretching mode (Table 3.8). In solid phase, the carboxylic group forms stable dimers of L–aspartic acid by direct interaction with OH and NH_2 groups through hydrogen bonds, O···H–N–H and O···H–O (Fig. 3.2). The intermolecular interaction affects the vibrational frequencies due to charge delocalization through hydrogen bonds (section 3.4.3). In dimers, the calculated vibrational frequencies of C=O stretching vibrations (mode 8 and 9) are found lower than those of monomer. The scaled frequencies of C=O stretching vibrations are 1774 and 1648 cm^{-1} at B3LYP/6–311++G(d,p) level of theory (for D1). The other frequencies in Table 3.6 for the case of dimer D1 can be seen to be little affected by the intermolecular interactions, except that of the O–H stretching vibrations.

The carboxylic acid O–H stretching bands are weak in the Raman spectrum while have moderate intensity in the IR spectrum. A very broad band appearing around 3400 cm^{-1} characterizes the O–H stretching [89–91]. The hydrogen bonding in solid phase makes vibrational spectra more complicated in this region. Therefore, we could not observe strong and sharp bands due to O–H vibration in the vibrational spectra. However, this band is predicted at 3469 cm^{-1} in dimer D1 using B3LYP/6–311++G(d,p) approach. The harmonic vibrational frequency of O–H stretching vibration in dimer D1 is lowered by 169 cm^{-1} than that of monomer.

In the present investigation, the anharmonic effects are quite large for the hydrogenic stretching, OH (mode 1), NH_2 (modes 2 and 3) and CH_2 (modes 5 and 7). The contribution of anharmonicity to observable transitions can exceed 5% for these

vibrations [92]. The largest discrepancy is observed between calculated anharmonic frequency and observed FTIR frequency at 3024 cm^{-1} (broad band). This may be because of the large anharmonicity associated to the mode and due to strong effect of the hydrogen bond between H16 and N9. This broad band is assigned to O1–H16 stretching vibration with 77% PED value in mode 4, which has 22% PED contribution from NH_2 symmetric stretching vibration. Other skeletal vibrations show a mixing of many modes. It is difficult to assign them to a pure vibration. In the present work, many bands are assigned to mixed vibrations with the help of PED values (Table 3.4).

From the values of RMS and MAD in Table 3.4, it can be seen that the calculated frequencies at HF theory deviate more from experimental frequencies than those at B3LYP level due to absence of electron correlation term in the HF calculations. The frequencies calculated by MP2 method are found close to those obtained from B3LYP calculations. Therefore, the B3LYP method approximates the frequencies much better than the HF but close to MP2 methods at same basis set. The anharmonic wavenumbers calculated by B3LYP/cc–pVTZ method show good agreement with experimentally observed data. The anharmonic method at PT2–B3LYP/6-311++G(d,p) level have predicted very low frequency e.g. 4 cm^{-1} for lower torsional mode (mode 42). This is because of the limitation or incapability of anharmonic methods for these modes in the present molecule.

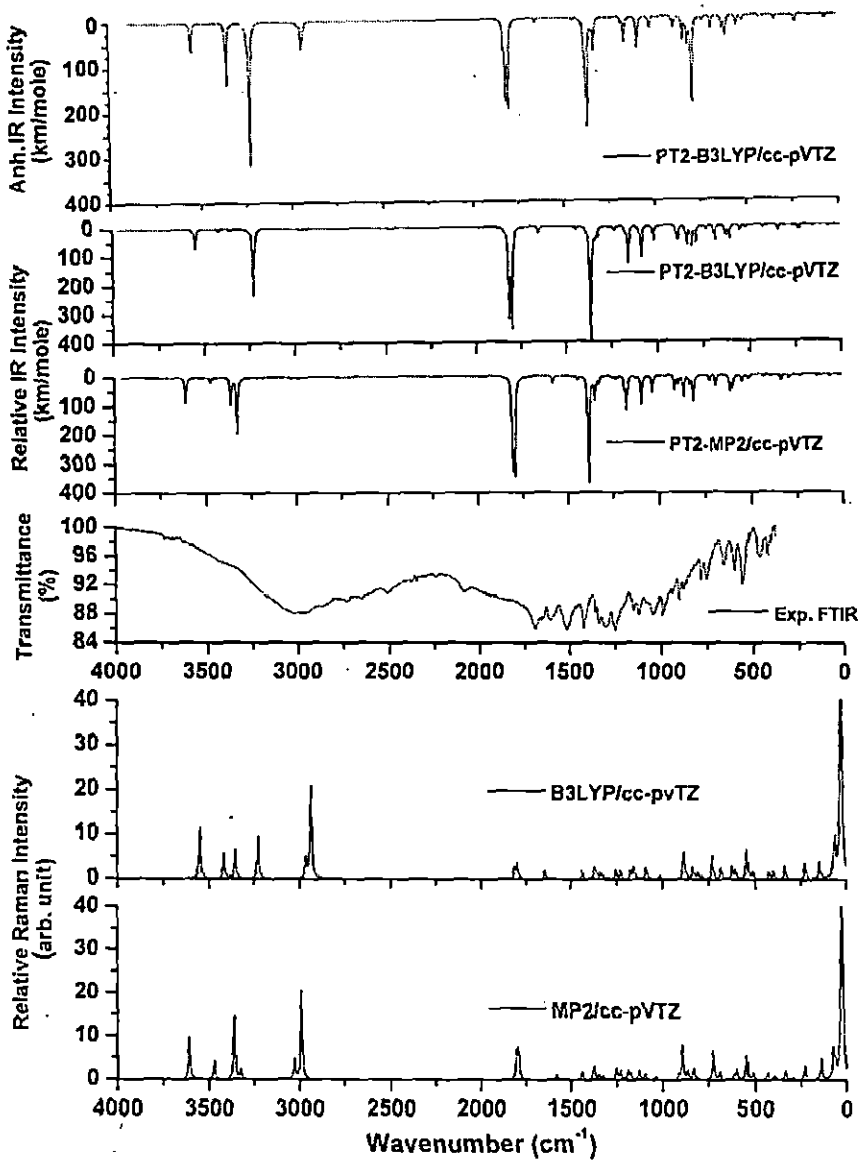

Fig. 3.5 Simulated and experimental vibrational spectra of L–aspartic acid.

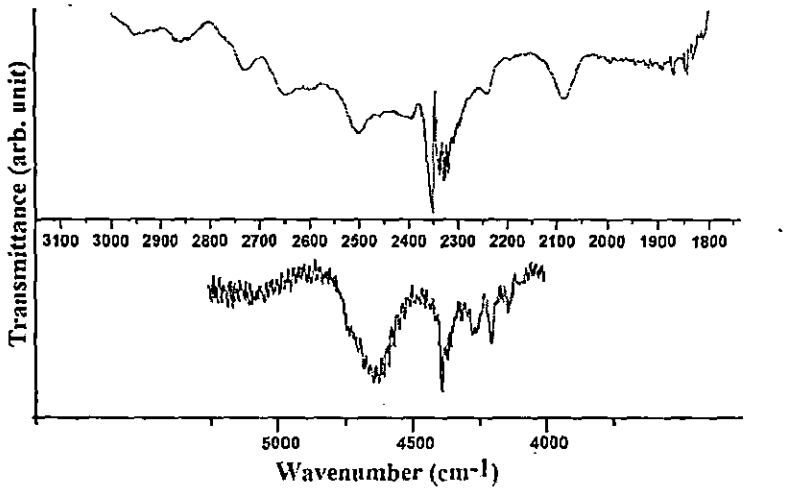

Fig. 3.6 FTIR spectra of L–aspartic acid in 4000-5000 and 1800-3000 cm^{-1} regions.

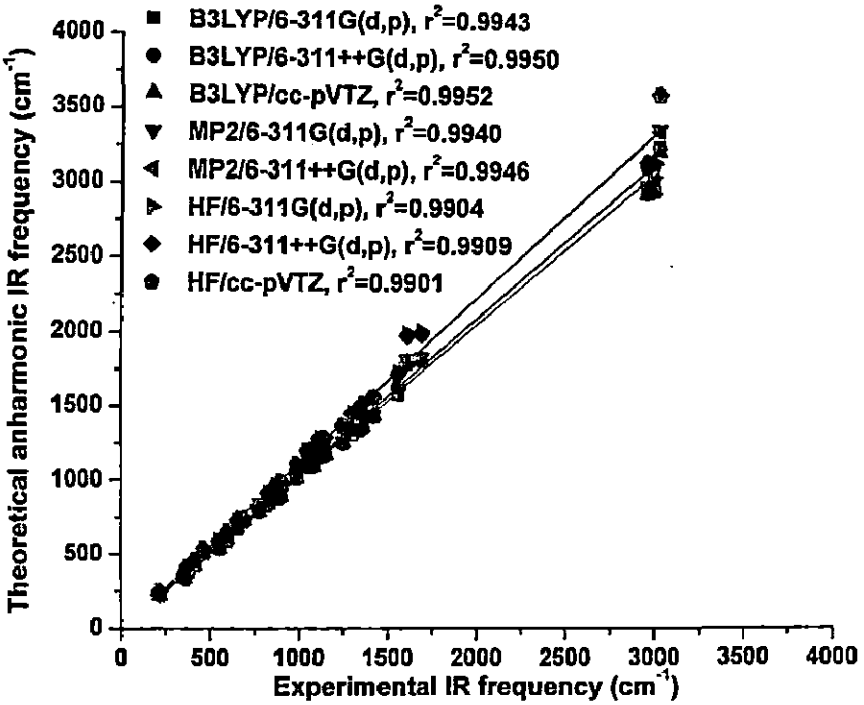

Fig. 3.7 Correlation plot between experimental and theoretical anharmonic frequencies (PT2).

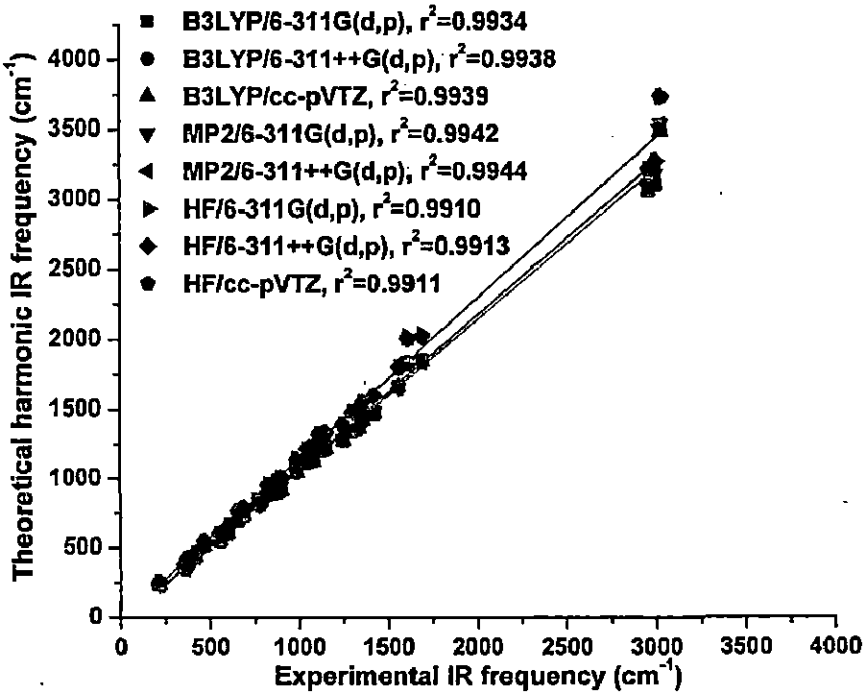

Fig. 3.8 Correlation plot between experimental and theoretical harmonic frequencies.

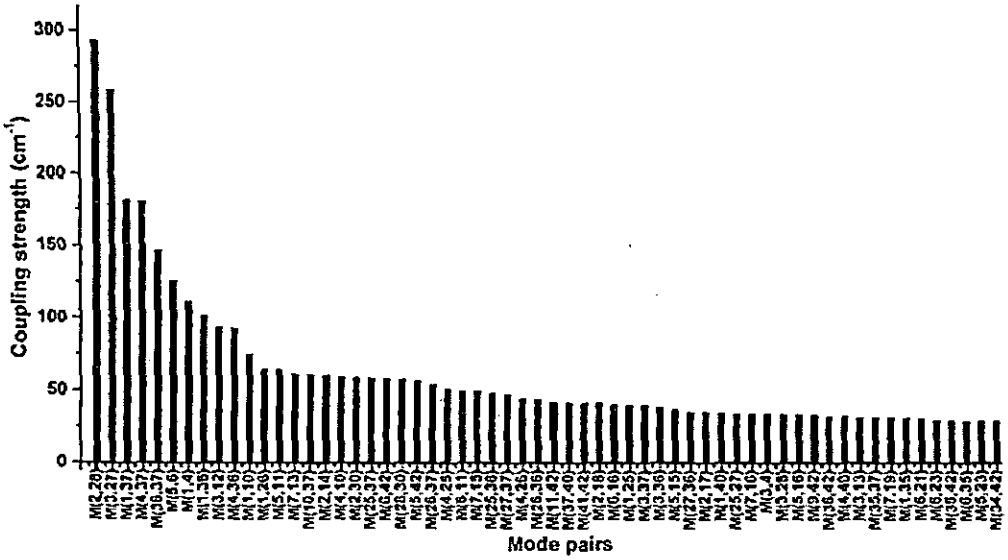

Fig. 3.9 Anharmonic mode–mode coupling strength between pair of modes.

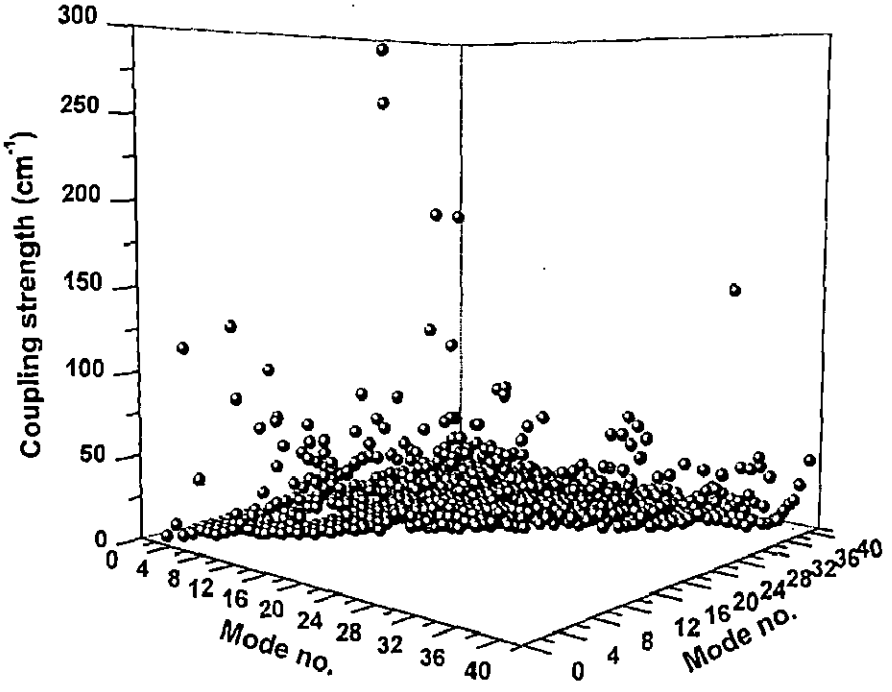

Fig. 3.10 3D Graph for anharmonic mode–mode coupling strengths between pair of modes.

Experimental and theoretical vibrational frequencies (cm^{-1}) along with intensities and vibrational assignments for L–aspartic acid monomer.

ved mbers	B3LYP															PED(>5%) and assignment
	6–311G(d,p)					6–311++G(d,p)					cc-pVTZ					
Raman[a]	ω_h	ω^b_{scaled}	ω_{anh}	A (km/ mole)	R_i (arb. unit)	ω_h	ω^c_{scaled}	ω_{anh}	A (km/ mole)	R_i (arb. unit)	ω_h	ω^b_{scaled}	ω_{anh}	A (km/ mole)	R_i (arb. unit)	
	3756	3423	3553	69.0	194.5	3758	3633	3559	81.0	180.8	3742	3626	3547	71.5	184.4	νH_{16}–O_4(100)
	3588	3272	3420	7.9	99.0	3596	3477	3423	13.6	85.5	3590	3470	3414	10.4	91.4	$\nu_{as} NH_2$(99)
	3505	3198	3334	36.7	69.1	3512	3395	3351	16.6	90.4	3506	3389	3351	7.1	101.6	$\nu_s NH_2$(73) + νH_{16}–O_1(22)
3016s	3489	3183	3253	213.0	178.0	3492	3376	3251	255.0	189.7	3483	3370	3225	235.1	153.9	νH_{16}–O_1(77)+ $\nu_s NH_2$(22)
2999vs	3102	2836	2952	6.3	72.8	3111	3008	2962	5.9	67.4	3109	3002	2960	5.8	70.1	$\nu_{as} CH_2$(92) + νC_6–H_{15} (6)
	3064	2802	2926	6.2	103.8	3068	2966	2925	6.8	68.1	3066	2961	2925	7.7	54.3	νC_6–H_{15}(84) + νC_7–H_{11} (9)
2958vs	3056	2795	2936	2.4	281.4	3060	2958	2936	1.2	310.5	3060	2953	2934	0.5	318.9	$\nu_s CH_2$(89) + νC_6–H_{15} (9)
1692m	1852	1714	1820	289.0	39.6	1836	1775	1804	327.9	61.2	1843	1772	1812	290.6	41.1	νC_5=O_2(85)+ βH_{16}–O_1–C_5(6)
	1837	1700	1807	327.0	42.8	1816	1756	1783	383.5	87.4	1823	1752	1796	329.6	53.8	νC_8=O_3(86)
	1664	1545	1582	31.0	29.6	1662	1607	1638	28.0	20.9	1660	1604	1645	24.5	26.4	$\beta_{asis} NH_2$(77)
1422ms	1464	1365	1424	10.6	32.4	1470	1421	1432	11.2	28.7	1471	1419	1437	10.6	28.9	$\beta_{scis} CH_2$(87)
1359m	1429	1334	1365	436.0	27.7	1411	1364	1345	410.6	25.6	1416	1362	1360	420.7	20.2	βH_{16}–O_1–C_5(73) + βO_1–C_5=O_2 (8) + νO_1–C_5 (8)
	1407	1314	1377	6.6	46.5	1404	1357	1368	11.8	39.7	1405	1355	1369	10.4	33.9	τH_{15}–C_6–C_5–O_1 (49) + τNH_2(14) + βH_{15}–C_6–C_5(13)
1336s	1368	1279	1331	19.8	17.6	1363	1318	1333	23.6	19.7	1363	1315	1336	33.3	17.6	ωCH_2 (42) + τH_{15}–C_6–C_5–O_1 (7) + ν [{C7–C8} + {O4–C8}] (7) + βH_{16}–O_1–C_5(6)
	1352	1265	1301	28.8	6.8	1346	1301	1318	46.2	8.0	1353	1299	1322	32.1	8.3	βH_{16}–O_1–C_5(33) + ν [{C7–C8} + {O4–C8}] (23) + βO_1–C_5–O_4 (15) + τH–C_7–C_8–O_4(12) + β[{ H_{11}–C_7–C_8}+ {H_{15}–C_6–C_5}] (6)
1249m	1277	1198	1251	4.7	32.4	1274	1232	1248	6.8	42.2	1276	1229	1254	5.3	30.8	β[{ H_{11}–C_7–C_8}+ {H_{15}–C_6–C_5}] (30)+ τH_{11}–C_7–C_8–O_4 (20) + τNH_2(12) + τH_{15}–C_6–C_5–O_1 (10)
	1257	1180	1223	15.8	33.7	1258	1216	1223	20.2	31.3	1258	1214	1227	16.8	27.2	βH_{15}–C_6–C_5 (39) + β[{ H_{11}–C_7–C_8}+ {H_{15}–C_6–C_5}] (12) + τ H–C_7–C_8–O_4(12)
1145w	1214	1141	1175	25.0	25.5	1208	1168	1164	16.7	31.8	1215	1166	1171	14.4	29.7	νO_1–C_5 (41) + βH_{15}–C_6–C_5 (18) + βH_{16}–O_1–C_5(9) + νC_5–C_6 (7)
1120m	1195	1124	1162	144.0	36.6	1200	1160	1151	145.1	49.8	1200	1158	1153	132.8	39.5	βH_{16}–O_4–C_8(29) + ν [{C_7–C_8} + {O_4–C_8}] (23) + τNH_2(13) + β[{ H_{11}–C_7–C_8}+ {H_{15}–C_6–C_5}] (9)
1082m	1133	1068	1100	27.2	35.4	1123	1086	1089	16.6	39.1	1123	1084	1088	15.0	34.2	νN_9–C_6 (49)+ β [H_{11}–C_7–C_8 + H_{15}–C_6–C_5] (11) + βH_{15}–N_9–C_6(6)
	1122	1058	1099	94.7	10.2	1112	1075	1088	111.0	17.9	1112	1073	1082	104.1	10.1	ν[{C_7–C_8} + {O_4–C_8}] (20) + νN_9–C_6 (15)+ τNH_2(15) + τH_{15}–C_6–C_5–O_1 (14) + βH_{16}–O_4–C_8(9)+ β[{ H_{11}–C_7–C_8}+ {H_{15}–C_6–C_5}] (9)

(continued)

991w	1054	997	1025	50.2	12.6	1041	1006	1010	49.7	13.0	1046	1005	1013	49.8	10.9	ν[{C5–C7} + {N9–(18)+ ν O1–C1 (1 O4}] (9)
900w	920	877	897	57.9	36.2	920	889	883	43.2	31.1	922	888	885	43.2	32.9	β H10–N9–C6 (17) + O1–C5–C7 {(+ τ I
870m	890	850	870	7.1	84.3	898	868	876	17.3	97.2	899	867	879	17.9	82.2	OUT [{O2–C6–O1– ν [(C5–C7) + {C3–(C6}] (14)+ ν + γ (
	885	846	858	70.2	37.8	880	851	832	76.4	40.8	880	849	833	65.2	40.2	ν[{C5–C7} + {C3 {(C5–C7} + {N9–C6 +
	860	823	815	91.5	29.2	855	827	809	75.1	13.7	854	825	808	67.9	20.3	τ H10–O1–C
777s	838	804	816	48.8	11.9	833	805	784	66.0	23.0	835	804	785	57.6	9.7	ν C3–C6 (34) + ω N C6}] (6)
	737	713	727	16.0	72.5	734	710	723	14.9	88.2	736	708	727	13.6	82.3	β O1–C5=O2 (27)+ (C7–O4–C8}] (18)+ τ C7} + {C5–C6}](9)
661vw	695	675	669	78.8	35.9	703	680	678	54.8	36.8	706	678	681	52.3	36.5	[τ H10–O4–C5–C τ H10–O4–C5–C·
	638	624	623	12.7	34.5	632	611	620	43.5	23.0	635	610	620	34.8	41.7	τ H10–O4–C5–C7 (2 C7–C6 (11)+ β[· +{C
599w	607	596	602	52.5	35.2	605	585	596	45.5	30.5	605	584	601	46.5	30.1	β O3–C5–O + ν [{C7
552m	552	547	542	15.1	132.5	551	533	541	21.6	101.1	552	532	540	18.4	104.1	OUT [{O2–C6–O1– β O1–C5=O2 (21)+ τ C5–O1}+ {C5–(+
466m	511	510	507	13.9	13.1	515	498	511	10.9	25.7	515	497	510	10.0	22.5	β[{ C6–C5–O1)+ {C OUT [{O2–C5–O1–(τ H10–O4–C5–C
412vw	441	447	440	10.9	32.9	432	418	428	11.4	23.6	433	417	424	10.4	22.4	β[{ C7–C8–O4}+ {· C8–C7 (10)
368w	381	393	375	4.3	39.0	393	380	394	3.9	27.2	392	379	398	3.5	26.2	β[{ C7–C6–N9}+ {C· O1 (15)+ ν [{
356m	356	371	363	21.2	61.8	350	338	338	19.7	58.5	351	338	336	20.2	46.0	β[{ C5–C6–N9}+ {C N9–C6 (10)
	327	345	375	12.2	26.4	311	301	328	12.8	8.5	305	300	220	14.0	15.5	
217w	239	266	235	6.3	49.3	233	225	228	6.7	51.7	234	225	226	6.5	50.7	β[{ C5–C6–N9}+ {C (16)+ ν [{C8–C7) +

(continued)

																N_9–C_6 (10)+ β[{ C_7
																β[{ C_6–C_5–O_1)+ (C
	145	181	147	5.8	39.2	143	138	142	5.8	70.5	143	138	145	5.3	58.2	β C_8–C_7–C_6 (38)+
																β[{ C_7–C_5–O
	83	126	91	1.7	76.8	75	73	71	1.8	88.0	76	72	66	1.2	63.3	τ O_1–C_5–C_6–C
																τ C_8–(
	69	113	80	5.3	128.7	66	64	58	5.5	101.8	64	64	60	5.4	105.4	τ O_1–
																τ O_1–(
	16	66	73	0.9	1522.0	24	23	4	2.0	1327.0	19	23	26	1.8	1330.0	τ O_1–
	113	68	65			110	74	62			110	72	61			
	72	45	37			69	34	35			70	33	36			

ed: M–modes, ω_h– harmonic frequencies, ω_{anh} – Anharmonic frequencies, A– IR intensity, R_I– Raman intensity, ν– stretching, β– bending, τ– torsional, γ– out o
ng, sh–shoulder, b–broad, s–strong, vs–very strong, OUT ABCD: angle between vector AD and plane BCD
ng factor obtained from Ref. [66] , [b]scaling factor obtained from Ref. [65]

Table 3.5 Theoretical harmonic and anharmonic vibrational frequencies (cm^{-1}) alongwith intensities for L–aspartic

	MP2								HF							
	6-311G(d, p)				6-311++G(d, p)				6-311G(d, p)				6-311++G(d, p)				
#M	ω_h	ω_{anh}	A (km/ mole)	R_I (arb. unit)	ω_h	ω_{anh}	A (km/ mole)	R_I (arb. unit)	ω_h	ω_{anh}	A (km/ mole)	R_I (arb. unit)	ω_h	ω_{anh}	A (km/ mole)	R_I (arb. unit)	ω_h	ω_a
1	3810	3623	81.1	149.0	3797	3610	89.4	152.0	4114	3942	132.0	103.0	4112	3941	140.8	101.0	4099	392
2	3644	3474	11.4	77.1	3641	3472	16.5	67.2	4037	3855	203.0	38.3	4035	3853	211.8	43.2	4025	384
3	3565	3334	212.0	41.7	3554	3325	196.0	33.2	3822	3671	14.8	74.4	3826	3675	19.1	63.0	3820	366
4	3538	3374	60.3	173.0	3533	3361	93.6	230.0	3734	3610	7.9	108.0	3737	3613	9.9	117.0	3732	360
5	3178	3029	3.3	80.0	3175	3029	3.4	69.6	3275	3144	8.2	78.1	3275	3146	7.9	67.9	3269	314
6	3120	2994	4.9	49.2	3117	2991	4.5	49.8	3224	3114	8.2	63.4	3225	3112	8.1	47.5	3220	306
7	3112	2991	0.7	269.0	3108	2990	0.7	280.0	3218	3151	2.3	250.0	3219	3153	1.6	270.0	3209	311
8	1859	1826	237.0	56.7	1835	1804	279.0	93.0	2033	2006	365.0	28.5	2018	1986	391.9	44.7	2020	198
9	1841	1813	249.0	54.4	1817	1793	299.0	104.0	2020	1991	469.0	27.5	2004	1975	520.4	43.2	2004	197
10	1656	1590	29.8	24.9	1652	1583	27.0	16.5	1801	1727	36.0	16.8	1800	1716	34.5	10.8	1798	172
11	1484	1440	17.2	34.7	1483	1441	14.3	30.4	1595	1555	15.1	27.8	1597	1556	13.5	25.1	1599	156
12	1456	1402	397.0	24.0	1434	1382	355.0	19.2	1555	1517	255.0	9.9	1549	1514	201.4	12.3	1549	151
13	1421	1381	15.1	40.7	1415	1375	32.8	39.9	1526	1487	99.4	37.4	1523	1481	87.0	31.2	1520	148
14	1393	1359	68.0	13.4	1381	1348	78.0	16.6	1506	1467	258.0	13.0	1501	1457	312.4	11.9	1502	146
15	1369	1333	12.1	18.9	1360	1328	25.1	12.7	1480	1453	39.8	16.3	1475	1447	43.2	12.1	1477	144
16	1289	1257	7.5	37.0	1285	1253	8.7	44.0	1393	1368	2.8	33.1	1392	1366	5.5	30.3	1393	136
17	1271	1234	5.8	23.4	1267	1232	11.6	32.7	1374	1340	54.4	23.3	1373	1336	52.9	30.6	1371	133

Table: 3.5 (*continued*)

18	1237	1199	67.4	27.3	1230	1188	41.2	35.3	1336	1288	151.0	27.6	1331	1282	153.1	22.8	1330	1280	117.0	24.0
19	1217	1180	97.7	27.0	1215	1174	114.0	24.9	1322	1285	14.8	10.3	1320	1278	6.3	14.5	1323	1280	36.0	9.6
20	1170	1138	9.4	33.4	1163	1129	7.3	33.4	1237	1209	33.5	49.3	1235	1207	34.8	48.0	1231	1205	31.0	42.0
21	1127	1102	89.8	13.2	1123	1094	100.0	20.3	1216	1197	67.8	7.3	1215	1195	69.5	9.2	1212	1194	69.0	7.4
22	1076	1046	56.7	14.7	1066	1034	57.7	11.8	1144	1114	57.3	14.9	1139	1108	55.7	14.7	1140	1111	56.0	13.0
23	946	916	54.8	24.1	944	913	48.1	18.3	1008	991	38.3	39.9	1008	987	38.6	43.0	1009	990	35.0	38.0
24	917	890	47.4	79.2	916	893	30.2	124.0	982	963	11.9	68.3	981	964	12.6	78.8	983	966	15.0	70.0
25	912	879	39.9	43.6	905	865	72.3	31.1	961	916	109.0	27.6	955	911	98.6	28.0	954	911	95.0	28.0
26	877	816	102.0	15.4	868	810	87.8	7.8	918	891	38.2	21.4	914	881	47.4	22.1	915	887	41.0	14.0
27	864	842	15.0	35.7	860	832	28.3	38.6	811	804	13.7	64.2	809	801	10.7	69.6	810	802	8.9	65.0
28	742	732	18.7	81.0	738	725	18.3	108.0	791	738	124.0	17.2	789	738	121.0	18.5	790	742	95.0	25.0
29	713	683	48.4	23.9	712	690	38.3	28.8	769	730	82.5	36.6	768	733	85.6	33.0	774	730	89.0	34.0
30	641	618	41.3	50.3	631	612	52.7	18.5	677	659	54.3	23.0	670	654	56.5	12.6	671	651	51.0	18.0
31	609	602	52.2	42.6	605	597	44.3	35.3	659	656	69.4	27.1	657	653	63.9	20.7	657	652	62.0	21.0
32	558	549	16.3	113.0	554	547	23.0	85.8	604	592	28.9	101.0	601	588	34.9	79.9	602	586	31.0	80.0
33	521	512	13.8	20.1	522	514	12.4	26.7	548	543	17.8	11.9	548	541	18.3	12.5	549	539	16.0	13.0
34	434	435	9.2	32.4	434	434	8.6	28.7	460	463	12.6	27.9	460	462	13.4	27.4	459	463	12.0	23.0
35	404	389	4.6	19.4	403	396	5.2	13.8	425	415	4.0	22.9	426	420	4.2	19.9	428	421	4.6	18.0
36	358	346	22.6	24.5	350	337	21.0	35.7	381	368	21.6	29.1	376	361	20.3	35.1	374	363	21.0	29.0
37	326	313	11.5	19.2	315	294	12.6	6.2	326	313	10.1	22.5	318	304	11.3	9.1	308	296	12.0	15.0
38	237	231	6.0	57.3	234	229	6.3	55.7	254	250	6.9	51.1	252	248	7.0	49.3	251	247	7.0	50.0
39	142	142	5.3	61.3	142	140	5.7	71.9	152	151	6.1	46.6	153	157	6.3	51.1	152	153	5.8	44.0
40	76	74	1.1	64.6	74	73	4.6	101.0	78	79	4.1	71.6	77	76	5.8	69.7	75	70	5.1	56.0
41	71	74	4.8	80.0	67	63	2.0	51.7	70	71	2.9	30.3	67	63	1.7	25.0	66	61	2.0	23.0
42	19	21	1.1	1463.0	29	26	1.6	1188.0	22	34	2.3	838.0	31	32	2.8	738.0	27	33	2.8	686.0
RMS	132	85			127	79			219	177			217	173			216	171		
MAD	92	51			86	46			172	135			170	131			169	129		

Abbreviation used: M–mode number, ω_h – harmonic frequencies, ω_{anh} – Anharmonic frequencies, A– IR intensity, R_i– Raman intensity

Table 3.6 Theoretical harmonic and scaled vibrational frequencies (cm^{-1}) for L–aspartic acid dimer

#M	D1				D2			
	B3LYP/6–311G(d,p)		B3LYP/6–311++G(d,p)		B3LYP/6–311G(d,p)		B3LYP/6–311++G(d,p)	
	ω_h	ω_{scaled}	ω_h	ω_{scaled}	ω_h	ω_{scaled}	ω_h	ω_{scaled}
1	3587, 3587	3469, 3469	3593, 3593	3474, 3474	3757, 3756	3633, 3632	3757, 3757	3632, 3632
2	3503, 3503	3387, 3387	3511, 3511	3394, 3394	3590, 3590	3472, 3472	3596, 3596	3477, 3477
3	3489, 3489	3374, 3374	3498, 3498	3382, 3382	3494, 3492	3379, 3377	3489, 3487	3373, 3371
4	3154, 3039	3050, 2939	3185, 3082	3079, 2980	3434, 3434	3321, 3321	3440, 3439	3326, 3325
5	3088, 3088	2986, 2986	3093, 3092	2990, 2989	3125, 3125	3022, 3022	3121, 3120	3017, 3016
6	3061, 3061	2960, 2960	3064, 3064	2962, 2962	3065, 3065	2964, 2964	3065, 3065	2963, 2963
7	3051, 3051	2950, 2950	3051, 3051	2950, 2950	3058, 3058	2957, 2957	3059, 3059	2957, 2957
8	1852, 1851	1791, 1790	1836, 1835	1775, 1774	1850, 1849	1789, 1788	1834, 1833	1773, 1772
9	1769, 1717	1711, 1660	1755, 1705	1697, 1648	1805, 1798	1745, 1739	1792, 1787	1733, 1728
10	1667, 1666	1612, 1611	1663, 1663	1608, 1608	1681, 1680	1626, 1625	1679, 1677	1623, 1621
11	1453, 1448	1405, 1400	1455, 1443	1407, 1395	1461, 1458	1413, 1410	1467, 1462	1418, 1413
12	1428, 1426	1381, 1379	1410, 1408	1363, 1361	1442, 1440	1394, 1392	1426, 1425	1379, 1378
13	1406, 1406	1360, 1360	1404, 1404	1357, 1357	1410, 1410	1363, 1363	1407, 1406	1360, 1359
14	1371, 1371	1326, 1326	1367, 1367	1322, 1322	1378, 1374	1333, 1329	1366, 1366	1321, 1321
15	1333, 1320	1289, 1276	1325, 1313	1281, 1269	1370, 1365	1325, 1320	1359, 1355	1314, 1310
16	1285, 1285	1243, 1243	1282, 1282	1239, 1239	1284, 1284	1242, 1242	1281, 1281	1238, 1238
17	1253, 1252	1212, 1211	1249, 1248	1208, 1207	1267, 1265	1225, 1223	1263, 1262	1221, 1220
18	1214, 1214	1174, 1174	1207, 1207	1167, 1167	1223, 1223	1183, 1183	1218, 1218	1178, 1178
19	1156, 1155	1118, 1117	1151, 1151	1113, 1113	1213, 1210	1173, 1170	1208, 1207	1168, 1167
20	1140, 1140	1102, 1102	1134, 1134	1096, 1096	1144, 1141	1106, 1103	1136, 1133	1098, 1095
21	1062, 1061	1027, 1026	1052, 1051	1017, 1016	1128, 1127	1091, 1090	1125, 1124	1088, 1087
22	1033,953	999, 922	1021, 974	987, 942	1051, 1059	1016, 1024	1039, 1038	1005, 1004
23	926, 925	895, 894	923, 922	892, 891	945, 944	914, 913	939, 938	908, 907
24	916, 916	886, 886	909, 908	879, 878	906, 905	876, 875	905, 905	875, 875
25	887, 887	858, 858	887, 887	858, 858	895, 894	865, 864	893, 893	863, 863
26	863, 862	835, 834	857, 856	829, 828	882, 882	853, 853	875, 874	846, 845
27	851, 851	823, 823	840, 839	812, 811	852, 848	824, 820	846, 844	818, 816
28	747, 743	722, 718	744, 740	719, 715	740, 740	716, 716	737, 737	713, 713
29	665, 651	643, 630	667, 655	645, 633	705, 702	682, 679	704, 702	681, 679
30	638, 636	617, 615	635, 634	614, 613	642, 641	621, 620	637, 635	616, 614
31	593, 584	573, 565	594, 587	574, 568	610, 609	590, 589	608, 608	588, 588
32	536, 532	518, 514	528, 525	510, 508	552, 551	534, 533	550, 550	532, 532
33	475, 457	459, 442	477, 457	461, 442	516, 516	499, 499	518, 518	501, 501
34	390, 375	377, 363	391, 379	378, 366	449, 444	434, 429	444, 440	429, 425
35	368, 365	356, 353	355, 351	343, 339	396, 390	383, 377	394, 391	381, 378
36	344, 344	333, 333	330, 329	319, 318	376, 374	364, 362	373, 373	361, 361
37	280, 256	271, 248	274, 248	265, 240	358, 357	346, 345	352, 352	340, 340
38	210, 202	203, 195	208, 196	201, 189	241, 241	233, 233	235, 235	227, 227
39	134, 126	130, 122	129, 123	125, 119	153, 149	148, 144	149, 144	144, 139
40	101, 92	98, 89	96, 88	93, 85	123, 120	119, 116	116, 115	112, 111
41	91, 75	88, 73	83, 78	80, 75	88, 84	85, 81	79, 74	76, 72
42	71, 47	69, 45	67, 46	65, 44	74, 62	72, 60	69, 59	67, 57
RMS	68, 60	34, 38	67, 57	33, 32	108, 107	68, 67	105, 104	66, 65
MAD	53, 48	25, 30	52, 46	25, 27	77, 76	39, 38	73, 72	35, 34

Note: Scaling factor, 0.967 at B3LYP/6–311G(d,p) [66], 0.9668 at B3LYP/6–311++G(d,p) [65]

Table 3.7 Assignments of combinations and overtones bands (in cm^{-1}) in FTIR spectrum of L–aspartic acid.

FTIR	B3LYP							MP2					Interpretation
	6–311G (d,p)		6–311++G(d,p)			cc–pVTZ		6–311G (d,p)		6–311++G(d,p)			
	ω_h	ω_{anh}	ω_h	ω_{anh}	A_{anh} (km/mole)	ω_h	ω_{anh}	ω_h	ω_{anh}	ω_h	ω_{anh}	A_{anh} (km/mole)	
4372	4520	4313	4530	4319	0.060	4531	4329	4596	4391	4591	4387	0.041	$\nu_{11}+\nu_7$
4316	4485	4281	4471	4264	0.004	4476	4275	4568	4379	4542	4357	0.002	$\nu_{12}+\nu_7$
4294	4424	4259	4423	4253	0.050	4423	4250	4504	4332	4488	4323	0.059	$\nu_{14}+\nu_7$
4254	4408	4227	4406	4211	0.047	4413	4226	4481	4306	4467	4291	0.013	$\nu_{15}+\nu_7$
4202	4333	4164	4334	4156	0.048	4336	4164	4401	4228	4393	4223	0.029	$\nu_{16}+\nu_7$
4008	4178	4014	4172	3996	0.009	4172	3995	4239	4076	4231	4063	0.010	$\nu_{21}+\nu_7$
2938	3129	3070	3111	3050	0.004	3118	3063	3148	3081	3120	3055	0.116	$\nu_{16}+\nu_8$
2860	3015	2915	3008	2900	0.022	3013	2927	3024	2921	3012	2909	0.037	$\nu_{15}+\nu_{10}$
2845	2927	2824	2940	2836	0.088	2942	2844	2968	2857	2966	2858	0.054	$2\nu_{11}$
2729	2815	2735	2816	2730	0.028	2824	2749	2853	2770	2843	2761	0.073	$\nu_{15}+\nu_{11}$
2650	2797	2701	2785	2686	0.091	2783	2698	2826	2728	2815	2717	0.078	$\nu_{20}+\nu_{10}$
2603	2706	2617	2685	2597	0.034	2692	2614	2746	2657	2719	2636	0.100	$\nu_{16}+\nu_{12}$
	2703	2616	2692	2591	0.448	2705	2620	2737	2654	2720	2637	0.066	$2\nu_{15}$
2502	2642	2529	2620	2502	1.482	2631	2518	2693	2593	2664	2561	1.549	$\nu_{18}+\nu_{12}$
	2554	2500	2548	2492	0.078	2552	2503	2579	2506	2570	2501	0.108	$2\nu_{16}$
2460	2584	2491	2582	2473	0.090	2582	2489	2602	2498	2596	2495	0.091	$\nu_{23}+\nu_{10}$
2435	2554	2474	2559	2474	0.054	2559	2490	2573	2476	2568	2480	0.033	$\nu_{24}+\nu_{10}$
2397	2491	2427	2483	2410	0.090	2491	2424	2526	2452	2515	2440	0.096	$\nu_{18}+\nu_{16}$
2328	2410	2345	2397	2332	0.037	2399	2337	2459	2389	2448	2378	0.038	$\nu_{20}+\nu_{16}$
	2383	2318	2390	2310	0.105	2393	2316	2430	2352	2427	2350	0.143	$\nu_{23}+\nu_{11}$
2319	2383	2318	2390	2310	0.105	2393	2316	2430	2352	2427	2350	0.143	$\nu_{23}+\nu_{11}$
2241	2331	2274	2315	2255	0.099	2322	2263	2365	2299	2352	2285	0.137	$\nu_{22}+\nu_{16}$
	2318	2236	2309	2225	0.006	2315	2238	2374	2291	2350	2276	0.011	$\nu_{24}+\nu_{12}$
2193	2314	2218	2291	2177	0.098	2296	2188	2369	2280	2339	2247	0.026	$\nu_{25}+\nu_{12}$
	2271	2209	2266	2182	0.138	2275	2198	2315	2247	2304	2234	0.089	$\nu_{23}+\nu_{15}$
2163	2265	2188	2247	2168	0.020	2247	2166	2340	2266	2325	2250	0.042	$2\nu_{20}$
	2253	2190	2243	2163	0.055	2243	2159	2305	2229	2286	2208	0.046	$\nu_{25}+\nu_{14}$
2086	2159	2090	2173	2105	0.068	2177	2109	2198	2116	2195	2127	0.063	$\nu_{29}+\nu_{11}$
	2189	2128	2178	2081	0.003	2187	2098	2232	2171	2220	2151	0.045	$\nu_{27}+\nu_{15}$
2016	2124	2034	2114	2027	0.006	2122	2039	2170	2083	2146	2072	0.003	$\nu_{29}+\nu_{12}$
	2071	2026	2075	2027	0.015	2076	2038	2093	2042	2088	2038	0.009	$\nu_{31}+\nu_{11}$
1998	2089	2038	2080	2022	0.021	2089	2039	2111	2061	2098	2044	0.013	$\nu_{28}+\nu_{15}$
	2084	2026	2097	2024	0.322	2099	2028	2135	2065	2131	2064	0.417	$\nu_{24}+\nu_{19}$
1991	2063	2006	2066	2014	0.016	2069	2008	2106	2025	2093	2038	0.007	$\nu_{29}+\nu_{14}$
1974	2015	1966	2021	1972	0.014	2023	1975	2042	1989	2037	1987	0.006	$\nu_{32}+\nu_{11}$
1966	2036	1966	2016	1945	0.148	2021	1960	2065	2004	2039	1980	0.130	$\nu_{31}+\nu_{12}$
1954	2022	1973	2021	1963	0.041	2022	1968	2087	2031	2078	2022	0.025	$\nu_{24}+\nu_{20}$
1942	2014	1979	2008	1970	0.010	2012	1980	2032	1986	2023	1977	0.000	$\nu_{28}+\nu_{16}$
1933	1975	1935	1968	1927	0.090	1968	1928	2001	1952	1986	1941	0.184	$\nu_{31}+\nu_{14}$
1908	1980	1908	1962	1891	0.057	1968	1903	2015	1955	1988	1931	0.094	$\nu_{32}+\nu_{12}$
1902	1972	1923	1977	1927	0.006	1982	1936	2003	1937	1997	1942	0.001	$\nu_{29}+\nu_{16}$
1895	1959	1913	1950	1894	1.162	1958	1913	1977	1932	1965	1917	0.291	$\nu_{31}+\nu_{15}$
1889	1920	1876	1914	1873	0.071	1915	1868	1951	1901	1935	1892	0.011	$\nu_{32}+\nu_{14}$
1876	2008	1953	1992	1914	0.902	1992	1910	2039	1979	2028	1956	0.554	$\nu_{25}+\nu_{21}$
1868	1943	1898	1939	1886	0.272	1942	1893	1994	1935	1982	1926	0.070	$\nu_{24}+\nu_{22}$
1851	1971	1913	1956	1871	0.458	1958	1871	2033	1980	2023	1962	0.158	$\nu_{27}+\nu_{20}$
1844	1884	1854	1879	1843	0.539	1881	1854	1898	1857	1890	1850	0.403	$\nu_{31}+\nu_{16}$
1829	1960	1911	1945	1866	0.185	1947	1863	1991	1943	1983	1924	0.210	$\nu_{27}+\nu_{21}$
1817	1939	1878	1921	1838	0.020	1926	1840	1988	1920	1971	1892	0.058	$\nu_{25}+\nu_{22}$
1810	1909	1845	1911	1841	0.981	1921	1851	1951	1878	1942	1877	0.383	$\nu_{29}+\nu_{18}$
1656	1771	1712	1759	1660	1.659	1760	1661	1825	1755	1810	1726	4.481	$2\nu_{25}$
1648	1748	1697	1744	1691	0.230	1752	1699	1790	1733	1779	1724	0.983	$\nu_{29}+\nu_{22}$
1380	1437	1400	1430	1373	5.360	1432	1372	1471	1428	1459	1411	0.214	$\nu_{32}+\nu_{25}$
934	933	917	944	935	0.176	944	938	962	939	958	943	0.745	$\nu_{35}+\nu_{32}$

Table: 3.7 (*continued*)

828	882	873	864	853	2.402	865	841	868	862	867	858	37.947	$2\nu_{34}$
748	763	739	786	790	0.027	784	794	807	773	807	793	0.068	$2\nu_{35}$

Abbreviation used: M–mode no., ω_h – harmonic frequencies, ω_{anh} – anharmonic frequencies, A– IR intensity

Table 3.8 Comparison of vibrational frequencies (cm^{-1}) calculated at B3LYP/6–311G (d,p) level of theory, anharmonic IR intensities (km/mole), $\Delta E_{diag.}$ (cm^{-1}) and $\Delta E_{coupl.}$ (cm^{-1}) calculated for each mode.

#M	$\omega_{harm.}$	$\omega_{diagonal}$	ω_{VSCF}	$\omega_{CC-VSCF}$	$I_{anh.}$	$\Delta E_{diag.}$	$\Delta E_{coupl.}$
1	3597	3609	3357	3336	7.1	12	273
2	3572	3430	3283	3311	56.0	–142	119
3	3527	3402	3222	3243	212.0	–125	159
4	3498	3434	3308	3310	23.0	–64	124
5	3133	3188	2968	2958	4.0	55	230
6	3080	3029	2938	2942	2.8	–51	87
7	3052	2955	2858	2877	5.7	–97	78
8	1868	1858	1833	1830	284.0	–10	28
9	1821	1811	1790	1788	306.0	–10	23
10	1663	1662	1641	1636	25.0	–1	26
11	1469	1473	1469	1467	13.0	4	6
12	1420	1430	1397	1388	349.0	10	42
13	1407	1415	1389	1385	84.0	8	30
14	1372	1376	1359	1354	25.0	4	22
15	1353	1361	1335	1332	21.0	8	29
16	1278	1285	1268	1264	8.1	7	21
17	1257	1262	1258	1255	72.0	5	7
18	1213	1217	1210	1206	123.0	4	11
19	1204	1205	1181	1177	12.0	1	28
20	1120	1120	1095	1092	22.0	0	28
21	1111	1119	1130	1127	76.0	8	–8
22	1045	1047	1044	1042	67.0	2	5
23	931	939	964	969	29.0	8	–30
24	900	900	896	901	55.0	0	–1
25	870	888	921	884	63.0	18	4
26	844	857	872	858	37.0	13	–1
27	833	935	890	842	89.0	102	93
28	772	888	833	858	113.0	116	30
29	740	740	735	733	7.8	0	7
30	690	699	724	706	1.9	9	–7
31	604	606	609	607	43.0	2	–1
32	571	572	579	576	6.4	1	–4
33	516	517	525	533	3.4	1	–16
34	426	433	470	460	8.5	7	–27
35	391	400	425	405	11.0	9	–5
36	375	415	471	340	21.0	40	75
37	334	432	448	311	3.3	98	121
38	227	228	229	228	4.7	1	0
39	138	140	148	146	8.2	2	–6
40	79	92	107	98	0.9	13	–6
41	55	75	84	79	2.2	20	–4
42	47	79	118	113	5.4	32	–34
RMS	116	116	92	86			
MAD	76	82	71	63			

Abbreviation useds: M– mode number, $\omega_{harm.}$, $\omega_{diagonal}$, ω_{VSCF}, $\omega_{CC-VSCF}$, ω_{PT2}–frequencies using harmonic, diagonal, VSCF, CC–VSCF and PT2 approaches respectively, I_{anh}– anharmonic intensity using VSCF, $\Delta E_{diag.}$– contribution of intrinsic anharmonicity , $\Delta E_{coupl.}$– contribution of mode–mode coupling anharmonicity

3.4.3 Natural bond orbital analysis

The natural bond orbitals (NBOs) and their interactions were analyzed at B3LYP/6–311G(d,p) level of theory with the NBO 3.0 program [68] implemented in Gaussian 09 software [57]. NBOs are localized centre orbitals that explain the Lewis like molecular bonding patterns of electron pairs or individual electrons in the open shell case [93, 94]. NBO analysis gives the information about interactions in both filled and virtual orbitals that help to know intramolecular and intermolecular interactions [94]. The hybridization of filled orbital for monomer is shown in Table 3.9. The second order perturbation energy values, $E^{(2)}$ [95], corresponding to the interactions and the overlap integral of orbital pair are presented in Table 3.10. The large values of $E^{(2)}$, 40.44 and 40.25 kcal/mole (Table 3.10) represent strong hyperconjugative interactions between the orbital containing the lone pair of electron of O_1, O_4 and the neighbour O_2=C_5, O_3=C_8 antibonding orbitals of carboxylic acid group respectively. Relatively high stabilization energies were observed from the interactions $n(LP_2O1) \rightarrow \pi^*(O2=C5)$, $n(LP_2O2) \rightarrow \sigma^*(O1=C5)$, $n(LP_2O2) \rightarrow \sigma^*(C5–C6)$, $n(LP_2O3) \rightarrow \sigma^*(O4–C8)$ and $n(LP_2O4) \rightarrow \pi^*(O3=C8)$. The hyperconjugative interaction and electron density transfer from lone pair electrons of the N9 atom to the O1–H16 antibonding orbital in the O1–H16···N9 system have been predicted. This hydrogen bonding is formed by the orbital overlap between $n(LP_1N9)$ and $\sigma^*(O1–H16)$ which consequences intramolecular charge transfer (ICT) causing stabilization of the hydrogen bonded system. Hence, hydrogen bonding interaction leads to an increase in electron density of O–H antibonding orbital. The NBO analysis of L–aspartic acid clearly shows the evidences of the formation of strong hydrogen bond. The stabilization energy, $E^{(2)}$, associated with hyperconjugative interaction $n(LP_1N9) \rightarrow \sigma^*(O1–H16)$, $n(LP_1N9) \rightarrow \sigma^*(C5–C6)$ and $n(LP_1N9) \rightarrow \sigma^*(C6–C7)$ are 10.26, 3.61and 6.85 kcal/mole respectively (Table 3.10) which quantify the intramolecular hydrogen bonding.

The NBO analysis of L–aspartic acid dimers has shown evidences of the formation of stabilized hydrogen bonded intermolecular interaction between lone pair LP (O) and antibonding σ* N–H/O–H orbitals at B3LYP/6–311G(d,p) level of theory. The NBO analysis of monomer and dimers has also revealed the presence of intramolecular interactions between lone pair LP (N) and antibonding σ* O–H orbital. The intermolecular charge transfer due to $n(LPO) \rightarrow \sigma^*(O–H)$ and $n(LPO) \rightarrow$

σ*(N–H) causes the stabilization of dimers D1 and D2 respectively. The stabilization energy, $E^{(2)}$, between hydrogen bonded orbitals determined by second order perturbation analysis of Fock matrix for L–aspartic acid dimers, are summerized in Table 3.11. This stabilization energy measures the strength of the hydrogen bonding. The intermolecular hydrogen bonds are formed by overlapping between the orbitals n(LPO) and σ*(N–H)/(O–H) and, hence, it leads to increase the electron density of antibonding orbital. The stabilization energy, $E^{(2)}$, associated with hyperconjugative interactions $n(LP_1O) \rightarrow \sigma^*(O–H)$, $n(LP_2O) \rightarrow \sigma^*(O–H)$ and $n(LP_1O) \rightarrow \sigma^*(N–H)$ were, respectively, 8.7, 23.6 and 2.8 kcal mol^{-1}, which measure the extent of intermolecular hydrogen bonding. The low value of stabilization energy is found for interaction $n(LP_1O) \rightarrow \sigma^*(N–H)$ that shows weak strength of hydrogen bond. Moreover, it is predicted that the total minimum SCF energy in the dimeric form is more than twice of the total energy of the monomer (Table 3.1). This shows that dimer is more stable than the monomer because of the existence of intermolecular hydrogen bonding.

Table 3.9 NBO analysis for L–aspartic acid at B3LYP/6–311G(d,p) level of theory.

Bond (A–B)	Occupancy	ED_A %	ED_B %	NBO (% p character)
σ(O1–C5)	1.99562	68.15	31.85	$0.8256\ sp^{2.02}(66.86)_O + 0.5643\ sp^{2.51}(71.33)_C$
σ(O1–H16)	1.98494	76.04	23.96	$0.8720\ sp^{3.41}(77.25)_O + 0.4895\ sp^{0.00}(0.25)_H$
σ(O2–C5)	1.99551	65.86	34.14	$0.8115\ sp^{1.55}(60.71)_O + 0.5843\ sp^{2.11}(67.73)_C$
π(O2–C5)	1.99155	68.96	31.04	$0.8304\ sp^{30.82}(96.74)_O + 0.5571\ sp^{40.16}(97.12)_C$
σ(O3–C8)	1.99627	65.89	34.11	$0.8117\ sp^{1.41}(58.50)_O + 0.5840\ sp^{1.98}(66.37)_C$
π(O3–C8)	1.99202	69.17	30.83	$0.8317\ sp^{99.99}(98.94)_O + 0.5553\ sp^{99.99}(98.75)_C$
σ(O4–C8)	1.99583	69.17	30.83	$0.8317\ sp^{1.94}(65.91)_O + 0.5553\ sp^{2.76}(73.20)_C$
σ(O1–H10)	1.98736	74.65	25.35	$0.8640\ sp^{3.76}(78.93)_O + 0.5035\ sp^{0.00}(0.18)_H$
σ(C5–C6)	1.97957	46.90	53.10	$0.6849\ sp^{1.72}(63.18)_C + 0.7287\ sp^{2.93}(74.51)_C$
σ(C6–C7)	1.97270	49.80	50.20	$0.7057\ sp^{2.38}(70.41)_C + 0.7085\ sp^{2.42}(70.77)_C$
σ(C6–N9)	1.98997	39.74	60.26	$0.6304\ sp^{3.20}(76.12)_C + 0.7763\ sp^{1.98}(66.39)_N$
σ(C6–H15)	1.95545	61.32	38.68	$0.7831\ sp^{3.67}(78.50)_C + 0.6219\ sp^{0.00}(0.04)_H$
σ(C7–C8)	1.97967	51.75	48.25	$0.7194\ sp^{2.76}(73.37)_C + 0.6946\ sp^{1.55}(60.77)_C$
σ(C7–H11)	1.95322	62.62	37.38	$0.7913\ sp^{3.56}(78.02)_C + 0.6114\ sp^{0.00}(0.04)_H$
σ(C7–H12)	1.97475	61.18	38.82	$0.7822\ sp^{3.47}(77.57)_C + 0.6231\ sp^{0.00}(0.02)_H$
σ(N9–H13)	1.99180	68.27	31.73	$0.8263\ sp^{3.17}(75.97)_N + 0.5633\ sp^{0.00}(0.06)_H$
σ(N9–H14)	1.98976	68.86	31.14	$0.8298\ sp^{3.09}(75.47)_N + 0.5580\ sp^{0.00}(0.06)_H$
Lone Pairs				
LP_1O1	1.97294			$sp^{1.26}(55.70)$
LP_2O1	1.79293			$sp^{1.00}(99.92)$
LP_1O2	1.97898			$sp^{0.73}(42.30)$
LP_2O2	1.84442			$sp^{99.99}(99.91)$
LP_1O3	1.97737			$sp^{0.73}(42.30)$
LP_2O3	1.84212			$sp^{1.00}(99.92)$
LP_1O4	1.97888			$sp^{1.22}(54.99)$
LP_2O4	1.82788			$sp^{1.00}(99.94)$
LP_1N9	1.92679			$Sp^{4.57}(82.01)$

Abbreviation used: ED– Electron density

Table 3.10 Second order perturbation theory analysis of Fock matrix in NBO basis for L aspartic acid at B3LYP/6–311G(d,p) level of theory.

Donor–acceptor interaction	$E^{(2)a}$ (kcal/mol)	E(j)–E(i)[b] (a.u.)	F(i, j)[c] (a.u.)
$n(LP_1O1) \rightarrow \sigma^*(O2–C5)$	0.96	1.19	0.030
$n(LP_1O1) \rightarrow \sigma^*(C5–C6)$	5.86	0.94	0.067
$n(LP_2O1) \rightarrow \sigma^*(O2–C5)$	1.49	0.91	0.034
$n(LP_2O1) \rightarrow \pi^*(O2–C5)$	40.44	0.39	0.111
$n(LP_1O2) \rightarrow \sigma^*(O1–C5)$	1.41	1.06	0.035
$n(LP_1O2) \rightarrow \sigma^*(C5–C6)$	2.60	1.02	0.047
$n(LP_2O2) \rightarrow \sigma^*(O1–C5)$	30.61	0.64	0.127
$n(LP_2O2) \rightarrow \sigma^*(C5–C6)$	21.04	0.59	0.101
$n(LP_2O2) \rightarrow \sigma^*(C6–N9)$	0.55	0.57	0.016
$n(LP_1O3) \rightarrow \sigma^*(O4–C8)$	1.33	1.03	0.034
$n(LP_1O3) \rightarrow \sigma^*(C7–C8)$	2.56	1.07	0.047
$n(LP_2O3) \rightarrow \sigma^*(O4–C8)$	33.95	0.61	0.130
$n(LP_2O3) \rightarrow \sigma^*(C7–C8)$	18.31	0.65	0.100
$n(LP_1O4) \rightarrow \sigma^*(O3–C8)$	5.54	1.24	0.074
$n(LP_2O4) \rightarrow \pi^*(O3–C8)$	40.25	0.37	0.109
$n(LP_1N9) \rightarrow \sigma^*(O1–H16)$	10.26	0.74	0.078
$n(LP_1N9) \rightarrow \sigma^*(C5–C6)$	3.61	0.69	0.045
$n(LP_1N9) \rightarrow \sigma^*(C6–C7)$	6.85	0.70	0.063

[a]Energy of hyper conjugative interaction (stabilization energy).
[b]Energy difference between donor and acceptor; i and j NBO orbitals.
[c]Fock matrix element between i and j NBO orbitals.

Table 3.11 Important donor–accepter inter/intra–molecular interactions based on second order perturbation theory analysis of Fock matrix in NBO basis for L–aspartic acid dimer at B3LYP/6–311G(d,p) level of theory.

Donor–acceptor intermolecular interaction	ED_i (e)	ED_j (e)	$E^{(2)a}$ (kcal/mol)	E(j)–E(i)[b] (a.u.)	F(i, j)[c] (a.u.)
unit 1 (D1)					
$n(LP_1N9) \rightarrow \sigma^*(O1–H16)$	1.92721	0.03673	9.93	0.74	0.077
from unit 1 to 2 (D1)					
$n(LP_1O3) \rightarrow \sigma^*(O20–H26)$	1.95556	0.07505	8.72	1.05	0.086
$n(LP_2O3) \rightarrow \sigma^*(O20–H26)$	1.84397	0.07505	23.58	0.70	0.117
from unit 2 to 1 (D1)					
$n(LP_1O19) \rightarrow \sigma^*(O4–H10)$	1.95556	0.07505	8.72	1.05	0.086
$n(LP_2O19) \rightarrow \sigma^*(O4–H10)$	1.84397	0.07505	23.58	0.70	0.117
unit 2 (D1)					
$n(LP_1N9) \rightarrow \sigma^*(O1–H16)$	1.92721	0.03673	9.93	0.74	0.077
unit 1 (D2)					
$n(LP_1N9) \rightarrow \sigma^*(O1–H16)$	1.91837	0.04253	12.14	0.72	0.084
from unit 1 to 2 (D2)					
$n(LP_1O3) \rightarrow \sigma^*(N25–H29)$	1.97152	0.01383	2.82	1.16	0.051
from unit 2 to 1 (D2)					
$n(LP_1O19) \rightarrow \sigma^*(N9–H13)$	1.97152	0.01383	2.82	1.16	0.051
unit 2 (D2)					
$n(LP_1N25) \rightarrow \sigma^*(O17–H32)$	1.91837	0.04253	12.14	0.72	0.084

Abbreviation used: ED_i - Electron density (e) for donor orbital, ED_j - Electron density (e) for acceptor orbital
[a]Energy of hyper conjugative interaction (stabilization energy).
[b]Energy difference between donor and acceptor; i and j NBO orbitals.
[c]Fock matrix element between i and j NBO orbitals.

3.4.4 Molecular electrostatic potential map

The Molecular electrostatic potential (MEP) maps have been used to predict the behaviour and reactivity of the molecules (section 2.2.7). MEP map is very useful in studying the electrophilic and nucleophilic reactions for the study of biological recognition process and hydrogen bonding interactions [96]. The surfaces over MEP maps with blue, red and green colours indicate the positive, negative, and zero potential respectively. MEP map for the L–aspartic acid at B3LYP/6–311G(d,p) level of theory is shown in Fig. 3.11 with colour range from –6.29E–2 (deepest red) to +6.29E–2 (deepest blue). The red colour surfaces with negative MEP correspond to high electron density, indicating a strong attraction between the proton and points on the molecular surface. The blue colour surfaces correspond to areas of low electron density. In MEP map, the surfaces over the O2 (–0.056 a.u.) and O1 (–0.048 a.u.) oxygen atoms, representing high value of negative electrostatic potential and the surfaces over the H10 (0.067 a.u.) with high value of positive electrostatic potential may be site of electrophilic and nucleophilic reactions respectively. The knowledge of the molecular reactive site enables workers to predict how complex drugs interact with proteins.

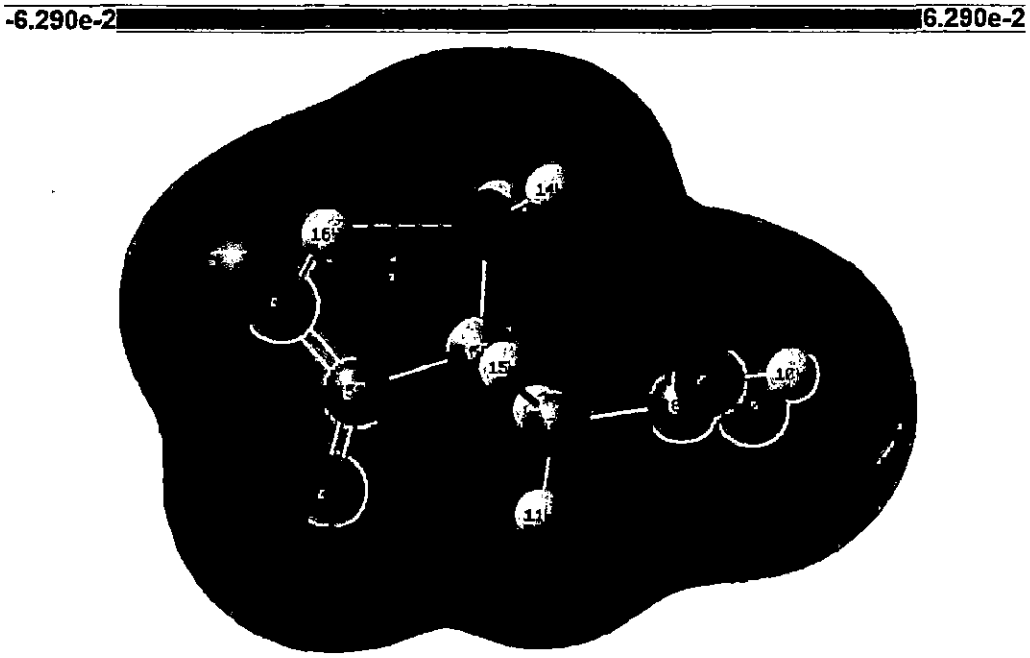

Fig. 3.11 Molecular electrostatic potential map for L–aspartic acid.

3.4.5 Frontier molecular orbitals

The frontier orbitals, HOMO and LUMO are very important parameters for determining the way the molecule interacts with other species. HOMO, the outermost orbital containing electrons has tendency to release electrons as an electron donor. On the other hand, LUMO orbital has free space to accept electrons as electron acceptor. The ability of charge transfer interactions within molecule can be explained by the HOMO–LUMO energy gap. The lowest excitation energy can be approximated as HOMO–LUMO gap using TD–DFT theory [97]. The density of state (DOS) spectrum and 3D frontier molecular orbitals (FMOs) plots are shown in Fig. 3.12. The positive and negative phases are represented by red and green colour respectively. The number of molecular orbitals between energy intervals of E and E+dE defines DOS for the molecule. It can be seen from this figure, that FMOs are localized on almost the whole molecule. The negative orbital energy of the HOMO and the energy of the LUMO provides the 1st ionization energy and electron affinity of a molecular system respectively [98]. The energy values of HOMO and LUMO and their energy gap show the chemical activity and kinetic stability of the molecule. The HOMO, LUMO energy eigenvalues and gap between them at B3LYP/cc–pVTZ level are shown in Fig. 3.12. The lowering of HOMO–LUMO energy gap supports bioactive property of the molecule.

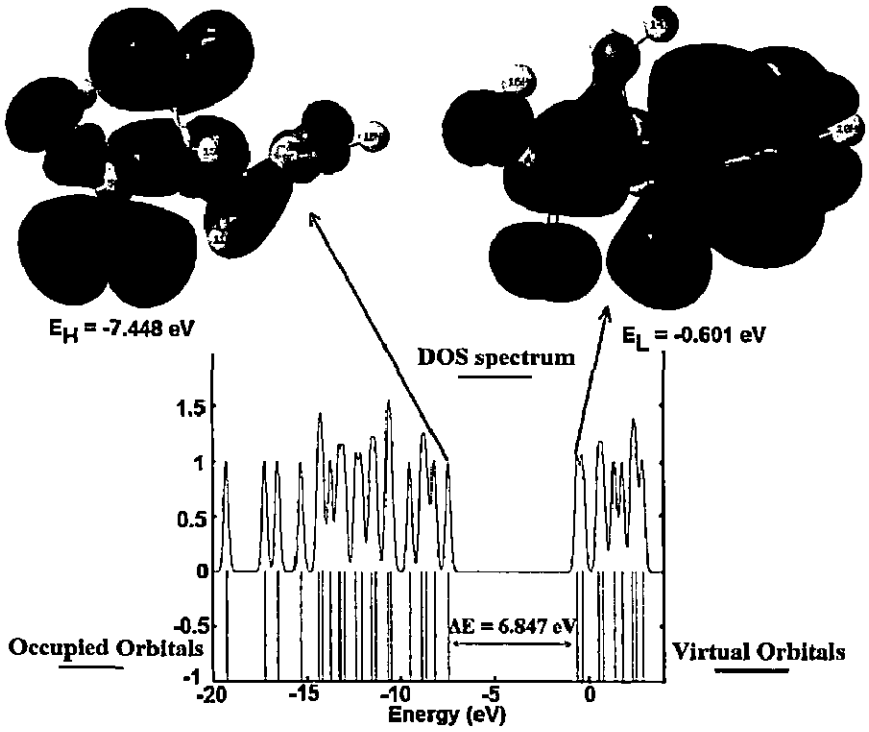

Fig. 3.12 HOMO, LUMO plots and DOS spectrum for L–aspartic acid at B3LYP/cc–pVTZ.

3.4.6 Other molecular properties

The theoretical data obtain during geometry optimization provides various molecular properties. The atomic charge on the each atom in molecule was computed at B3LYP/6–311G(d,p) level of theory by NBO analysis. Mullikan atomic charges were also computed using HF, MP2 and DFT (B3LYP) methods with 6–311G(d,p), 6–311++G(d,p) and cc–pVTZ basis sets. These are presented in Table 3.12. In NBO analysis, atomic charges are calculated by summing occupancy of natural atomic orbitals. It may be noted that the nitrogen atom (N9) and carbon atom (C8) have large negative and positive net natural charge respectively. All the hydrogen atoms connected with large electronegative atoms have net positive charge. The negative natural charge on N9 (–0.875), O1 (–0.676), O2 (–0.589), O3 (–0.585) and O4 (–0.710) atoms may support the formation of intermolecular interactions in solid form. In the present work, the large negative charge on N9 (–0.875) and positive charge on H16 (0.490) also support the formation of strong hydrogen bonding between them. The comparisons of atomic charges for L–aspartic acid monomer and dimers at different theories are shown in Fig. 3.13. The natural atomic charges for L–aspartic acid in monomer and dimers computed at B3LYP/6–311G(d,p) level of theory are depicted in Table 3.12. The shifts in natural atomic charges in dimers have been noticed due to presence of intermolecular hydrogen bonding interactions. The atoms O3, C7, C8 and H10, which are involved in formation of intermolecular hydrogen bonded dimer D1, show the significant changes in the charge values. This strengthens the hydrogen bond and stabilizes the dimeric structures.

Table 3.12 Atomic charges (e) for L–aspartic acid at different levels of theory.

Atoms	B3LYP				MP2		HF			D1	D2
	6–311 G(d,p)		6–311++ G(d,p)	cc–pVTZ	6–311 G(d,p)	6–311++ G(d,p)	6–311 G(d,p)	6–311++ G(d,p)	cc–pVTZ	B3LYP/ 6–311 G(d,p)	B3LYP/ 6–311 G(d,p)
O1	–0.296	–0.675	–0.179	–0.232	–0.404	–0.260	–0.394	–0.257	–0.287	–0.675	–0.675
O2	–0.329	–0.589	–0.274	–0.295	–0.455	–0.348	–0.441	–0.346	–0.372	–0.589	–0.595
O3	–0.319	–0.585	–0.249	–0.293	–0.443	–0.318	–0.435	–0.331	–0.376	–0.667	–0.646
O4	–0.331	–0.710	–0.159	–0.269	–0.431	–0.220	–0.421	–0.231	–0.331	–0.7	–0.692
C5	0.400	0.819	–0.064	0.291	0.584	–0.035	0.586	–0.022	0.387	0.82	0.82
C6	–0.168	–0.118	–0.116	–0.067	–0.102	–0.003	–0.115	–0.004	–0.034	–0.122	–0.115
C7	–0.232	–0.512	–0.467	–0.176	–0.197	–0.540	–0.193	–0.548	–0.199	–0.508	–0.513
C8	0.328	0.833	0.033	0.268	0.5012	0.104.	0.495	0.157	0.380	0.868	0.861
N9	–0.506	–0.875	–0.369	–0.348	–0.576	–0.383	–0.565	–0.388	–0.430	–0.872	–0.891
H10	0.257	0.482	0.292	0.219	0.282	0.315	0.279	0.318	0.245	0.508	0.482
H11	0.177	0.258	0.232	0.136	0.176	0.245	0.169	0.245	0.152	0.263	0.259
H12	0.145	0.222	0.230	0.117	0.143	0.256	0.139	0.250	0.137	0.226	0.233
H13	0.218	0.359	0.260	0.149	0.224	0.281	0.219	0.271	0.166	0.354	0.393

Table: 3.12 (*continued*)

H14	0.228	0.372	0.273	0.155	0.232	0.297	0.227	0.292	0.171	0.377	0.365
H15	0.177	0.228	0.257	0.131	0.173	0.289	0.166	0.282	0.144	0.228	0.224
H16	0.251	0.490	0.300	0.213	0.292	0.320	0.283	0.311	0.246	0.49	0.491

Note: The underlined values are natural charges and the others are Mullikan charges

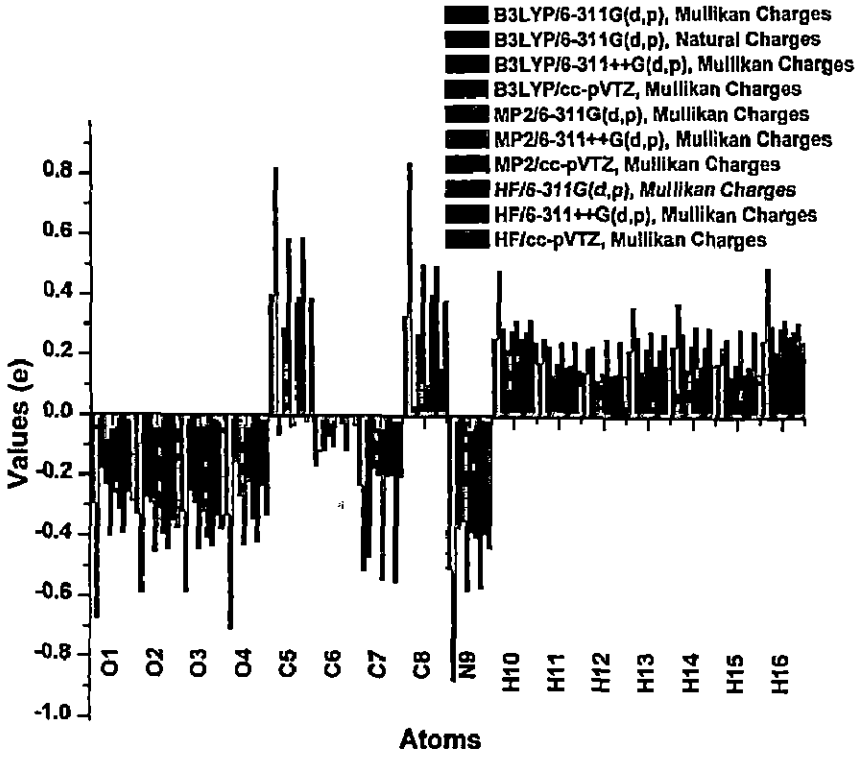

Fig. 3.13 Atomic charges for L–aspartic acid at different theories.

The quantum chemical calculations play crucial role in designing non–linear optical (NLO) molecules and predicting some related properties such as molecular dipole moments, polarizabilities and hyperpolarizabilities [99, 100]. The computation of polarizabilities and hyperpolarizabilities of the organic compounds are of great significance to study the phenomenon induced by intermolecular interactions and non–linear optical effects (section 2.2.7). The total molecular dipole moment and mean first order hyperpolarizability of L–aspartic acid are 5.873 Debye and 1.403 x 10^{-30} esu respectively at B3LYP/cc–pVTZ level of theory. The value of mean first order hyperpolarizability of L–aspartic acid is about 4 times greater than the value for urea (β_o = 0.3728 x 10^{-30} esu) [101]. The high value of first order hyperpolarizability of L–aspartic acid reflects its non–linear property. The permanent electric dipole moment of a molecule is an important indicator of its behaviour in physical, chemical and biological process [102]. It is measure of the charge density in a molecule and is a reactivity index, which is important to study biological properties related to the

interaction with active site of an enzyme [103]. The magnitude and direction of dipole moment are sensitive to molecular size and shape and they serve as tool in conformational analysis [104]. Molecular polarizability and first order static hyperpolarizability values are collected in Table 3.13. Calculated dipole moments are tabulated in Table 3.14. The high values of dipole moment and first order hyperpolarizability are indicating nonlinearity.

Knowledge on thermodynamic properties is a key in understanding the rate and selectivity of chemical process including design of feasible industrial chemical process. The experimental determination of such properties is not possible in some cases [105]. Computational methods are valuable and sometimes indispensable tool in obtaining the thermodynamic quantities of molecules. The lack of thermodynamic data for the gas phase of amino acids is explained by the limitations that are due to their ion volatility and low thermal stability. Several thermodynamic parameters such as enthalpy, heat capacity, free energy and entropy of L–aspartic acid have been computed at different levels of theory. The values related to thermodynamic and other molecular properties are tabulated in Table 3.14. In this work, the global reactivity descriptors based on HOMO and LUMO energy eigenvalues such as electronic chemical potential (μ), the absolute chemical hardness (η), chemical softness (S) and the global electrophilicity (ω) are computed using DFT calculations. The theory related to chemical reactivity descriptors can be found in texts [73–75, 106]. The global electrophilicity index measures the tendency of chemical species to accept the electrons. Thus, the good electrophile and nucleophile can be characterized by low and high value of electrophilicity index respectively [106, 107]. The HOMO and LUMO energy eigenvalues, HOMO–LUMO energy gap and chemical reactivity descriptors are presented in Table 3.14.

Table 3.13 Calculated components of polarizability (a.u.), first order hyperpolarizability β (a.u.), mean polarizability $\langle\alpha\rangle$ (a.u.), anisotropy of the polarizability γ (a.u.) and the mean first order hyperpolarizability β_0 (esu, 1 a.u.=8.639 x 10^{-33} esu) of L–aspartic acid.

	B3LYP			MP2			B3LYP			MP2	
	6–311 G(d,p)	6–311++ G(d,p)	cc–pVTZ	6–311 G(d,p)	6–311++ G(d,p)		6–311 G(d,p)	6–311++ G(d,p)	cc–pVTZ	6–311 G(d,p)	6–311++ G(d,p)
α_{xx}	71.858	81.697	77.752	68.339	78.213	β_{xxx}	86.207	121.354	98.462	66.639	69.848
α_{xy}	0.755	2.012	1.720	2.268	2.634	β_{xxy}	35.945	23.307	13.383	12.297	13.405
α_{yy}	60.292	67.698	63.540	58.550	67.552	β_{xyy}	43.096	26.720	34.464	32.975	19.230
α_{xz}	–0.705	–1.116	–0.363	–0.772	–1.121	β_{yyy}	13.567	23.747	8.998	–25.158	–7.516
α_{yz}	1.424	0.044	0.266	0.299	–0.460	β_{xxz}	44.175	33.462	42.159	28.533	14.702

Table: 3.13 (*continued*)

α_{xx}	50.996	59.972	56.430	51.791	59.477	β_{xyz}	9.656	4.559	9.260	7.662	3.101
$\langle\alpha\rangle$	61.049	69.789	65.907	59.560	68.414	β_{yyz}	11.966	12.345	6.049	11.603	10.699
γ	18.360	19.486	19.054	15.005	17.034	β_{xzz}	22.084	8.520	22.043	19.067	3.293
						β_{yzz}	7.310	14.308	11.410	7.019	13.421
						β_{zzz}	–23.396	–16.188	–13.263	–26.678	–29.708
						β_0 x 10^{-30}	1.425	1.475	1.403	1.033	0.816

Table 3.14 Calculated zero point vibrational energy, thermodynamic quantities (at 298.15 K), rotational constants, rotational temperatures, energies of frontier molecular orbitals, global reactivity descriptors and dipole moment of L–aspartic acid.

Parameters	B3LYP			MP2		HF		
	6–311 G(d,p)	6–311 ++G(d,p)	cc–pVTZ	6–311 G(d,p)	6–311 ++G(d,p)	6–311 G(d,p)	6–311 ++G(d,p)	cc–pVTZ
Zero point vibrational energy (kcal mole^{-1})	77.729 76.816[a]	77.586 76.470[a]	77.589 76.463[a]	78.915 77.847[a]	78.559 77.471[a]	84.142 83.179[a]	84.001 83.009[a]	83.916 82.935[a]
Rotational constants (GHz)								
A	3.373	3.333	3.349	3.378	3.352	3.464	3.452	3.457
B	0.881	0.878	0.881	0.895	0.897	0.894	0.893	0.895
C	0.793	0.802	0.805	0.819	0.819	0.817	0.817	0.819
Rotational temperatures (K)	0.162 0.042 0.038	0.160 0.042 0.038	0.161 0.042 0.039	0.162 0.042 0.039	0.161 0.043 0.039	0.166 0.043 0.039	0.166 0.043 0.039	0.166 0.043 0.039
Total energy (thermal) (kcal mol^{-1})	83.492 82.505[a]	83.377 82.376[a]	83.387 82.426[a]	84.637 83.662[a]	84.302 83.329[a]	89.668 88.764[a]	89.532 88.626[a]	89.462 88.566[a]
Molar capacity at const. volume, C_v (cal mol^{-1} K^{-1})	32.410 32.894[a]	32.522 33.250[a]	32.493 33.389[a]	31.989 32.756[a]	32.163 32.940[a]	30.540 31.176[a]	30.626 31.276[a]	30.631 31.283[a]
Molar capacity at const. pressure, C_p (cal mol^{-1} K^{-1})	34.398 34.880[a]	34.510 35.239[a]	34.479 35.378[a] 37.089	33.977 34.742[a]	34.152 34.926[a]	32.526 33.162[a]	32.615 33.262[a]	32.617 33.272[a]
Total Entropy, S (cal mol^{-1} K^{-1})	97.572 94.089[a]	97.237 101.575[a]	97.701 98.435[a]	97.103 97.371[a]	96.613 97.553[a]	95.657 95.203[a]	95.203 95.655[a]	95.593 95.880[a]
Total Enthalpy, H (kcal mol^{-1})	84.085 83.098[a]	83.970 82.968[a]	83.979 83.019[a]	85.227 84.254[a]	84.895 83.922[a]	90.258 89.357[a]	90.124 89.218[a]	90.055 89.159[a]
Field independent dipole moment (Debye)								
μ_x	2.742 (3.384)	2.827 (3.481)	2.664 (3.278)	3.267	3.273	2.750	2.753	2.605
μ_y	3.772 (4.765)	3.325 (4.633)	3.321 (4.655)	3.260	3.110	3.478	3.405	3.278
μ_z	0.622 (1.100)	1.361 (1.664)	1.299 (1.440)	1.453	1.700	1.361	1.493	1.588
μ_{total}	4.704 (5.947)	4.572 (6.030)	4.451 (5.873)	4.839	4.824	4.638	4.627	4.478
Frontier MO Energies (eV)								
E_{LUMO+1}	–0.163 (–0.089)	–0.884 (–0.559)	–0.294 (–0.008)	4.010	2.410	4.254	1.269	4.002
E_{LUMO}	–0.490 (–0.345)	–1.014 (–0.774)	–0.601 (–0.458)	3.174	2.174	3.292	0.787	3.036
E_{HOMO}	–7.347 (–7.314)	–7.619 (–7.559)	–7.448 (–7.402)	–11.740	–11.850	–11.606	–11.722	–11.616
E_{HOMO-1}	–8.163 (–7.991)	–8.412 (–8.269)	–8.207 (–8.082)	–12.752	–12.890	–12.649	–12.800	–12.665
$E_{LUMO} - E_{HOMO}$	6.857 5.554	6.605 5.430	6.847 5.544	14.914	14.024	14.898	12.509	14.652

Table: 3.14 (*continued*)

	(5.620)	(5.507)	(5.616)
Global reactivity descriptors (eV)			
Ionization potential, I	7.347	7.619	7.448
Electron affinity, A	0.490	1.014	0.601
Electronegativity, χ	–3.919	–4.317	–4.025
Chemical potential, μ	3.919	4.317	4.025
Electrophilicity, ω	2.240	2.821	2.366
Hardness, η	3.429	3.303	3.424
Softness, S	0.146	0.151	0.146

*anharmonic value

Note: the numerical values given in parenthesis are calculated using PCM model (ethanol solution), the underline values are calculated using TD–B3LYP

3.5 Conclusion

Complete vibrational studies of L–aspartic acid molecule have been carried out using experimental information and quantum chemical HF, MP2 and DFT computations. The optimized geometrical parameters, harmonic and anharmonic vibrational frequencies along with relative intensities, vibrational assignments, MEP mapping, various molecular properties, HOMO–LUMO and NBO analysis of L–aspartic acid have been presented using quantum chemical calculations. The RMS and MAD values reflect the accuracy of the MP2 and DFT values. The calculated structural parameters and anharmonic vibrational spectra show good correlation with experimentally observed data. Vibrational assignments have been made with high degree of accuracy using PED values and animated modes. Combination and overtone bands in the FTIR are also assigned with the help of theoretical anharmonic force field calculations. The frequencies of stretching and torsional vibrations are appeared with large deviation from experimental values. This may be due to large anharmonicity associated to these vibrations (i.e large amplitude of vibrations) and rectilinear coordinates used in calculations to define vibrations. Rectilinear coordinates are useful to define small amplitude of vibrations. Any further discrepancy noted between calculated and experimental results may be due to the fact that the calculations have been done on a single molecule in gaseous state contrary to the experimental results carried out in the presence of intermolecular interactions. The present studies demonstrate that DFT (B3LYP) calculations with anharmonic approximations are powerful approach for understanding the vibrational spectra of L–aspartic acid. The atomic charge calculations and NBO analysis confirm the presence of intramolecular hydrogen bonding O1– –H16–N9 in L–aspartic acid. The molecular structure and vibrational analysis along with NBO analysis have been also

carried out for L–aspartic molecule in dimeric form using DFT/B3LYP method in the harmonic approximation. The dimeric parameters are well comparable with solid phase experimental data. The scaled harmonic frequencies of many vibrational modes of L–aspartic acid in intermolecular complexes have lower values than those of monomer, which reveals the existence of intermolecular hydrogen bonds. The NBO analysis has also shown the presence of strong intermolecular interactions: O···H–N–H and O···H–O. In MEP map, the surfaces over the O2 and O1 oxygen atoms with high value of negative electrostatic potential are the predicted site for electrophilic attack while the surface over the H10 with high value of positive electrostatic potential may be site of nucleophilic attack.

References

[1]. http://dx.doi.org/10.1351/pac198456050595.
[2]. P. M. Helfman, J. L. Bada, Proc. Nat. Acad. Sci. 72 (1975) 2891–2894.
[3]. E. R. Waite, M. J. Collins, S. R. Timme, H. W. Schutz, C. Cattaneo, H. I. M. Borrman, Forensic Sci. Int. 103 (1999) 113–124.
[4]. L. E. Nita, A. P. Chiriac, C. M. Popescu, I. Neamtu, L. Alecu, J. Optoelec. and Adv. Materials 8 (2006) 663–666.
[5]. Y. H. Hofstee et al. Human Mutation 31 (2010) 1915–1927.
[6]. P. S. Kushwaha, P. C. Mishra, J. Mol. Struct. (Theochem) 549 (2001) 229–242.
[7]. M. E. Sanz, J. C. Lopez, J. L. Alonso, Phys. Chem. Chem. Phys. 12 (2010) 3573–3578.
[8]. W. S. Aroon, V. Ruangpornvisuti, J. Mol. Struct. (Theochem) 758 (2006) 181–187.
[9]. M. Chen, Z. Lin, J. Chem. Phys. 127 (2007) 154314–154325.
[10]. J. T. L. Navarrete, V. Hernandez, F. J. Ramirez, Biopolymers 34 (1994) 1065–1077.
[11]. J. T. L. Navarrete, V. Hernandez, F. J. Ramirez, J. Mol. Struct. 348 (1995) 249–252.
[12]. J. L. Castro, M. A. Montanez, J. C. Otero, J. I. Marcos, J. Mol. Struct. 349 (1995) 113–116.
[13]. M. E. Mohamed, A. M. A. Mohammed, Int. J. Lett. Chem. Phys. Astro. 10 (2013) 1–17.
[14]. R. Flaig, T. Koritsanszky, D. Zobel, P. Luger, J. Am. Chem. Soc. 120 (1998) 2227–2238.
[15]. J. L. Derissen, H. J. Endeman, A. F. Peerdeman, Acta Cryst. B 24 (1968) 1349–1354.
[16]. T. Kimura, N. Matubayasi, H. Sato, F. Hirata, M. Nakahara, J. Phys. Chem. B 106 (2002) 12336–12343.
[17]. P. I. Nagy, B. Noszal, J. Phys. Chem. A 104 (2000) 6834–6843.
[18]. J. O. Hutchens, A. G. Cole, R. A. Robie, J. W. Stout, J. Biol. Chem. 238 (1963) 2407–2412.
[19]. Z. Li, M. H. Matus, H. A. Velazquez, D. A. Dixon, C. J. Cassady, Int. J. Mass Spectrom. 265 (2007) 213–223.
[20]. M. A. Palafox, J. Talaya, A. G. Martinez, G. Tardajos, H. Kumar, J. K. Vats, V. K. Rastogi, Spect. Lett. 43 (2010) 51–59.
[21]. K. K. Irikura, R. D. Johnson, R. N. Kacker, J. Phys. Chem. A 109 (2005) 8430–8437.
[22]. M. A. Palafox, V. K. Rastogi, Spectrochim. Acta A 58 (2002) 411–440.
[23]. M. A. Palafox, M. Gill, N. J. Nunez, V. K. Rastogi, L. Mittal, R. Sharma, Int. J. Quant. Chem. 103 (2005) 394–421.
[24]. M. A. Palafox, V. K. Rastogi, Perspectives in Modern Optics and Optical Instrument, Edited by, A Sharma, J. Joseph, V. K. Rastogi, Anita Publications, Delhi–Ghaziabad, India, 2002.
[25]. M. A. Palafox, N. J. Nunez, M. Gill, V. K. Rastogi, Perspectives in Engineering Optics, Edited by, K. Singh, V. K. Rastogi, Anita Publications, Delhi–Ghaziabad, India, 2003.
[26]. V. Barone, J. Chem. Phys. 122 (2005) 014108–014118.
[27]. G. M. Chaban, J. O. Jung, R. B. Gerber, J. Chem. Phys. 111 (1999) 1823–1829.
[28]. V. Barone, J. Chem. Phys. 101 (1994) 10666–10676.
[29]. C. Minichino, V. Barone, J. Chem. Phys. 100 (1994) 3717–3741.

[30]. V. Barone, C. Minichino, J. Mol. Struct. (Theochem) 330 (1995) 365–376.
[31]. V. Barone, M. Cossi, N. Rega, G. Scalmani, J. Comp. Chem. 24 (2003) 669–681.
[32]. V. Barone, J. Chem. Phys. 120 (2004) 3059–3065.
[33]. V. Parchansky, P. Bour, J. Chem. Phys. 133 (2010) 044117–044126.
[34]. J. Antony, G. V. Helden, G. Meijer, B. Schmidt, J. Chem. Phys. 123 (2005) 014305–014316.
[35]. A. Miani, E. Cane, P. Palmieri, A. Trombetti, N. C. Handy, J. Chem. Phys. 112 (2000) 248–259.
[36]. V. Barone, Chem. Phys. Lett. 383 (2004) 528–532.
[37]. R. Gerber, M. Ratner, Adv. Chem. Phys. 70 (1988) 97–132.
[38]. T. K. Roy, R. B. Gerber, Phys. Chem. Chem. Phys. 15 (2013) 9468–9492.
[39]. G. C. Carney, L. L. Sprandel, C. W. Kern, Adv. Chem. Phys. 37 (1978) 305–379.
[40]. J. M. Bowman, J. Chem. Phys. 68 (1978) 608–610.
[41]. J. M. Bowman, Acc. Chem. Res. 19 (1986) 202–208.
[42]. N. Tasinato, A. P. Charmet, P. Stoppa, S. Giorgianni, A. Gambi, Chem. Phys. 397 (2012) 55–64.
[43]. P. Wojciechowski, K. Helios, D. Michalska, Vib. Spectrosc. 57 (2011) 126–134.
[44]. V. M. R. Betancourtt, V. M. Q. Navarro, M. Neff, G. Rauhut, Chem. Phys. 387 (2011) 1–4.
[45]. K. Ohno, S. Maeda, Chem. Phys. Lett. 503 (2011) 322–326.
[46]. C. Puzzarini, M. Biczysko, V. Barone, J. Chem. Theo. Comput. 7 (2011) 3702–3710.
[47]. L. Pele, J. Sebek, E. O. Potma, R. B. Gerber, Chem. Phys. Lett. 515 (2011) 7–12.
[48]. V. P. Gupta, P. Tandon, Spectrochim. Acta A 89 (2012) 55–66.
[49]. P. Klaeboe, A. Horn, C. J. Nielsen, G. A. Guirgis, Vib. Spectrosc. 56 (2011) 136–145.
[50]. G. O. Ildiz, S. Akyuz, Vib. Spectrosc. 58 (2012) 12–18.
[51]. T. Rasheed, S. Ahmad, S. M. Afzal, K. Rahimullah, J. Mol. Struct. (Theochem) 895 (2009) 18–20.
[52]. M. J. Alam, S. Ahmad, J. Mol. Struct. 1059 (2014) 239–254.
[53]. M. J. Alam, S. Ahmad, Spectrochim. Acta A 128 (2014) 653–664.
[54]. M. J. Alam, S. Ahmad, Spectrochim. Acta A 96 (2012) 992–1004.
[55]. M. J. Alam, S. Ahmad, Spectrochim. Acta A 136 (2015) 961–978.
[56]. P. Seidler, T. Kaga, K. Yagi, O. Christiansen, K. Hirao, Chem. Phys. Lett. 483 (2009) 138–142.
[57]. M. J. Frisch et al., Gaussian 09, Revision D.01, Gaussian, Inc., Wallingford CT, 2009.
[58]. M. W. Schmidt, K. K. Baldridge, J. A. Boatz, S. T. Elbert, M. S. Gordon, J. H. Jensen, S. Koseki, N. Matsunaga, K. A. Nguyen, S. J. Su, T. L. Windus, M. Dupuis, J. A. Montgomery, J. Comput. Chem. 14 (1993) 1347–1363.
[59]. D. Michalska, R. Wysokiński, Chem. Phys. Lett. 403 (2005) 211–217.
[60]. B. D. Becke, Phys. Rev. A 38 (1988) 3098–3100.
[61]. C. Lee, W. Yang, R. G. Parr, Phys. Rev. B 37 (1988) 785–789.
[62]. Y. Miller, G. M. Chaban, R. B. Gerber, J. Phys. Chem. A 109 (2005) 6565–6574.
[63]. K. Yagi, K. Hirao, T. Taketsugu, M. W. Schmidt, M. S. Gordon, J. Chem. Phys. 121 (2004) 1383–1389.
[64]. T. Rasheed, S. Ahmad, Vib. Spectrosc. 56 (2011) 51–59.

[65]. N. Sundaraganesan, G. Elango, S. Sebastian, P. Subramani, Ind. J. Pure & Appl. Phys. 47 (2009) 481–490.
[66]. http://cccbdb.nist.gov/vibscalejust.asp
[67]. M. H. Jamroz, Vibrational Energy Distribution Analysis VEDA 4, Warsaw, 2004.
[68]. E. D. Glendening, A. E. Reed, J. E. Carpenter, F. Weinhold, NBO Version 3.1.
[69]. A. R. Allouche, J. Comp. Chem. 32 (2011) 174–182.
[70]. R. G. Parr, W. Yang, Density–Functional Theory of Atoms and Molecules, Oxford University Press, New York, 1989.
[71]. R. G. Parr, W. T. Yang, Annu. Rev. Phys. Chem. 46 (1995) 701–728.
[72]. W. Kohn, A. D. Becke, R. G. Parr, J. Phys. Chem. 100 (1996) 12974–12980.
[73]. P. Geerlings, F. De Proft, W. Langenaeker, Chem. Rev. 103 (2003) 1793–1874.
[74]. P. Geerlings, F. De Proft, Phys. Chem. Chem. Phys. 10 (2008) 3028–3042.
[75]. P. W. Ayers, J. S. M. Anderson, L. J. Bartolotti, Int. J. Quantum Chem. 101 (2005) 520–534.
[76]. H. Chermette, J. Comput. Chem. 20 (1999) 129–154 and ref. cited therein.
[77]. C. A. Morgado, P. Jurecka, D. Svozil, P. Hobza, J. Sponer, Phys. Chem. Chem. Phys. 12 (2010) 3522–3534.
[78]. P. Hobza, R. Zahradnik, Int. J. Quantum Chem. 42 (1992) 581–590.
[79]. J. Leszczynski, Handbook of Computational Chemistry, Springer, New York, 2012.
[80]. I. Georgieva, D. Binev, N. Trendafilova, G. Bauer, Chem. Phys. 286 (2003) 205–217.
[81]. A. F. de C. Alcantara, A. F. Teixeira, I. F. da Silva, W. B. de Almeida, D. P. Veloso, Quim. Nova 27 (2004) 371–377.
[82]. A. R. Garcia, R. B. de Barros, J. P. Lourenco, L. M. Ilharco, J. Phys. Chem. A 112 (2008) 8280–8287.
[83]. E. Pretsch, P. Buhlmann, C. Affolter, Structure Determination of Organic Compounds: Tables of Spectral Data, 3rd edition, Springer–Verlag, Berlin Heidelberg, New York, 2000.
[84]. G. Socrates, Infrared Characteristic Group Frequencies, 3rd edition, Wiley Interscience Publications, New York, 1980.
[85]. B. Smith, Infrared Spectral Interpretation: A Systematic Approach, CRC Press, Washington DC, 1999.
[86]. N. B. Colthup, L. H. Daly, S. E. Wiberley, Introduction to Infrared and Raman Spectroscopy, Academic Press, New York, 1990.
[87]. M. Govindarajan, M. Karabacak, S. Periandy, D. Tanuja, Spectrochim. Acta A 97 (2012) 231–245.
[88]. K. Meng, J. Wang, Phys. Chem. Chem. Phys. 13 (2011) 2001–2013.
[89]. A. Nataraj, V. Balachandran, T. Karthick, M. Karabacak, A. Atac, J. Mol. Struct. 1027 (2012) 1–14.
[90]. D. Lin–Vein, N. B. Colthup, W. G. Fateley, J. G. Grasselli, The Handbook of Infrared an Raman Characteristic Frequencies of Organic Molecules, Academic Press, San Diego, 1991.
[91]. M. Silverstein, G. C. Basseler, C. Morill, Spectrometric Identification of Organic Compounds, Wiley, New York, 1981.
[92]. R. B. Gerber, B. Brauer, S. K. Gregurick, G. M. Chaban, Phys. Chem. Comm. 5 (2002) 142–150.
[93]. A. E. Reed, L. A. Curtiss, F. Weinhold, Chem. Rev. 88 (1988) 899–926.

[94]. F. Weinhold, C. R. Landis, Chemistry Education: Research and Practice in Europe 2 (2001) 91–104.
[95]. E. Kavitha, N. Sundaraganesan, S. Sebastian, M. Kurt, Spectrochim. Acta A 77 (2010) 612–619.
[96]. B. Kosar, C. Albayrak, Spectrochim. Acta A 78 (2011) 160–167.
[97]. G. Zhang, C. B. Musgrave, J. Phys. Chem. A 111 (2007) 1554–1561.
[98]. T. Koopmans, Physica 1 (1934) 104–113.
[99]. H. Sun, S. J. Mumby, J. Chem. Phys. 104 (1996) 1018–1024.
[100]. O. Christiansen, J. Gauss, J. F. Stanton, J. Chem. Phys. Lett. 305 (1999) 147–155.
[101]. M. Arivazhagan, J. S. Kumar, Indian J. Pure Appl. Phys. 50 (2012) 363–373.
[102]. G. U. Bublitz, S. G. Boxer, Annu. Rev. Phys. Chem. 48 (1997) 213–242.
[103]. J. O. Verbal, L. P. Londono, J. Chem. Inf. Comput. Sci. 42 (2002) 1241–1246.
[104]. T. V. Nguyen, D. W. Pratt, J. Chem. Phys. 124 (2006) 1216–1219.
[105]. V. V. Speybroeck, R. Gani, R. J. Meier, Chem. Soc. Rev. 39 (2010) 1764–1779.
[106]. R. V. Reyes, F. N. Zarur, E. Martinez, Org. Elect. 9 (2008) 625–634 and ref; cited therein.
[107]. L. H. M. Huizar, C. H. R. Reyes, J. Mex. Chem. Soc. 55 (2011) 142–147.

Chapter 4

Molecular structure and anharmonic vibrational analysis of ortho–, meta–, para–iodonitrobenzene

4.1 Introduction

Nitro aromatic compounds are widely used as intermediates in the synthesis of pharmaceuticals, dyes, polymers, pesticides, biologically active substances, explosives, etc. The molecules, o–, m–, and p–iodonitrobenzen (OINB, MINB and PINB) have wide applications in biochemistry, organic chemistry and electrochemistry [1–6]. These molecules play an important role in formation of radicals upon their electrochemical reduction [4, 5]. MINB (1–iodo–3–nitrobenzene) is used in synthesis of N–phenyl–N'–(2–chlroethyl) ureas which are antineoplastic agents [2]. OINB molecule shows high reactivity due to electron withdrawing and electron–donating substituents connected in the neighbouring positions of benzene ring, therefore, it plays a role in many chemical reactions for example in palladium–catalyzed N–arylation reaction of nucleo–bases for synthesis of DNA adducts with carcinogenic compounds [6]. The nitro and halogen substituents in the benzene ring affect its overall stability and other properties due to their electron withdrawing nature. These are also molecules of scientific interest for understanding the deformation in benzene ring due to influence of nitro group and iodine atom.

Spectroscopic techniques with aid of quantum chemical calculations are widely used to understand structure, vibrations and various other properties of molecules. Several authors [7–23] have studied structures and spectra of substituted nitrobenzenes. The molecular structures of several aromatic nitro compounds [12], o–, m–, p–iodonitrobenzene [13, 14] and o–fluoronitrobenzene [15] have been measured using diffraction experiments. The structures of o–, m–, p–iodonitrobenzene [14], o–fluoronitrobenzene [15] and o–, m–, p–halonitrobenzene radical anions [16] were

theoretically calculated. The electronic structures of chloro, bromo and iodonitrobenzene were studied by UV photoelectron spectroscopy [17, 18]. Various descriptors such as LUMO energy, electron affinity, electrophilicity index and group electronegativity of 12 para substituted nitrobenzenes have been computed [22]. The vibrational spectra of 1, 2–dichloro–4–nitrobenzene [19], p–fluoronitrobenzene [20] and isomeric chloronitrobenzenes [21] have been carried out by using FTIR, FT–Raman and quantum chemical calculations. The spectral studies of o–, m–, p–iodonitrobenzene are inadequate in the literature. The vibrational spectra of these molecules are analyzed earlier using infrared spectra [10], Raman spectra [7, 23] and normal coordinate analysis by Wilson's GF matrix method [7]. To the best of our knowledge, harmonic and anharmonic quantum chemical calculations, combination and overtone bands, MEP mapping, HOMO–LUMO and NBO analysis of OINB, MINB and PINB have not been reported so far. Therefore, there is need to supplement the existing experimental and theoretical data to help in making correct assignments. In the present work, all these computations are carried out and theoretical as well as experimental studies of the FTIR and Raman spectra of OINB, MINB and PINB have been presented. The theoretical vibrational spectra are simulated using the anharmonic frequencies obtained by Barone's PT2 method [24] within DFT, MP2 and HF approaches along with different basis sets. The fundamental, combination and overtone bands of the FTIR spectra have been assigned using anharmonic force field calculations. All the fundamental vibrational modes are assigned with the help of visual inspection of atomic displacement and PED calculations. The effect of substitution of iodine in nitrobenzene and benzene has been also studied. Many workers have performed vibrational analysis of polyatomic molecules in the harmonic approximation and various scaling procedures [25–28] were used for compensating discrepancies. Harmonic calculations are of computationally low cost even for relatively large organic molecules but the accuracy is inadequate in particularly for stretching vibrations appearing at higher wavenumbers. In order to get reliable results without any scaling, a great effort has been made to carry out anharmonic computations [29–34]. Recently, vibrational spectra of polyatomic molecules are well–interpreted using anharmonic calculations [35–40].

The aim of this work is to use anharmonic method for analysis of the vibrational spectra of substituted benzenes and to test the capability of the method for medium

sized molecules containing heavier atom like iodine. The HF computations provide inadequate results due to ignorance of electron–electron correlation term. The anharmonic force field calculations using MP2 and DFT methods have comparable accuracy but anharmonic MP2 computations are of very high computational cost. Therefore, present study encourages the use of anharmonic method within the DFT framework for calculating vibrational spectra of medium sized polyatomic molecules containing heavy elements.

4.2 Experimental details

The samples of OINB, MINB and PINB, obtained from Koch–Light Laboratories and Colnbrook Bucks (England), were used as such for the spectral measurements. FTIR spectra of the samples were recorded on Tensor 37 Spectrometer (Bruker) in the region of 370–4000 cm^{-1} with a spectral resolution of 1 cm^{-1} using KBr pellet technique. A minimum of 32 scans were accumulated to increase the signal–to–noise ratio.

4.3 Computational details

The quantum chemical calculations on compounds containing iodine atom are not much accurate because of unavailability of basis sets for iodine atom in most of quantum mechanical programs, although various accurate theoretical methods (B3LYP, MPn and QCISD, etc.) have been developed. Gaussian type basis sets for the heavy elements beyond the fourth row in the periodic table, are relatively limited. In the present investigation, the quantum chemical calculations were carried out at DFT/B3LYP [41,42] level of theory using LANL2DZ (with effective core potential) as well as 3–21G* (without effective core potential) on iodine atom and basis sets 6–311G(d,p), 6–311++G(d,p) and cc–pVTZ on other atoms using Gaussian 09 software [43]. The computations have been also done using MP2 and HF methods. The effective core potential and valence double zeta basis set, LANL2DZ, was used for the consideration of relativistic effect. The basis set 3–21G* on iodine atom is used because this is relatively more accurate and least expensive. In the present calculations, the MP2 method with some basis sets unable to compute molecular geometry of MINB and PINB at local minimum on PES. Therefore, the calculations for MINB and PINB are presented respectively at MP2/cc–pVTZ/LANL2DZ and

MP2/6–311G(d,p)/LANL2DZ levels of theory. The stable molecular structures of OINB, MINB and PINB in the ground state were obtained using Berny's optimization algorithm under tight convergence criterion. To determine the stable conformations of these molecules, the torsional angle T (C–C–N–O) was varied from 0 to 180° with step size of 10° and the energy profiles were obtained at B3LYP/6–311G(d,p)/3–21G* level of theory. The optimized structural parameters have been computed for stable molecular structures and were used for the calculations of the harmonic and anharmonic vibrational frequencies. The anharmonic frequencies were calculated using the second order perturbative method elaborated by Barone [24, 43]. The combination and overtone frequencies were also computed and are compared with experimental non–fundamental bands of the FTIR. All the real values of calculated frequencies confirm that optimized molecular geometries correspond to true energy minima on the potential energy surface. Vibrational spectra of the molecules have been assigned using PED values that were computed with the help of VEDA4 program [44]. Electronic properties like HOMO and LUMO energy eigenvalues along with HOMO–LUMO gaps were also deduced for the stable structure at B3LYP/6–311G(d,p) level of theory in gaseous and solution phases. HOMO–LUMO energy gaps were also computed by TD–DFT calculations. The chemical reactivity descriptors are obtained using HOMO and LUMO energy eigenvalues for understanding the reactivity (section 2.2.7) of present molecules. For the plots of simulated IR and Raman spectra, pure Lorentzian band shape was used with full width at half maxima (FWHM) of 5 cm^{-1} [45]. Raman intensities were computed by RAINT program [46]. The calculated harmonic IR and Raman intensities were used for the simulation of vibrational spectra. The root mean square (RMS) error and mean absolute deviation (MAD) values (Eq. 3.1 and 3.2) have been used for the comparisons between experimental and theoretical data. The gas phase thermodynamic properties such as entropy, heat capacity and enthalpy change have been calculated in the temperatures range 77–700K at B3LYP/6–311G(d,p)/3–21G* level of theory. The NBO analysis was performed B3LYP/6–311G(d,p)/3–21G* level of theory by using the NBO 3.1 program [47, 48] implemented in Gaussian 09 software.

4.4 Results and discussion

4.4.1 Molecular geometry and potential energy surface scan

The OINB, MINB and PINB molecules contain an iodine atom and a nitro group attached to a benzene ring. The optimized molecular structures with labelling of atoms are shown in Fig. 4.1. The minimum self–consistent field (SCF) energies for OINB, MINB and PINB at different levels of theory are presented in Table 4.1. The experimental and optimized molecular structural parameters along with RMS and MAD values are listed in Table 4.2–4.4. The calculated structural parameters are in good agreement with data obtained from electron diffraction experiment [14]. In order to describe stable structure on potential energy surface, the energy profile has been achieved as a function of C4–C5–N3–O1 dihedral angle (Fig. 4.2). In the case of OINB, two maxima are found at 0° and 90° with relative energy values –4597341.675 and –4597335.400 kcal/mol respectively at B3LYP/6–311G(d,p)/3–21G* level of theory. The values of dihedral angle, O–N–C–C, (Table 4.3 and 4.4) show that aromatic rings are co–planar with nitro group for MINB and PINB. In OINB, the nitro group is twisted by significant degree of angle (Table 4.2) with the plane of aromatic ring for obtaining stable conformation. The angle of twist is confirmed by PES scan. This twist angle for OINB calculated at MP2 theory is found more comparable with experimental value than those obtained by other methods (Table 4.2). The comparison between structural parameters of OINB, MINB and PINB obtained from electron diffraction data and theory are shown in Fig. 4.3 and 4.4. The structure of PINB is more stable (Table 4.1) than OINB and MINB due to its predominant resonance structure and the larger separation between electron withdrawing nitro group and electronegative iodine atom. In the case of OINB, nitro group gets twist and the activation effect of nitro group is diminished by the steric effect and may result in a net deactivation [20, 49]. The computed potential barrier heights (V_{max}– V_{min}) due to torsional motion of the nitro group of OINB are 3.14 and 0.94 kcal/mole at 90° and 0° torsional angle respectively at B3LYP/6–311G(d,p)/3–21G* level of theory. The substitution of the iodine atom to the different positions in aromatic ring does not cause any noticeable change in C–C, C–H, C–N, N–O and C–I bond lengths in the investigated molecules (Table 4.2– 4.4, Fig. 4.3). It is also found that the N3–C5–C4, N3–C5–C6 and C–C–I bond angles are approximately same in MINB and PINB but they differ in OINB. The differences in the bond angles for OINB can be attributed to

steric effect of nitro group and iodine atom. The RMS error and MAD between theoretical and experimental structural parameters were also calculated and are given in Table 4.2–4.4. According to RMS and MAD values, the good correlations are found for bond lengths at MP2/6–311G(d,p)/LANL2DZ level for OINB, at B3LYP/6–311++G(d,p)/3–21G* level for MINB and at MP2/6–311G(d,p)/LANL2DZ level for PINB. In the case of bond angles, the good correlations are obtained at MP2/6–311++G(d,p)/LANL2DZ level for OINB, at B3LYP/6–311++G(d,p)/LANL2DZ level for MINB and at HF/6–311G(d,p)/LANL2DZ theory for PINB. The theoretical structural parameters, calculated with and without electron core potential for iodine atom, are found almost same.

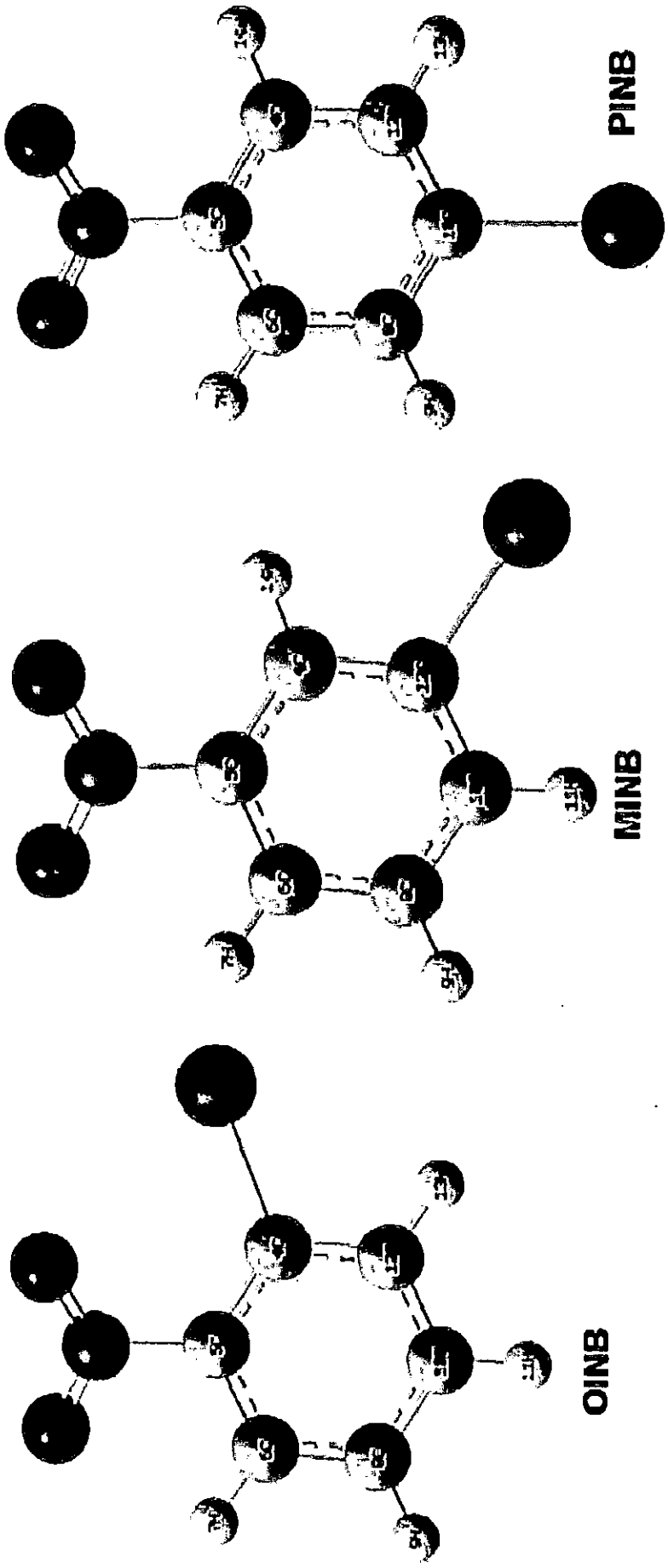

Fig. 4.1 The molecular structure of OINB, MINB and PINB with numbering scheme.

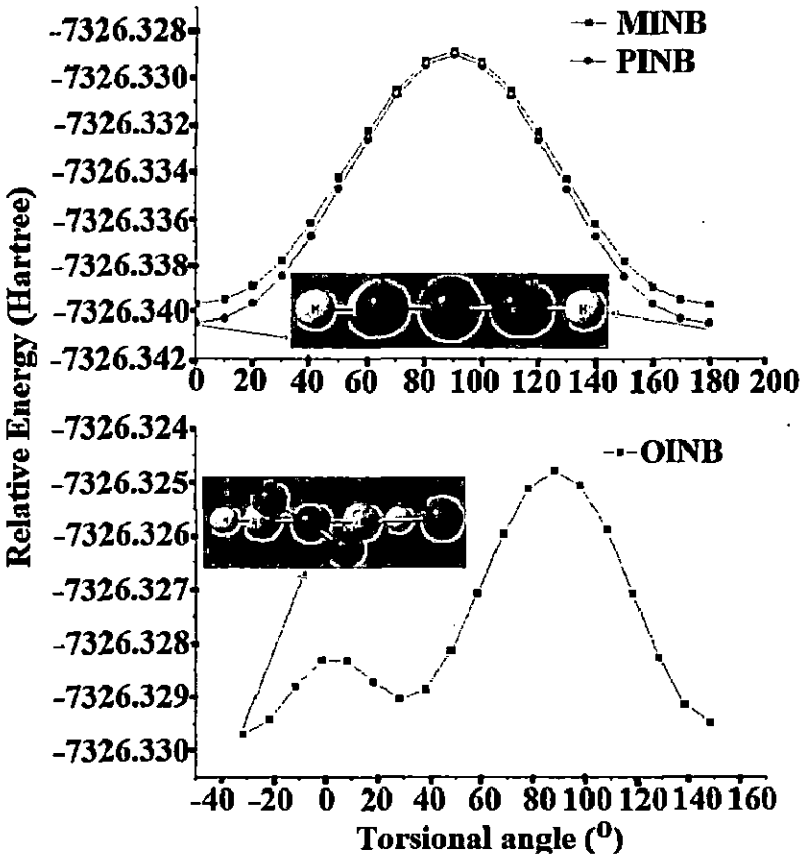

Fig. 4.2 PES scans for the selected T(C–C–N–O) dihedral angle of OINB, MINB and PINB.

Table 4.1 Calculated minimum SCF energies (a. u.) for the o–, m–, p–iodonitrobenzene at different levels of theory.

	OINB			MINB			PINB		
	B3LYP	MP2	HF	B3LYP	MP2	HF	B3LYP	MP2	HF
p) Z	–447.62502115	–446.25608685	–444.82480906	–447.63682111	–	–444.83866796	–447.63754051	–446.26448235	–444.83936770
p)	–7326.32982071	–	–	–7326.33977197	–	–	–7326.34046669	–	–
l,p) Z	–447.63744871	–446.28515457	–444.83504754	–447.64820065	–	–444.84815435	–447.64903772	–	–444.84888285
p)	–7326.34786435	–	–	–7326.35636269	–	–	–7326.35709611	–	–
Z	–447.67748542	–446.54963334	–444.88550565	–447.68868056	–446.55738288	–444.89885061	–447.68958154	–	–444.89972802
p)	–7326.38435540	–	–	–7326.39395808	–	–	–7326.39484299	–	–

2DZ (with ECP) and 3–21G* basis sets are used on iodine atom

able 4.2 Comparison of structural parameters obtained from electron diffraction data and quantum chemical methods for OINB.

		B3LYP						MP2			HF		
ters	ED[a]	6–311 G(d,p) /3–21G*	6–311 G(d,p) /LANL2DZ	6–311++ G(d,p) /3–21G*	6–311++ G(d,p) /LANL2DZ	cc–pVTZ /3–21G*	cc–pVTZ /LANL2DZ	6–311 G(d,p) /LANL2DZ	6–311++ G(d,p) /LANL2DZ	cc–pVTZ /LANL2DZ	6–311 G(d,p) /LANL2DZ	6–311++ G(d,p) /LANL2DZ	cc–pVTZ /LANL2DZ
Å)													
3		1.22 0	1.219	1.221	1.220	1.219	1.218	1.229	1.232	1.229	1,182	1.183	1.182
3		1.224	1.224	1.225	1.225	1.222	1.222	1.231	1.233	1.230	1.188	1.188	1.186
5	1.468	1.482	1.482	1.480	1.480	1.478	1.479	1.469	1.466	1.462	1.467	1.468	1.466
5		1.399	1.397	1.398	1.397	1.394	1.394	1.399	1.397	1.393	1.386	1.385	1.382
2		1.398	1.396	1.398	1.396	1.394	1.393	1.403	1.402	1.398	1.387	1.388	1.385
4	2.101	2.115	2.131	2.112	2.125	2.096	2.102	2.099	2.091	2.035	2.116	2.110	2.086
5		1.394	1.394	1.393	1.394	1.39	1.391	1.396	1.395	1.390	1.383	1.383	1.380
7		1.081	1.082	1.082	1.082	1.079	1.079	1.085	1.086	1.080	1.072	1.073	1.070
8		1.386	1.387	1.387	1.388	1.383	1.384	1.393	1.396	1.388	1.379	1.380	1.377
9		1.083	1.083	1.083	1.083	1.081	1.081	1.086	1.086	1.080	1.074	1.074	1.072
0		1.393	1.393	1.393	1.393	1.389	1.389	1.399	1.400	1.393	1.383	1.384	1.380
11		1.084	1.084	1.084	1.084	1.081	1.081	1.086	1.086	1.081	1.075	1.075	1.073
12		1.390	1.391	1.391	1.392	1.387	1.388	1.396	1.398	1.390	1.383	1.384	1.380
13		1.082	1.082	1.082	1.082	1.080	1.079	1.085	1.086	1.080	1.073	1.073	1.071

Table: 4.2 (*continued*)

<C–C>[b]	1.398	1.393	1.393	1.393	1.393	1.390	1.390	1.398	1.398	1.392	1.384	1.384	1.381
<C–H>[b]	1.117	1.083	1.083	1.083	1.083	1.080	1.080	1.086	1.086	1.080	1.074	1.074	1.072
<O=N>[b]	1.238	1.222	1.222	1.223	1.223	1.221	1.220	1.230	1.233	1.230	1.185	1.186	1.184
RMS		0.019	0.023	0.018	0.021	0.019	0.019	0.014	0.015	0.034	0.032	0.031	0.033
MAD		0.017	0.020	0.015	0.018	0.015	0.015	0.008	0.010	0.025	0.025	0.024	0.027
Bond angle (°)													
O1=N3=O2		125.2	125.5	125.2	125.3	125.2	125.4	126.0	126.0	125.9	125.5	125.4	125.5
O1=N3–C5	118.8	117.9	117.9	117.7	117.9	117.8	117.9	117.4	117.1	117.3	117.9	117.8	117.7
O2=N3–C5	118.8	116.9	116.6	117.0	116.8	116.9	116.7	116.6	116.9	116.8	116.6	116.7	116.7
C5–C4–C12	118.6	117.6	118.3	117.5	118.1	117.3	117.8	117.3	117.4	116.5	118.0	117.8	117.5
C5–C4–I14	124.1	125.8	125.2	125.2	124.8	125.5	125.2	124.5	122.2	124.3	125.3	125.0	125.2
C12–C4–I14		116.5	116.4	117.3	117.0	117.1	116.9	118.1	120.2	119.1	116.6	117.1	117.2
N3–C5–C4	121.1	123.1	123.5	122.6	123.0	122.8	123.1	122.5	120.9	121.9	123.0	122.7	122.7
N3–C5–C6	116.1	115.5	115.5	115.6	115.6	115.5	115.5	115.4	116.4	115.3	115.4	115.5	115.3
C4–C5–C6	122.8	121.4	121.0	121.8	121.3	121.7	121.4	122.1	122.7	122.7	121.5	121.9	122.0
C5–C6–H7		118.3	118.3	118.7	118.6	118.5	118.5	118.7	119.3	118.8	119.0	119.2	119.1
C5–C6–C8	116.8	120.1	120.1	119.8	119.9	120.0	120.0	119.6	119.1	119.5	119.8	119.6	119.7
H7–C6–C8	121.6	121.6	121.6	121.5	121.5	121.5	121.5	121.7	121.7	121.7	121.2	121.2	121.2
C6–C8–H9		120.0	119.9	120.0	119.9	120.0	120.0	119.9	119.9	120.1	119.9	119.9	120.0
C6–C8–C10	122.4	119.3	119.4	119.3	119.4	119.3	119.3	119.4	119.5	119.2	119.4	119.4	119.3
H9–C8–C10	118.8	120.7	120.7	120.7	120.6	120.7	120.7	120.7	120.6	120.8	120.7	120.7	120.7
C8–C10–H11		120.3	120.4	120.3	120.3	120.3	120.4	120.4	120.2	120.3	120.3	120.3	120.3
C8–C10–C12	118.9	120.3	120.3	120.4	120.4	120.3	120.4	120.1	120.4	120.2	120.4	120.5	120.4
H11–C10–C12	120.6	119.3	119.3	119.3	119.2	119.3	119.3	119.4	119.3	119.4	119.3	119.3	119.3
C4–C12–C10	120.5	121.2	120.8	121.2	120.8	121.4	121.1	121.4	120.9	121.8	120.9	120.8	121.1
C4–C12–H13		119.0	119.3	119.1	119.4	119.0	119.3	119.0	119.3	119.0	119.5	119.5	119.4
C10–C12–H13		119.8	119.9	119.7	119.8	119.6	119.6	119.7	119.8	119.2	119.7	119.7	119.5
RMS		1.750	1.764	1.626	1.644	1.704	1.715	1.598	1.529	1.655	1.671	1.593	1.647
MAD		1.514	1.464	1.407	1.371	1.493	1.471	1.371	1.257	1.379	1.450	1.371	1.450
Dihedral angle (°)													
O1=N3–C5–C4	60.0	–31.6	–37.5	–39.2	–41.73	–36.2	–40.5	–52.2	–66.6	–54.3	–43.3	–47.3	–47.4
O1=N3–C5–C6		147.8	142.0	140.4	137.8	143.0	138.9	127.7	113.3	125.1	136.0	132.3	132.0
O2=N3–C5–C4		149.5	144.1	142.2	139.9	145.1	141.2	129.5	114.6	127.6	139.0	134.7	135.0
O2=N3–C5–C6		–31.0	–36.4	–38.2	–40.51	–35.6	–39.4	–50.6	–65.5	–53.1	–41.8	–45.7	–46.2

[a]Electron diffraction data in gaseous phase (dynamical model), Ref. [14].

[b]Mean value

Table 4.3 Comparison of structural parameters obtained from electron diffraction data and quantum chemical methods for MINB.

Parameters	ED[a]	B3LYP						MP2	HF		
		6-311 G(d,p) /3-21G*	6-311 G(d,p) /LANL2DZ	6-311++ G(d,p) /3-21G*	6-311++ G(d,p) /LANL2DZ	cc-pVTZ /3-21G*	cc-pVTZ /LANL2DZ	cc-pVTZ /LANL2DZ	6-311 G(d,p) /LANL2DZ	6-311++ G(d,p) /LANL2DZ	cc-pVTZ /LANL2DZ
Bond length (Å)											
C12–I13	2.102	2.116	2.133	2.115	2.128	2.098	2.104	2.036	2.116	2.111	2.086
C5–N3		1.484	1.484	1.483	1.484	1.480	1.481	1.473	1.467	1.468	1.466
C5–C4		1.390	1.391	1.390	1.392	1.386	1.388	1.387	1.382	1.382	1.379
C5–C6		1.389	1.389	1.390	1.390	1.386	1.386	1.387	1.380	1.380	1.377
C10–H11		1.083	1.082	1.083	1.082	1.080	1.080	1.080	1.073	1.073	1.071
C10–C12		1.396	1.394	1.396	1.395	1.392	1.391	1.395	1.385	1.386	1.382
C10–C8		1.394	1.395	1.394	1.395	1.390	1.391	1.392	1.385	1.385	1.382
O1=N3		1.222	1.222	1.224	1.223	1.221	1.221	1.228	1.186	1.187	1.185
N3=O2		1.223	1.222	1.224	1.224	1.221	1.221	1.228	1.186	1.187	1.185
C4–H14		1.080	1.080	1.080	1.080	1.078	1.078	1.078	1.070	1.070	1.068
C4–C12		1.391	1.389	1.391	1.390	1.387	1.386	1.392	1.381	1.382	1.378
C8–H9		1.083	1.083	1.083	1.084	1.081	1.081	1.081	1.074	1.074	1.072
C8–C6		1.391	1.391	1.391	1.391	1.387	1.387	1.391	1.382	1.383	1.379
C6–H7		1.081	1.081	1.081	1.081	1.078	1.078	1.078	1.071	1.071	1.069
<C–C>[b]	1.392	1.392	1.392	1.392	1.392	1.388	1.388	1.391	1.383	1.383	1.380
<C–H>[b]	1.114	1.082	1.082	1.082	1.082	1.079	1.079	1.079	1.072	1.072	1.070
<O=N>[b]	1.226	1.223	1.222	1.224	1.224	1.221	1.221	1.228	1.186	1.187	1.185
RMS		0.018	0.022	0.017	0.021	0.018	0.018	0.037	0.030	0.029	0.032
MAD		0.012	0.017	0.012	0.015	0.012	0.012	0.026	0.026	0.025	0.028
Bond angle (°)											
N3–C5–C4	118.0	118.4	118.4	118.3	118.4	118.4	118.4	118.3	118.4	118.4	118.5
N3–C5–C6	118.0	119.0	119.0	119.0	118.9	119.0	119.0	118.8	118.9	118.9	118.9
C4–C5–C6	124.0	122.6	122.7	122.7	122.7	122.5	122.6	122.9	122.7	122.7	122.6
I11–C10–C12	120.3	120.1	120.4	120.2	120.4	120.0	120.3	120.0	120.3	120.3	120.2
I11–C10–C8		120.0	120.1	119.8	120.1	119.7	119.9	119.4	119.9	119.8	119.6
12–C10–C8	119.4	119.9	119.5	120.0	119.6	120.2	119.9	120.5	119.9	119.9	120.2
5–N3=O1	118.0	117.5	117.5	117.6	117.6	117.6	117.6	117.5	117.5	117.6	117.6
5–N3=O2	118.0	117.4	117.4	117.5	117.5	117.4	117.4	117.3	117.4	117.4	117.4
1=N3=O2		125.1	125.1	124.9	124.9	124.9	124.9	125.3	125.1	125.0	125.0
5–C4–H14	121.8	119.4	119.5	119.5	119.7	119.3	119.4	119.0	119.9	120.0	119.8
5–C4–C12	116.4	118.3	117.9	118.3	117.9	118.6	118.3	118.9	118.0	118.0	118.4
14–C4–C12		122.3	122.6	122.1	122.4	122.1	122.3	122.1	122.0	122.0	121.9

ble: 4.3 (*continued*)

3–C12–C10	118.4	120.2	119.8	120.4	119.8	120.4	120.0	120.7	119.8	119.8
3–C12–C4	118.4	119.4	119.2	119.3	119.3	119.7	119.5	119.9	119.5	119.5
0–C12–C4	121.9	120.4	121.0	120.3	120.9	120.0	120.5	119.3	120.7	120.7
10–C8–H9	119.5	119.6	119.5	119.6	119.5	119.6	119.5	119.5	119.7	119.7
10–C8–C6	121.1	120.6	120.7	120.6	120.7	120.6	120.6	120.9	120.5	120.5
9–C8–C6		119.8	119.8	119.7	119.8	119.8	119.8	119.6	119.8	119.8
5–C6–C8	117.2	118.1	118.2	118.0	118.2	118.0	118.1	117.5	118.3	118.2
5–C6–H7		119.6	119.6	119.9	119.8	119.8	119.8	120.1	120.1	120.2
8–C6–H7	121.4	122.3	122.2	122.1	122.0	122.1	122.1	122.4	121.7	121.6
RMS		1.166	1.007	1.152	0.971	1.286	1.133	1.447	1.000	0.977
MAD		0.975	0.819	0.938	0.794	1.063	0.925	1.125	0.850	0.825
Dihedral angle (°)										
-C5–N3=O1	0.0	0.0	0.0	0.0	0.0	0.0	0.0	0.0	0.0	0.0
-C5–N3=O2		180.0	180.0	180.0	180.0	180.0	180.0	180.0	180.0	180.0
-C5–N3=O1		180.0	180.0	180.0	180.0	180.0	180.0	180.0	180.0	180.0
-C5–N3=O2		0.0	0.0	0.0	0.0	0.0	0.0	0.0	0.0	0.0

ctron diffraction data in gaseous phase (dynamical model), Ref. [14].

an value

4.4 Comparison of structural parameters obtained from electron diffraction data and different quantum chemical meth

Parameters	ED[a]	B3LYP						MP2	HF		
		6-311 G(d,p) /3-21G*	6-311 G(d,p) /LANL2DZ	6-311++ G(d,p) /3-21G*	6-311++ G(d,p) /LANL2DZ	cc-pVTZ /3-21G*	cc-pVTZ /LANL2DZ	6-311 G(d,p) /LANL2DZ	6-311 G(d,p) /LANL2DZ	6-311++ G(d,p) /LANL2DZ	cc /L
Bond length (Å)											
C–I	2.102	2.112	2.13	2.111	2.124	2.094	2.101	2.098	2.115	2.109	
O1=N3		1.223	1.223	1.225	1.225	1.222	1.222	1.230	1.186	1.187	
O2=N3		1.223	1.223	1.225	1.225	1.222	1.222	1.230	1.186	1.187	
C10–C8		1.396	1.394	1.396	1.395	1.392	1.392	1.401	1.385	1.385	
C10–C12		1.396	1.394	1.396	1.395	1.392	1.392	1.401	1.385	1.385	
N3–C5		1.478	1.479	1.478	1.478	1.474	1.475	1.477	1.465	1.466	
C5–C4		1.390	1.390	1.391	1.391	1.387	1.387	1.394	1.380	1.381	
C5–C6		1.390	1.390	1.391	1.391	1.387	1.387	1.394	1.380	1.381	
C4–C12		1.390	1.390	1.390	1.391	1.386	1.387	1.396	1.383	1.383	
C4–H14		1.081	1.081	1.081	1.081	1.079	1.079	1.084	1.071	1.072	
C6–C8		1.390	1.390	1.390	1.391	1.386	1.387	1.396	1.383	1.383	

Table: 4.4 (*continued*)

C6–H7		1.081	1.081	1.081	1.081	1.079	1.079	1.084	1.071	1.072	1.069
C8–H9		1.082	1.082	1.082	1.082	1.080	1.080	1.085	1.072	1.073	1.071
C12–H13		1.082	1.082	1.082	1.082	1.080	1.080	1.085	1.072	1.073	1.071
<C–C>[b]	1.396	1.392	1.391	1.392	1.392	1.388	1.389	1.397	1.383	1.383	1.380
<C–H>[b]	1.107	1.082	1.082	1.082	1.082	1.080	1.080	1.085	1.072	1.073	1.070
<O=N>[b]	1.228	1.223	1.223	1.225	1.225	1.222	1.222	1.230	1.186	1.187	1.185
RMS		0.014	0.019	0.014	0.017	0.015	0.014	0.011	0.029	0.028	0.031
MAD		0.011	0.016	0.010	0.014	0.012	0.010	0.007	0.026	0.024	0.028
Bond angle (°)											
I–C10–C8		119.7	119.4	119.8	119.4	119.9	119.7	120.1	119.4	119.5	119.7
I–C10–C12		119.7	119.4	119.8	119.4	119.9	119.7	120.1	119.4	119.5	119.7
C8–C10–C12	122.2	120.6	121.2	120.4	121.1	120.1	120.7	119.8	121.1	121.0	120.6
O1=N3=O2		125.0	125.0	124.8	124.8	124.8	124.8	125.3	125.1	125.0	125.0
O1=N3–C5	117.9	117.5	117.5	117.6	117.6	117.6	117.6	117.4	117.5	117.5	117.5
O2=N3–C5	117.9	117.5	117.5	117.6	117.6	117.6	117.6	117.4	117.5	117.5	117.5
N3–C5–C4		119.0	119.0	119.0	119.0	119.1	119.1	118.9	119.0	118.9	119.0
N3–C5–C6		119.0	119.0	119.0	119.0	119.1	119.1	118.9	119.0	118.9	119.0
C4–C5–C6	122.2	121.9	122.0	121.9	121.9	121.7	121.8	122.1	122.1	122.1	121.9
C5–C4–C12	118.9	118.9	119.0	118.8	119.0	119.0	119.0	118.6	118.9	118.8	118.9
C5–C4–H14	120.6	119.6	119.6	119.8	119.8	119.7	119.7	119.9	120.1	120.2	120.2
C12–C4–H14		121.5	121.4	121.4	121.2	121.3	121.3	121.5	121.0	120.9	120.9
C5–C6–C8	119.2	118.9	119.0	118.8	119.0	119.0	119.0	118.6	118.9	118.8	118.9
C5–C6–H7		119.6	119.6	119.8	119.8	119.7	119.7	119.9	120.1	120.2	120.2
C8–C6–H7		121.5	121.4	121.4	121.2	121.3	121.3	121.5	121.0	120.9	120.9
C10–C8–C6	118.8	119.8	119.4	120.0	119.5	120.1	119.7	120.4	119.5	119.6	119.9
C10–C8–H9		120.4	120.7	120.4	120.7	120.4	120.6	120.2	120.7	120.7	120.6
C6–C8–H9		119.8	119.9	119.6	119.8	119.5	119.7	119.4	119.7	119.7	119.5
C10–C12–C4	118.9	119.8	119.4	120.0	119.5	120.1	119.7	120.4	119.5	119.6	119.9
C10–C12–H13		120.4	120.7	120.4	120.7	120.4	120.6	120.2	120.7	120.7	120.6
C4–C12–H13		119.8	119.9	119.6	119.8	119.5	119.7	119.4	119.7	119.7	119.5
RMS		0.808	0.579	0.880	0.579	0.991	0.738	1.156	0.551	0.599	0.777
MAD		0.656	0.489	0.700	0.489	0.767	0.600	0.911	0.456	0.500	0.611
Dihedral angle (°)											
O1=N3–C5–C4	0.0	0.0	0.0	0.0	0.0	0.0	0.0	0.0	0.0	0.0	0.0
O1=N3–C5–C6		180.0	180.0	180.0	180.0	180.0	180.0	180.0	180.0	180.0	180.0
O2=N3–C5–C4		180.0	180.0	180.0	180.0	180.0	180.0	180.0	180.0	180.0	180.0
O2=N3–C5–C6		0.0	0.0	0.0	0.0	0.0	0.0	0.0	0.0	0.0	0.0

[a]Deformation parameters on the benzene ring caused by nitro group and iodine atom, Ref. [14], [b]Mean value

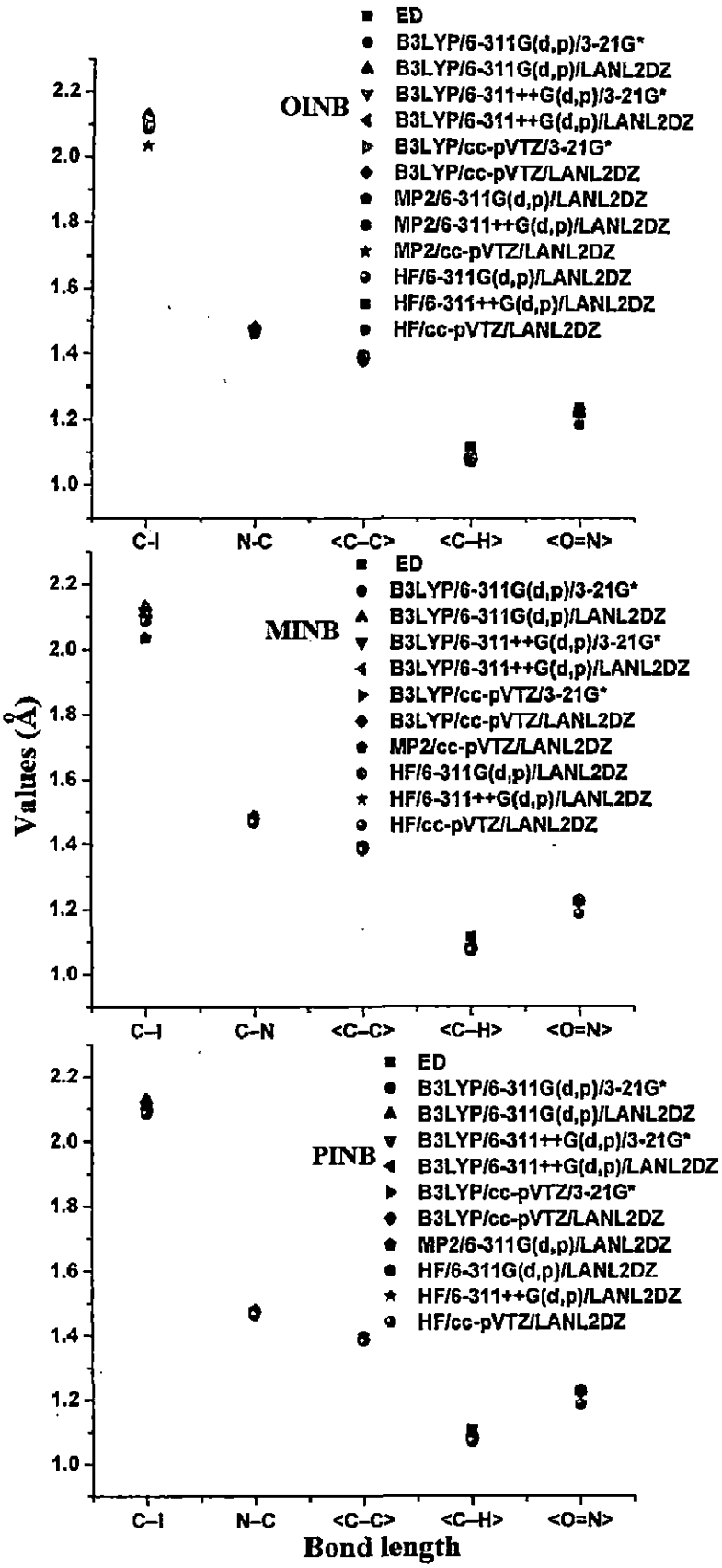

Fig. 4.3 Comparison between experimental and theoretical bond lengths.

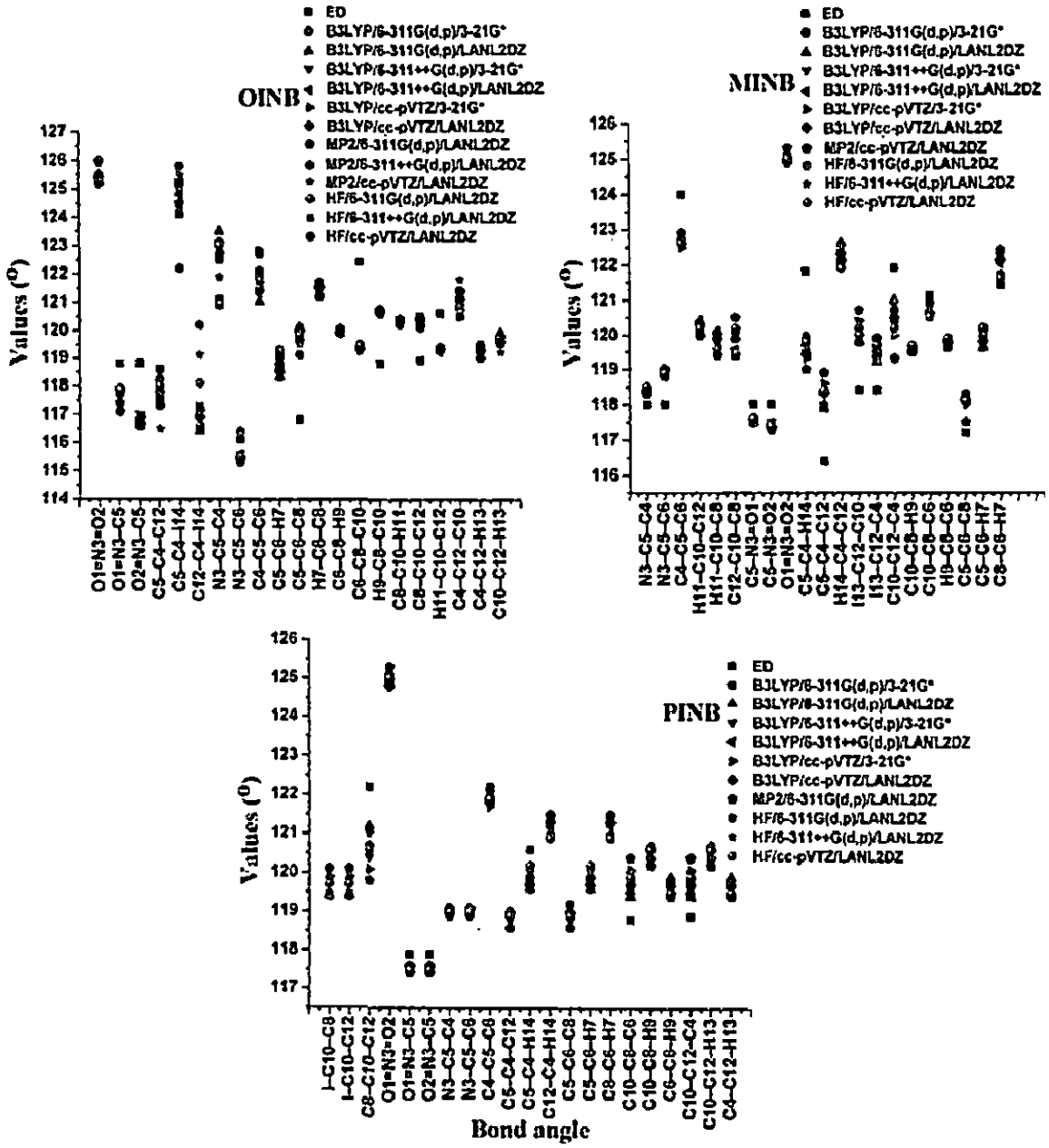

Fig. 4.4 Comparison between experimental and theoretical bond angles.

4.4.2 Vibrational analysis

The theoretical vibrational frequencies at different levels of theory as well as experimental vibrational frequencies along with their assignments for OINB, MINB and PINB are depicted in Tables 4.5–4.10. The comparison between theoretical and experimental vibrational frequencies has been made using correlation plots, RMS error and MAD values. The far–IR and Raman wavenumbers are taken from the earlier reported spectra [7, 23]. The FTIR and simulated spectra of the molecules are shown in Fig. 4.5 and 4.6. The correlation plots between experimental and theoretical vibrational frequencies are depicted in Fig. 4.7, 4.8 and 4.9. The broad bands,

appeared around 3400 cm^{-1} in the FTIR spectra of MINB and PINB, are attributed to presence of water in KBr or semisolid state of the compounds at room temperature [7]. Under symmetry consideration, OINB, MINB and PINB belong to C_1, C_S and C_{2v} point group respectively. The 36 normal modes of MINB are classified into the irreducible representations $\Gamma_{vib} = 25a' + 11a''$ under C_S point group, where a′ and a″ species represent in plane and out of plane mode of vibrations respectively. For PINB molecule, all the 36 fundamental modes of vibrations are distributed among four symmetry species of C_{2v} point group as $\Gamma_{vib} = 13a_1 + 4a_2 + 7b_1 + 12b_2$. The vibrations of a_1 and b_2 symmetry species are the in-plane modes and those of a_2 and b_1 species are out of plane modes. Under C_{2v} symmetry, a_1, a_2 and b_1 vibrations are Raman and IR active while a_2 vibrations are allowed in Raman but forbidden in infrared spectra. All the fundamental vibrations of OINB, MINB and PINB have been assigned using PED values, their animated modes and the vibrational assignments of benzene, nitrobenzene and iodobenzene (Table 4.11). In the FTIR spectra of OINB, MINB and PINB, the combination and overtone bands are also assigned with the help of calculated anharmonic frequencies. The calculated and experimental wavenumbers of non–fundamental bands for OINB, MINB and PINB are given in Table 4.12–4.14. The most of the observed non–fundamentals are combination bands. The assignments of the fundamental normal modes of the molecules are discussed in the following sections.

Nitro group vibrations

The characteristic infrared frequencies of organic nitro compounds show strong absorptions due to the asymmetric and symmetric stretching vibrations of the nitro group in the region 1600–1510 cm^{-1} and 1385–1325 cm^{-1} respectively [8, 10, 11, 50]. The strong infrared bands observed in the respective ranges are assigned to NO_2 asymmetric (mode 7) and symmetric stretching (mode 10) vibrations for OINB, MINB and PINB and they have more than 70% contributions in these modes. The average error between calculated anharmonic and experimental wavenumbers at B3LYP/6–311G(d,p)/3–21G* is about 2% for NO_2 asymmetric stretching vibrations. This could be related to either limitations of the calculations or higher order effects neglected in PT2 computations of anharmonicity. For symmetric stretching vibrations, the differences are relatively low which give an average error of 0.3% at B3LYP/6–311G(d,p)/3–21G*. The Raman band corresponding to NO_2 asymmetric stretching

vibration is stronger in OINB while NO_2 symmetric stretching vibrations have appeared with strong intensity in all the isomers. The wavenumbers of NO_2 stretching vibrations for OINB, MINB and PINB have appeared consistently with similar magnitude of frequencies. For OINB, MINB and PINB, the anharmonic frequencies of NO_2 stretching vibrations (Mode 7 and 10) calculated at B3LYP/6–311++G(d,p) and B3LYP/cc–pVTZ levels of theory are found more close to experimental data. The diffuse functions, included in 6–311G(d,p), define accurately the lone pair electrons of the oxygen atom in the present calculation. The NO_2 deformation vibrations appear in the low wavenumber region. It is identified in mode 21 with major contribution (about 50%) in all the molecules. The symmetric NO_2 in–plane bending vibration (Mode 21) in OINB has appeared at higher wavenumber with weak intensity in FTIR spectrum as compared with those in MINB and PINB. The wagging vibration of NO_2 group normally occurs in the region 730–590 cm^{-1}. In the present work, mode 24 in OINB and mode 23 in MINB and PINB are assigned to wagging vibrations which have appeared with strong intensity in the FTIR spectra whereas with very weak intensity in the Raman spectra of the molecules. The wagging vibration is observed at lower wavenumber in OINB than those identified in MINB and PINB. The assignments of NO_2 group vibrations are coherent with earlier reports [7, 8, 10, 11, 20, 21, 23, 51]. All NO_2 group vibrational frequencies have close similarity in magnitude in OINB, MINB and PINB.

C–H vibrations of the aromatic ring

The IR spectra of aromatic compounds contain multiple weak peaks due to the C–H stretching vibrations in the region 3100–3000 cm^{-1} [50]. In Raman spectra, these vibrations may appear as strong bands. The bands observed in FTIR at 3084 cm^{-1} in OINB, at 3095 and 3035 cm^{-1} in MINB and at 3093 and 3051 cm^{-1} in PINB are assigned to C–H stretching vibrations. They are also found with strong to medium intensity in Raman spectra. These modes are pure C–H stretching vibrations as evident from corresponding PED values given in Table 4.5, 4.7 and 4.9. The calculated anharmonic frequencies of C–H stretching vibrations for MINB and PINB are found at higher wavenumber than those for the OINB. The average deviation of calculated frequencies from experimental values for C–H stretching vibrations is about 1% in the case of anharmonic calculations (at B3LYP/6–311G(d,p)/3–21G*). On the other hand, it is 4% for the harmonic frequencies (at B3LYP/6–311G(d,p)/3–

21G*). The improvement in results of anharmonic DFT calculations over harmonic one is largest for these modes. The deviations for C–H stretching vibrations in isomeric iodonitrobenzenes are larger in comparison to those of benzene, nitrobenzene and iodobenzene (Table 4.11). The analysis of data also shows that some vibrational modes in OINB, MINB and PINB molecules involve stronger anharmonic effects as compared to benzene, nitrobenzene and iodobenzene. The aromatic C–H in plane bending vibrations occur in the region 1290–990 cm^{-1} [7, 8, 50]. These bands are observed with weak to medium intensities in FTIR and Raman spectra and are assigned (Table 4.5, 4.7 and 4.9). The C–H out of plane bending vibrations appear in the region 950–600 cm^{-1} [21]. These modes are also identified in iodonitrobenzenes and they have higher PED contributions than in plane bending vibrations (Table 4.5, 4.7 and 4.9).

C–X vibrations

The C–NO_2 stretching vibrations normally show their presence in the region 1180–865 cm^{-1} in aromatic nitro compounds [7, 8, 10, 50]. In IR spectrum of nitrobenzene, C–NO_2 stretching vibration, mixed with ring vibrations, is reported at 1108 and 392 cm^{-1} [51]. According to PED values, the maximum contributions of C–NO_2 stretching vibrations (about 45%) are obtained in the mode 30 for OINB and MINB. In the case of PINB, the contribution of this vibration is 58% in mode 29. The vibrational band due to C–NO_2 stretching vibration is observed at lower wavenumbers in OINB and MINB than that for PINB. The pure torsional vibrations of C–NO_2 are found at very low wavenumbers in mode 36 for OINB, MINB and PINB. For the nitrobenzene, it was observed at 51 cm^{-1} [51]. A comparison of C–NO_2 torsional vibrational frequencies revealed close similarity in magnitude in all these molecules. It should be emphasized that the calculated frequencies for these vibrations are in good agreement with the corresponding experimental values. Due to the large mass of iodine atom, the C–I stretching vibration appears in low wavenumber region, 610–200 cm^{-1} and it mixes with ring vibrations [19, 50, 52, 54]. The C–I stretching vibration is reported at 269 cm^{-1} in the Raman spectrum of 2–iodopyridine [52]. This vibration has been calculated at 109 cm^{-1} [53] in p–iodobenzene sulfonyl chloride, at 238 cm^{-1} in 5–iodouracil [54] and at 262 cm^{-1} in 2–iodopyridine [52] using DFT/B3LYP theory. In the present investigation, C–I stretching vibrations have high PED contribution in mode 32 for OINB, MINB and in mode 33 for PINB. These vibrations are observed

with weak intensities in FTIR and Raman spectra of all the molecules except Raman spectrum of MINB. In the present work, the C–I stretching vibrations are found at very low wavenumbers as a contradiction to spectral region of 500 ± 100 cm^{-1} reported for other compounds containing iodine [55]. The remarkable reduction in the frequencies may be due to interaction of C–I stretching vibration with ring vibrations [54]. The C–I in plane bending vibrations have been calculated at 151, 126, 152 cm^{-1} in OINB, MINB and PINB respectively at B3LYP/6–311G(d,p)/3–21G* level of theory. The computed frequencies at 193, 184 and 71 cm^{-1} at B3LYP/6–311G(d,p)/3–21G* level of theory with very weak IR intensities in OINB, MINB and PINB, respectively, are assigned to C–I out of plane bending vibrations and are in good agreement with the experimental values.

Ring vibrations

The C–C stretching vibrations of the phenyl ring occur in the region 1650–1100 cm^{-1} [56, 22]. In the present FTIR and Raman spectra, these vibrational bands are observed with variable intensity in the region 1600–1000 cm^{-1} in OINB, MINB and PINB. As compared to range cited in literature, noticeable decrements in frequencies are found. These vibrations are affected by the nature of attached substituent (heavy iodine atom) with the phenyl ring [53]. The calculated anharmonic frequencies are found to be in good agreement with experimental values. Other observed skeletal vibrations are mixed to a considerable extent in all investigated molecules (Table 4.5, 4.7 and 4.9). The ring breathing and Kekule modes appear at 993 and 1309 cm^{-1} in benzene molecule respectively [57, 58]. From the PED values and animated modes, the IR bands due to ring breathing and Kekule modes are assigned, respectively, at 1015 and 1261 cm^{-1} in iodobenzene; at 1039 and 1290 cm^{-1} in OINB; at 1052 and 1303 cm^{-1} in MINB; and at 1053 and 1307 cm^{-1} in PINB. Kekule mode is assigned at 1325 cm^{-1} in nitrobenzene [51] and around 1300 cm^{-1} in monohalogenated nitrobenzenes [7]. The ring twist mode is found at 1350 cm^{-1} in benzene molecule [58]. The infrared bands observed at 1321, 1316, 1265 and 1272 cm^{-1} in iodobenzene, nitrobenzene, MINB and PINB, respectively, are assigned to the ring twist modes. In the case of OINB, it is observed at 1428 cm^{-1} with very low PED value. The other important mode of vibration "Star of David (trigonal ring breathing)" is assigned with the help of PED and visual inspection that can be seen in Table 4.5, 4.7, 4.9 and 4.11. This mode is reported at 1000 (1001) cm^{-1} in the IR (Raman) spectra of 3–fluoroaniline [36].

4.5 Theoretical and experimental vibrational frequencies along with intensities, vibrational assignments and PED values for OINB.

Observed wavenumbers (cm^{-1})		B3LYP												Assignment and PED values (%)
		6-311G(d,p)/3-21G*				6-311++G(d,p)/3-21G*				cc-pVTZ/3-21G*				
FTIR	Raman[a]	ω^{har}	ω^{anh}	I^{IR}	I^{RA}	ω^{har}	ω^{anh}	I^{IR}	I^{RA}	ω^{har}	ω^{anh}	I^{IR}	I^{RA}	
3084vw	3091m	3220	3076	1.9	380.6	3214	3066	2.0	469.4	3220	3073	1.7	395.5	νCH (87)
	3069m	3207	3068	2.8	284.1	3207	3067	1.4	226.0	3210	3071	2.4	273.9	νCH (83)
		3195	3067	7.2	425.7	3195	3065	5.2	384.8	3197	3067	6.2	411.1	νCH (77)
		3179	3053	2.8	203.2	3180	3056	2.4	184.5	3181	3059	2.5	192.3	νCH (86)
1582s	1580s	1639	1604	176.4	571.1	1628	1585	107.3	172.8	1634	1591	105.3	144.1	νCC (71) + βCNO (7)
	1560m	1617	1580	34.4	238.5	1612	1575	36.2	241.0	1616	1578	44.6	184.8	νCC (50) + βHCC (10) + βCCC (9)
1525vvs	1525m	1598	1562	66.4	138.3	1588	1549	182.5	159.0	1593	1557	143.3	127.3	$\nu_{as}NO_2$ (73)
1462w	1460vw	1489	1459	25.4	7.1	1491	1455	21.1	13.9	1494	1465	23.8	8.7	βHCC (51) + βCCC (25)
1428w		1462	1435	5.2	6.5	1462	1430	4.6	10.6	1468	1440	4.4	8.0	βHCC (53)[b] + νCC (19)
1334vs	1341vs	1380	1349	225.3	848.3	1379	1350	211.8	815.9	1379	1347	208.7	776.8	$\nu_s NO_2$ (75) + νNC (8)
1290m		1331	1304	10.3	107.0	1331	1299	9.0	104.6	1331	1300	9.0	103.6	νCC (63)[c] + βHCC (8)
1243m	1250vw	1286	1261	7.2	25.3	1289	1258	6.7	14.9	1285	1264	6.1	19.7	βHCC (56) + νCC (21)
1165w	1158w	1189	1179	0.9	98.9	1190	1175	0.8	95.7	1191	1175	0.7	95.3	βHCC (80) + νCC (9)
1136w	1135w	1164	1145	7.4	177.3	1166	1142	6.0	198.9	1167	1148	5.3	169.2	νCC (37) + βHCC (28)
1101m	1104w	1127	1111	10.4	229.3	1132	1104	6.8	209.7	1133	1113	8.2	258.4	βCCC (20) + βHCC (18) + νCC (10) + νNC (8)
1039w	1035s	1065	1048	0.8	455.0	1110	417	0.4	23.4	1070	1047	7.4	200.4	νCC (53)[d] + βCCC (15) + βHCC (12)
1019m	1016w	1043	1024	31.8	190.2	1066	1039	3.9	282.5	1056	1036	21.9	458.7	βCCC (50)[e] + νCC (22)
946w		1030	943	0.2	2.2	1049	1024	24.8	457.3	1040	978	0.2	2.4	τHCCC (57) + τCCCC (18)
930w		993	940	2.2	2.2	1003	865	1.6	1.6	999	962	1.7	1.4	τHCCC (78)
852m	854w	910	854	0.2	15.8	938	782	0.8	17.5	916	878	0.1	12.4	τHCCC (76)
872w		871	862	35.1	167.3	870	857	28.9	225.1	870	860	31.7	177.9	βNO_2 (53) + νNC (11) + βCCC (8)
779s	778vw	811	779	11.7	5.4	835	688	5.2	29.9	820	790	9.1	6.4	γNCCC (42) + τHCCC (20) + τCCCC (12)
727vs		762	724	45.6	33.2	785	703	32.4	26.4	771	740	43.9	31.3	τHCCC (53) + γNCCC (21) + τCCCC (6)
692s	691vw	724	691	12.5	19.2	737	698	29.1	32.4	733	709	11.8	16.9	ωNO_2 (73) + τHCCC (10)
		714	704	13.7	21.5	714	701	11.9	33.2	717	706	13.1	26.6	βCCC (40) + βNO_2 (18) + νNC (8)
639w	635w	653	644	5.2	94.8	655	645	4.8	93.5	658	649	4.9	86.5	βCCC (72)
556w		571	558	0.5	56.5	588	538	0.5	52.2	579	566	0.5	39.9	βCNO (45) + τHCCC (9)
466w	465w	487	471	5.6	32.3	499	444	9.1	58.8	493	478	4.8	44.8	τC-C-C-C (69) + τHCCC (9)

Table: 4.5 (*continued*)

29	424w	420w	430	414	0.4	9.8	427	390	0.6	16.9	428	412	0.4	12.2	τCCCC (49) + βCNO (12) + τHCCC (12) + γOCON (6)
30	379vw		406	403	1.9	284.9	403	398	1.4	262.4	405	401	1.6	279.5	νNC (42) + βCCC (11)
31	250w	244w	302	298	1.2	128.4	302	296	1.4	138.9	305	300	1.2	128.2	βCNO (67)
32	238w	244m	249	244	0.3	218.3	248	242	0.5	181.9	251	247	0.2	186.5	νCl (49) + βCCl (18)
33	202w	200w	198	192	0.2	263.3	196	183	0.5	299.1	196	190	0.2	218.8	γ[NCCC + ICCC] (78)
34	139w	132w	153	151	1.8	41.7	146	142	2.5	51.1	150	146	1.8	56.6	β[CCl + CCN] (68)
35		92vs	113	106	1.0	649.2	114	103	1.2	522.6	114	108	1.0	607.3	τNCCC (57) + γCCCC (19) + τONCC (7)
36	70w		51	49	0.2	1093.8	46	39	0.3	1345.9	49	40	0.2	1156.6	τNO_2 (82)
RMS			50	15			55	32			53	19			
MAD			39	11			45	22			42	16			

Abbreviation used: ν–stretching, ν_a, ν_s–asymmetric and symmetric stretching, β–bending, τ–torsional motion, γ–out of plane motion, ω– wagging motion; vw–very weak, w–weak, m–medium, s–strong, vs– very strong, vvs–very very strong, RMS– Root Mean Square, MAD–Mean Absolute Deviation, ω^{har}: harmonic wavenumber (cm^{-1}), ω^{anh}: anharmonic wavenumber (cm^{-1}), I^{IR}– IR intensity (km/mole), I^{RA}– Raman intensity (arb. unit), M– mode no.
[a]Ref. [7, 23], [b]ring twist, [c]Kekule, [d]ring breathing, [e]trigonal ring breathing

Table 4.6 Theoretical harmonic and anharmonic vibrational frequencies (cm^{-1}) for OINB.

#M	B3LYP						MP2						HF					
	6–311G(d,p) /LANL2DZ		6–311++G(d,p) /LANL2DZ		cc–pVTZ /LANL2DZ		6–311G(d,p) /LANL2DZ		6–311++G(d,p) /LANL2DZ		cc–pVTZ /LANL2DZ		6–311G(d,p) /LANL2DZ		6–311++G(d,p) /LANL2DZ		cc–pVTZ /LANL2DZ	
	ω^{har}	ω^{anh}	ω^{har}	ω^{anh}	ω^{har}	ω^{anh}	ω^{har}	ω^{anh}	ω^{har}	ω^{anh}	ω^{har}	ω^{anh}	ω^{har}	ω^{anh}	ω^{har}	ω^{anh}	ω^{har}	ω^{anh}
1	3217	3075	3213	3068	3218	3072	3244	3109	3239	3123	3250	3113	3384	3262	3379	3258	3377	3257
2	3209	3069	3208	3071	3211	3075	3236	3113	3231	3129	3243	3119	3371	3245	3370	3242	3366	3244
3	3195	3066	3195	3068	3197	3067	3229	3096	3223	3117	3235	3100	3357	3222	3356	3221	3352	3222
4	3179	3055	3179	3057	3182	3056	3216	3093	3212	3099	3223	3095	3339	3194	3338	3193	3334	3189
5	1638	1603	1625	1583	1631	1588	1797	1785	1777	1788	1765	1751	1848	1805	1819	1778	1823	1783
6	1617	1578	1612	1574	1617	1577	1631	1590	1627	1724	1640	1598	1770	1731	1765	1729	1768	1730
7	1603	1567	1590	1554	1597	1557	1618	1580	1615	1701	1619	1579	1755	1715	1752	1713	1752	1714
8	1488	1461	1487	1457	1496	1467	1495	1467	1494	1564	1503	1472	1652	1615	1649	1611	1649	1617
9	1462	1436	1461	1435	1469	1436	1469	1437	1471	1587	1484	1439	1622	1591	1620	1588	1626	1595
10	1384	1353	1381	1348	1383	1347	1451	1418	1452	1513	1456	1420	1584	1559	1582	1556	1587	1560
11	1327	1300	1326	1298	1328	1302	1401	1381	1397	1397	1396	1377	1402	1379	1401	1376	1406	1381
12	1286	1263	1286	1262	1291	1266	1291	1270	1290	1363	1295	1270	1315	1303	1315	1301	1314	1302

Table: 4.6 (*continued*)

13	1189	1178	1190	1177	1192	1175	1188	1171	1187	1235	1187	1170	1272	1252	1270	1249	1271	1249
14	1165	1146	1164	1145	1168	1145	1182	1167	1182	1220	1184	1161	1227	1210	1227	1209	1230	1212
15	1127	1109	1128	1106	1132	1109	1142	1126	1142	1220	1149	1129	1188	1176	1186	1174	1181	1170
16	1064	1046	1062	1045	1068	1046	1066	1053	1062	1102	1082	1059	1140	1122	1138	1120	1145	1125
17	1027	1013	1028	1014	1043	1022	1035	1024	1038	1175	1059	1039	1124	1101	1119	1103	1137	1106
18	1006	991	1001	1018	1022	991	912	1022	921	875	1014	973	1108	1093	1108	1094	1119	1102
19	975	956	972	967	987	964	905	1041	912	1075	974	954	1092	1068	1089	1069	1099	1076
20	886	866	883	871	902	877	865	860	864	904	897	871	994	972	991	971	1004	980
21	871	862	868	856	870	857	842	890	849	931	864	855	972	962	969	959	970	961
22	800	785	798	786	809	791	777	791	767	909	805	782	904	889	900	885	910	894
23	748	737	745	737	757	741	730	735	729	742	753	742	838	824	836	824	844	830
24	707	698	706	699	721	701	706	702	703	795	733	719	785	768	778	781	799	782
25	705	694	695	721	710	699	643	644	645	825	711	703	767	759	766	757	770	761
26	647	641	648	641	654	645	620	715	630	955	652	644	694	689	695	689	700	693
27	573	564	575	573	579	566	494	993	496	524	592	582	631	623	632	628	637	627
28	470	464	463	463	478	464	437	470	416	806	464	468	515	506	510	503	518	509
29	419	410	412	402	417	406	403	400	397	538	409	401	453	443	447	434	447	436
30	398	393	397	392	400	393	392	394	374	651	401	387	436	432	434	429	436	430
31	296	294	295	293	300	294	299	297	300	465	307	304	325	323	324	323	330	327
32	238	234	238	235	245	239	239	236	237	528	251	247	256	253	256	254	263	260
33	189	186	186	181	189	184	176	179	163	554	180	179	206	202	203	199	204	200
34	147	145	144	141	147	139	138	136	128	429	138	134	157	154	153	151	156	152
35	110	105	108	102	110	109	106	106	105	1234	109	106	123	120	121	118	122	117
36	53	51	48	41	49	21	51	49	46	732	42	39	57	55	50	48	49	44
RMS	47	18	44	21	50	20	70	93	67	286	71	44	145	114	141	112	145	115
MAD	34	14	32	15	39	15	48	47	47	194	53	30	119	96	116	95	121	98

Abbreviation used: M–mode no., RMS– Root Mean Square, MAD -Mean Absolute Deviation, ω^{har}: harmonic wavenumber, ω^{anh}: anharmonic wavenumber

Table 4.7 Theoretical and experimental vibrational frequencies along with intensities, vibrational assignments and PED values for MINB.

#M	Species	Observed wavenumbers (cm^{-1})		B3LYP												Assignment and PED values (%)
				6–311G(d,p)/3–21G*				6–311++G(d,p)/3–21G*				cc–pVTZ/3–21G*				
		FTIR	Raman[a]	ω^{har}	ω^{anh}	I^{IR}	I^{RA}	ω^{har}	ω^{anh}	I^{IR}	I^{RA}	ω^{har}	ω^{anh}	I^{IR}	I^{RA}	
1	a'			3235	3091	7.5	89.2	3233	3087	8.7	84.8	3237	3093	7.2	84.3	vCH (100)
2	a'	3095m	3092s	3229	3098	3.6	249.1	3227	3096	4.4	252.2	3232	3102	3.8	247.3	vCH (97)
3	a'		3072m	3203	3077	3.1	323.1	3203	3075	2.2	317.4	3204	3082	3.2	335.8	vCH (87)

continued)

3035w		3185	3054	4.1	252.1	3186	3031	3.3	232.2	3187	3042	3.4	228.3	νCH (88)
1599m		1651	1613	39.6	12.8	1641	1600	17	21.8	1646	1610	15.0	32.4	νCC(67) + β CNO (7)
	1563s	1614	1575	7.0	374.1	1612	1572	6	483.7	1615	1579	8.3	377.1	νCC (55) + βCCC (13) + βHCC (7)
1527vvs	1524w	1600	1561	228.0	148.6	1584	1545	300	221.9	1592	1555	266.0	153.6	$\nu_{as}NO_2$ (83)
1456m	1454vw	1495	1462	24.5	6.0	1495	1458	20	16.2	1502	1473	21.0	6.4	βHCC (60)
1414w	1412vw	1448	1421	7.1	11.9	1447	1416	5.5	25.1	1451	1423	5.2	13.1	νCC (49) + βHCC (24)
1348vvs	1345vvs	1380	1350	291.3	1281.7	1371	1342	300	1538.7	1375	1347	280	1304.1	ν_sNO_2 (79) + νNC (7)
1303m		1337	1307	10.1	28.9	1337	1307	10	35.8	1338	1305	9.5	29.2	νCC (69)[b] + βHCC (10)
1265m		1303	1278	5.2	9.8	1305	1275	7.1	11.0	1305	1285	6.1	10.0	βHCC (75)[b] + νCC (7)
1178w		1196	1178	0.0	42.6	1197	1171	0	40.9	1198	1186	0.0	43.7	βHCC (72) + νCC (6)
1101m	1108m	1123	1100	56.7	303.2	1123	1099	44	278.3	1130	1103	52.0	323.3	βHCC (27) + ν[CC + NC] (25) + βCCC (8)
1072m	1067m	1116	1090	12.0	86.0	1116	1085	27	190.7	1117	1096	14.0	101.5	βHCC (26) + νCC (15) + βCCC (14)
1052m	1044w	1082	1063	11.5	113.0	1082	1063	12	144.3	1087	1071	12.0	84.3	βCCC (16) + βHCC (14) + νCC (12)[d]
963w		1021	961	0.1	0.2	1037	779	0.0	9.2	1030	1000	0.1	0.3	τHCCC (71) + τCCCC (15)
1009w	1010vvs	1011	1002	6.3	584.1	1010	995	5.4	624.6	1022	1003	4.1	628.2	βCCC (45)[c] + νCC (32)
928w		973	921	4.7	13.1	968	893	2.5	4.5	982	942	4.1	10.8	τHCCC (73)
885s	890vw	946	888	5.8	3.8	939	874	5.3	10.1	950	937	5.5	3.8	τHCCC (65) + τCCCC (13)
863s	854w	882	872	29.0	64.6	880	871	26.8	96.4	882	870	27.6	82.5	βNO_2 (48) + νNC (14) + βCCC (6)
776sh		823	798	22.0	15.8	809	815	31.5	3.7	836	821	12.9	11.5	τHCCC (74)
729vs	725vw	740	737	29.8	35.7	728	752	16.6	43.3	762	757	38.8	15.7	ωNO_2 (80) + τHCCC (10)
711s	706w	732	723	41.0	17.2	732	721	37.2	27.7	735	726	39.4	23.4	βCCC (33) + βNO_2 (26) + νIC (12) + νCC (9) + νNC (7)
659s	654s	694	660	14.6	1.3	651	818	15.5	59.5	700	697	9.6	1.1	τCCCC (55) + τHCCC (15)
639m	638m	659	651	4.0	124.3	659	651	3.7	131.8	664	656	3.4	116.0	βCCC (53) + νIC (13)
529w		538	525	1.3	49.7	537	525	1.3	48.3	538	526	1.3	46.1	βCNO (77)
485w		505	489	4.3	8.2	505	494	7.9	53.5	518	505	3.6	16.1	[τCCCC + γNCCC] (81) + τHCCC (6)
422m	425vw	438	422	0.9	0.5	436	464	2.0	20.2	446	432	0.7	1.9	τCCCC (70) + τHCCC (19)
381w	390vw	400	396	0.9	70.3	399	395	0.6	60.2	400	396	0.9	63.6	νNC (45) + βCCC (20)
252w	250w	302	301	0.7	84.7	300	299	0.8	63.0	303	306	0.5	83.2	βCNO (90)
238w		257	253	0.4	442.4	257	253	0.3	442.6	260	261	0.4	400.3	νIC (58) + βCCC (21)
212w		188	184	1.5	241.5	187	182	1.9	229.0	190	189	1.4	201.9	[τCCCC + γICCC] (80)
140m	140s	143	143	0.1	235.0	146	144	0.0	182.9	147	155	0.2	200.3	γICCC (80) + τCCCC (10)
	128m	127	126	1.1	211.7	126	123	1.2	161.7	127	135	1.2	232.9	β[CCI + CCN] (78)
70w	68m	45	62	0.1	273.8	42	48	0.2	407.9	45	111	0.1	219.3	τNO$_2$ (91)
		53	15			51	45			55	23			
		40	10			37	22			43	19			

ed: ν–stretching, ν_s, ν_{as}–asymmetric and symmetric stretching, β–bending, τ–torsional motion, γ–out of plane motion, ω– wagging motion; vw–very weak, w–weak, m–medium, s–strong, , vvs–very very strong, RMS– Root Mean Square, MAD–Mean Absolute Deviation, ω^{har}: harmonic wavenumber (cm^{-1}), ω^{anh}: anharmonic wavenumber (cm^{-1}), I^{IR}– IR intensity (km/mole), ensity (arb. unit), M– mode no.

ing twist, [c]Kekule, [d]ring breathing, [e]trigonal ring breathing

Table 4.8 Theoretical harmonic and anharmonic vibrational frequencies (cm^{-1}) for MINB.

#M	Species	B3LYP						MP2		HF					
		6-311G(d,p) /LANL2DZ		6-311++G(d,p) /LANL2DZ		cc-pVTZ /LANL2DZ		cc-pVTZ /LANL2DZ		6-311G(d,p) /LANL2DZ		6-311++G(d,p) /LANL2DZ		cc-pVTZ /LANL2DZ	
		ω^{har}	ω^{anh}	ω^{har}	ω^{anh}	ω^{har}	ω^{anh}	ω^{har}	ω^{anh}	ω^{har}	ω^{anh}	ω^{har}	ω^{anh}	ω^{har}	ω^{anh}
1	a'	3237	3102	3234	3096	3238	3094	3269	3122	3408	3281	3405	3277	3404	3280
2	a'	3230	3094	3227	3089	3231	3102	3266	3135	3401	3284	3398	3283	3397	3282
3	a'	3207	3076	3206	3064	3206	3083	3242	3116	3368	3230	3367	3247	3362	3229
4	a'	3186	3051	3186	3049	3188	3043	3226	3102	3347	3224	3346	3220	3343	3216
5	a'	1650	1611	1639	1601	1644	1607	1765	1749	1853	1812	1829	1790	1832	1794
6	a'	1615	1575	1611	1572	1616	1580	1649	1609	1766	1728	1762	1722	1763	1723
7	a'	1599	1558	1583	1544	1591	1556	1622	1581	1760	1723	1752	1712	1755	1718
8	a'	1491	1456	1490	1455	1501	1469	1503	1470	1639	1599	1630	1596	1634	1602
9	a'	1448	1425	1446	1421	1453	1421	1492	1453	1620	1590	1616	1586	1621	1591
10	a'	1380	1349	1371	1340	1375	1348	1437	1406	1565	1535	1562	1532	1565	1538
11	a'	1335	1303	1335	1299	1337	1308	1393	1373	1426	1404	1427	1405	1435	1409
12	a'	1300	1273	1302	1277	1308	1284	1306	1280	1314	1301	1313	1299	1314	1299
13	a'	1194	1175	1195	1179	1199	1179	1201	1185	1235	1221	1231	1201	1236	1206
14	a'	1118	1090	1118	1093	1124	1096	1157	1134	1229	1213	1228	1213	1229	1211
15	a'	1113	1081	1112	1086	1118	1093	1130	1108	1189	1169	1188	1172	1187	1170
16	a'	1075	1054	1075	1054	1082	1064	1094	1070	1156	1138	1155	1136	1163	1144
17	a''	1006	986	1004	990	1020	999	1002	1003	1122	1099	1122	1078	1135	1107
18	a'	1013	1002	1013	1000	1022	1007	1018	1007	1083	1075	1083	1073	1090	1082
19	a''	954	934	948	941	969	943	938	929	1074	1048	1068	1049	1084	1060
20	a''	921	905	915	917	942	927	900	918	1044	1017	1039	1026	1060	1033
21	a'	879	869	877	866	880	869	884	873	981	970	979	969	981	971
22	a''	811	801	803	819	828	820	814	819	906	896	894	913	925	912
23	a''	735	735	722	757	756	757	741	736	835	834	813	857	857	845
24	a'	723	713	722	711	729	718	740	731	788	779	788	779	795	785
25	a''	679	671	659	756	694	702	678	728	733	723	715	806	747	731
26	a'	654	647	654	645	660	652	658	650	701	695	701	695	707	700
27	a'	538	521	538	522	538	530	535	520	584	591	583	570	581	566
28	a''	489	484	482	492	500	509	498	510	537	529	530	541	544	536
29	a''	431	425	427	436	436	431	436	433	469	464	466	477	473	466
30	a'	399	394	398	393	400	396	404	399	437	434	435	432	436	433
31	a'	303	300	302	297	305	308	305	305	331	329	330	329	332	330
32	a'	242	239	244	238	252	254	271	266	262	259	264	261	274	270

Table: 4.8 (*continued*)

33	a"	183	181	182	180	185	188	185	185	204	202	204	201	205	202
34	a"	138	139	138	138	141	154	144	146	154	153	154	155	156	155
35	a'	127	123	128	124	129	138	130	126	138	136	139	137	140	139
36	a"	45	49	41	45	44	121	33	33	42	46	42	49	46	46
	RMS	50	15	48	24	53	23	73	43	149	114	145	115	150	115
	MAD	35	11	32	15	40	18	52	33	122	98	118	99	125	99

Abbreviation used: M–mode no., RMS– Root Mean Square, MAD–Mean Absolute Deviation, ω^{har}: harmonic wavenumber, ω^{anh}: anharmonic wavenumber

Table 4.9 Theoretical and experimental vibrational frequencies along with intensities, vibrational assignments and PED values for PINB.

#M	Species	Observed wavenumbers (cm^{-1})		B3LYP												Assignment and PED values (%)
				6–311G(d,p)/3–21G*				6–311++G(d,p)/3–21G*				cc–pVTZ/3–21G*				
		FTIR	Raman[a]	ω^{har}	ω^{anh}	I^{IR}	I^{RA}	ω^{har}	ω^{anh}	I^{IR}	I^{RA}	ω^{har}	ω^{anh}	I^{IR}	I^{RA}	
1	a1		3078m	3225	3086	3.0	451.4	3223	3088	3.7	453.7	3227	3089	3.5	443.6	νCH (91)
2	b2	3093m		3224	3094	1.5	75.9	3223	3088	2.1	64.3	3227	3098	1.3	69.6	νCH (94)
3	b2	3051w		3201	3064	1.5	116.4	3200	3056	0.8	102.1	3202	3066	1.5	107.7	νCH (94)
4	a1			3201	3084	0.2	139.5	3200	3081	0.3	126.4	3202	3089	0.2	144.2	νCH (91)
5	b2	1595m	1590w	1649	1610	101.7	14.9	1639	1599	73.7	16.2	1643	1602	74.5	9.1	νCC (68) + βCNO (9)
6	a1	1570m	1562s	1616	1577	69.6	1702.3	1614	1579	76.0	2018.4	1619	1581	71.3	1793.0	νCC (69) + βHCC (17) + βCCC (12)
7	b2	1513vvs	1510w	1593	1554	135.2	66.3	1575	1536	210.7	143.5	1582	1544	177.0	81.1	$\nu_{as}NO_2$ (76)
8	a1	1470w	1463w	1506	1470	34.1	14.2	1506	1463	30.3	25.9	1514	1480	33.0	13.9	βHCC (67) + βCCC (11)
9	b2	1394vw	1404w	1423	1392	8.1	7.2	1421	1396	5.6	16.2	1426	1397	6.1	7.8	νCC (32) + βHCC (32) + βCCC (16)
10	a1	1343vvs	1340vvs	1377	1347	414.4	4712.0	1367	1338	446.6	5918.1	1372	1344	410.3	4931.0	ν_sNO_2 (79) + νNC (7)
11	b2	1307m		1339	1313	9.3	3.1	1341	1313	11.8	3.0	1341	1304	9.4	3.2	νCC (40)[c] + βHCC (31)
12	b2	1272w		1316	1285	2.4	0.4	1319	1284	3.3	1.0	1317	1291	2.6	0.0	βHCC (57)[b] + νCC (29)
13	a1	1179m	1179w	1206	1186	6.6	40.5	1208	1181	9.8	82.4	1208	1190	8.8	45.7	βHCC (68) + νCC (17)
14	b2	1104m	1104s	1124	1103	9.0	0.4	1126	1111	7.2	1.0	1127	1108	7.9	0.5	βHCC (65) + νCC (23)
15	a1	1073w	1067m	1120	1092	38.5	1574.2	1118	1100	43.1	1837.2	1124	1094	31.8	1527.4	νCC (37) + νNC (17) + βHCC (10)
16	a1	1053w	1052vs	1079	1055	22.1	634.4	1080	1044	24.7	881.2	1090	1066	31.4	836.2	βCCC (34) + βHCC (18) + νCC (13)[d]
17	a1	1008m	1002w	1027	1009	28.7	43.0	1030	1043	28.1	36.8	1037	1017	25.1	34.6	βCCC (61)[e] + νCC (16)
18	a2			1019	955	0.00	0.10	1026	882	0.0	1.1	1027	981	0.0	1.3	τHCCC (74) + τCCCC (25)
19	b1	915vw		1016	925	0.3	12.7	1043	701	1.6	62.7	1024	975	0.6	8.2	τHCCC (68) + τCCCC (25)
20	b1	837s	835vw	872	843	39.1	22.0	860	835	34.3	3.9	887	867	28.9	21.9	τHCCC (85)
21	a1	851sh	845w	869	859	78.7	232.1	868	847	71.6	294.4	869	858	73.4	260.2	βNO_2 (54) + νCC (12) + νNC (6)
22	a2			860	828	0.0	25.4	852	808	0.0	2.1	864	839	0.0	17.0	τHCCC (100)

ble: 4.9 (*continued*)

b1	734s	732vw	751	725	14.8	26.9	740	733	1.6	165.4	779	752	23.2	4.3	[τCCCC + ωNO$_2$] (67) + τHCCC (16)
a1	700vw	698w	719	710	0.7	57.7	718	690	0.7	55.0	722	712	0.2	51.2	βCCC (42) + ν[NC + IC] (15)
b1	671w		710	677	17.5	13.3	704	658	26.6	10.6	722	695	13.9	12.2	τCCCC (64) + τHCCC (14) + γOCON (7)
b2	621w	618w	638	631	0.5	145.2	638	628	0.4	167.7	643	634	0.4	132.8	βCCC (81) + β CCI (7)
b2	530vw		533	535	1.5	78.7	532	516	1.7	64.0	532	518	1.6	78.6	βCNO (77)
b1	468w		477	466	8.5	0.2	472	472	15.1	58.8	488	475	7.2	3.8	[τCCCC + γNCCC] (92)
a1	455w	460w	465	457	6.3	3.2	465	450	5.1	6.6	468	461	5.7	4.9	νNC (58) + βCCC (14)
a2		400vw	427	411	0.0	0.7	431	402	0.0	0.6	435	415	0.0	1.2	τCCCC (75) + τHCCC (25)
b2	266m		296	292	0.8	18.9	295	290	1.1	34.9	296	291	0.5	10.4	βCNO (87)
b1	248s	250w	257	250	2.9	87.3	261	246	3.6	171.5	264	254	2.6	55.6	γNCCC (84)
a1	222w	216w	215	214	0.0	151.3	215	182	0.0	122.9	218	216	0.0	126.7	νIC (61) + βCCC (22)
b2	125w	130w	151	152	1.7	127.4	150	196	1.6	54.5	152	150	1.8	117.9	βCCI (82)
b1	70w		74	71	2.0	2.4	75	73	2.2	43.9	76	72	2.1	0.6	γ[NCCC + ICCC] (90)
a2		79w	57	56	0.0	51.6	53	56	0.0	0.9	57	57	0.0	61.0	τNO$_2$ (98)
RMS			55	13			55	42			58	18			
MAD			40	9			39	18			44	14			

eviation used: ν-stretching, ν$_s$, ν$_a$-asymmetric and symmetric stretching, β–bending, τ–torsional motion, γ–out of plane motion, ω– wagging motion; vw–very weak, w–weak, m–um, s–strong, vs– very strong, vvs–very very strong, RMS– Root Mean Square, MAD–Mean Absolute Deviation, ω^{har}: harmonic wavenumber (cm^{-1}), ω^{anh}: anharmonic number (cm^{-1}), I^{IR} – IR intensity (km/mole), I^{RA} – Raman intensity (arb. unit), M – mode n.

[7, 23], [b]ring twist, [c]Kekule, [d]ring breathing, [e]trigonal ring breathing

Table 4.10 Theoretical harmonic and anharmonic vibrational frequencies (cm^{-1}) for PINB.

Species	B3LYP						MP2				HF					
	6-311G(d,p) /LANL2DZ		6-311++G(d,p) /LANL2DZ		cc-pVTZ /LANL2DZ		6-311G(d,p) /LANL2DZ		6-311G(d,p) /LANL2DZ		6-311++G(d,p) /LANL2DZ		cc-pVTZ /LANL2DZ	
	ω^{har}	ω^{anh}	ω^{har}	ω^{anh}	ω^{har}	ω^{anh}	ω^{har}	ω^{anh}	ω^{har}	ω^{anh}	ω^{har}	ω^{anh}	ω^{har}	ω^{anh}
a1	3225	3084	3222	3082	3227	3087	3258	3116	3398	3276	3395	3273	3395	3274
b2	3225	3093	3222	3093	3227	3098	3258	3128	3398	3277	3395	3279	3395	3279
b2	3204	3066	3202	3063	3205	3068	3230	3105	3369	3251	3368	3251	3364	3249
a1	3203	3086	3202	3084	3205	3090	3229	3116	3369	3241	3367	3240	3364	3241
b2	1651	1611	1640	1598	1644	1604	1797	1778	1853	1813	1829	1791	1832	1794
a1	1613	1575	1610	1571	1616	1577	1626	1594	1768	1732	1764	1729	1766	1731
b2	1595	1555	1576	1539	1584	1546	1635	1598	1753	1710	1744	1703	1746	1706
a1	1501	1469	1501	1465	1512	1478	1508	1478	1646	1611	1642	1609	1650	1619

Table: 4.10 (*continued*)

9	b2	1423	1401	1421	1397	1427	1404	1468	1429	1535	1508	1532	1507	1535	1511
10	a1	1378	1346	1368	1335	1373	1344	1407	1389	1628	1600	1620	1590	1623	1586
11	b2	1338	1311	1338	1311	1343	1320	1411	1385	1438	1419	1439	1417	1447	1426
12	b2	1314	1284	1315	1288	1319	1286	1315	1300	1279	1261	1277	1262	1273	1258
13	a1	1202	1181	1203	1183	1208	1187	1209	1190	1298	1283	1297	1282	1301	1286
14	b2	1123	1108	1125	1110	1128	1100	1124	1107	1178	1166	1178	1166	1176	1164
15	a1	1120	1094	1118	1091	1123	1093	1142	1130	1232	1208	1228	1204	1231	1205
16	a1	1066	1044	1065	1043	1076	1053	1086	1071	1149	1130	1148	1129	1160	1141
17	a1	1021	1006	1021	1006	1034	1015	1014	1024	1095	1082	1096	1082	1107	1090
18	a2	995	980	992	995	1009	988	923	1059	1116	1089	1115	1086	1127	1100
19	b1	990	968	978	1002	1009	976	895	1035	1101	1072	1092	1089	1120	1083
20	b1	855	851	845	869	879	863	792	888	958	945	947	955	980	962
21	a1	869	858	867	855	868	856	867	864	970	959	967	956	968	957
22	a2	843	831	839	834	853	838	821	859	944	922	942	920	950	930
23	b1	738	745	719	793	767	757	692	724	837	841	810	892	868	856
24	a1	714	704	714	706	719	708	713	707	774	765	774	764	779	769
25	b1	693	683	665	821	707	693	430	1219	759	744	733	874	772	753
26	b2	636	630	636	629	640	633	629	627	683	678	683	677	687	681
27	b2	533	517	532	521	532	518	534	557	577	583	576	566	574	557
28	b1	468	467	458	491	478	473	420	840	516	512	504	554	525	517
29	a1	453	449	453	450	459	453	465	458	496	494	497	495	504	499
30	a2	418	413	417	418	422	415	398	432	454	448	455	450	458	451
31	b2	296	291	296	292	298	292	298	295	324	320	324	321	326	321
32	b1	249	248	249	249	254	252	240	284	280	277	279	280	282	280
33	a1	205	203	206	204	212	209	210	209	221	220	223	222	230	227
34	b2	152	151	153	152	154	152	152	153	166	166	167	167	168	168
35	b1	72	72	72	71	73	72	72	77	83	81	83	84	84	83
36	a2	56	62	52	59	56	59	13	119	50	56	50	57	56	53
	RMS	53	16	51	35	56	18	88	126	154	119	149	124	155	119
	MAD	36	12	34	19	41	14	60	62	122	99	118	104	125	101

Abbreviation used: M–mode no., RMS– Root Mean Square, MAD–Mean Absolute Deviation, ω^{har}: harmonic wavenumber, ω^{anh}: anharmonic wavenumber

Note: a2 species are IR inactive

perimental and calculated vibrational frequencies (cm^{-1}) along with their assignments (PED, in %) for benzene, nitrobenzene and iodobenzene 3LYP/6–311G(d,p)/3–21G* level of theory.

Benzene					Nitrobenzene					Iodobenzene				
arsanyi[b]	ω^{har}	ω^{anh}	Species	PED (%)	Exp[c]	ω^{har}	ω^{anh}	Species	PED (%)	Exp[c]	ω^{har}	ω^{anh}	Species	PED (%)
3073	3192	3053	a1g	νCH (99)	3107	3225	3102	b2	νCH (97)	3064	3196	3065	b2	νCH (89)
	3181	3033	e1u	νCH (99)	3076	3225	3088	a1	νCH (90)	3064	3188	3073	a1	νCH (95)
3064	3181	3035	e1u	νCH (97)		3196	3040	a1	νCH (93)	3031	3199	3043	a1	νCH (94)
	3165	3035	e2g	νCH (99)		3187	3052	b2	νCH (97)	3048	3174	3035	b2	νCH (89)
3056	3165	3038	e2g	νCH (98)		3175	3013	a1	νCH (92)	3050	3166	3046	a1	νCH (88)
3057	3155	2994	b1u	νCH (100)										
1599	1637	1594	e2g	νCC (66)	1588	1631	1584	a1	νCC(65) + βHCC (19)	1575	1619	1568	a1	νCC (64)
	1637	1594	e2g	νCC (64)	1620	1660	1628	b2	νCC(63)	1575	1619	1579	b2	νCC (67) + βHCC (21)
					1523	1603	1563	b2	$\nu_{as}NO_2$ (81)					
1482	1513	1484	e1u	βHCC (67)	1479	1510	1476	a1	βHCC (69) + βCCC (12)	1473	1507	1473	a1	βHCC (67) + νCC(23)
	1513	1485	e1u	βHCC (62)	1455	1489	1458	b2	βHCC (40) + νCC(38)	1435	1469	1443	b2	βHCC (61) + βCCC (–17)
					1347	1381	1349	a1	ν_sNO_2 (79)					
1350	1381	1352	a2g	βHCC (97)[e]	1316	1336	1307	b2	βHCC (80)[e]	1321	1347	1320	b2	βHCC (79)[e]
1309	1335	1314	b2u	νCC (82)[f]	1325	1353	1322	b2	νCC(71)[f]	1261	1312	1270	b2	νCC (82)[f]
1178	1197	1183	e2g	βHCC (71)	1174	1195	1179	a1	βHCC (67) + νCC (21)	1178	1208	1188	a1	βHCC (73) + νCC (23)
	1197	1185	e2g	βHCC (70)	1162	1184	1170	b2	βHCC (78)	1159	1183	1170	b2	βHCC (78) + νCC (11)
1146	1175	1163	b2u	βHCC (82)						1068	1097	1074	b2	βCCC (40) + βHCC (36)
					1108	1118	1095	a1	νCC (32) + νNC (20)	1060	1086	1060	a1	νCC (43) + βHCC (26)
1037	1060	1040	e1u	νCC(66) + βHCC (22)	1070	1099	1074	b2	βHCC (46) + νCC (19)					
	1060	1042	e1u	βCCC (67)+βHCC (34)	1021	1043	1023	a1	βCCC (45) + βHCC (21)					
1010	1023	1011	b1u	βCCC (95)[h]	1004	1019	1006	a1	βCCC (42)[h] + νCC (35)	998	1011	998	a1	βCCC[h] (72) + νCC (13)
990	1018	998	b2g	τHCCC (70)	990	1019	998	b1	τHCCC (75)	987	1018	945	b1	τHCCC (50) + τCCCC (39)
993	1013	998	a1g	νCC(93)[g]						1015	1037	1020	a1	νCC(71)[g]
967	983	975	e2u	τHCCC (89)	975	999	987	a2	τHCCC (95)	963	1000	944	a2	τHCCC (83) + τCCCC (14)
	983	976	e2u	τHCCC (79)		965	945	b1	τHCCC (88)	904	940	889	b1	τHCCC (91)
	864	851	e1g	τHCCC (94)										
					852	871	859	a1	βNO_2 (57) + νCC (11)					
846	864	850	e1g	τHCCC (100)	840	859	848	a2	τHCCC (–100)	835	862	830	a2	τHCCC (100)
					793	798	795	b1	τHCCC (52) + ωNO_2 (31)	730	761	722	b1	τHCCC (62) + τCCCC (19)
707	724	711	b2g	τCCCC (72)						684	718	681	b1	τHCCC (39) + τCCCC (38)
					710	714	711	b1	ωNO_2 (54) + τHCCC (32)					
673	691	683	a2u	τHCCC (100)	676	697	688	a1	βCCC (41) + βNO_2 (19)	654	671	663	a1	βCCC (–65) + νCl (19)
606	623	618	e2g	βCCC (89)										

ontinued)

					681	692	687	b1	τCCCC (70)					
	623	618	e2g	βCCC (90)	611	627	620	b2	βCCC (79)	613	628	621	b2	βCCC (85)
					532	528	529	b2	βCNO (73)					
398	414	405	e2u	τCCCC (87)	436	445	442	b1	τCCCC (77)	448	472	458	b1	τCCCC (81)
	414	406	e2u	τCCCC (82)	417	418	413	a2	τCCCC (92)	398	418	404	a2	τCCCC (77)
					392	396	390	a1	νNC (45) + βCCC (27)	266	273	268	a1	νCl (71)
					255	258	255	b2	β[CNO+NCC] (82)	220	220	220	b2	βICC (92)
					182	169	168	b1	γNCCC (83)	181	158	153	b1	γICCC (-93)
					51	53	59	a2	τNO$_2$					
	54	18				42	10				61	12		
	40	11				28	7				45	9		

ted: ν–stretching, ν_s, ν_a–asymmetric and symmetric stretching, β–bending, τ–torsional motion, γ–out of plane motion, ω– wagging motion; RMS– Root Mean Square, MAD–Mean Absolute
: harmonic wavenumber, ω^{anh}: anharmonic wavenumber
[58], [51], [74] , [a]ring twist, [b]Kekule, [c]ring breathing, [d]trigonal ring breathing

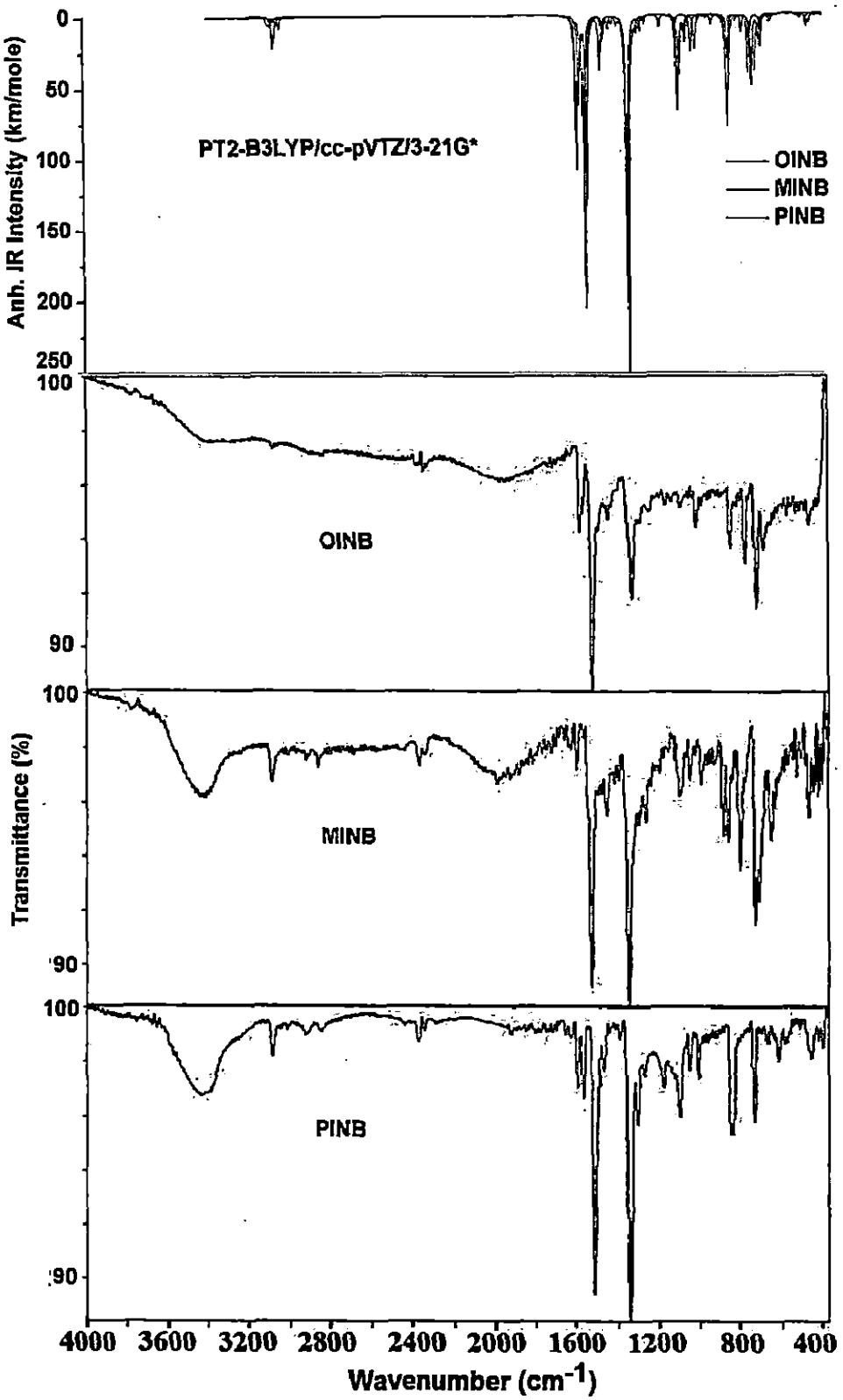

Fig. 4.5 Experimental FTIR and theoretical anharmonic (Anh.) IR spectra of OINB, MINB and PINB.

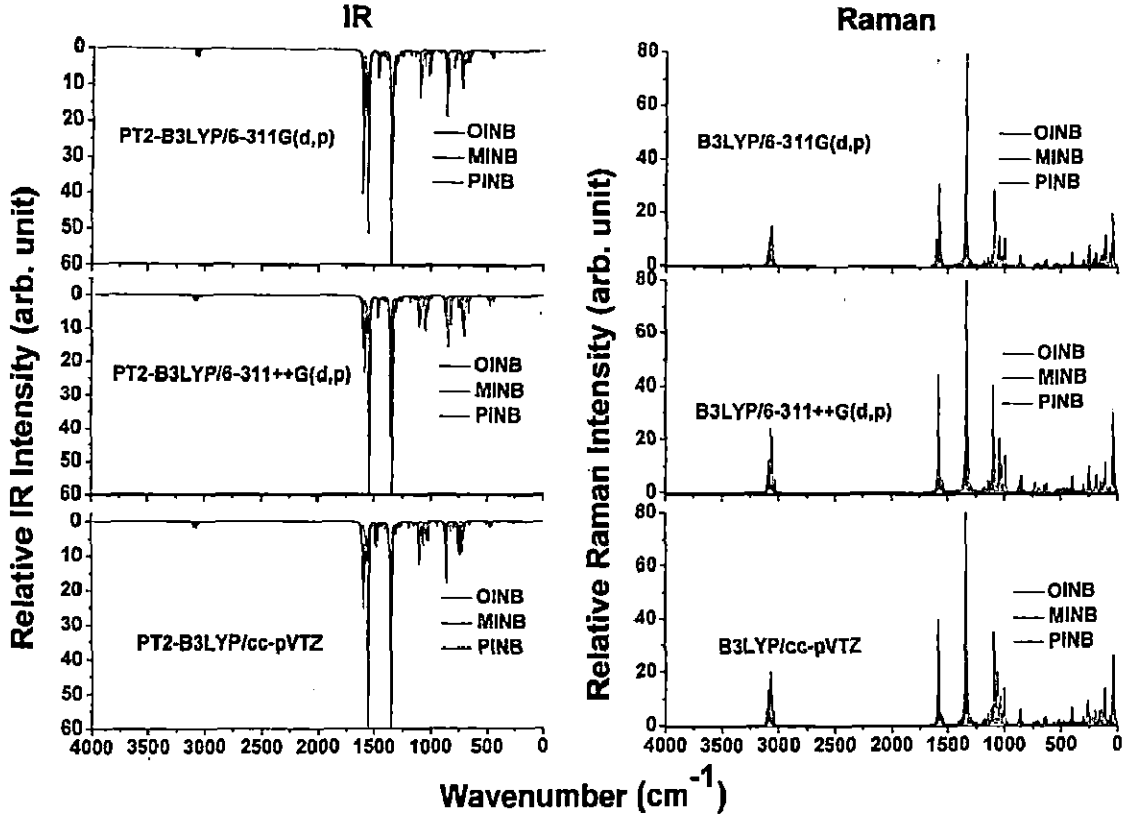

Fig. 4.6 Simulated IR and Raman spectra of OINB, MINB and PINB.

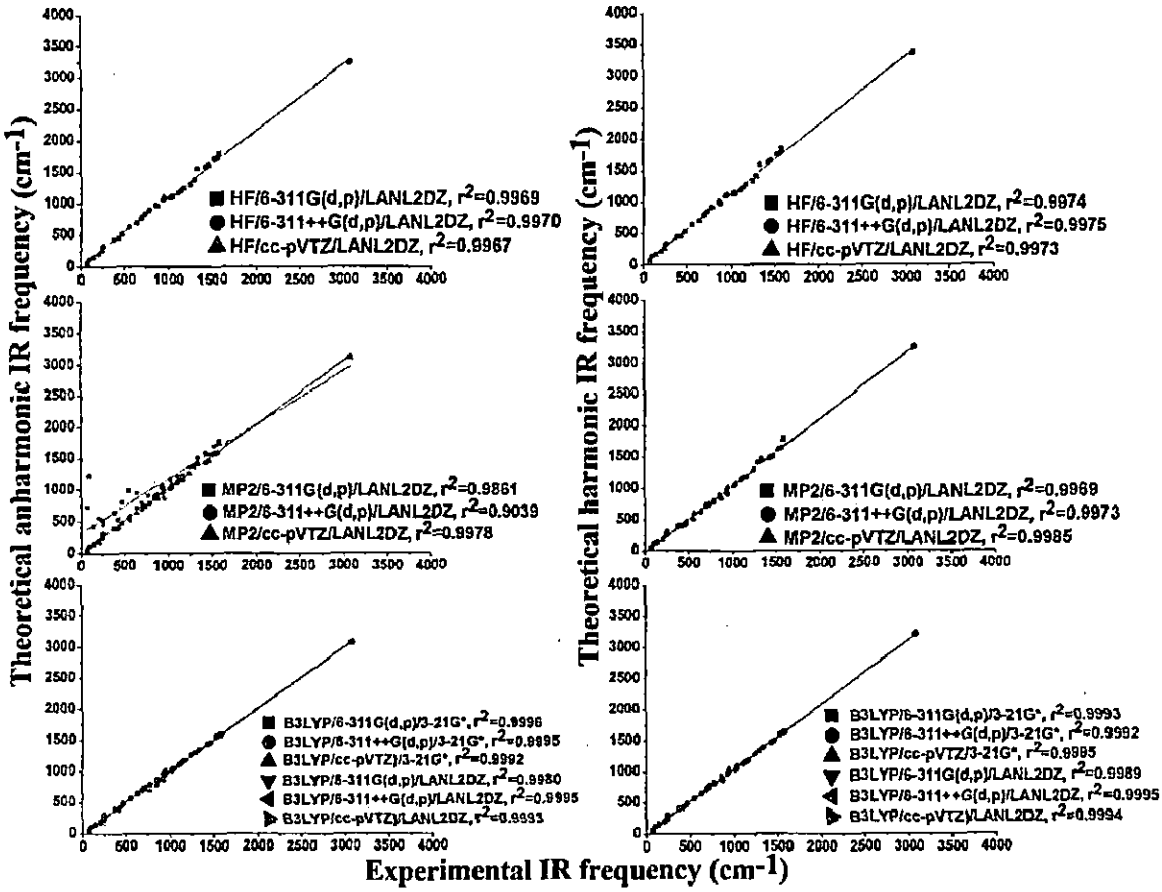

Fig. 4.7 Correlation plots between experimental and computed frequencies for OINB.

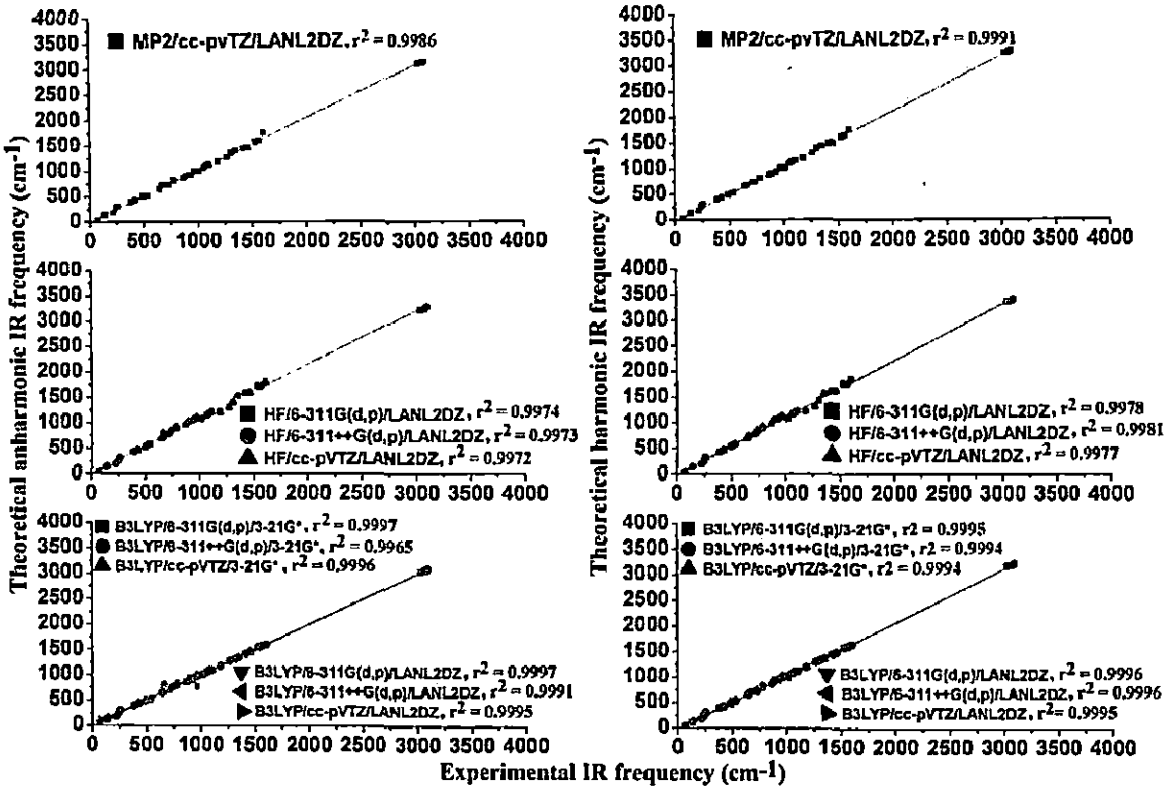

Fig. 4.8 Correlation plots between experimental and computed frequencies for MINB.

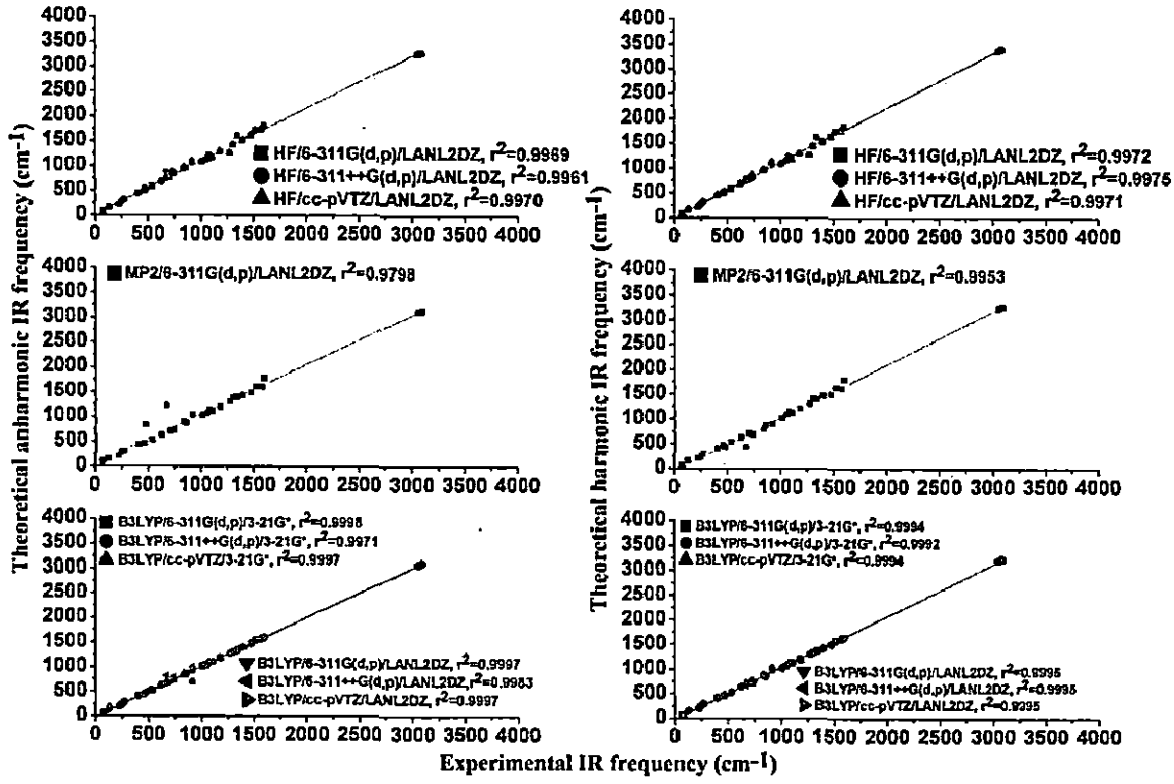

Fig. 4.9 Correlation plots between experimental and computed frequencies for PINB.

Table 4.14 Assignments of combination and overtone bands in the FTIR spectra of PINB.

FTIR (cm^{-1})	ω^{anh} (cm^{-1}) at DFT/B3LYP						Assignment
	6-311G (d,p) /3-21G*	6-311G (d,p) /LANL2DZ	6-311++ G(d,p) /3-21G*	6-311++ G(d,p) /LANL2DZ	cc-pVTZ/ 3-21G*	cc-pVTZ/ LANL2DZ	
2848	2856	2855	2855	2853	2864	2858	$\nu_6+\nu_{12}$
2442	2446	2439	2438	2439	2462	2450	$\nu_9+\nu_{16}$
	2450	2451	2449	2445	2451	2451	$\nu_{10}+\nu_{14}$
2370	2386	2388	2390	2395	2395	2393	$\nu_{12}+\nu_{14}$
2342	2375	2378	2380	2377	2382	2379	$\nu_{12}+\nu_{15}$
1924	1925	1912	1911	1909	1936	1927	$\nu_8+\nu_{29}$
	1919	1923	1921	1922	1921	1922	$\nu_9+\nu_{27}$
1801	1805	1793	1789	1782	1806	1795	$\nu_{10}+\nu_{29}$
	1812	1813	1807	1814	1814	1812	$\nu_{12}+\nu_{27}$
1780	1779	1789	1775	1836	1817	1809	$\nu_{16}+\nu_{23}$
	1772	1780	1781	1802	1783	1783	$\nu_{11}+\nu_{28}$
1755	1764	1748	1733	1749	1778	1760	$\nu_{15}+\nu_{24}$
	1754	1818	1509	1877	1837	1836	$\nu_{19}+\nu_{20}$
1722	1731	1725	1700	1861	1760	1744	$\nu_{16}+\nu_{25}$
1705	1718	1716	1690	1710	1714	1712	$2\nu_{21}$
	1713	1708	1707	1709	1714	1711	$\nu_{13}+\nu_{27}$
1688	1702	1709	1682	1724	1724	1719	$\nu_{20}+\nu_{21}$
1657	1653	1647	1653	1675	1664	1661	$\nu_{13}+\nu_{28}$
1625	1641	1638	1672	1637	1650	1648	$\nu_{17}+\nu_{26}$
1443	1451	1494	1226	1528	1499	1500	$\nu_{19}+\nu_{27}$
1412	1396	1432	1381	1667	1441	1450	$\nu_{23}+\nu_{25}$
1148	1157	1156	1153	1154	1158	1157	$\nu_{26}+\nu_{27}$

Abbreviation used: ω^{anh} – Calculated anharmonic frequencies

4.4.3 Frontier molecular orbitals

The frontier orbitals, HOMO and LUMO indicate the ability to donate and accept the electron respectively. These orbitals are important to determine the way the molecules interact with other molecular species. The calculated frontier orbitals (HOMO and LUMO) at B3LYP/6–311G(d,p)/3–21G* level of theory are shown in Fig. 4.10. The HOMO and LUMO energy eigenvalues are useful for computing various global chemical reactivity indices (chemical hardness–softness, electronic chemical potential and electrophilicity) and Fukui functions [60] which predict relative stability and reactivity of the molecules [61, 62]. These values are tabulated in Table 4.15. The description regarding chemical reactivity descriptors can be seen in section 2.2.7. In iodonitrobezes, the most of the part of HOMOs are located over iodine atoms and benzene rings whereas the LUMOs are delocalized over the C–C bonds and NO_2 groups (Fig. 4.10). The HOMO–LUMO excitations in these molecules imply an electron density transfer from iodine atoms to NO_2 groups and redistribution of the charge density on aromatic part. The HOMO and LUMO energy eigenvalues along with their gaps are computed for OINB, MINB and PINB and are presented in Table 4.15. It is clear from Table 4.15, PINB molecule is most stable in gaseous state

because of its largest HOMO–LUMO gap among the investigated molecules as well as it is least reactive than those having smaller gaps. The calculated excitation energies at TD–DFT level for transitions between HOMO and LUMO are reasonable approximations to the HOMO–LUMO gaps. The HOMO–LUMO gaps calculated at TD–DFT level have more physical meaning than those derived directly from the energy differences between HOMO and LUMO energy eigenvalues obtained in DFT calculations. The least value of HOMO–LUMO gap (at TD–B3LYP/6–311G(d,p)/3–21G*) in OINB predicts its high reactivity in chemical reactions.

Table 4.15 SCF, HOMO and LUMO energies; HOMO–LUMO energy gaps (kcal/mol) and reactivity descriptors (eV) for OINB, MINB and PINB.

Parameters	PCM–B3LYP/6–311G(d,p)/3–21G*			PCM–B3LYP/6–311G(d,p)/LANL2DZ		
	OINB	MINB	PINB	OINB	MINB	PINB
SCF	–4597349.110[a]	–4597354.848[a]	–4597355.520[a]	–280893.937[a]	–280900.656[a]	–280901.150[a]
	–4597341.562[b]	–4597347.807[b]	–4597348.243[b]	–280888.953[b]	–280896.358[b]	–280896.809[b]
HOMO	–157.649[a]	–157.599[a]	–159.136[a]	–163.730[a]	–163.372[a]	–164.891[a]
	–159.682[b]	–162.217[b]	–164.401[b]	–164.464[b]	–166.434[b]	–168.499[b]
LUMO	–63.253[a]	–66.378[a]	–66.008[a]	–63.404[a]	–67.351[a]	–66.729[a]
	–60.605[b]	–65.154[b]	–64.872[b]	–59.852[b]	–66.027[b]	–65.474[b]
LUMO–HOMO gap	94.396[a]	91.221[a]	93.129[a]	100.326[a]	96.021[a]	98.162[a]
	99.077[b]	97.063[b]	99.529[b]	104.612[b]	100.407[b]	103.025[b]
	78.918[d]	83.664[d]	90.988[d]	88.536[d]	86.894[d]	94.055[d]
	76.330[c]	77.711[c]	83.942[c]	82.594[c]	82.384[c]	88.633[c]
[b]Reactivity descriptors						
IP	6.924	7.034	7.129	7.132	7.217	7.307
EA	2.628	2.825	2.813	2.595	2.863	2.839
η	2.148	2.105	2.158	2.269	2.177	2.234
S	0.233	0.238	0.232	0.220	0.230	0.224
μ	–4.776	–4.930	–4.971	–4.864	–5.040	–5.073
χ	4.776	4.930	4.971	4.864	5.040	5.073
ω	5.310	5.773	5.725	5.213	5.834	5.760

Abbreviation used:: IP–ionization potential, EA–electron affinity, η–chemical hardness, S–chemical softness, μ–chemical potential, χ–electronegativity, ω–electrophilicity

Note: HOMO→LUMO excitation energy at [c]PCM–TD–B3LYP/6–311G(d,p) and [d]TD–B3LYP,

[b]values in gaseous phase, [a]values in ethanol

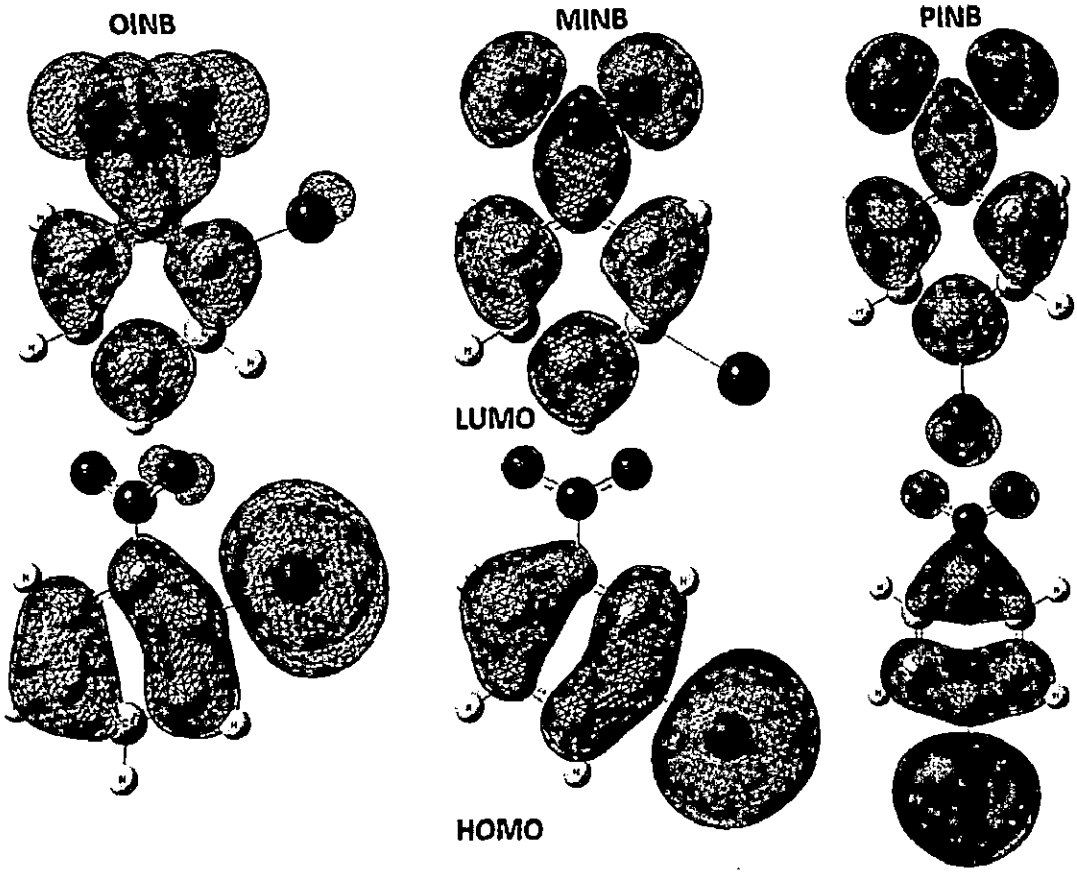

Fig. 4.10 The HOMOs and LUMOs of OINB, MINB and PINB at B3LYP/6–311G(d,p)/3–21G*.

4.4.4 Thermodynamic properties

Thermodynamic data are important for understanding the chemical processes. The density functional theory is a well–established and efficient tool to predict various statistical thermodynamic properties of molecules (section 2.2.7). Nowadays, due to theoretical predictions of thermodynamic properties, their experimental measurements are possible with high accuracy. This information constitutes the spectroscopy of the molecule of interest [63].

In the present investigations, the parameters such as zero–point vibrational energies, specific heat capacities, rotational constants, rotational temperatures, dipole moments, entropies and enthalpies of OINB, MINB and PINB are computed at B3LYP/6–311G(d,p)/3–21G* level of theory (Table 4.16). Based on harmonic vibrational analysis, the statistical thermodynamic functions: molar entropy (S_m^0), molar enthalpy change (ΔH_m^0) and molar heat capacity ($C_{p,m}^0$) for the molecules are calculated in the temperature range, 77– 700 K (Table 4.17). It can be seen that these thermodynamic functions are increasing with temperature because the molecular

vibrational intensities increase with temperature [64]. The statistical thermodynamic functions and ZPE with anharmonic corrections at 298.15K are also presented. The correlation equations for entropies, enthalpy changes and heat capacities are fitted by quadratic polynomial in temperature (Fig. 4.11). The corresponding fitting equations with fitting factors (r^2) are given as follows.

For OINB, the corresponding fitting equations are

$$S^0_{p,m} = 57.0595 + 0.1405\,T - 0.4799 \times 10^{-4}\,T^2 (r^2 = 0.9996)$$

$$C_p = 5.4169 + 0.1031\,T - 0.4318 \times 10^{-4}\,T^2 (r^2 = 0.9989)$$

$$\Delta H = -0.2965 + 0.0102\,T + 0.3579 \times 10^{-4}\,T^2 (r^2 = 0.9998).$$

For MINB, the corresponding fitting equations are

$$S^0_{p,m} = 57.5931 + 0.1408\,T - 0.4815 \times 10^{-4}\,T^2\,(r^2 = 0.9996)$$

$$C_p = 5.4801 + 0.1026\,T - 0.4256 \times 10^{-4}\,T^2 (r^2 = 0.9989)$$

$$\Delta H = -0.2764 + 0.0101\,T + 0.3582 \times 10^{-4}\,T^2 (r^2 = 0.9998).$$

For PINB, the corresponding fitting equations are

$$S^0_{p,m} = 57.606 + 0.1405\,T - 0.4792 \times 10^{-4}\,T^2\,(r^2 = 0.9996)$$

$$C_p = 5.4278 + 0.1027\,T - 0.4271 \times 10^{-4}\,T^2 (r^2 = 0.9989)$$

$$\Delta H = -0.2933 + 0.0101\,T + 0.3578 \times 10^{-4}\,T^2 (r^2 = 0.9998).$$

All the computed gaseous phase thermodynamic data will be helpful for calculating other thermodynamic energies and for predicting directions of chemical reactions using second law of thermodynamics [65].

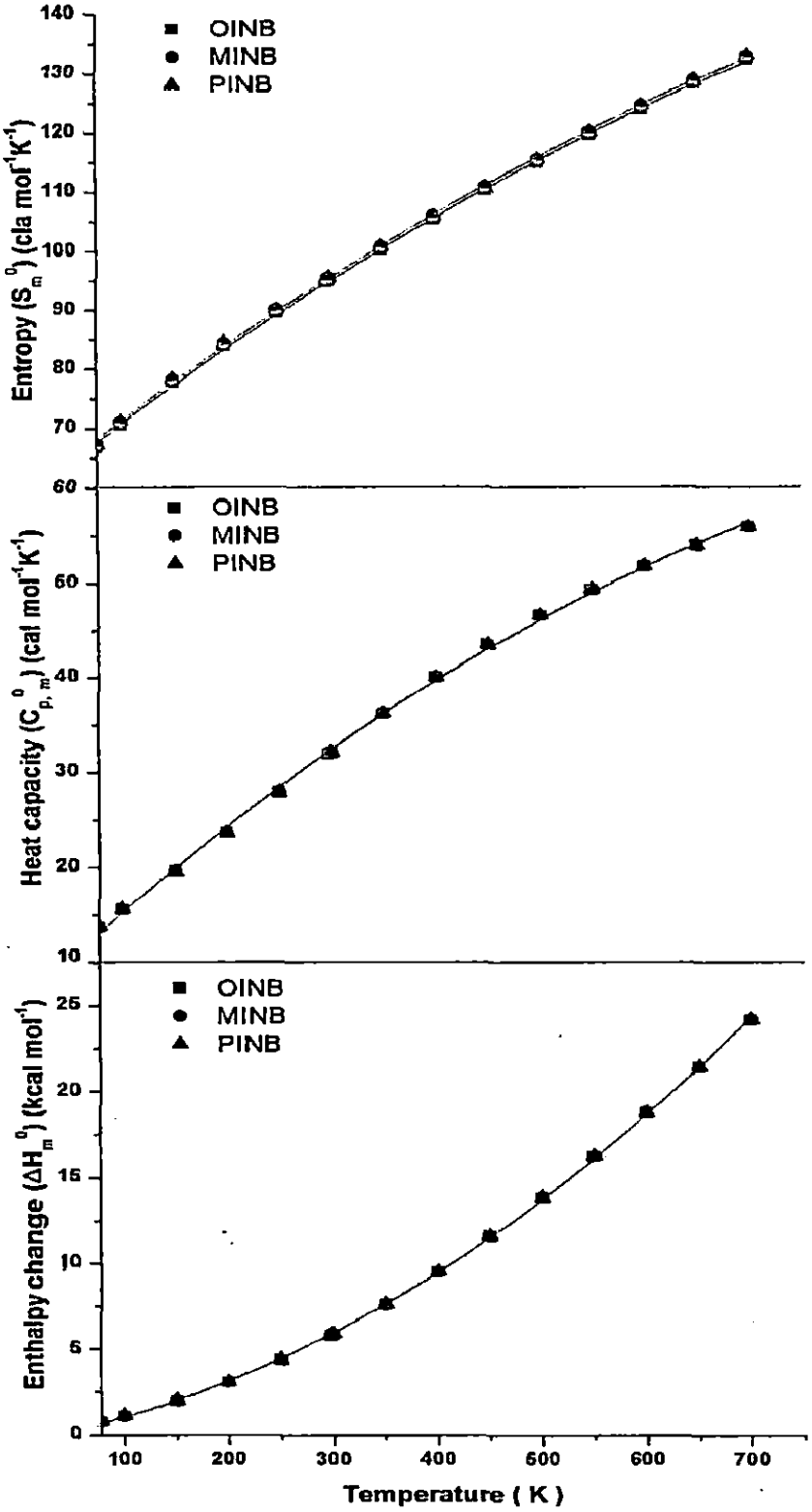

Fig. 4.11 Temperature dependence thermodynamic properties (Entropy, Heat capacity and enthalpy change) for the OINB, MINB and PINB.

Table 4.16 Theoretical zero point vibrational energies (kcal/mol), rotational constants (GHz), rotational temperatures (Kelvin), thermal energies (kcal/mol), molar capacity at constant volume and at constant pressure (cal mol^{-1} K^{-1}), entropies (cal mol^{-1} K^{-1}), enthalpies (kcal/mol) and dipole moments (Debye) of OINB, MINB and PINB at STP.

Parameters (at 298 K)	B3LYP/6-311G(d,p)/3-21G*		
	OINB	MINB	PINB
Zero point vibrational energy	58.067	58.071	58.091
	57.302[a]	57.380[a]	57.352[a]
Rotational constants			
X	1.257	2.026	3.982
Y	0.649	0.365	0.286
Z	0.436	0.309	0.267
Rotational temperatures	0.060	0.097	0.191
	0.031	0.017	0.014
	0.021	0.015	0.013
Thermal Energy			
Total	63.300	63.317	63.341
	62.629[a]	62.689[a]	62.689[a]
Translational	0.889	0.889	0.889
Rotational	0.889	0.889	0.889
Vibrational	61.523	61.540	61.564
Molar capacity at constant volume			
Total	29.961	30.034	29.991
	30.722[a]	30.681[a]	30.693[a]
Translational	2.981	2.981	2.981
Rotational	2.981	2.981	2.981
Vibrational	23.999	24.072	24.030
Molar capacity at constant pressure	31.948	32.022	31.979
	32.708[a]	32.667[a]	32.682[a]
Entropy			
Total	94.811	95.453	93.981
	95.174[a]	95.282[a]	94.503[a]
Translational	42.436	42.436	42.436
Rotational	31.180	31.620	29.957
Vibrational	21.194	21.397	21.587
Total Enthalpy	63.893	63.910	63.934
	63.222[a]	63.282[a]	63.282[a]
Dipole Moment			
μ_x	−1.305	−0.393	0.000
μ_y	−4.219	3.999	−0.002
μ_z	0.043	0.001	3.678
μ	4.417	4.018	3.678

[a]anharmonic value

Table 4.17 Thermodynamic properties at different temperatures for OINB, MINB and PINB.

T(K)	B3LYP/6-311G(d,p)/3-21G*								
	OINB			MINB			PINB		
	$C^0_{p,m}$ (cal mol^{-1} K^{-1})	S^0_m (cal mol^{-1} K^{-1})	ΔH^0_m (kcal mol^{-1})	$C^0_{p,m}$ (cal mol^{-1} K^{-1})	S^0_m (cal mol^{-1} K^{-1})	ΔH^0_m (kcal mol^{-1})	$C^0_{p,m}$ (cal mol^{-1} K^{-1})	S^0_m (cal mol^{-1} K^{-1})	ΔH^0_m (kcal mol^{-1})
77	13.706	66.732	0.801	13.728	67.289	0.803	13.841	67.272	0.818
100	15.618	70.556	1.138	15.635	71.118	1.141	15.637	71.115	1.157
150	19.585	77.641	2.019	19.611	78.211	2.022	19.546	78.191	2.036
200	23.643	83.827	3.099	23.687	84.406	3.104	23.631	84.368	3.114
250	27.862	89.554	4.386	27.921	90.145	4.394	27.878	90.096	4.401
298.15	31.948	94.812	5.826	32.014	95.413	5.837	31.978	95.357	5.843
300	32.103	95.010	5.885	32.169	95.612	5.897	32.134	95.556	5.902
350	36.191	100.268	7.593	36.259	100.881	7.608	36.228	100.820	7.612
400	40.000	105.353	9.499	40.067	105.975	9.517	40.037	105.910	9.520
450	43.467	110.268	11.588	43.528	110.897	11.609	43.501	110.829	11.610
500	46.576	115.012	13.840	46.631	115.647	13.865	46.607	115.576	13.864
550	49.344	119.583	16.239	49.392	120.224	16.266	49.370	120.150	16.265
600	51.802	123.984	18.769	51.844	124.629	18.799	51.824	124.553	18.796
650	53.987	128.219	21.415	54.022	128.866	21.446	54.004	128.789	21.443
700	55.934	132.292	24.164	55.963	132.942	24.197	55.947	132.864	24.193

4.4.5 Molecular electrostatic potential map

The molecular electrostatic potential (MEP) is a tool for understanding and predicting the reactive behaviour of molecules [66]. There are many applications of the electrostatic potential in the fields such as molecular recognition, hydrogen bonding and understanding of variety of physiochemical properties related to molecular interactions (section 2.2.7). The MEP maps for iodonitrobenzenes at B3LYP/6–311G(d,p)/3–21G* level of theory are shown in Fig. 4.12. The values of electrostatic potentials on the surface increase in the order red < yellow < green < blue. In the MEP plots, the colour–coded high potential values (a.u.) are shown over the surfaces. The electrostatic potential values on the surface are specified in the range –0.0442 a.u. (deepest red) to 0.0442 a.u. (deepest blue) in the present molecules (Fig. 4.12). In any particular region around a molecule, the sign of the electrostatic potential depends upon whether the effects of the nuclei or electrons are dominant. It is a key to assessing its reactivity there. In the MEP, the negative regions with high electron density (high negative potential) are preferred site for electrophilic attack indicated by deep red colour. The deep blue colour surfaces represent positive regions with low electron density (high positive potential) that are preferred site for nucleophilic attack. The almost neutral part, having electrostatic potentials close to zero, is indicated by green colour. Electrostatic potential contour maps obtained at B3LYP/6–311G(d,p)/3–21G* level of theory are also presented in Fig. 4.13. In the iodonitrobenzenes, negative regions are localized on surface around the oxygen while positive regions are confined over hydrogen atoms. The surfaces over the aromatic ring and iodine atom are showing neutral part (green colour).

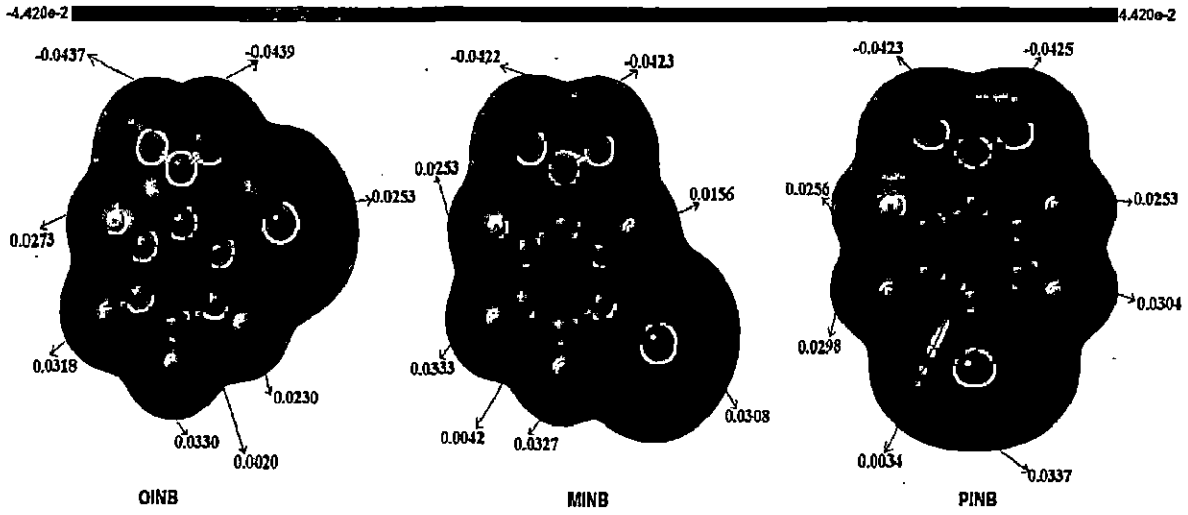

Fig. 4.12 Molecular electrostatic potential map (MEP) for OINB, MINB and PINB.

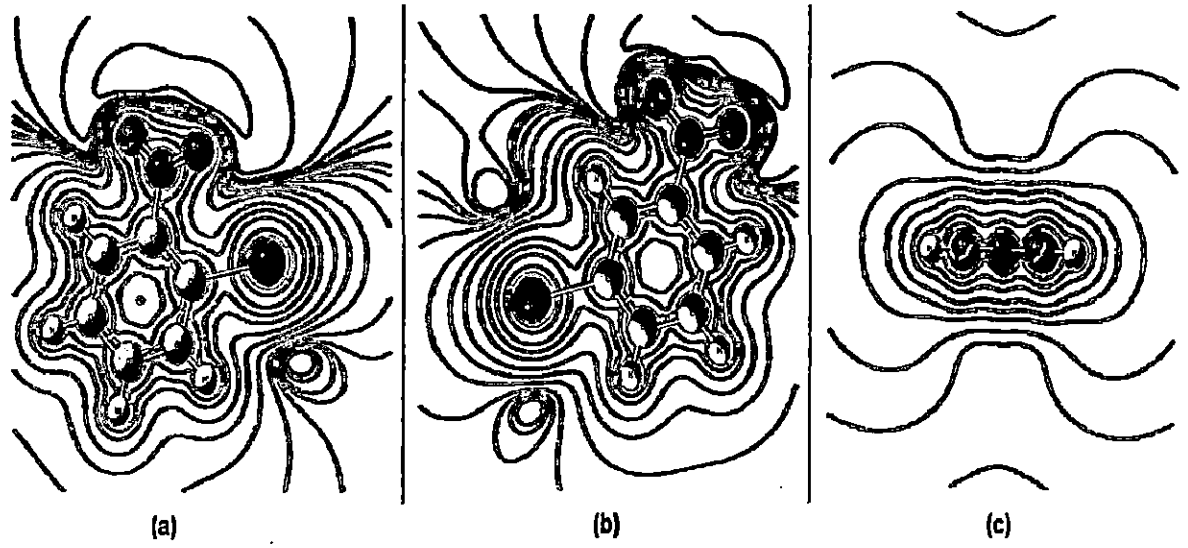

Fig. 4.13 Electrostatic potential contour map for (a) OINB, (b) MINB and (c) PINB.

4.4.6 Natural bond orbital analysis

NBO analysis is an important technique for studying intra and intermolecular bonding, hybridization and charge transfer in the molecular systems (section 2.2.7). The natural bond orbital (NBO) analysis has been carried out at the B3LYP/6–311G(d,p)/3–21G* level of theory using NBO 3.1 program [43, 47]. The hybridization of filled orbital is shown in Table 4.18. The second order perturbation energy values [67, 68], $E^{(2)}$, corresponding the important interactions between the electron donors and acceptors, are presented in Table 4.19. The larger value of polarization coefficients (section 2.2.7) represents larger electron density value (%) of NBO which shows higher electronegativity (Table 4.18). It should be noted that a decrease in occupancy of third lone pair of oxygen and iodine atoms has been found in iodonitrobenzenes. The interaction energies, $E^{(2)}$, are representing delocalization of electron density between Lewis (bond or lone pair) and non Lewis (anti bond) NBO orbital's (Table 4.19). The larger the $E^{(2)}$ value, the more intensive is the interaction between electron donors and electron acceptors. The important donor–acceptor interactions between NBO's with large value of $E^{(2)}$ are n(LP2O1) → σ*(O2–N3), n(LP2O1) → σ*(N3–C5), n(LP2O2) → σ*(O1–N3) and n(LP2O2) → σ*(N3–C5) in OINB, MINB and PINB; π(O1–N3) → n(LP3O2) and n(LP3O2) → π*(O1–N3) in OINB and PINB; n(LP3O1) → π*(O2–N3) and n(LP3I) → π*(C10–C12) in PINB; n(LP3I) → σ*(C4–C12) in OINB and n(LP3I) → π*(C4–C12) in MINB.

Table 4.18 NBO analysis of OINB, MINB and PINB at B3LYP/6-311G(d,p)/3-21G* level of theory.

Bond	Occupancy			ED_A %			ED_B %			NBO (% p character)		
A–B)	OINB	MINB	PINB	OINB	MINB	PINB	OINB	MINB	PINB	OINB	MINB	PINB
O1–N3)	1.99483	1.99498	1.99503	51.63	51.55	51.52	48.37	48.45	48.48	$0.7185\ sp^{2.80}(74.23)_O$ $+0.6955\ sp^{2.10}(67.68)_N$	$0.7180\ sp^{2.87}(74.05)_O$ $+0.6961\ sp^{2.11}(67.78)_N$	$0.7177\ sp^{2.81}(74.11)_O$ $+0.6963\ sp^{2.12}(67.86)_N$
O1–N3)	1.98566	1.98630		59.23	59.94		40.77	40.06		$0.7696\ sp^{99.99}(99.57)_O$ $+0.6385\ sp^{99.99}(99.65)_N$	$0.7742\ sp^{1.00}(99.85)_O$ $+0.6329\ sp^{1.00}(99.74)_N$	
O2–N3)	1.99382	1.99482	1.99503	51.61	51.54	51.52	48.39	48.46	48.48	$0.7184\ sp^{2.94}(74.53)_O$ $+0.6956\ sp^{2.13}(67.90)_N$	$0.7179\ sp^{2.87}(74.06)_O$ $+0.6961\ sp^{2.11}(67.80)_N$	$0.7177\ sp^{2.81}(74.11)_O$ $+0.6963\ sp^{2.12}(67.86)_N$
O2–N3)			1.98601			60.02			39.98			$0.7747\ sp^{1.00}(99.85)_O$ $+0.6323\ sp^{1.00}(99.74)_N$
N3–C5)	1.98852	1.98834	1.98904	62.19	62.49	62.43	37.81	37.51	37.57	$0.7886\ sp^{1.82}(64.52)_N$ $+0.6149\ sp^{2.25}(76.41)_C$	$0.7905\ sp^{1.81}(64.43)_N$ $+0.6124\ sp^{3.21}(76.17)_C$	$0.7901\ sp^{1.80}(64.29)_N$ $+0.6129\ sp^{3.15}(75.83)_C$
C4–C5)	1.97603	1.96764	1.97586	48.87	49.52	49.16	51.13	50.48	50.84	$0.6991\ sp^{1.59}(61.42)_C$ $+0.7150\ sp^{1.56}(60.88)_C$	$0.7037\ sp^{1.89}(65.26)_C$ $+0.7105\ sp^{1.64}(62.05)_C$	$0.7011\ sp^{1.86}(65.01)_C$ $+0.7130\ sp^{1.64}(62.06)_C$
C4–C5)			1.64363			45.10			54.90			$0.6716\ sp^{1.00}(99.94)_C$ $+0.7409\ sp^{1.00}(99.99)_C$
C4–C12)	1.97563	1.97587	1.96680	50.36	50.77	50.08	49.64	49.23	49.92	$0.7096\ sp^{1.58}(61.14)_C$ $+0.7046\ sp^{1.77}(63.84)_C$	$0.7125\ sp^{1.22}(63.13)_C$ $+0.7016\ sp^{1.56}(60.98)_C$	$0.7077\ sp^{1.76}(63.71)_C$ $+0.7065\ sp^{1.80}(64.28)_C$
C4–C12)	1.66179	1.66553		52.23	45.56		47.77	54.44		$0.7227\ sp^{1.00}(99.96)_C$ $+0.7046\ sp^{1.00}(99.95)_C$	$0.6750\ sp^{1.00}(99.95)_C$ $+0.7378\ sp^{1.00}(99.98)_C$	
(C4–I)	1.97329			58.07			41.93			$0.7620\ sp^{3.40}(77.23)_C$ $+0.6475\ sp^{7.66}(88.19)_I$		
C12–I)		1.97464			56.61			43.39			$0.7524\ sp^{2.61}(78.23)_C$ $+0.6587sp^{1.36}(87.78)_I$	
C10–I)			1.97517			56.47			43.53			$0.7515\ sp^{3.63}(78.41)_C$ $+0.6598\ sp^{7.24}(87.62)_I$
C4–H14)		1.97366	1.97409		62.77	62.17		37.23	37.83		$0.7923\ sp^{2.50}(71.35)_C$ $+0.6101\ sp^{0.00}(0.01)_H$	$0.7885\ sp^{2.47}(71.17)_C$ $+0.6151\ sp^{0.00}(0.05)_H$
C5–C6)	1.96533	1.97612	1.97586	51.27	50.96	50.84	48.73	49.04	49.16	$0.7160\ sp^{1.68}(62.68)_C$ $+0.6981sp^{1.87}(65.12)_C$	$0.7139\ sp^{1.62}(61.76)_C$ $+0.7003\ sp^{1.58}(65.21)_C$	$0.7130\ sp^{1.64}(62.06)_C$ $+0.7011\ sp^{1.86}(65.01)_C$
C5–C6)	1.65159	1.64754		54.44	54.28		45.56	45.72		$0.7379\ sp^{1.00}(99.97)_C$ $+0.6750\ sp^{59.99}(99.92)_C$	$0.7368\ sp^{1.00}(99.98)_C$ $+0.6762\ sp^{1.00}(99.94)_C$	
C6–H7)	1.97346	1.97519	1.97409	61.91	62.12	62.17	38.09	37.88	37.83	$0.7868\ sp^{2.31}(71.50)_C$ $+0.6172\ sp^{0.00}(0.05)_H$	$0.7882\ sp^{2.43}(70.83)_C$ $+0.6154\ sp^{0.00}(0.05)_H$	$0.7885\ sp^{2.47}(71.17)_C$ $+0.6151\ sp^{0.00}(0.05)_H$
C6–C8)	1.97556	1.97482	1.96680	50.55	50.48	50.08	49.45	49.52	49.92	$0.7110\ sp^{1.23}(63.31)_C$ $+0.7032\ sp^{1.80}(64.23)_C$	$0.7105\ sp^{1.77}(63.85)_C$ $+0.7037\ sp^{1.78}(64.05)_C$	$0.7077\ sp^{1.76}(63.71)_C$ $+0.7065\ sp^{1.80}(64.28)_C$
C6–C8)			1.64608			48.52			51.48			$0.6965\ sp^{1.00}(99.94)_C$ $+0.7175\ sp^{1.00}(99.95)_C$
C8–H9)	1.97851	1.97731	1.97744	60.77	60.82	61.32	39.23	39.18	38.68	$0.7795\ sp^{2.32}(71.57)_C$ $+0.6264\ sp^{0.00}(0.05)_H$	$0.7799\ sp^{2.37}(71.95)_C$ $+0.6260\ sp^{0.00}(0.05)_H$	$0.7831\ sp^{2.58}(72.02)_C$ $+0.6220\ sp^{0.00}(0.04)_H$
C8–C10)	1.97970	1.97148	1.98077	49.98	49.60	50.17	50.02	50.40	49.83	$0.7070\ sp^{1.49}(64.10)_C$ $+0.7073\ sp^{1.76}(63.95)_C$	$0.7042\ sp^{1.77}(63.92)_C$ $+0.7100\ sp^{1.79}(64.07)_C$	$0.7083\ sp^{1.73}(63.57)_C$ $+0.7059\ sp^{1.53}(60.68)_C$
C8–C10)	1.62914	1.63908		51.10	51.03		48.90	48.97		$0.7148\ sp^{1.00}(99.95)_C$ $+0.6993\ sp^{1.00}(99.95)_C$	$0.7144\ sp^{1.00}(99.95)_C$ $+0.6998\ sp^{1.00}(99.95)_C$	
C10–H11)	1.97778	1.97778		60.67	61.20		39.33	38.80		$0.7789\ sp^{2.35}(72.05)_C$ $+0.6271\ sp^{0.00}(0.05)_H$	$0.7823\ sp^{2.60}(72.18)_C$ $+0.6229\ sp^{0.00}(0.04)_H$	

Table: 4.18 (*continued*)

(C10–C12)	1.97277	1.98099	1.98077	49.58	50.11	49.83	50.42	49.89	50.17	$0.7041\ sp^{1.77}(63.91)_C$ $+0.7101\ sp^{1.76}(63.73)_C$	$0.7079\ sp^{1.75}(63.61)_C$ $+0.7063\ sp^{1.54}(60.59)_C$	$0.7059\ sp^{1.55}(60.68)_C$ $+0.7083\ sp^{1.73}(63.57)_C$
(C10–C12)			1.65650			52.13			47.87			$0.7220\ sp^{1.00}(99.97)_C$ $+0.6919\ sp^{1.00}(99.95)_C$
(C12–H13)	1.97689		1.97744	61.23		61.32	38.77		38.68	$0.7825\ sp^{2.42}(72.31)_C$ $+0.6226\ sp^{0.00}(0.05)_H$		$0.7831\ sp^{2.58}(72.02)_C$ $+0.6220\ sp^{0.00}(0.04)_H$
one Pairs												
LP_1O_1	1.98139	1.98135	1.98142							$sp^{0.33}(25.82)$	$sp^{0.33}(25.74)$	$sp^{0.35}(25.69)$
LP_2O_1	1.89240	1.89660	1.89746							$sp^{1.00}(99.92)$	$sp^{99.99}(99.92)$	$sp^{99.99}(99.91)$
LP_3O_1			1.44227									$sp^{1.00}(99.87)$
LP_1O_2	1.98138	1.98131	1.98142							$sp^{0.34}(25.56)$	$sp^{0.33}(25.73)$	$sp^{0.35}(25.69)$
LP_2O_2	1.89510	1.89621	1.89746							$sp^{1.00}(99.93)$	$sp^{99.99}(99.92)$	$sp^{99.99}(99.91)$
LP_3O_2	1.43921	1.43956								$sp^{99.99}(99.55)$	$sp^{1.00}(99.87)$	
LP_1I	1.99547	1.99518	1.99528							$sp^{0.14}(12.52)$	$sp^{0.13}(11.42)$	$sp^{0.13}(11.58)$
LP_2I	1.97269	1.97673	1.97706							$sp^{61.89}(98.50)$	$sp^{1.00}(99.99)$	$sp^{1.00}(99.99)$
LP_3I	1.92405	1.93736	1.92651							$sp^{99.99}(99.96)$	$sp^{1.00}(99.98)$	$sp^{1.00}(99.98)$

bbreviation used: ED– Electron Density

Table 4.19 Second order perturbation theory analysis of Fock matrix in NBO basis for OINB, MINB and PINB at B3LYP/6–311G(d,p)/3–21G* level of theory.

Donor–acceptor interaction	$E^{(2)a}$ (kcal/mol)			E(j)–E(i)^b (a.u.)			F(i, j)^c (a.u.)		
	OINB	MINB	PINB	OINB	MINB	PINB	OINB	MINB	PINB
π(O1–N3) → n(LP3O2)	12.31	12.66		0.19	0.18		0.080	0.079	
σ(O2–N3) → n(LP3O2)	1.50			0.81			0.058		
π(O2–N3) → n(LP3O2)			12.56			0.18			0.079
n(LP1O1) → σ*(O2–N3)	2.57	2.40	2.36	1.22	1.22	1.22	0.050	0.049	0.048
n(LP1O1) → σ*(N3–C5)	4.20	4.16	4.20	1.05	1.05	1.06	0.061	0.061	0.061
n(LP2O1) → n(LP3O2)	0.63			0.02			0.005		
n(LP2O1) → σ*(O2–N3)	19.09	18.74	18.75	0.72	0.73	0.73	0.106	0.106	0.105
n(LP2O1) → σ*(N3–C5)	13.93	13.89	13.56	0.55	0.56	0.56	0.078	0.079	0.078
n(LP2O1) → σ*(C5–C6)	0.52	0.68	0.69	0.83	0.84	0.84	0.019	0.022	0.022
n(LP2O1) → σ*(C4–C12)		0.52	0.55		0.84	0.85		0.019	0.020
n(LP2O1) → σ*(O1–N3)			2.36			1.22			0.048
n(LP1O2) → σ*(O1–N3)	2.48	2.41		1.22	1.23		0.050	0.049	
n(LP1O2) → σ*(N3–C5)	4.12	4.15	4.20	1.05	1.05	1.06	0.060	0.060	0.061
n(LP2O2) → σ*(O1–N3)	18.29	18.69	18.75	0.72	0.73	0.73	0.104	0.105	0.105
n(LP2O2) → π*(O1–N3)	0.99			0.17			0.013		
n(LP2O2) → σ*(N3–C5)	14.09	13.83	13.56	0.55	0.56	0.56	0.079	0.078	0.078
n(LP2O2) → σ*(C5–C4)		0.70	0.69		0.84	0.84		0.022	0.022
n(LP2O2) → σ*(C8–C6)		0.54	0.55		0.85	0.85		0.020	0.020
n(LP3O1) → π*(O2–N3)			166.29			0.14			0.140
n(LP3O2) → π*(O1–N3)	159.82	166.93		0.15	0.14		0.141	0.140	
n(LP3O2) → σ*(O2–N3)	3.35			0.70			0.050		
n(LP1I) → σ*(C4–C5)	1.66			1.39			0.043		

Table: 4.19 (*continued*)

n(LP1I) → σ*(C4–C12)	1.26	1.36		1.40	1.43		0.038	0.040	
n(LP1I) → σ*(C10–C8)			1.41			1.43			0.040
n(LP2I) → σ*(C10–C8)			2.63			0.82			0.041
n(LP2I) → σ*(C4–C5)	3.92			0.80			0.050		
n(LP2I) → σ*(C4–C12)	1.73	2.67		0.81	0.82		0.034	0.042	
n(LP2I) → σ*(C10–C12)	0.53	2.59	2.63	0.83	0.82	0.82	0.019	0.041	0.041
n(LP1I) → σ*(C10–C12)		1.43	1.41		1.43	1.43		0.041	0.040
n(LP3I) → σ*(C4–C12)	8.17			0.26			0.045		
n(LP3I) → π*(C4–C12)		8.02			0.27			0.045	
n(LP5I) → π*(C10–C12)			8.44			0.27			0.046

[a]Energy of hyper conjugative interaction (stabilization energy).
[b]Energy difference between donor and acceptor i and j NBO orbitals.
[c]Fock matrix element between i and j NBO orbitals.

4.4.7 Other molecular properties

In the present work, natural atomic charges of isomeric iodonitrobenzenes calculated at B3LYP/6–311G(d,p) level of theory are presented in Table 4.20. The plots of natural atomic charges on different atoms for the molecules are shown in Fig. 4.14. Atomic charges have a significant importance in the application of quantum chemical calculations for molecular system because they are related to dipole moment, electronic structure, molecular polarizability and other various properties of the molecules. Among all carbon atoms in the ring, the C5 atom has less positive charge in all the iodonitrobenzenes. This may be due to attached electron withdrawing group, NO_2, on C5 atom. The charges on N3 atoms in the iodonitrobenzenes are found larger than other atoms due to electron withdrawing inductive effect of NO_2.

DFT calculations are efficient tool for predicting some important quantities such as molecular dipole moments, polarizabilities and hyperpolarizabilities [69–73]. The computation of polarizabilities and hyperpolarizabilities of the organic molecules are of great importance to study the phenomenon induced by intermolecular interactions and non–linear optical effects. Theoretical molecular polarizability and first order static hyperpolarizability values are reported (Table 4.21). Measurements of electric dipole moment give the understanding about the degree of polarity (Table 4.16). This important property is used to study the intermolecular interactions involving the non–bonded type dipole–dipole interactions because higher the dipole moment, stronger will be the intermolecular interactions. The calculated value of the dipole moment of OINB is largest among the investigated molecules. The polarizability and hyperpolarizability describe the response of molecular system in the presence of weak homogeneous electric field. The high values of dipole moment and first order hyperpolarizability are indicating nonlinearity of isomeric iodonitrobenzenes. The MINB is found with large non–linear optical potential due to large mean first hyperpolarizablity value among the others. The lower HOMO–LUMO gap and higher dipole moment of OINB show its higher activity and lesser stability in comparison to MINB and PINB. The order of stability increases as OINB < MINB < PINB.

Table 4.20 Natural atomic charges (*e*) for iodonitrobenzenes.

Atoms	OINB		MINB		PINB	
	B3LYP/ 6–311G(d,p)/ 3–21G*	B3LYP/ 6–311G(d,p)/ LANL2DZ	B3LYP/ 6–311G(d,p)/ 3–21G*	B3LYP/ 6–311G(d,p)/ LANL2DZ	B3LYP/ 6–311G(d,p)/ 3–21G*	B3LYP/ 6–311G(d,p)/ LANL2DZ
O1	–0.360	–0.350	–0.380	–0.380	–0.380	–0.380
O2	–0.380	–0.380	–0.380	–0.380	–0.380	–0.380
N3	0.516	0.516	0.517	0.517	0.515	0.516
C4	–0.210	–0.210	–0.210	–0.220	–0.170	–0.170
C5	0.036	0.038	0.074	0.075	0.0590	0.0590
C6	–0.170	–0.170	–0.190	–0.190	–0.170	–0.170
H7	0.237	0.236	0.241	0.241	0.242	0.243
C8	–0.190	–0.190	–0.180	–0.180	–0.220	–0.220
H9	0.213	0.214	0.215	0.215	0.223	0.224
C10	–0.160	–0.16	–0.20	–0.200	–0.190	–0.190
H11	0.212	0.212	0.221	0.222		
C12	–0.210	–0.210	–0.20	–0.200	–0.220	–0.220
H13	0.221	0.222			0.223	0.224
H14			0.252	0.253	0.242	0.243
I	0.259	0.246	0.214	0.208	0.222	0.214

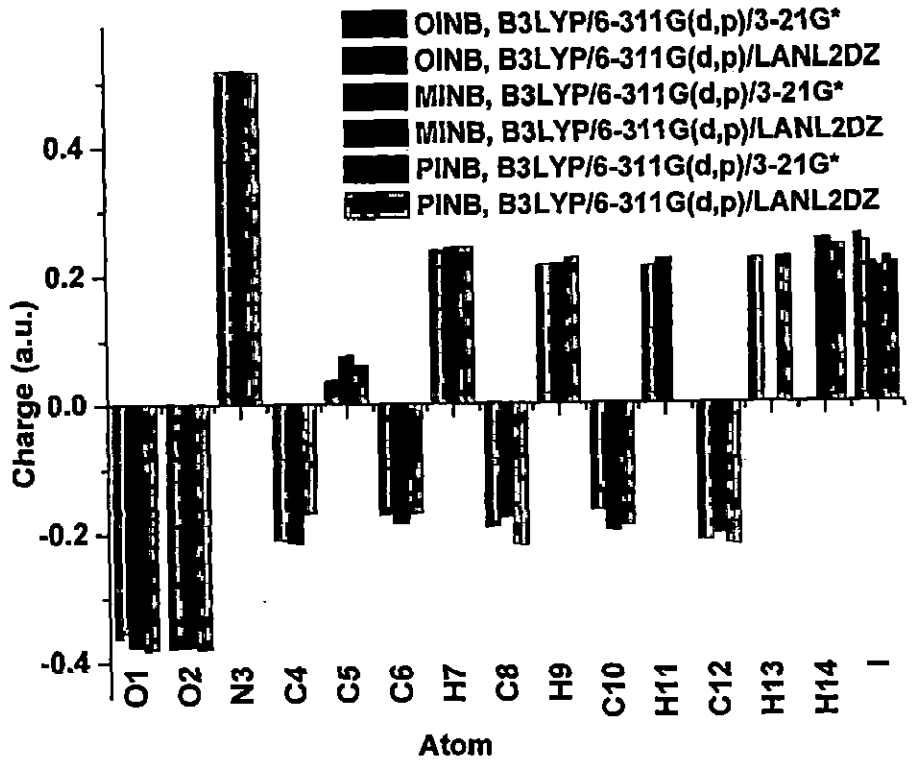

Fig. 4.14 The correlation of natural atomic charges for OINB, MINB and PINB.

Table 4.21 Calculated molecular polarizabilities (a.u) with their components, polarizability anisotropy invariant (a.u.), hyperpolarizabilities components (a.u.) and mean first hyperpolarizabilities (in esu, 1 a.u.= 8.639 x 10^{-33} esu) of iodonitrobenzenes at B3LYP/6–311G(d,p)/3–21G*.

	OINB	MINB	PINB
α_{xx}	144.727	149.062	46.412
α_{xy}	8.037	–16.516	0.000
α_{yy}	115.124	117.470	101.665
α_{xz}	3.760	–0.012	0.000
α_{yz}	–1.590	0.001	0.016
α_{zz}	50.189	46.384	175.474
$<\alpha>$	103.347	104.305	107.850
γ	85.199	95.474	112.155
β_{xxx}	–398.451	276.553	0.000
β_{xxy}	–44.209	–22.406	0.000
β_{xyy}	–27.156	166.834	0.000
β_{yyy}	75.012	–237.306	0.000
β_{xxz}	17.032	0.000	7.798
β_{xyz}	–5.388	0.000	0.000
β_{yyz}	5.786	0.000	45.583
β_{xzz}	–8.665	2.218	0.000
β_{yzz}	–16.935	11.962	0.000
β_{zzz}	0.998	0.000	–1735.590
β_0 (in esu)	3.754 x 10^{-30}	4.404 x 10^{-30}	0.365 x 10^{-30}

4.5 Conclusion

The optimization of geometry and PES scan reveal that MINB and PINB are planer while OINB is non–planar in geometry due to steric effect. The substitution of iodine at different sites of the nitrobenzene ring leads to significant changes in structures and modes of vibration. It is also found that the N3–C5–C4, N3–C5–C6 and C–C–I bond angles are approximately same in MINB and PINB but they differ in OINB. In addition to fundamentals and combinations, some important vibrations such as Kekule, ring breathing, Star of David and ring twisting vibrations in OINB, MINB and PINB are assigned. The calculated harmonic frequencies for higher modes have shown large deviations from the experiment than those obtained in anharmonic approximation. Good agreement between the experimental and simulated anharmonic vibrational spectra has been achieved without any scaling. The differences between anharmonic and experimental wavenumbers for some modes are found large which may be either due to limitations of the calculations or neglect of higher order potential energy terms in PT2 approach. The PT2 method with 6–311G(d,p) and 3–21G* basis set have performed reasonably well in reproducing the experimental spectra. The studies demonstrate that the 3–21G* basis set is suitable for iodine atom in iodo–substituted molecules to understand their molecular properties as well as spectra. The

low values of the RMS and MAD are found for anharmonic vibrational frequencies at B3LYP/6–311G(d,p)/3–21G* level of theory. Electrostatic potential contour maps show that negative regions are localized on surface around the oxygen while positive regions are confined over hydrogen atoms. The surfaces over the aromatic ring and iodine atom are neutral in the all iodonitrobenzenes. The important donor–acceptor interactions between NBO's are n(LP3O2) → π^*(O1–N3) in OINB and PINB and n(LP3O1) → π^*(O2–N3) in MINB with larger two electron stabilization energy ($E^{(2)}$). The value of HOMO–LUMO energy gap for the OINB is least that attributes to high reactivity the molecule. The high values of mean first hyperpolarizability of OINB and MINB show their non–linear potential.

References

[1]. H. Zollinger, Colour Chemistry: Properties and Applications of Organic Dyes, 2nd edition, John Wiley, New York, 1991.

[2]. E. Moreau, S. Fortin, M. Desjardins, J. L. C. Rousseau, E. Petitclerc, R. C. Gaudreault, Bioorg. Med. Chem. 13 (2005) 6703–6712.

[3]. R. Meyer, J. Kholar, A. Homburg, Explosives, 5th edition, John Wiley, New York, 2002.

[4]. Y. C. Tsai, B. A. Coles, R. G. Compton, F. Marken, J. Am. Chem. Soc. 124 (2002) 9784–9788.

[5]. J. G. Lawless, M. D. Hawley, J. Electroanal. Chem. 21 (1969) 365–375.

[6]. T. T. Enya, S. Enomoto, K. Wakabayashi, J. Org. Chem. 71 (2006) 5599–5606.

[7]. P. M. Rao, G. R. Rao, J. Raman Spectrosc. 20 (1989) 529–540 and ref therein.

[8]. K. C. Mehdi, Spectrochim. Acta. 20 (1964) 675–683.

[9]. C. G. Lagrange, J. M. Lebas, M. L. Josien, Spectrochim. Acta. 12 (1958) 305–320.

[10]. E. F. Mooney, Spectrochim. Acta. 20 (1964) 1021–1032.

[11]. J. H. S. Green, D. J. Harrison, Spectrochim. Acta. 26 (1970) 1925–1937.

[12]. N. I. Sadova, L. V. Vikov, Russian Chem. Rev. 51 (1982) 153–184.

[13]. J. Brunvoll, S. Samdal, H. Thomassen, L. V. Vilkov, H. V. Volden, Acta. Chem. Scand. 44 (1990) 23–30.

[14]. S. Samdal, L. V. Vilkov, H. V. Volden, Acta. Chem. Scand. 46 (1992) 712–719.

[15]. I. F. Shishkov, L. V. Khristenko, L. V. Vilkov, S. Samdal, S. Gundersen, Struct. Chem. 14 (2003) 151–157.

[16]. A. B. Pierini, Jr. J. S. Duca, D. M. A. Vera, J. Chem. Soc., Perkin Trans. 2. 7 (1999) 1003–1009.

[17]. M. Ge, L. Yao, Spectrochim. Acta A 71 (2008) 1499–1502.

[18]. L. Yao, L. Du, M. Ge, C. Ma, D. Wang, J. Phys. Chem. A 111 (2007) 10105–10110.

[19]. M. Arivazhagan, S. Jeyavijayan, Spectrochim. Acta A 79 (2011) 376–383.

[20]. V. Udayakumara, S. Periandyb, M. Karabacakc, S. Ramalingamd, Spectrochim. Acta A 83 (2011) 575– 586.

[21]. V. Arjunan, A. Raj, S. Sakiladevi, K. Carthigayan, S. Mohan, J. Mol. Struct. 1007 (2012) 122–135.

[22]. A. Kunh, K. G. V. Eschwege, J. Conradie, J. Phys. Org. Chem. 25 (2012) 58–68.

[23]. S. Ahmad, S. Mathew, P. K. Verma, Indian J. Pure & Appl. Phys. 31 (1993) 395–398.

[24]. V. Barone, J. Chem. Phys. 122 (2005) 14108–14118.

[25]. M. A. Palafox, J. Talaya, A. G. Martinez, G. Tardajos, H. Kumar, J. K. Vats, V. K. Rastogi, Spect. Lett. 43 (2010) 51–59.

[26]. K. K. Irikura, R. D. Johnson, R. N. Kacker, J. Phys. Chem. A 109 (2005) 8430–8437.

[27]. M. A. Palafox, V. K. Rastogi, Spectrochim. Acta A 58 (2002) 411–440.

[28]. M. A. Palafox, M. Gill, N. J. Nunez, V. K. Rastogi, L. Mittal, R. Sharma, Int. J. Quantum Chem. 103 (2005) 394–421.

[29]. G. M. Chaban, J. O. Jung, R. B. Gerber, J. Chem. Phys. 111 (1999) 1823–1829.

[30]. V. Barone, J. Chem. Phys. 101 (1994) 10666–10676.

[31]. C. Minichino, V. Barone, J. Chem. Phys. 100 (1994) 3717–3741.

[32]. V. Barone, M. Cossi, N. Rega, G. Scalmani, J. Comput. Chem. 24 (2003) 669–681.

[33]. V. Barone, J. Chem. Phys. 120 (2004) 3059–3065.

[34]. A. Miani, E. Cane, P. Palmieri, A. Trombetti, N. C. Handy, J. Chem. Phys. 112 (2000) 248–259.
[35]. S. V. Krasnoshchekov, N. C. Craig, N. F. Stepanov, J. Phys. Chem. A 117 (2013) 3041–3056.
[36]. P. Wojciechowski, K. Helios, D. Michalska, Vib. Spectrosc. 57 (2011) 126–134.
[37]. V. M. R. Betancourtt, V. M. Q. Navarro, M. Neff, G. Rauhut, Chem. Phys. 387 (2011) 1–4.
[38]. G. O. Ildiz, S. Akyuz, Vib. Spectrosc. 58 (2012) 12–18.
[39]. T. Rasheed, S. Ahmad, Vib. Spectrosc. 56 (2011) 51–59.
[40]. M. J. Alam, S. Ahmad, Spectrochim. Acta A 96 (2012) 992–1004.
[41]. B. D. Becke, Phys. Rev. A 38 (1988) 3098–3100.
[42]. C. Lee, W. Yang, R. G. Parr, Phys. Rev. B 37 (1988) 785–789.
[43]. M. J. Frisch et al., Gaussian 09, Revision D.01, Gaussian, Inc., Wallingford CT, 2009.
[44]. M. H. Jamroz, Vibrational Energy Distribution Analysis: VEDA 4, Warsaw, 2004.
[45]. A. R. Allouche, J. Comput. Chem. 32 (2011) 174–182.
[46]. D. Michalska, R. Wysokiński, Chem. Phys. Lett. 403 (2005) 211–217.
[47]. E. D. Glendening, A. E. Reed, J. E. Carpenter, F. Weinhold, NBO Version 3.1.
[48]. J. P. Foster, F. Weinhold, J. Am. Chem. Soc. 102 (1980) 7211–7218.
[49]. V. Krishnakumar, N. Prabavathi, Spectrochim. Acta A 72 (2009) 738–742.
[50]. G. Socrates, Infrared Characteristic Group Frequencies, 3rd edition, Wiley Interscience Publications, New York, 1980.
[51]. J. Clarkson, W. E. Smith, J. Mol. Struct. 655 (2003) 413–422.
[52]. V. Sortur, J. Yenagi, J. Tonannavar, Spectrochim. Acta A 69 (2008) 604–611.
[53]. M. Arivazhagan, S. Prabhakaran, R. Gayathri, Spectrochim. Acta A 82 (2011) 332–339.
[54]. M. A. Palafox, V. K. Rastogi, A. G. Martinez, G. Tardajos, H. Joe, J. K. Vats, Vib. Spectrosc. 52 (2010) 108–121.
[55]. D. L. Vien, N. B. Colthup, W. G. Fateley, J. G. Grasselli, The Handbook of Infrared and Raman Characteristic Wavenumber of Organic Molecules, Academic Press, San Diego, CA, USA, 1991.
[56]. L. J. Bellamy, The Infrared Spectra of Complex Molecules, 3rd edition, Wiley, New York, 1975.
[57]. G. Herzberg, Molecular Spectra and Molecular Structure II: Infrared and Raman Spectra of Polyatomic Molecules, Van Nostrand, New York, 1945.
[58]. G. Varsanyi, Assignments of the Vibrational Spectra of Seven Hundred Benzene Derivatives, Vol. 1 and 2, Wiley, New York, 1974.
[59]. A. Dreuw, Chem. Rev. 105 (2005) 4009–4037.
[60]. F. D. Proft, J. M. L. Martin, P. Geerlings, Chem. Phys. Lett. 256 (1996) 400–408.
[61]. M. Oftadeh, S. Naseh , M. Hamadanian , Comput. and Theor. Chem. 966 (2011) 20–25.
[62]. C. A. Mebi, J. Chem. Sci. 123 (2011) 727–731.
[63]. K. K. Irikura, D. J. Frurip, Computational Thermochemistry: Prediction and Estimation of Molecular Thermodynamics, American Chemical Society, 1998.
[64]. M. Govindarajan, M. Karabacak, V. Udayakumar, S. Periandy, Spectrochim. Acta A 88 (2012) 37–48.
[65]. R. Zhang, B. Dub, G. Sun, Y. Sun, Spectrochim. Acta A 75 (2010) 1115–1124.

[66]. A. M. Sapse, Molecular Orbital Calculations for Biological Systems, Oxford University Press, 1998.
[67]. A. E. Reed, L. A. Curtiss, F. Weinhold, Chem. Rev. 88 (1988) 899–926.
[68]. F. Weinhold, C. R. Landis, Chemistry Education: Research and Practice in Europe, 2 (2001) 91–104.
[69]. K. Wu, C. Liu, C. Mang, Opt. Mater. 29 (2007) 1129–1137.
[70]. T. M. Kolev, D. Y. Yancheva, B. A. Stamboliyska, M. D. Dimitrov, R. Wortmann, Chem. Phys. 348 (2008) 45–52.
[71]. I. M. Kenawi, A. H. Kamel, R. H. Hilal, J. Mol. Struct. (Theochem) 851 (2008) 46–53.
[72]. P. A. Fantin, P. L. Barbieri, A. C. Neto, F. E. Jorge, J. Mol. Struct. (Theochem) 810 (2007) 103–111.
[73]. M. Drozd, M. K. Marchewka, Spectrochim. Acta A 64 (2006) 6–23.
[74]. A. M. Gardner, T. G. Wright, J. Chem. Phys. 135 (2011) 114305–114321.

Chapter 5

Structural and vibrational studies of 3–methyladenine based on monomer, dimer and trimer calculations

5.1 Introduction

Adenine is a most widespread nucleic acid base found in the DNA and RNA that are involved in the storage and transfer of the genetic information [1–3]. Adenine is a key component in adenosine triphosphate (ATP), which is a primary energy carrier in all living organisms. The purine bases, adenine and guanine, are important structural constituents of the second messengers cAMP and cGMP, and are often involved in mutations leading to carcinogenesis [4]. In addition, these are the preferred biological targets of platinum–based drugs mediating the cytotoxic effect of these anticancer agents [1, 2, 4]. Therefore, the knowledge of structures and spectra of nucleic acids and their derivatives are helpful in understanding the biological processes and mechanisms of action of drugs. The present investigations have been carried out on 3–methyladenine (3MA) using vibrational spectroscopy with aid of quantum chemical calculations. The compound, 3–methyladenine is widely used as an inhibitor of autophagy. It inhibits P13K activity [5]. The molecule 3MA has been shown to stimulate cell death of tumour cells under nutrient–starved conditions by inhibiting autophagy [6]. It also inhibits autophagy in tobacco culture cells under sucrose starvation conditions [7]. 3–Methylation of adenine does not influence base pairing, rather, the methyl group blocks replication by interfering with the interactions of DNA polymerase [8].

A critical survey of the most recent quantum chemical studies on nucleic acids and their constituents was carried out [9]. Extensive studies have been done on adenine along with its hydrogen–bonded dimers, derivatives, base pairs and tautomers by using various spectroscopic techniques and theoretical approaches [10–45].

9–methyladenine and its tautomers as well as complexes have been thoroughly studied using vibrational spectroscopy and quantum chemical calculations [11, 15, 24, 25, 35, 39, 43, 44]. The polarized Raman scattering measurements were done for monoclinic crystal of 1:1 hydrogen bonded complex between 9–methyladenine and 1–methylthymine [45]. The base pair formation energy of the pair between 1–methyluracil and 9–methyladenine was obtained at HF and MP2 level of theory [46]. The electronic spectra of 9–methyladenine were investigated using UV photoelectron spectroscopy [18, 29, 33], resonantly enhanced multiphoton ionization spectroscopy [47], UV resonance Raman spectroscopy [48], polarization spectroscopy [37] and theoretical approaches [18, 41, 45]. The molecular structures of platinum–9–methyladenine complex [49], 3–ethyladenine [50], 3–methyladenine hydrochloride [51], tautomers of 1–methyladenine [52, 53], 9–methyladenine [54], 9–methyladenine dihydrobromide [55] and cis–Diamminebis (3–methyladenine) platinum (II) Nitrate Trihydrate have been also reported [49, 56]. Orbell et al. [56] computed electrostatic potential maps for 3–methyladenine and 9–methyladenine using INDO molecular orbital approximation. The IR spectra of 1–methyladenine tautomers were investigated using argon matrix [52], quantum chemical calculations [57], normal coordinate analysis [52], SQM force field [53] and PM3 method [57]. Moreover, the vibrational spectra of 8–azaadenine [58] and 2–chloroadenine [13, 59] were analysed using quantum chemical computations. Many workers have performed vibrational analysis of molecules in the harmonic approximation and used various empirical scaling factors for compensating discrepancies between calculated and experimental results [60–63]. To the best of our knowledge the anharmonic force field computations, mode–mode coupling strengths, NBO analysis, vibrational spectroscopy of 3–methyladenine and simulations on its dimeric and trimeric structures have not been reported so far. Therefore, there is a scope of study of the vibrational spectra of this molecule, which is of biological importance.

The vibrational calculations at harmonic level do not represent nature of anharmonic part of the potential that is itself of great interest. Some successful efforts have been made to carry out anharmonic calculations [64–80] in order to get reliable results without any scaling. Recently, many workers have reported anharmonic vibrational frequencies of various polyatomic molecules [81–90].

In the present work, the optimized structural parameters and vibrational spectra of isolated 3MA have been computed using the *ab initio* HF and DFT (B3LYP, B3PW91) methods with 6–311G(d,p), 6–311++G(d,p) and cc–pVTZ basis sets. The MP2 method has been also utilized for calculations only at 6–311G(d,p) basis set. For treating anharmonic effects, the second order perturbation theory (PT2) method given by Barone [64], vibrational self–consistent field (VSCF) [65, 66, 79, 80] and correlation corrected vibrational self–consistent field (CC–VSCF or PT2–VSCF) [91, 92] methods based on two mode coupling representation of the quartic force field (2MR–QFF) potential energy function were employed. The details of VSCF, CC–VSCF and 2MR–QFF theories are given in section 2.2.6. In order to make good correlation between theoretical and experimental data, the simulations have been performed also on dimeric and trimeric structures of 3MA at DFT/6–311G(d,p) level of theory in the harmonic approximation. The DFT calculations with 6–311G(d,p) basis set for dimer and trimer in the anharmonic approximation are of very high computational cost, therefore, anharmonicity was not included. Anharmonicity, which causes coupling between different vibrational modes, shifts the frequencies of the modes. Therefore, to understand the coupling behaviour between pair of modes in isolated 3MA, the strength of mode–mode coupling based on 2MR–QFF for the ground state are computed and discussed [93]. Moreover, the NLO properties, MEP mapping, HOMO–LUMO and NBO analysis have been also presented. The theoretical results are compared with experiments (FTIR, FT–Raman, XRD) and are found in good agreement.

5.2 Experimental details

The compound 3–methyadenine was obtained from Sigma Aldrich chemicals company, USA and was used as such for recording of FTIR and FT–Raman spectra. FTIR spectrum of the compound was recorded at room temperature on Tensor 37 spectrometer (Bruker) in the spectral region of 400–4000 cm^{-1} with a spectral resolution of 2 cm^{-1} using KBr pellet technique. To increase the signal–to–noise ratio, a minimum of 32 scans were accumulated. FT–Raman spectrum was recorded on FT–Raman spectrometer (Bruker RFS 27) in the spectral region 50–4000 cm^{-1} with a spectral resolution 2 cm^{-1}. The Nd:YAG laser (1064 nm, 100mW) was used as excitation source.

5.3 Computational details

All the calculations were performed using Gaussian 09 software package [94] except few that were done by GAMESS-US package [95]. In DFT calculations, the functionals B3LYP [96, 97] and B3PW91 [98-101] were used. The basis sets 6-311G(d,p), 6-311++G(d,p) and cc-pVTZ were utilised with HF, B3LYP and B3PW91 methods while 6-311G(d,p) was used with MP2 method. The anharmonic force field calculations with large basis set in MP2 framework are of very high computational cost and less accurate than DFT method at same basis set. Therefore, only 6-311G(d,p) basis set has been taken for the MP2 anharmonic computations. The optimized structural parameters of the molecule in the ground state were obtained under tight convergence criterion using Berny's algorithm at same level of theory. Subsequently, vibrational frequencies (harmonic and anharmonic) along with infrared intensities and Raman activities were calculated. Anharmonic corrections in vibrational frequencies were computed using Barone's PT2 approach with Gaussian 09 package as well as VSCF and CC-VSCF methods implemented into GAMESS-US package [95]. The PT2 method is used within the HF, MP2 and DFT framework while VSCF and CC-VSCF approaches are adopted only at B3LYP/6-311G(d,p) level of theory. Gaussian program does not provide Raman intensities. Therefore, Raman intensities were computed using RAINT program [102]. The optimized structural parameters and vibrational spectra of the hydrogen bonded dimer and trimer of 3MA have been also computed at B3LYP/6-311G(d,p) level of theory in the harmonic approximation. The theoretical vibrational frequencies are, in general, overestimated from the corresponding experimental data. Therefore, it is customary to scale down the calculated harmonic vibrational frequencies for compensating discrepancies between theory and experiment. In the present case of dimer and trimer, a uniform scaling factor (0.967) was used [103]. The assignments were made with a high degree of accuracy using literature [42] and visual inspection of atomic displacements with the help of Gauss-View program [104]. In general, the highly anharmonic modes show large mode-mode coupling strengths. In order to know the coupling magnitude between pair of modes, the magnitudes of mode-mode coupling for the ground state has been estimated at B3LYP/6-311G(d,p) level of theory. The 2MR-QFF potential energy function was used for calculating anharmonic mode-mode coupling strengths [93, 105]. NBO analysis was performed and natural

atomic charges were calculated for monomeric, dimeric and trimeric strutures of 3MA with the NBO 3.1 program [106]. For the plots of simulated IR and Raman spectra, pure Lorentzian band shapes were used with full width at half maxima (FWHM) of 5 cm^{-1} [107]. The chemical behaviour and the reactivity of the 3MA monomer were investigated using HOMO (ionization potential) and LUMO (electron affinity) energy eigenvalues calculated at DFT level. These values have been used to compute chemical reactivity descriptors such as chemical potential (μ), electronegativity (χ), chemical hardness (η), chemical softness (S) and electrophilicity index (ω). These so called global quantities describe the reactivity of the molecule [108–114]. The theory related to chemical reactivity descriptors is presented in the section 2.2.7.

5.4 Results and discussion

5.4.1 Molecular geometry

Isolated form

The optimized molecular geometry of 3MA has been calculated using HF, MP2 and DFT (B3LYP and B3PW91) methods and the geometry of molecule with labelling of atoms is shown in Fig. 5.1. The molecular energies related to optimized geometries are presented in Table 5.1. From Table 5.1, it is clear that the molecular geometry calculated at B3LYP/cc–pVTZ level of theory is more stable. The calculated structural parameters and comparison with experiments for the molecule in monomer, dimer and trimer form are listed in Table 5.2 and 5.3. The RMS error and MAD between theoretical and experimental structural parameters were also presented in these tables. According to RMS and MAD values, the theoretical structural parameters are found in good agreement with XRD data [50, 51]. All real values of frequencies in vibrational calculations confirm that the optimized geometry belongs to a true minimum. The differences between theoretical and experimental structural parameters of 3MA monomer have been shown in Fig. 5.2 and 5.3. To the best of our knowledge, the experimental data on the structural parameters of 3MA are not available in the literature. Therefore, the calculated geometrical parameters are compared with available experimental data on 3–methyladenine hydrochloride and 3–ethyladenine [50, 51]. Few experimental values of bond angles, C6–C5–N11, C5–C6–C10, N7–C6–C10, C6–N7–C8, N7–C8–N9 and C6–C10–N9 of 3–methyladenine hydrochloride deviate by 4° from calculated bond angles of 3MA.

This may be because of intermolecular and intramolecular interactions in solid phase of 3MA while the theoretical calculations belong to isolated molecule in gas phase. Experimental values of these bond angles in 3–ethyladenine are comparatively close to calculated values for 3MA. The most of the calculated structural parameters at HF level show better agreement with experiments.

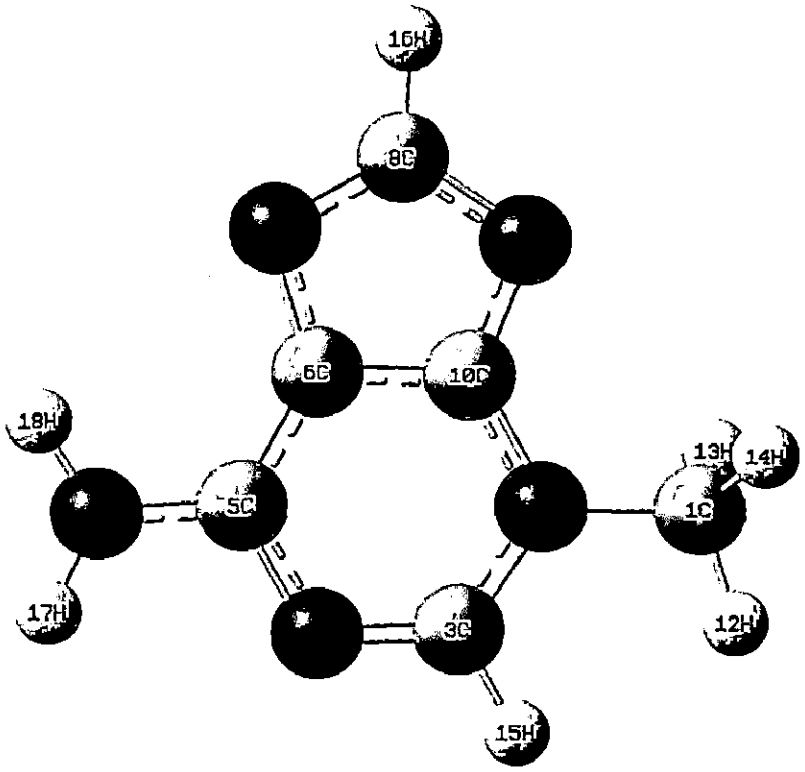

Fig. 5.1 Molecular geometry of 3MA with numbering scheme.

Dimer and trimer form

In this work, the discrepancies between theoretical and measured values of structural parameters have been noticed. These discrepancies can be associated to the fact that the calculations assume a gas phase isolated molecule, whereas the experimental result corresponds to interacting molecules in the crystal lattice for the same compound. The intermolecular interaction affects the molecular structure, vibrational frequencies and hence various other molecular properties of those of monomer. The simulation of intermolecular hydrogen bonded dimer and trimer can improve these discrepancies. The experimental data on structure of 3MA molecule have not been reported so far. The molecular structure of the similar compound, 3–ethyladenine shows the intermolecular interaction by hydrogen bonds, N···H–N–H in crystal [50].

The 1:1 molecular complex of 9–methyladenine and 2–thiohydantoin shows the hydrogen bonded dimer by H–N–H···N [115]. The single crystal structure (1 0 0) plane of 9–methyladenine shows the H–N–H···N hydrogen bonded trimer [116]. Therefore, it is expected that the 3MA molecule form intermolecular complexes in solid phase that are stabilized by hydrogen bonding, N···H–N–H. In this work, the dimeric and trimeric structures of 3MA were obtained in the ground state at B3LYP/6–311G(d,p) level of theory. The optimized geometries of the dimer and trimer with intermolecular hydrogen bond (N···H–N–H) description are given in Fig. 5.4. The predicted lengths of intermolecular hydrogen bonds are different in the dimer and trimer. The calculated structural parameters for the hydrogen bonded dimer and trimer are presented in Table 5.2 and 5.3. These tables also show the RMS errors and MAD values for the structural parameters of the monomer, dimer and trimer at different theories. According to RMS and MAD values, the bond lengths for 3MA molecule in dimer and trimer are very close to monomer while bond angles are slightly different but in good correlation with solid phase experimental data. The minimum SCF energies for the monomer, dimer and trimer are −506.74742005, −1013.51686836 and −1520.28601146 a. u. respectively at B3LYP/6–311G(d,p) level of theory. The formation of intermolecular non–covalent bondings between nitrogen atom of ring and amine group make the present dimeric and trimeric structures stable. In the most stable trimer, the calculated bond angle values of N4–C5–C6, C5–N11–H17 and H17–N11–H18 are shortened by ca. 1°, 2.7° and 2.6° respectively while C5–N11–H18 is increased by ca. 3.7° upon trimerization. The predicted values of these bond angles show excellent agreement with solid phase XRD data [50, 51]. Thus, the changes in structural parameters that involved in formation of dimer and trimer are predicted and that show the presence of intermolecular interactions in solid phase. For the present case, the supermolecular approach [117–119] was used to calculate the interaction energy of pair of interacting molecules (dimer). The computed interaction energy ($E_{int} = E_{AB} - E_A - E_B$) of the formation of hydrogen bonded dimer is 13.823 kcal/mole at B3LYP/6–311G(d,p) level of theory. The electronic energy of rigid monomer is only considered and the energy associated with the deformation of the monomer is not used. The minimum electronic energy of trimer is found more than three times of that monomer and, in dimer, it is more than two times that of monomer because of high stabilization of hydrogen bonded complex. The dipole moment for the monomer, dimer and trimer are predicted ca.

4.0160, 8.2617 and 12.8619 Debye respectively at B3LYP/6–311G(d,p) level of theory. The high dipole moment values could be contributing to favour the formation of intermolecular complexes [120].

Table 5.1 Calculated minimum SCF energies (a. u.) of the 3MA in monomer, dimer and trimer forms at different levels of theory.

Basis Sets	Monomer				Dimer	Trimer
	B3LYP	B3PW91	MP2	HF	B3LYP	B3LYP
6-311G(d,p)	-506.74742005	-506.55180603	-505.33062479	-503.65168764	-1013.51686836	-1520.28601146
6-311++G(d,p)	-506.75982280	-506.56244865	--	-503.66163309	--	--
cc-pVTZ	-506.79999250	-506.60316712	--	-503.71094364	--	--

Table 5.2 Comparison of theoretical bond lengths of 3MA monomer, dimer and trimer with experiment (XRD).

Bond length (Å)	XRD[a]	XRD[b]	Monomer									B3LYP/ 6-311G(d,p)	
			B3LYP			B3PW91			MP2	HF			
			6-311 G(d,p)	6-311++ G(d,p)	cc-pVTZ	6-311 G(d,p)	6-311++ G(d,p)	cc-pVTZ	6-311 G(d,p)	6-311 G(d,p)	6-311++ G(d,p)	cc-pVTZ	Dimer U1, U2	Trimer U1, U2, U3
C1-N2	1.473	1.476	1.464	1.465	1.460	1.457	1.457	1.453	1.462	1.457	1.458	1.454	1.464, 1.463	1.463, 1.463, 1.464
C1-H12		0.990	1.089	1.089	1.087	1.090	1.090	1.088	1.090	1.081	1.081	1.079	1.089, 1.089	1.089, 1.089, 1.089
C1-H13		1.000	1.090	1.090	1.088	1.091	1.091	1.089	1.091	1.081	1.081	1.079	1.090, 1.090	1.090, 1.090, 1.090
C1-H14		1.510	1.090	1.090	1.088	1.091	1.091	1.089	1.091	1.081	1.081	1.079	1.090, 1.090	1.090, 1.091, 1.090
N2-C3	1.328	1.350	1.355	1.355	1.351	1.351	1.351	1.347	1.352	1.335	1.336	1.332	1.354, 1.350	1.349, 1.351, 1.354
N2-C10	1.374	1.371	1.376	1.375	1.372	1.372	1.371	1.368	1.369	1.369	1.368	1.366	1.376, 1.379	1.379, 1.379, 1.376
C3-N4	1.315	1.314	1.310	1.310	1.307	1.307	1.308	1.305	1.322	1.289	1.290	1.287	1.307, 1.312	1.309, 1.312, 1.307
C3-H15		0.980	1.085	1.085	1.082	1.086	1.086	1.084	1.086	1.075	1.075	1.073	1.085, 1.085	1.085, 1.085, 1.085
N4-C5	1.382	1.365	1.364	1.364	1.361	1.360	1.360	1.357	1.358	1.358	1.358	1.356	1.370, 1.376	1.381, 1.374, 1.369
C5-C6	1.380	1.402	1.396	1.396	1.393	1.395	1.395	1.393	1.401	1.380	1.380	1.378	1.404, 1.403	1.410, 1.403, 1.404
C5-N11	1.323	1.330	1.346	1.348	1.344	1.343	1.344	1.341	1.356	1.335	1.336	1.333	1.338, 1.333	1.325, 1.334, 1.338
C6-N7	1.399	1.379	1.367	1.368	1.366	1.363	1.363	1.362	1.360	1.368	1.368	1.367	1.371, 1.366	1.371, 1.367, 1.371
C6-C10	1.375	1.383	1.414	1.414	1.410	1.410	1.411	1.407	1.419	1.396	1.396	1.392	1.411, 1.410	1.407, 1.410, 1.410
N7-C8	1.333	1.332	1.335	1.335	1.332	1.333	1.333	1.331	1.353	1.301	1.302	1.299	1.338, 1.336	1.338, 1.336, 1.338
C8-N9	1.338	1.363	1.373	1.372	1.369	1.368	1.367	1.365	1.371	1.365	1.364	1.363	1.363, 1.372	1.363, 1.372, 1.363
C8-H16		0.970	1.082	1.082	1.080	1.083	1.083	1.082	1.084	1.073	1.073	1.071	1.082, 1.082	1.082, 1.082, 1.082
N9-C10	1.357	1.345	1.329	1.330	1.328	1.327	1.328	1.326	1.337	1.307	1.308	1.307	1.332, 1.330	1.333, 1.330, 1.333
N11-H17		0.860	1.006	1.006	1.003	1.005	1.005	1.003	1.008	0.991	0.992	0.989	1.007, 1.031	1.028, 1.030, 1.007
N11-H18		0.940	1.006	1.007	1.004	1.006	1.006	1.004	1.009	0.992	0.993	0.990	1.023, 1.008	1.023, 1.008, 1.023
		RMS	0.114	0.114	0.113	0.114	0.114	0.114	0.114	0.113	0.113	0.113	0.114, 0.116	0.116, 0.115, 0.114
		MAD	0.061	0.061	0.060	0.061	0.061	0.061	0.063	0.062	0.062	0.062	0.061, 0.062	0.062, 0.620, 0.061

Abbreviation used: XRD- X-ray diffraction data, RMS-root mean square error, MAD- mean absolute deviation, U1, U2, U3- unit1, unit2 and unit3 in hydrogen bonded complex, [a]Ref [50], [b]Ref [51]

Table 5.3 Comparison of theoretical bond angles of 3MA monomer, dimer and trimer with experiment (XRD).

Bond angle (°)	XRD[a]	XRD[b]	Monomer										B3LYP/ 6-311G(d,p)	
			B3LYP			B3PW91			MP2	HF				
			6-311 G(d,p)	6-311++ G(d,p)	cc-pVTZ	6-311 G(d,p)	6-311++ G(d,p)	cc-pVTZ	6-311 G(d,p)	6-311 G(d,p)	6-311++ G(d,p)	cc-pVTZ	Dimer U1, U2	Trimer U1, U2, U3
N2-C1-H12			109.1	109.0	109.1	109.1	109.0	109.1	108.7	109.1	109.0	109.1	109.0, 109.2	109.1, 109.1, 109.0
N2-C1-H13			109.6	109.6	109.7	109.6	109.6	109.7	109.1	109.6	109.6	109.7	109.6, 109.5	109.5, 109.5, 109.7
N2-C1-H14			109.6	109.6	109.7	109.6	109.6	109.7	109.0	109.6	109.6	109.7	109.6, 109.6	109.7, 109.6, 109.6
H12-C1-H13			110.1	110.0	110.0	110.0	110.0	110.0	110.5	109.9	109.9	109.8	110.0, 110.1	110.1, 110.1, 110.0
H12-C1-H14			110.1	110.0	110.0	110.0	110.0	110.0	110.5	109.9	109.9	109.8	110.0, 110.0	110.0, 110.1, 110.0
H13-C1-H14			108.5	108.6	108.4	108.5	108.6	108.3	109.0	108.8	108.9	108.7	108.5, 108.4	108.5, 108.4, 108.5
C1-N2-C3	122.0	122.8	123.0	122.9	122.8	123.0	122.9	122.8	123.0	123.3	123.2	123.1	123.2, 123.1	123.3, 123.0, 123.1
C1-N2-C10	121.3	121.2	120.2	120.4	120.4	120.2	120.4	120.4	119.7	120.3	120.4	120.4	120.3, 120.2	120.3, 120.3, 120.4
C3-N2-C10	116.7	115.9	116.8	116.7	116.8	116.8	116.7	116.7	117.3	116.5	116.4	116.4	116.5, 116.6	116.4, 116.7, 116.5
N2-C3-N4	126.7	126.4	125.8	125.8	125.8	125.9	125.9	125.9	125.6	126.4	126.3	126.4	125.8, 126.0	126.0, 125.8, 125.8
N2-C3-H15		114.0	115.7	115.7	115.6	115.6	115.6	115.5	115.8	115.9	115.9	115.8	115.7, 115.5	115.6, 115.9, 115.7
N4-C3-H15		120.0	118.5	118.5	118.6	118.5	118.5	118.6	118.6	117.8	117.8	117.9	118.5, 118.5	118.5, 118.3, 118.5
C3-N4-C5	118.9	118.9	119.3	119.4	119.4	119.2	119.3	119.3	118.9	119.1	119.2	119.2	119.9, 119.7	120.3, 120.0, 119.9
N4-C5-C6	116.3	118.5	119.5	119.4	119.3	119.5	119.4	119.3	119.8	119.3	119.2	119.2	118.5, 118.1	117.4, 118.1, 118.5
N4-C5-N11	116.9	118.6	117.6	117.6	117.7	117.6	117.6	117.7	117.7	117.1	117.1	117.1	116.7, 118.7	117.7, 118.3, 116.9
C6-C5-N11	126.7	122.9	122.9	123.1	123.0	122.9	123.0	123.0	122.4	123.7	123.7	123.7	124.7, 123.2	127.9, 123.6, 124.6
C5-C6-N7	134.1	132.2	133.2	133.2	133.2	133.2	133.3	133.2	132.8	133.7	133.7	133.7	134.0, 132.5	133.4, 132.6, 133.8
C5-C6-C10	122.6	119.5	118.7	118.7	118.8	118.6	118.6	118.6	118.5	118.8	118.8	118.8	118.8, 119.5	119.4, 119.4, 118.8
N7-C6-C10	103.3	108.4	108.1	108.0	108.0	108.2	108.1	108.1	108.6	107.5	107.5	107.5	107.2, 108.0	107.2, 108.0, 107.3
C6-N7-C8	106.5	101.5	102.0	102.2	102.1	101.9	102.1	102.0	101.3	102.3	102.4	102.3	102.7, 102.2	102.8, 102.1, 102.7
N7-C8-N9	114.6	118.3	117.7	117.5	117.6	117.9	117.8	117.8	118.4	117.7	117.6	117.7	117.3, 117.6	117.2, 117.6, 117.3
N7-C8-H16		120.0	121.8	121.9	121.9	121.7	121.8	121.7	121.2	122.1	122.2	122.1	121.9, 121.9	121.9, 121.9, 121.8
N9-C8-H16		122.0	120.4	120.6	120.5	120.4	120.5	120.4	120.4	120.2	120.3	120.2	120.9, 120.5	120.9, 120.5, 120.9
C8-N9-C10	101.9	100.3	101.0	101.2	101.1	100.9	101.0	100.9	100.3	101.3	101.4	101.3	101.3, 100.9	101.2, 101.0, 101.3
N2-C10-C6	118.7	120.8	119.9	120.0	120.0	120.0	120.1	120.1	119.8	120.0	120.1	120.1	120.4, 120.0	120.5, 120.1, 120.4
N2-C10-N9	127.5	127.6	128.9	129.0	128.9	128.8	128.9	128.8	128.9	128.8	128.8	128.7	128.1, 128.7	127.8, 128.7, 128.2
C6-C10-N9	113.8	111.6	111.1	111.0	111.1	111.2	111.1	111.1	111.3	111.2	111.1	111.2	111.5, 111.3	111.7, 111.3, 111.4
C5-N11-H17		116.0	119.8	119.8	119.8	119.7	119.8	119.8	116.7	119.7	119.7	119.8	116.9, 122.9	120.8, 122.1, 117.1
C5-N11-H18		122.0	119.3	119.6	119.5	119.3	119.5	119.4	116.1	119.6	119.7	119.7	123.2, 116.7	120.8, 117.1, 123.0
H17-N11-H18		117.0	120.9	120.6	120.7	121.0	120.7	120.8	118.0	120.7	120.5	120.5	119.8, 120.0	118.3, 120.4, 119.7
		RMS	1.552	1.504	1.500	1.530	1.498	1.492	1.546	1.608	1.584	1.570	1.269, 2.054	1.744, 1.962, 1.218
		MAD	1.196	1.192	1.158	1.150	1.150	1.121	1.038	1.292	1.283	1.250	1.092, 1.271	1.271, 1.308, 1.058

Abbreviation used: XRD- X-ray diffraction data, RMS-root mean square error, MAD- mean absolute deviation, U1, U2, U3-unit1, unit2 and unit3 in hydrogen bonded complex, [a]Ref [50], [b]Ref [51].

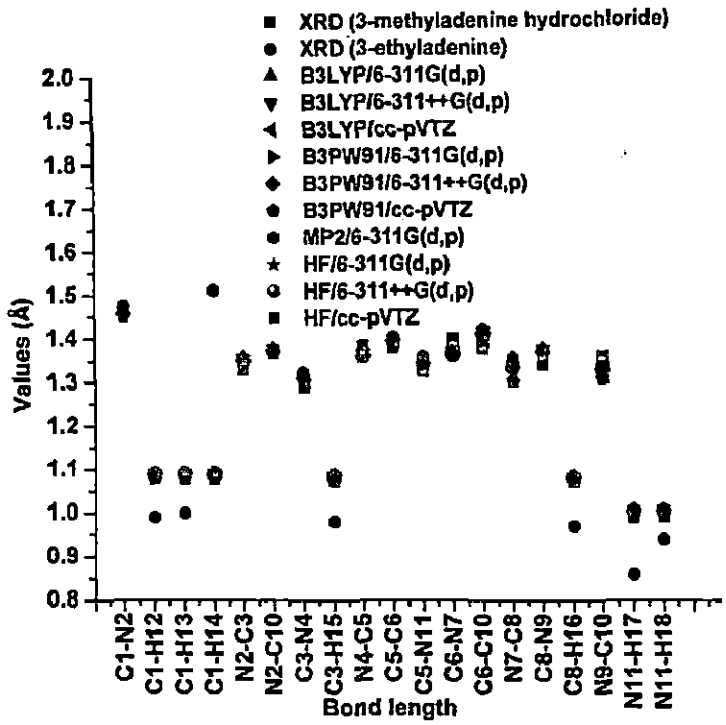

Fig. 5.2 Differences between experimental and theoretical bond lengths for 3MA monomer.

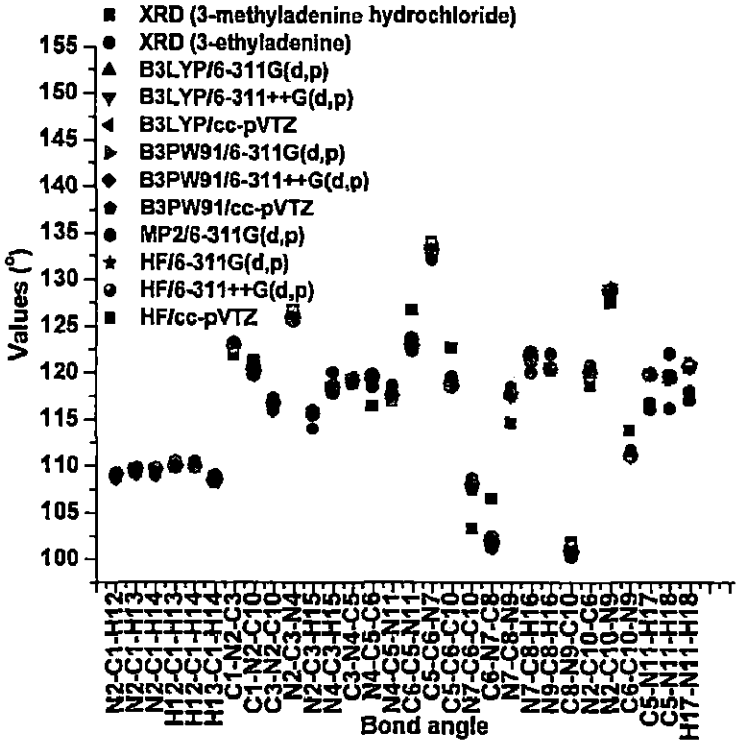

Fig 5.3 Differences between experimental and theoretical bond angles for 3MA monomer.

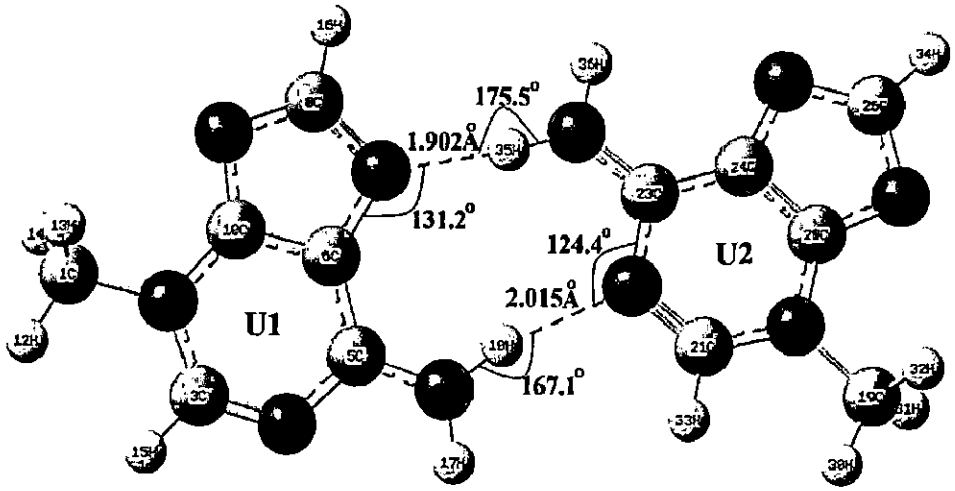

Hydrogen bonded dimer of 3MA

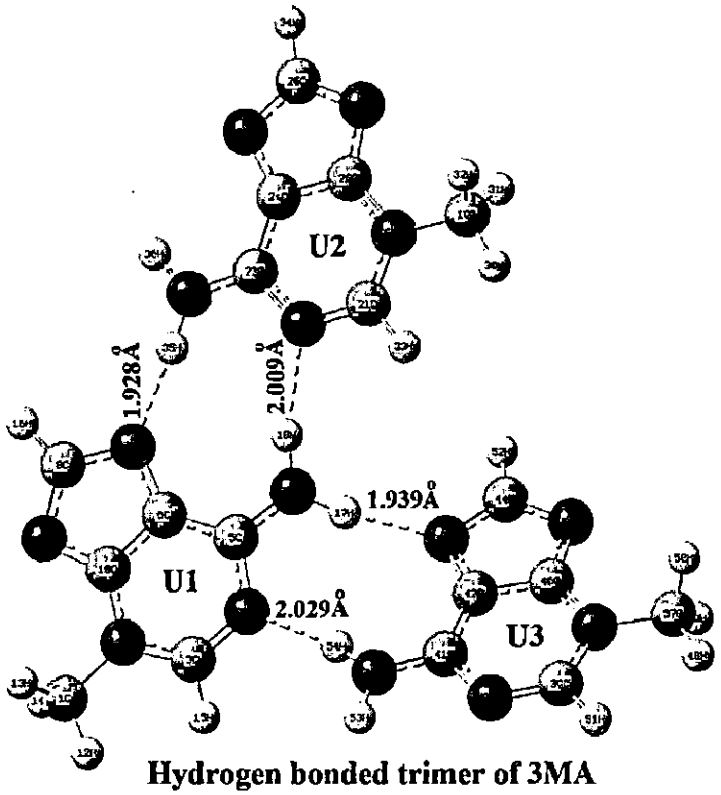

Hydrogen bonded trimer of 3MA

Fig. 5.4 Hydrogen bonded dimeric and trimeric molecular structures of 3MA.

5.4.2 Vibrational analysis

The molecule, 3MA, consists of 18 atoms and belongs to C_1 point group. It has non–planar geometry because of NH_2 and CH_3 functional groups. Therefore, all the 48 vibrational modes of 3MA are active in both IR and Raman spectra. The experimental and theoretical vibrational frequencies (at DFT/B3LYP) along with their assignments are tabulated in Table 5.4. The comparison among theoretical vibrational frequencies calculated at different theories like HF, MP2 and B3PW91 has been also presented in Table 5.5. The experimental and simulated vibrational spectra (FTIR and

FT–Raman) are presented in Fig. 5.5 and 5.6. The correlation plots between experimental and theoretical frequencies are given in Fig. 5.7 and 5.8. Vibrational assignments are based on the visualization of atomic displacements and with the help of literature [42]. The RMS and MAD values for different theories show that the B3LYP method is more reliable than others used in present work. The calculated frequencies at DFT level are found lower than those of HF due to inclusion of electron correlation term in DFT. The vibrational frequencies at MP2/6–311G(d,p) level of theory are found comparable to frequencies obtained using DFT method, however, MP2 calculations demand high computational cost. Comparison of calculated frequencies at harmonic level with respect to the experimental data shows overestimation due to neglect of anharmonicity. Therefore, in order to get good agreement between experimental and calculated wavenumbers, the anharmonic correction has been made to each vibrational mode. The calculated anharmonic wavenumbers show low RMS and MAD values in comparison to harmonic wavenumbers. It is found that the frequencies at PT2 level are more close to experimental IR frequencies except mode 46, 47 and 48.

It is considered that the amine group of 3MA form dimer and trimer by hydrogen bonding interactions with nitrogen atoms of its ring in solid phase. The intermolecular interaction can significantly affect the vibrational spectra. The calculation of vibrational frequencies for dimeric and trimeric structures of 3MA provides significant changes in many vibrational modes. The theoretical vibrational frequencies (at B3LYP/6–311G(d,p)) of dimer and trimer are presented in Table 5.6. It is interesting to note that the harmonic unscaled and scaled frequencies of many vibrational modes of dimer and trimer are found more close to solid phase FTIR data. In this work, the molecular vibrations for ring and NH_2 group in 3MA dimer and trimer are discussed because these are involve in formation of hydrogen bonded complex. In Table 5.6, the low values of the RMS and MAD for the trimer show the significant correction in theoretical vibrational spectra of 3MA monomer.

The coupling strengths between some important pair of modes are presented graphically in Fig. 5.9. In this plot, the CH_3 torsional vibration (mode 48) shows high value of coupling strengths with mode 5, 6 and 7, which correspond to stretching vibrations of CH_3 group. In addition to these, strong coupling between NH_2 wagging vibration (mode 46) and NH_2 stretching vibrations (mode 1 and 2) have been predicted. Anharmonic couplings between normal modes that involve the

displacements of the same atoms are typically stronger [67, 68]. The modes 1, 2, 5 and 6 also show medium to low coupling strength with other normal modes (Fig. 5.9). The lower modes 40, 41, 42 and 43 are found weakly coupled with the other vibrations. The 3D graphical representation of mode pair coupling strength in the 2-mode coupling representations of the quartic force field (2MR-QFF) calculated at B3LYP/6-311G(d,p) level for 3MA, is shown in Fig. 5.10. It indicates that most of the normal mode pairs have very low coupling strength except some mode pairs. The mode couplings between important pair of modes are also discussed in the relevant sections.

The molecule, 3-methyladenine, consists of one NH_2 and one CH_3 functional groups connected with purine ring. The vibrational modes of the molecule are classified into group vibrations in addition to skeletal vibrations. The vibrations related to each characteristic group of the molecule are discussed in the following sections.

NH_2 vibrations

The amino group (NH_2) is known as electron donating or activating group, which donates some of its electron density to a conjugated π system via resonance mechanism. The NH_2 group gives rise to six possible internal modes of vibrations that are defined as symmetric and asymmetric stretching, scissoring, rocking, wagging and twisting motions. The primary amines show their vibrational bands with weak to medium intensity in the region 3550-3300 cm^{-1} for asymmetric stretching and 3450-3250 cm^{-1} for symmetric stretching [121]. In the gas phase and matrix IR spectra of adenine molecule and its derivatives, the asymmetric and symmetric NH_2 stretching vibrations are reported in the region 3570-3500 and 3490-3435 cm^{-1} respectively [11-13, 16, 20, 52]. These vibrations are observed at 3426 cm^{-1} for asymmetric stretching and at 3296 cm^{-1} for symmetric stretching in the solid phase FTIR spectrum of adenine tautomer (N(9) H-*amino*-) [14]. In the present FTIR spectrum of 3MA, the bands 3365 and 3264 cm^{-1} are assigned to asymmetric and symmetric stretching vibrations respectively. The modes 1 and 2 correspond to these pure stretching vibrations as seen by animated modes. For these modes, the calculated frequencies at CC-VSCF/B3LYP/6-311G(d,p) level show comparatively low deviations from the experiment. The vibrational frequencies of N-H stretching modes show quite significant anharmonic corrections in the CC-VSCF treatment. The

significant corrections were predicted for the calculated vibrational frequencies of NH_2 group vibrations upon trimerization. The NH_2 asymmetric and symmetric stretching vibrations are predicted at 3392 and 3247 cm^{-1} respectively (harmonic frequencies for 3MA trimer) which are very close to solid phase FTIR data. Noticeable deviations are appeared between the harmonic vibrational frequencies in the monomer and the trimeric simulation of the NH_2 asymmetric stretching (by ca. 349 cm^{-1}) and symmetric stretching (by ca. 360 cm^{-1}) vibrations. Thus, it is worth to note that the harmonic vibrational frequencies for these vibrations of 3MA in dimer and trimer are well comparable to experimental FTIR without any scaling. This shows the presence of the intermolecular interactions for 3MA through the amino group in solid phase. The couplings between mode 1 and 2 to other modes of isolated 3MA are shown in Fig. 5.9. These appear strong [121] and these modes are coupled to other also. The N–H stretching modes are found strongly coupled with mode 46, which involves NH_2 wagging mixed with C1–NH_2 out of plane bending vibrations. This strong coupling may have affected the frequencies of NH_2 group vibrations.

The scissoring vibration of the NH_2 group shows strong band in the region 1650–1615 cm^{-1} [122–124]. The strong band observed at 1627 cm^{-1} in the FTIR spectrum of 3MA is identified as the scissoring of the NH_2. It is also observed in FT–Raman spectrum with weak intensity. The closest calculated harmonic frequencies for this vibration are 1627 and 1632 cm^{-1} at B3LYP/6–311G(d,p) and B3PW91/6–311G(d,p) respectively. These harmonic frequencies in the isolated state are almost the same to those of the dimer and trimer. In the gas and matrix infrared spectra of adenine, the bands in the region 1650–1612 cm^{-1} are assigned to NH_2 scissoring vibration [11, 16, 42]. This vibration, mixed with others, is reported at 1673 [14, 26], 1675 [22] and 1687 cm^{-1} [4] in the solid phase FTIR spectra of adenine. In the case of 9–methyladenine, it is assigned at 1644 cm^{-1} [11]. According to the magnitude of coupling, the scissoring vibration is found very weakly coupled to other modes. The harmonic frequencies (at MP2 and DFT levels) of this vibration for 3MA monomer, dimer and trimer are similar and close to experiment. The rocking vibration of NH_2 normally shows its presence in the region 1150–900 cm^{-1} while the wagging vibration shows band in the region 850–500 cm^{-1} [123, 124]. In the present work, the rocking motion mixed with purine ring vibrations is identified in mode 20, 21 and 27. All the calculated frequencies for this mode are in good accord with the experiment except those of HF. A high coupling strength is found between mode 46 and 47. The

anharmonic frequency of mode 46 (NH_2 wagging vibration) is predicted at 544 (PT2-B3LYP/6-311G(d,p)) and 454 (VSCF-B3LYP/6-311G(d,p)) cm^{-1}. The corresponding harmonic one is 136 cm^{-1} at B3LYP level. The difference between harmonic and anharmonic frequencies is very high indicating large anharmonicity associated in this mode or incapability of method to describe the mode. The IR bands at 566, 582 and 592 [11] in adenine and at 590 and 574 cm^{-1} in 9–methyladenine [11] are identified for wagging deformations of the amino group. In the case of adenine molecule, NH_2 rocking vibration is reported at 1229, 1017 and 1005 in the matrix; at 1234, 1018 and 961 in gas phase and at1025 and 913 cm^{-1} in solid phase FTIR spectra in the earlier reports [12, 14, 16, 22, 42]. The NH_2 twisting vibration has contributions to modes 37 and 39. The assignment is in good accord with the earlier reports in infrared spectra of adenine [14, 16, 26, 42, 125] and 9–methyladenine [15].

C–X vibrations

The C–H stretching vibrational bands normally occur in the region 3080–3010 cm^{-1} [122, 123]. FT–Raman spectrum shows the presence of C–H stretching vibrations at 3081 and 3026 cm^{-1}. These vibrations are pure stretching as visualized by animated modes. The bands due to C–H in plane bending and out of plane motion usually appear in the region 1430–990 cm^{-1} and 900–667 cm^{-1} respectively [126]. In the present work, the IR bands at 1453, 1400, 1365, 1319, 1272, 1231, 1216 and 1173 cm^{-1} are identified for C–H in plane bending vibrations have contributions in mode 13, 17, 18, 19, 20, 21 and 22 which are mixed with stretching vibrations of purine ring. The weak IR bands at 901 and 882 cm^{-1} are assigned to C–H out of plane bending modes 29 and 30, which are pure as noticed by animation. The C–H out of plane bending vibrations mixed with out of plane bending ring vibration show also their participation in mode 33.

For aromatic amines, the C–NH_2 stretching vibration appears in the region 1360–1180 cm^{-1} [122, 123]. The bands observed at 1216 and 1201 cm^{-1} in the present FTIR and FT–Raman spectra, respectively, are assigned to C–NH_2 stretching vibration, which is mixed with N–CH_3 stretching. It is reported at 1239 [11], 1368 [14], 1127 [16], 1254 [22] and 1253 cm^{-1} [26] for adenine molecule and at 1234 cm^{-1} for 9–methyladenine [11].

CH_3 vibrations

The C–H stretching vibrations in CH_3 group normally appear in the region 3010–2880 cm^{-1} [122, 123]. The bands at 2999 and 2957 cm^{-1} are assigned, respectively, to CH_3 asymmetric and C–H stretching vibrations of CH_3 group in the present FT–Raman spectrum. The symmetric CH_3 stretching vibration predicted at anharmonic frequency 2931 cm^{-1} (at PT2-B3LYP/6-311G(d,p)) is assigned to mode 7. These assignments are in agreement with those in 9–methyladenine and 1–methyladenine [15, 39, 43, 52, 57, 127]. The CH_3 umbrella vibration is observed in the present FTIR and FT–Raman spectra of 3MA, which has appeared in mode 13, 15 and 16. This vibration is reported at 1413 cm^{-1} in thymine [21], at 1429 cm^{-1} in 1–methylthymine [128], and at 1438 cm^{-1} in 9–methyladenine [11]. The CH_3 wagging vibration is assigned to mode 24 while the rocking vibration shows its presence in modes 25, 26 and 27.

The C–H bending motions in CH_3 group have shown contributions in modes 11 to 26. These vibrational assignments are within the region as reported in literature [15, 39, 43, 52, 57, 127]. The two strong Raman bands are observed at 75 and 121 cm^{-1}, first one is assigned to CH_3 torsional motion (mode 48) while the second band is appearing due to mixing of NH_2 inversion and CH_3 torsion (mode 47). The calculated anharmonic frequency for the vibrational mode 47 is 469 cm^{-1} (at PT2-B3LYP/6-311G(d,p)). It is far from those calculated using other methods. The anharmonic methods perhaps have not handled well the mode. This may also be due to strong mode coupling between mode 47 to 46 and 48 [129]. The CH_3 torsional motion is reported at theoretical wavenumber of 119 cm^{-1} [57] in 1–methyladenine molecule and at 37 cm^{-1} in 9–methyladenine [15].

Ring vibrations

The purine ring stretching vibrations appear in the region 1700–1200 cm^{-1} [52] and bending motions show their presence below 1100 cm^{-1} [10, 15, 52]. Purine ring stretching vibrations are also observed in the region 1630–1060 cm^{-1} [10, 15]. For the adenine and 9–methyladenine, the ring stretching bands have been reported in the region 1600–1060 and 1600–1300 cm^{-1} respectively [15]. In the present FTIR and FT–Raman spectra, the ring stretching vibrations are assigned within the said region and they are not pure as evident from animations (Table 5.4). The very strong to

medium bands in the FTIR spectrum of 3MA are observed at 1677, 1563, 1518, 1453, 1400, 1272, 1231, 1173 and 997 cm^{-1} which are assigned to C–N ring stretching vibrations mixed with other modes. The intensity of the stretching vibrational band at 1677 cm^{-1} is found the highest among these. These calculated results correlate reasonably with the experimental IR frequencies and intensities. For the present molecule, the ring breathing, twisting and butterfly motions are assigned to modes 35, 36 and 44 respectively. The ring breathing vibration is previously reported at 693, 721, 722, 723, 724 and 728 cm^{-1} for adenine molecule [21, 22, 26, 36, 130]. The calculated wavenumbers, 211 [14], 226, 199 [15], 209 [21], 196 [27], 204 [28], 182 [59], 209 [42] and 205 cm^{-1} [16] are assigned to butterfly motion of purine ring. Our assignments are in accordance with the earlier assignments [10, 14–16, 21, 27, 28, 42, 52, 59]. The high value of coupling strength is found between butterfly motion of purine ring (mode 44) and wagging motion of NH_2 group (mode 46).

The modes 46 and 47 appear at high energy in PT2 and VSCF calculations because of their soft character. These methods fail to describe large amplitude vibrations properly. Moreover, the anharmonicity in these two modes is due to non–diagonal coupling coefficients rather than the diagonal anharmonicity. The reason of failure of PT2 and VSCF [131] methods for defining such modes is the use of rectilinear normal coordinates in calculations. The molecular vibrations defined by rectilinear normal coordinates are based on the infinitesimal approximation of the nuclear displacements. Therefore, such coordinates are not the useful for describing the molecular vibrations involving large displacements from the equilibrium [132]. This leads to large coupling of the affected modes to their high energy counterparts (e.g. stretching vibrations) within groups capable of large amplitude of vibrations [133].

The anharmonic frequencies of lower modes 46, 47 and 48 have shown very large deviations from harmonic values which indicate large anharmonicity associated to these modes or failure of method to describe the modes. In dimer and trimer, the calculated lower wavenumbers show the complex vibrations mixed with dimer vibrations through hydrogen bonds, as seen by animated modes using GaussView.

4 Comparison of the calculated and experimental vibrational frequencies (cm^{-1}) along with intensities and probable assignments for 3MA.

Experimental		B3LYP/6-311G(d,p)							B3LYP/6-311++G(d,p)				B3LYP/cc-pVTZ				Assignment
			ω_{anh}			A*	A				A				A		
FTIR	FTR	ω_h	PT2	VSCF	CC-VSCF	(km /mole)	(km /mole)	R_i	ω_h	ω_{anh}	(km /mole)	R_i	ω_h	ω_{anh}	(km /mole)	R_i	
3365m		3741	3526	3488	3450	61.0	63.6	18.1	3737	3528	70.2	14.9	3738	3506	62.4	17.0	$\nu_{as}NH_2$
3264m		3607	3420	3412	3392	122.9	128.4	55.5	3604	3422	128.3	60.0	3604	3402	123.0	56.5	ν_sNH_2
	3081m	3213	3075	3008	3027	20.5	16.8	78.6	3218	3081	10.7	69.4	3212	3078	15.4	77.1	ν C8–H16
3025s	3026w	3178	3048	2980	2996	9.1	7.3	48.7	3182	3054	6.2	45.1	3178	3054	6.7	47.7	ν C3–H15
	2999w	3147	3003	2958	2920	7.2	7.2	26.8	3147	3003	6.1	24.9	3145	3003	6.0	24.6	$\nu_{as}CH_3$
	2957m	3127	2972	2928	2891	6.6	7.0	36.2	3129	2974	5.3	33.7	3124	2973	5.7	34.8	ν_{as} C–H of CH_3
		3057	2931	2923	2885	27.4	26.7	95.4	3058	2952	25.7	106.7	3058	2953	25.8	104.0	ν_sCH_3
1677vs		1682	1642	1651	1650	755.1	765.6	17.1	1677	1639	798.0	22.6	1677	1639	739.0	19.4	ν Rr, β_{sciss}. NH_2
1627vs	1629w	1627	1592	1599	1598	27.5	26.7	2.1	1624	1591	23.6	2.0	1624	1592	27.4	1.4	β_{sciss}. NH_2
1563m	1566s	1584	1554	1555	1552	55.8	55.9	79.0	1582	1547	54.9	94.0	1581	1546	52.8	79.7	ν Rr, β C–H of CH_3
1518m	1521m	1538	1502	1513	1513	9.4	10.4	22.1	1533	1498	13.7	35.4	1536	1499	9.9	19.6	β_{sciss}. NH_2, β_{sciss}.CH_3 of CH_3, ν Rr
		1509	1490	1488	1492	1.3	1.8	37.2	1507	1468	0.6	36.1	1509	1467	1.1	31.7	β_{sciss}.CH_2 of CH_3), β_{sciss}. NH_2
1453m	1457m	1481	1446	1456	1454	106.6	110.1	50.9	1477	1442	113.6	57.9	1479	1445	114.0	55.8	ν Rr, β N–H18 of NH_2, β C–H15, umb. CH_3
		1473	1434	1454	1459	12.2	11.0	33.6	1473	1437	11.3	26.1	1475	1430	10.1	23.9	β H–C–H of CH_3
		1461	1415	1423	1420	5.6	14.4	49.5	1458	1417	8.1	44.0	1461	1413	10.0	39.7	ν Rr, umb. CH_3
1428m	1432m	1454	1419	1426	1424	19.2	9.5	24.2	1452	1419	20.9	36.4	1456	1417	13.9	29.3	umb. CH_3, ν Rr
1400s	1410s	1420	1386	1401	1400	41.4	44.0	94.6	1418	1383	48.7	111.7	1421	1386	44.7	93.3	β C–H16, β_{sciss}. CH_3 of CH_3, ν Rr
1365sh	1371w	1383	1352	1369	1367	12.8	11.8	11.5	1381	1351	17.6	9.6	1385	1355	16.4	10.1	β H15–C, ν C5–N11, ν Rr
1319m	1322m	1343	1306	1319	1317	64.4	63.2	55.3	1341	1309	66.4	64.8	1344	1310	59.9	58.6	β C–H16, β CH_2 of CH_3, ν Rr
1272m	1269s	1301	1273	1281	1278	47.2	46.8	148.4	1302	1273	47.7	186.5	1300	1272	48.5	157.0	β C–H15, r NH_2, ν Rr
1231m	1239m	1258	1240	1245	1240	11.6	12.3	36.8	1258	1235	14.5	40.6	1260	1240	13.0	33.1	β C–H16, r NH_2, ν Rr
1216m	1201w	1232	1205	1217	1215	44.3	44.2	12.5	1229	1202	49.1	19.1	1231	1207	48.0	13.8	ν [C–NH_2 + N–CH_3], β C–H15, ν Rr
1173vs	1167s	1175	1146	1149	1146	77.2	78.4	12.9	1178	1148	85.0	23.7	1176	1146	78.2	13.4	ν N9–C8, β C–H16
		1150	1124	1145	1144	0.0	0.0	3.1	1147	1124	0.0	2.2	1153	1124	0.0	1.4	ω CH_3
1104m	1106w	1114	1099	1095	1092	4.4	4.1	23.1	1112	1095	4.8	26.6	1115	1102	4.4	20.9	r CH_3, r NH_2
1039w		1056	1036	1038	1035	4.2	5.0	46.6	1054	1034	4.7	60.2	1056	1037	4.7	47.9	β Rr, r CH_3, ν N2–CH_3
997sh	999vw	998	1008	1008	1002	15.4	15.0	5.6	997	1004	13.9	8.7	997	1013	14.6	5.1	r NH_2, r CH_3, ν Rr
946m	958m	953	941	942	941	2.1	1.9	22.8	950	937	3.8	10.3	951	938	2.6	19.3	β r2
931vw		914	894	927	916	1.2	3.2	1.6	912	891	6.2	2.8	923	905	3.2	0.1	γ H16–C
882w	892vw	912	895	924	913	9.7	8.2	0.0	908	906	6.9	0.2	921	900	7.3	0.7	γ H15–C
807m	804s	808	794	796	795	7.7	7.6	64.4	807	793	6.4	79.6	809	797	6.9	68.3	β Rr
774m	782vw	789	779	780	780	4.6	4.2	4.5	762	797	4.9	3.9	803	795	3.7	5.9	γ Rr

Table 5.4 (*continued*)

33	696vw	690vw	693	680	685	685	0.2	0.2	0.8	683	685	1.4	5.1	699	687	0.3	3.2	γ Rr, γ H16–C
34	668sh		671	657	670	669	29.1	29.9	4.4	665	656	26.6	2.4	672	660	26.7	2.6	γ Rr
35	650m	660vs	664	651	660	656	0.6	0.4	227.1	663	650	0.6	275.4	664	657	0.5	248.0	ν Rr (ring breathing)
36	615w		611	602	615	614	2.9	3.1	17.7	612	603	2.9	11.0	612	598	3.3	14.9	t Rr
37	542w		568	543	605	588	3.5	0.0	31.2	567	561	4.1	45.8	570	554	0.1	19.7	t NH_2, τ Rr
38	573m		567	562	639	599	1.0	4.2	42.5	558	550	0.04	8.0	568	561	3.9	39.7	β Rr
39			553	532	651	583	5.8	5.8	3.1	543	533	5.8	1.3	553	537	4.8	4.1	t NH_2, τ R2
40	474w	482m	476	472	473	472	2.4	2.5	92.8	476	473	3.1	103.3	477	477	2.7	95.3	β R1
41		324m	361	357	367	368	1.0	1.1	0.3	355	356	1.2	1.0	362	359	1.6	0.1	τ R1
42		288w	289	290	296	292	6.7	7.2	26.2	290	290	7.4	34.0	290	297	7.2	25.0	β [C5–N11 + C1–N2]
43			267	271	277	273	1.3	0.7	75.2	269	273	0.3	57.7	269	277	0.7	72.2	β [C5–N11 + C1–N2], β r1
44			228	282	335	284	29.0	25.8	6.4	225	285	38.6	1.3	226	289	13.7	4.1	τ Rr, ω NH_2
45		165w	187	185	205	200	0.1	0.1	1.1	180	194	0.3	10.2	188	194	0.0	1.7	τ r1, γ [C1–N2 + C5–N11]
46			136	544	454	118	122.2	140.3	62.3	150	586	174.0	8.9	132	224	31.9	47.7	ω NH_2, γ C1–N2
47		121vs	120	469	297	184	14.2	45.9	15.5	125	165	1.1	51.8	105	962	89.3	6.3	τ CH_3, inv. NH_2
48		75vs	82	126	244	96	0.0	0.1	5.5	91	136	0.1	7.8	92	923	50.1	13.5	τ CH_3
	RMS		96	68	56	37				96	42			96	195			
	MAD		46	29	33	24				45	24			47	63			

Abbreviation used: M–mode no., ω_h–harmonic wavenumbers, ω_{anh} –Anharmonic wavenumbers, A– IR intensity, R_i– Raman intensity (arb. unit), RMS–root mean square error, MAD–mean absolute deviation, ν– stretching, β– in–plane bending, τ– torsional, r–rocking motion, $\beta_{scis.}$–scissoring, ω–wagging, t–twisting, umb.–umbrella, γ– out of plane vibrations, τ Rr–butter fly motion of purine ring, Rr–purine ring, R1, R2– six membered ring, r1, r2–five membered ring, inv.–inversion motion,; w–weak, m–medium strong, sh–shoulder, b–broad, s–strong, vs–very strong., *Anharmonic IR intensity calculated by using VSCF method

Table 5.5 Theoretical harmonic and anharmonic vibrational frequencies (cm^{-1}) alongwith IR intensities of 3MA in isolated gas phase.

	B3PW91									MP2			HF								
	6–311G(d,p)			6–311++G(d,p)			cc–pVTZ			6–311G(d,p)			6–311G(d,p)			6–311++G(d,p)			cc–pVTZ		
#M	ω_h	ω_{anh}	A (km /mole)	ω_h	ω_{anh}	A (km /mole)	ω_h	ω_{anh}	A (km /mole)	ω_h	ω_{anh}	A (km /mole)	ω_h	ω_{anh}	A (km /mole)	ω_h	ω_{anh}	A (km /mole)	ω_h	ω_{anh}	A (km /mole)
1	3764	3555	68.8	3760	3555	73.4	3760	3533	65.3	3752	3590	56.4	3974	3774	85.3	3971	3784	91.2	3971	3761	81.3
2	3626	3444	134.4	3623	3445	130.3	3623	3428	126.0	3615	3469	117.0	3833	3670	158.0	3831	3675	154.6	3831	3659	148.1
3	3221	3088	15.8	3224	3087	11.1	3216	3085	14.9	3254	3125	12.6	3375	3261	26.5	3378	3262	19.4	3367	3256	25.0
4	3186	3051	7.0	3188	3053	6.3	3181	3049	6.6	3226	3096	5.9	3355	3214	10.2	3355	3211	8.4	3346	3208	9.5
5	3164	3020	6.0	3163	3020	5.2	3158	3017	4.9	3214	3076	3.6	3295	3167	12.3	3294	3164	10.8	3284	3161	10.7
6	3144	2990	5.4	3144	2993	4.3	3136	2990	4.5	3198	3061	3.4	3287	3155	12.3	3288	3158	10.2	3275	3154	10.8
7	3065	2979	25.2	3065	2942	24.8	3063	2960	24.4	3101	3005	22.3	3207	3024	33.8	3207	3030	33.3	3201	3021	33.1

le 5.5 (*continued*)

1699	1658	760	1695	1656	786.5	1693	1653	729.0	1713	1674	527.0	1836	1803	1039.0	1831	1797	1083.0
1632	1597	50.5	1629	1593	49.0	1627	1591	53.1	1637	1592	37.2	1782	1746	125.0	1779	1742	112.0
1603	1567	55.3	1601	1566	56.2	1599	1565	55.1	1605	1565	34.5	1748	1716	127.0	1744	1711	131.2
1550	1517	22.1	1547	1512	21.8	1546	1514	15.6	1581	1539	73.7	1679	1649	2.1	1674	1644	3.0
1507	1471	5.5	1505	1475	3.1	1505	1466	4.1	1526	1487	2.1	1639	1599	21.3	1638	1596	20.0
1498	1461	79.4	1494	1458	85.9	1493	1457	88.0	1514	1474	125.0	1611	1575	249.0	1606	1573	259.4
1481	1441	35.5	1477	1441	40.0	1479	1437	36.0	1495	1461	70.3	1595	1560	9.3	1595	1561	9.9
1466	1422	11.9	1466	1427	12.0	1465	1421	10.9	1490	1451	10.2	1592	1559	5.4	1588	1556	4.1
1450	1426	0.5	1449	1428	1.7	1450	1412	0.8	1465	1428	8.9	1581	1545	19.4	1577	1542	28.2
1432	1400	44.8	1431	1400	49.4	1431	1399	44.2	1435	1402	49.1	1557	1524	76.3	1553	1523	76.7
1386	1356	13.5	1384	1355	17.8	1386	1357	17.0	1389	1361	20.1	1496	1465	21.1	1494	1464	25.3
1356	1326	61.5	1354	1324	65.2	1355	1322	59.5	1373	1341	49.0	1447	1426	139.0	1445	1420	138.1
1318	1288	40.8	1319	1290	41.0	1315	1288	42.0	1311	1279	42.9	1419	1390	22.1	1417	1388	21.3
1268	1245	9.9	1268	1243	10.3	1268	1249	9.9	1251	1224	41.7	1370	1349	38.1	1368	1350	42.6
1244	1227	37.3	1242	1223	41.6	1242	1219	40.3	1239	1214	0.4	1338	1314	99.2	1335	1308	106.6
1193	1164	79.1	1194	1166	84.6	1191	1162	78.8	1211	1181	83.6	1256	1232	132.0	1256	1232	140.2
1145	1126	0.0	1142	1121	0.02	1147	1118	0.01	1163	1146	0.1	1255	1234	0.6	1252	1235	0.5
1115	1098	2.3	1114	1098	2.9	1115	1102	2.5	1136	1109	3.1	1206	1193	9.4	1204	1191	10.1
1063	1042	6.6	1061	1041	6.0	1062	1041	6.4	1068	1048	1.0	1143	1123	16.4	1141	1125	16.0
1004	1012	12.5	1002	1010	11.4	1001	1016	12.4	1027	1001	18.9	1086	1067	1.6	1080	1071	2.0
954	942	1.9	952	942	3.2	952	938	2.4	940	927	0.9	1081	1084	30.7	1079	1079	29.8
917	897	5.4	915	899	7.0	923	907	0.8	881	869	6.8	1055	1039	3.0	1051	1039	4.7
914	898	6.8	909	908	6.5	922	907	10.1	877	861	10.9	1024	1012	20.6	1021	1010	26.4
811	799	7.5	810	799	6.2	811	799	6.7	806	792	9.1	871	858	10.3	870	857	9.3
790	777	4.3	758	827	5.0	804	800	3.5	685	726	2.5	867	865	21.4	835	889	23.1
695	684	0.2	683	707	1.8	700	692	0.2	673	659	1.4	780	767	0.3	768	771	0.1
672	659	29.8	670	658	0.6	673	661	26.2	658	647	36.3	730	717	40.1	722	716	33.0
671	658	0.5	666	668	25.5	670	657	0.5	641	649	3.0	709	699	0.8	708	698	1.1
612	604	3.3	612	607	3.1	611	601	3.5	612	603	1.5	661	651	1.8	661	654	1.6
571	549	0.1	566	562	4.0	572	552	0.01	565	553	16.1	614	608	5.5	613	607	5.5
566	561	4.1	561	553	0.0	566	560	3.8	550	540	3.2	607	560	0.1	600	563	0.1
555	536	5.9	546	543	5.8	556	533	4.9	520	484	43.0	583	544	7.4	575	556	6.6
477	474	2.0	477	478	2.5	477	473	2.2	483	416	81.6	511	508	5.0	511	508	5.8
363	357	1.0	357	362	1.1	363	361	1.6	455	320	232.0	387	383	10.0	380	382	1.2
287	285	7.4	289	290	7.6	288	286	7.3	351	351	7.5	315	315	5.9	316	314	6.0
264	264	0.8	266	268	0.4	265	266	0.7	289	287	7.1	291	294	0.4	292	293	0.3
232	294	38.0	230	269	60.7	228	287	16.7	264	264	0.4	243	267	17.8	241	214	48.2
186	183	0.0	179	222	1.0	188	190	0.0	208	209	1.7	198	199	0.2	191	195	8.9

Table 5.5 (*continued*)

46	155	583	177.7	168	346	153.7	133	348	73.1	175	183	0.5	144	320	125.0	178	76	198.6
47	125	141	0.2	125	118	1.0	118	843	92.8	126	127	6.8	126	515	109.0	136	131	0.1
48	82	77	0.1	89	101	0.5	96	148	2.5	75	101	1.1	98	104	0.7	103	100	0.6
RMS	103	44		103	47		102	123		114	59		196	153		194	140	
MAD	53	20		52	24		52	40		67	34		147	120		144	110	

Abbreviation used: M–mode no., ω_h–harmonic wavenumbers, ω_{anh} –Anharmonic wavenumbers, A– IR intensity, RMS–root mean square error, MAD–mean absolu

Table 5.6 Theoretical vibrational frequencies (cm^{-1}) of 3MA in dimeric and trimeric form.

#M	B3LYP/6–311G(d,p)			
	Dimer		Trimer	
	ω_h U1, U2	ω_{scaled} U1, U2	ω_h U3, U2, U1	ω_{scaled} U3, U2, U1
1	3666, 3651	3545, 3531	3666, 3657, 3392	3545, 3536, 3280
2	3345, 3196	3235, 3091	3220, 3247, 3355	3114, 3140, 3244
3	3213, 3216	3107, 3110	3209, 3210, 3212	3103, 3104, 3106
4	3177, 3172	3072, 3067	3171, 3173, 3177	3066, 3068, 3072
5	3148, 3145	3044, 3041	3146, 3146, 3149	3042, 3042, 3045
6	3127, 3127	3024, 3024	3125, 3127, 3128	3022, 3024, 3025
7	3057, 3056	2956, 2955	3055, 3056, 3058	2954, 2955, 2957
8	1709, 1700	1653, 1644	1698, 1705, 1738	1642, 1649, 1681
9	1669, 1655	1614, 1600	1654, 1664, 1674	1599, 1609, 1619
10	1589, 1575	1537, 1523	1577, 1582, 1588	1525, 1530, 1536
11	1561, 1548	1509, 1497	1547, 1559, 1568	1496, 1508, 1516
12	1513, 1512	1463, 1462	1511, 1512, 1513	1461, 1462, 1463
13	1479, 1477	1430, 1428	1477, 1478, 1481	1428, 1429, 1432
14	1473, 1471	1424, 1422	1473, 1474, 1474	1424, 1425, 1425
15	1469, 1468	1421, 1420	1467, 1469, 1471	1419, 1421, 1422
16	1456, 1455	1408, 1407	1455, 1456, 1456	1407, 1408, 1408
17	1427, 1420	1380, 1373	1421, 1425, 1426	1374, 1378, 1379
18	1397, 1390	1351, 1344	1390, 1397, 1400	1344, 1351, 1354
19	1350, 1345	1305, 1301	1344, 1349, 1351	1300, 1304, 1306
20	1306, 1299	1263, 1256	1298, 1302, 1307	1255, 1259, 1264
21	1265, 1262	1223, 1220	1261, 1264, 1268	1219, 1222, 1226
22	1243, 1238	1202, 1197	1237, 1243, 1246	1196, 1202, 1205
23	1200, 1177	1160, 1138	1177, 1197, 1200	1138, 1157, 1160
24	1150, 1150	1112, 1112	1150, 1150, 1151	1112, 1112, 1113
25	1128, 1120	1091, 1083	1120, 1127, 1133	1083, 1090, 1096
26	1062, 1061	1027, 1026	1061, 1061, 1065	1026, 1026, 1030
27	1024, 1015	990, 982	1015, 1024, 1034	982, 990, 1000
28	968, 956	936, 924	956, 967, 969	924, 935, 937
29	922, 909	892, 879	919, 921, 924	889, 891, 894
30	907, 904	877, 874	903, 905, 906	873, 875, 876
31	817, 812	790, 785	815, 819, 834	788, 792, 806
32	811, 785	784, 759	787, 806, 811	761, 779, 784
33	784, 735	758, 711	750, 782, 785	725, 756, 759
34	696, 689	673, 666	693, 697, 737	670, 674, 713
35	674, 668	652, 646	672, 674, 690	650, 652, 667
36	664, 661	642, 639	664, 665, 669	642, 643, 647
37	627, 622	606, 601	627, 633, 661	606, 612, 639
38	577, 572	558, 553	573, 580, 621	554, 561, 601
39	557, 556	539, 538	557, 558, 571	539, 540, 552
40	529, 482	512, 466	485, 511, 553	469, 494, 535
41	476, 454	460, 439	466, 476, 479	451, 460, 463
42	359, 358	347, 346	359, 359, 367	347, 347, 355
43	338, 329	327, 318	330, 331, 357	319, 320, 345
44	278, 273	269, 264	273, 277, 278	264, 268, 269
45	223, 211	216, 204	213, 222, 226	206, 215, 219
46	191, 186	185, 180	186, 189, 193	180, 183, 187
47	133, 128	129, 124	131, 133, 140	127, 129, 135
48	102, 85	99, 82	91, 96, 118	88, 93, 114
RMS	82, 75	46, 51	77, 79, 72	51, 49, 42
MAD	57, 47	30, 34	48, 54, 58	34, 32, 30

Abbreviation used: M–mode no., RMS–root mean square error, MAD–mean absolute deviation, ω_h–harmonic wavenumbers, U1, U2, U3– unit1, unit2 and unit3 in hydrogen bonded complex ω_{scaled}– scaled vibrational frequency (uniform scaling factor ca. 0.967 was used) [99]

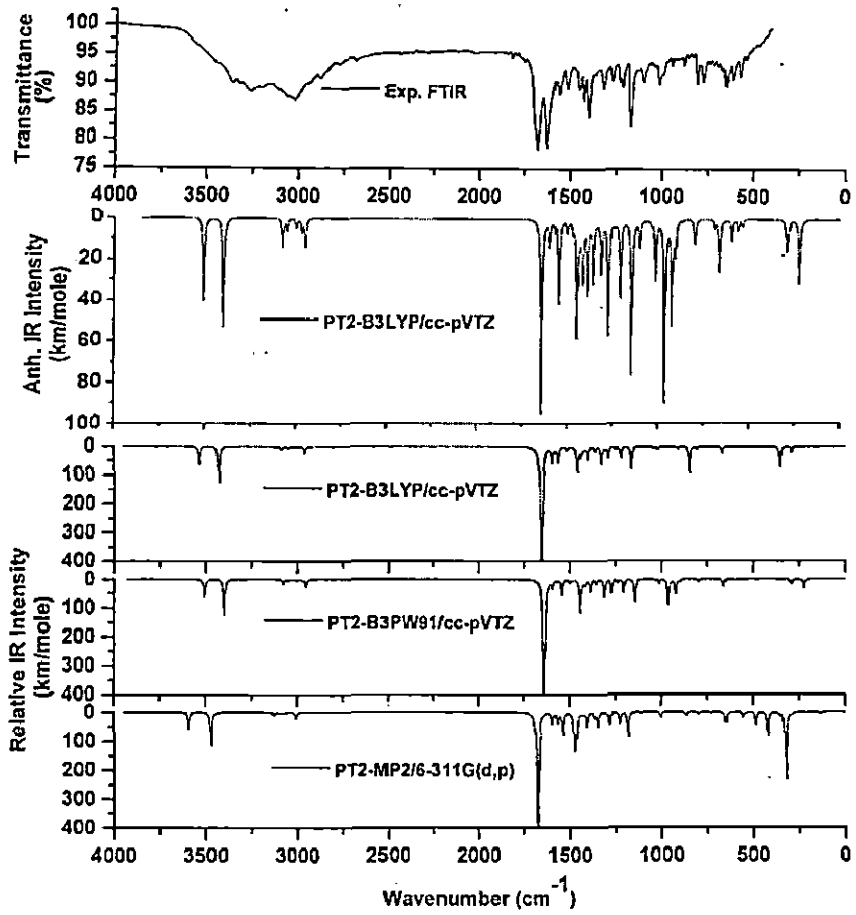

Fig. 5.5 Comparison of experimental and simulated IR spectra of 3MA.

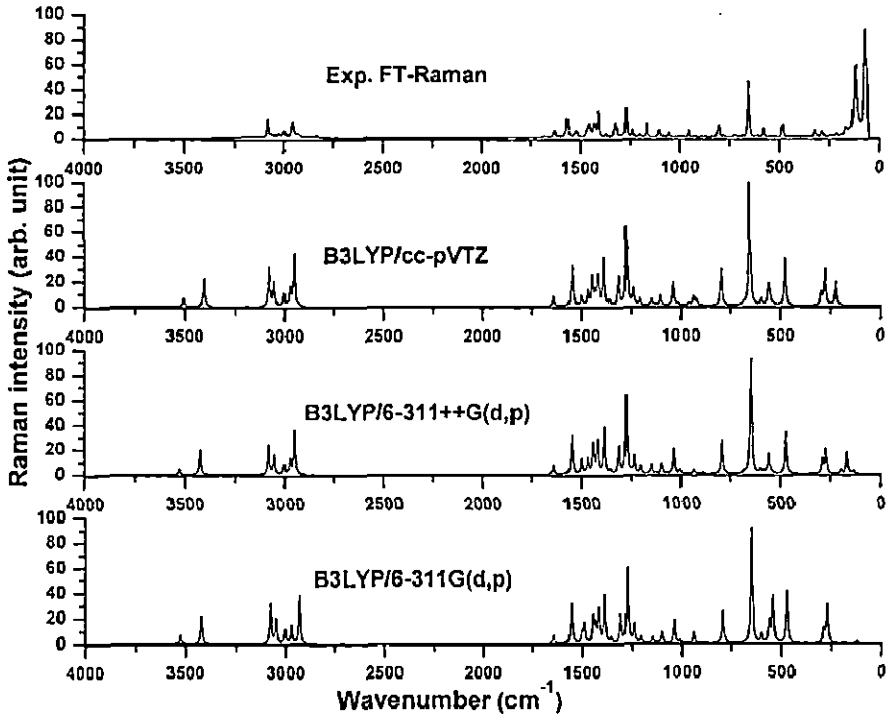

Fig. 5.6 Comparison of experimental and simulated Raman spectra of 3MA.

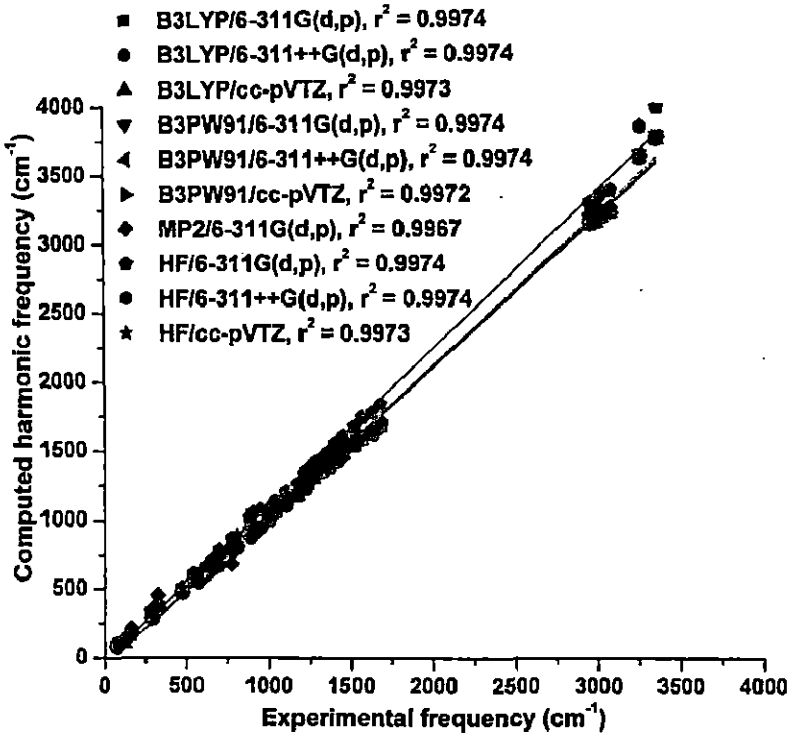

Fig. 5.7 Correlation graph between experimental and theoretical (harmonic) frequencies.

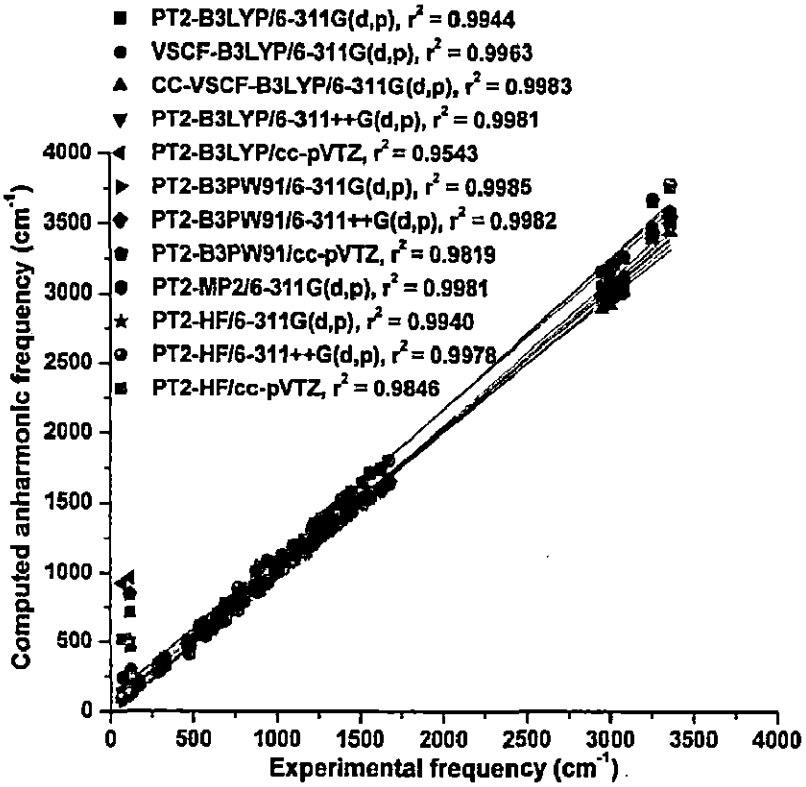

Fig. 5.8 Correlation graph between experimental and theoretical (anharmonic) frequencies.

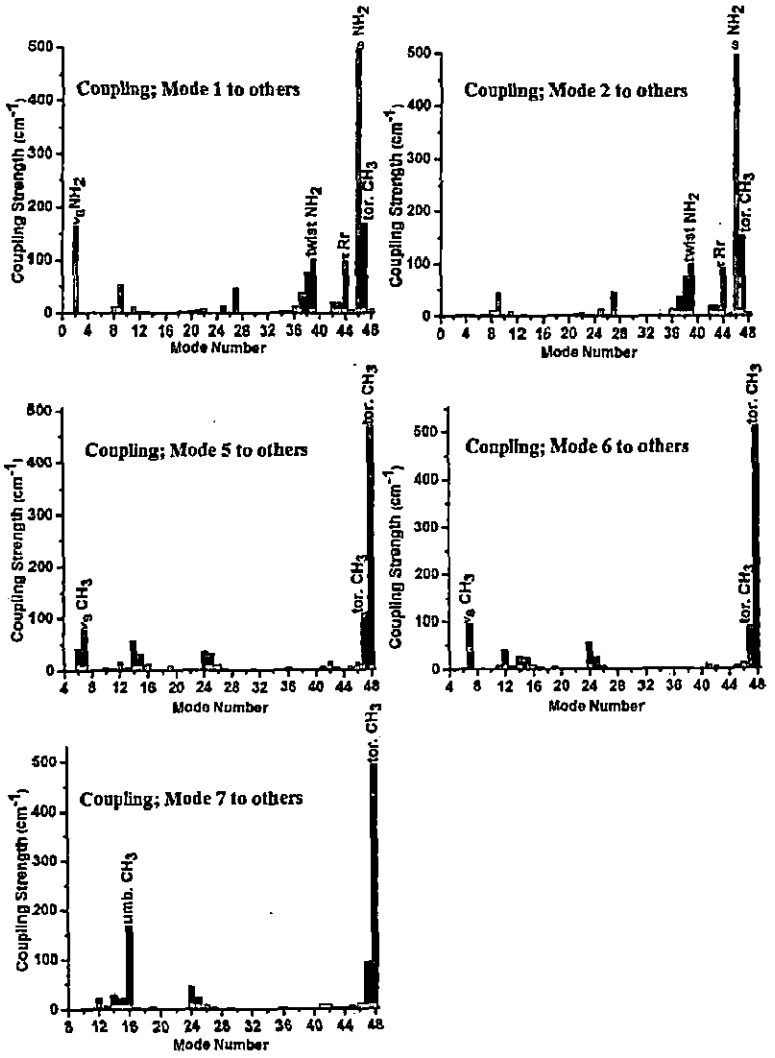

Fig. 5.9 Graph for mode–mode coupling strengths between some important modes of 3MA.

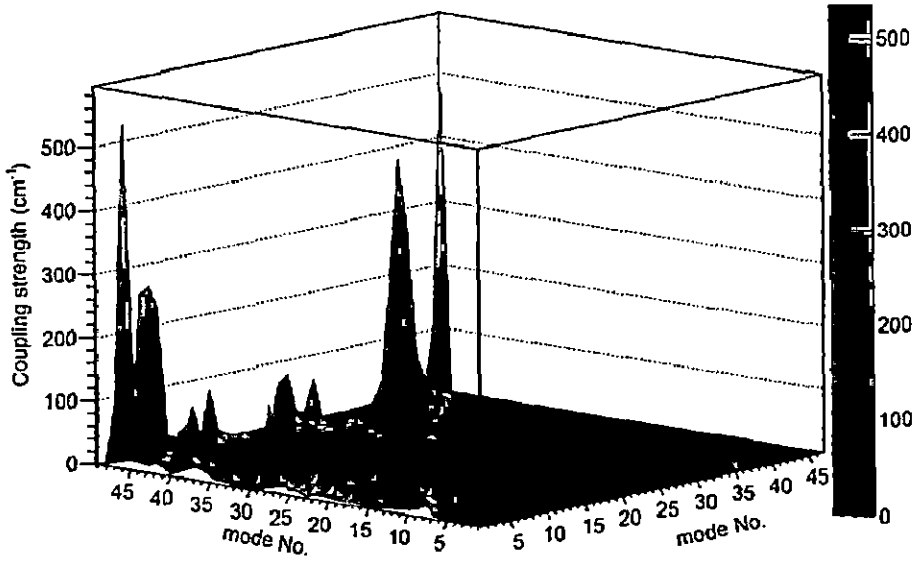

Fig. 5.10 3D Graphical representation of mode–mode coupling strengths for 3MA.

5.4.3 Natural bond orbital analysis

The natural bond orbitals (NBO) analysis is a useful technique for studying hybridization, intramolecular and intermolecular bonding, covalency effect and charge transfer in molecular systems. It provides most accurate Lewis structure of molecules [134, 135] and information about interactions between acceptor (empty NBOs) and donor (filled NBOs) orbitals. The stabilization energy $E^{(2)}$ associated with delocalization i→j for each donor NBO (i) and acceptor NBO (j) is computed by second order perturbation theory (section 2.2.7). The NBO analysis was carried out at the B3LYP/6−311G(d,p) level of theory using NBO 3.1 program as implemented in the Gaussian 09 package. The hybridization of filled orbitals is presented in Table 5.7. The second order perturbation energy values, $E^{(2)}$, corresponding to important interactions between electron donors and acceptors are given in Table 5.8. The larger value of stabilization energy, $E^{(2)}$, represents intensive interaction between filled and virtual NBOs. Larger polarization coefficient corresponds to higher electron density (in %) of NBO as well as electronegativity. In 3MA molecule, the nitrogen atoms show high electronegativity (Table 5.7). High values of polarization coefficient are predicted for carbon atoms in σ(C1−H12), σ(C1−H13), σ(C1−H14), σ(C3−H15), σ(C5−C6), π(C5−C6), σ(C6−C10) and σ(C8−H16) bonding. The carbon atoms, which are attached to nitrogen atoms, show low polarization coefficient because of high electronegativity of nitrogen atom. In Table 5.8, the intensive intramolecular interactions are observed for π*(C3−N4) → π*(C5−C6), π(C5−C6) → π*(N9−C10), π(N7−C8) → π*(C5−C6), π(N9−C10) → π*(N7−C8), π*(C3−N4) → π*(C5−C6), n(LP_1N2) → π*(C3−N4), n(LP_1N2) → π*(N9−C10) and n(LP_1N11) → π*(C5−C6) orbitals. These interactions are showing delocalization of electron density between NBO orbitals. The NBO analysis of 3MA dimer and trimer show evidences of the formation of stabilized hydrogen bonded intermolecular interaction between lone pair LP (N) and antibonding σ* N−H orbitals at B3LYP/6−311G(d,p) level of theory. Its existence is evident from the intermolecular charge transfer due to n(LPN) → σ*(N−H) which causes the stabilization of dimer and trimer. The stabilization energy values, $E^{(2)}$, between hydrogen bonded orbitals, n(LPN)···σ*(N−H), determined by second order perturbation analysis of Fock matrix of 3MA dimer and trimer, are summerized in Table. 5.9. The stabilization energy measures the strength of the hydrogen bonding. The intermolecular hydrogen bonds are formed by overlapping

between the orbitals n(LPN) and σ*(N–H) and, hence, it leads to increase the electron density of N–H antibonding orbital.

The comparison of NBO analysis between monomer and dimer or trimer clearly show the existence of H–N–H···N intermolecular hydrogen bonding in 3MA. This investigation obviously clarifies the formation of two intermolecular H–bonded interactions in dimer and four in trimer. These are formed between lone pair orbitals: n(N7), n(N4), n(N22), n(N43) and antibonding orbitals: σ*(N29–H35), σ*(N47–H54), σ*(N11–H18), σ*(N11–H17), respectively, causing stabilization of the Hydrogen–bonded complexes.

The stabilization energies, $E^{(2)}$, associated with hyperconjugative interactions $n(LP_1N7) \rightarrow \sigma^*(N29–H35)$, $n(LP_1N22) \rightarrow \sigma^*(N11–H18)$, $n(LP_1N7) \rightarrow \sigma^*(N29–H35)$, $n(LP_1N4) \rightarrow \sigma^*(N47–H54)$, $n(LP_1N22) \rightarrow \sigma^*(N11–H18)$ and $n(LP_1N43) \rightarrow \sigma^*(N11–H17)$ were respectively 17.30, 10.93, 15.88, 10.10, 10.81 and 15.40 kcal mol^{-1}, which measure the extent of intermolecular hydrogen bonding. Moreover, it is predicted that the total SCF energy in the dimeric form is more than twice of the total energy of the monomer and, for trimer, it is more than of thrice of that monomer (Table 5.1). This shows that dimer and trimer are more stable than the monomer because of the existence of intermolecular hydrogen bonding.

Table 5.7 NBO analysis of 3MA monomer at B3LYP/6–311G(d,p) level of theory.

Bond (A–B)	Occupancy	ED_A %	ED_B %	NBO (% p character)
σ(C1–N2)	1.98572	35.79	64.21	$0.5983\ sp^{3.08}(75.38)_C + 0.8013\ sp^{2.22}(68.96)_N$
σ(C1–H12)	1.99072	59.69	40.31	$0.7726\ sp^{2.99}(74.92)_C + 0.6349\ sp^{0.00}(0.04)_H$
σ(C1–H13)	1.98725	60.73	39.27	$0.7793\ sp^{2.95}(74.61)_C + 0.6267\ sp^{0.00}(0.04)_H$
σ(C1–H14)	1.98725	60.73	39.27	$0.7793\ sp^{2.95}(74.61)_C + 0.6267\ sp^{0.00}(0.04)_H$
σ(N2–C3)	1.98631	63.62	36.38	$0.7976\ sp^{1.91}(65.62)_N + 0.6032\ sp^{2.03}(66.97)_C$
σ(N2–C10)	1.98187	63.22	36.78	$0.7951\ sp^{1.89}(65.36)_N + 0.6065\ sp^{2.36}(70.21)_C$
σ(C3–N4)	1.98480	41.01	58.99	$0.6404\ sp^{1.76}(63.67)_C + 0.7680\ sp^{1.68}(62.65)_N$
π(C3–N4)	1.83308	36.60	63.40	$0.6050\ sp^{1.00}(99.82)_C + 0.7963\ sp^{1.00}(99.86)_N$
σ(C3–H15)	1.97887	59.48	40.52	$0.7712\ sp^{2.22}(68.90)_C + 0.6365\ sp^{0.00}(0.06)_H$
σ(N4–C5)	1.98013	58.60	41.40	$0.7655\ sp^{1.90}(65.50)_N + 0.6435\ sp^{2.26}(69.22)_C$
σ(C5–C6)	1.97494	50.00	50.00	$0.7071\ sp^{1.58}(61.18)_C + 0.7071\ sp^{1.75}(63.63)_C$
π(C5–C6)	1.56000	40.68	59.32	$0.6378\ sp^{1.00}(99.94)_C + 0.7702\ sp^{1.00}(99.98)_C$
σ(C5–N11)	1.98972	39.88	60.12	$0.6315\ sp^{2.31}(69.71)_C + 0.7754\ sp^{1.46}(59.37)_N$
σ(C6–N7)	1.97701	43.18	56.82	$0.6571\ sp^{2.16}(68.34)_C + 0.7538\ sp^{2.14}(68.07)_N$
σ(C6–C10)	1.96921	49.93	50.07	$0.7066\ sp^{2.14}(68.10)_C + 0.7076\ sp^{1.78}(63.95)_C$
σ(N7–C8)	1.98546	59.98	40.02	$0.7745\ sp^{1.91}(65.59)_N + 0.6326\ sp^{1.89}(65.31)_C$
π(N7–C8)	1.84437	61.43	38.57	$0.7838\ sp^{1.00}(99.84)_N + 0.6210\ sp^{1.00}(99.79)_C$
σ(C8–N9)	1.97799	39.70	60.30	$0.6301\ sp^{2.00}(66.56)_C + 0.7765\ sp^{2.15}(68.23)_N$
σ(C8–H16)	1.98356	59.20	40.80	$0.7694\ sp^{2.11}(67.84)_C + 0.6387\ sp^{0.00}(0.06)_H$
σ(N9–C10)	1.98125	57.20	42.80	$0.7563\ sp^{1.94}(65.97)_N + 0.6542\ sp^{1.94}(65.88)_C$
π(N9–C10)	1.80167	61.72	38.28	$0.7856\ sp^{1.00}(99.83)_N + 0.6187\ sp^{1.00}(99.84)_C$
σ(N11–H17)	1.99060	69.98	30.02	$0.8366\ sp^{2.38}(70.37)_N + 0.5479\ sp^{0.00}(0.06)_H$

Table 5.7 (*continued*)

σ(N11–H18)	1.98967	70.35	29.65	$0.8388\ sp^{2.36}\ (70.21)_N + 0.5445\ sp^{0.00}\ (0.06)_H$
Lone Pairs				
LP_1 N2	1.53267			$sp^{1.00}$ (99.99)
LP_1 N4	1.89810			$sp^{2.53}$ (71.62)
LP_1 N7	1.93063			$sp^{1.95}$ (66.09)
LP_1 N9	1.92723			$sp^{1.91}$ (65.54)
LP_1 N11	1.72625			$sp^{1.00}$ (99.99)

Abbreviation used: ED– Electron density

Table 5.8 Second order perturbation theory analysis of Fock matrix in NBO basis for 3MA monomer at B3LYP/6–311G(d,p) level of theory.

Donor–acceptor interaction	$E^{(2)a}$ (kcal/mol)	E(j)–E(i)[b] (a.u.)	F(i, j)[c] (a.u.)
π(C3–N4) → π*(C5–C6)	21.41	0.36	0.084
π(C5–C6) → π*(C3–N4)	12.81	0.24	0.049
π(C5–C6) → π*(N7–C8)	15.09	0.28	0.059
π(C5–C6) → π*(N9–C10)	31.96	0.28	0.085
π(N7–C8) → π*(C5–C6)	23.50	0.30	0.081
π(N7–C8) → π*(N9–C10)	8.21	0.29	0.048
σ(C8–N9) → σ*(N2–C10)	11.61	1.19	0.106
π(N9–C10) → π*(C5–C6)	9.60	0.31	0.052
π(N9–C10) → π*(N7–C8)	31.42	0.32	0.093
π*(C3–N4) → π*(C5–C6)	69.39	0.04	0.075
n(LP_1N2) → σ*(C1–H13)	4.06	0.67	0.053
n(LP_1N2) → σ*(C1–H14)	4.06	0.67	0.053
n(LP_1N2) → π*(C3–N4)	60.41	0.27	0.116
n(LP_1N2) → π*(N9–C10)	48.62	0.30	0.109
n(LP_1N4) → σ*(N2–C3)	13.41	0.80	0.094
n(LP_1N4) → σ*(C3–H15)	4.39	0.74	0.052
n(LP_1N4) → σ*(C5–C6)	8.98	0.91	0.082
n(LP_1N4) → σ*(C5–N11)	3.83	0.83	0.051
n(LP_1N7) → σ*(N2–C10)	0.55	0.80	0.019
n(LP_1N7) → σ*(C6–C10)	6.65	0.88	0.068
n(LP_1N7) → σ*(C8–N9)	7.58	0.85	0.072
n(LP_1N7) → σ*(C8–H16)	2.27	0.81	0.039
n(LP_1N9) → σ*(N2–C10)	1.61	0.80	0.032
n(LP_1N9) → σ*(C6–C10)	7.35	0.88	0.072
n(LP_1N9) → σ*(N7–C8)	6.14	0.91	0.068
n(LP_1N9) → σ*(C8–H16)	1.98	0.81	0.036
n(LP_1N11) → π*(C5–C6)	50.41	0.29	0.113

[a]Energy of hyper conjugative interaction (stabilization energy).
[b]Energy difference between donor and acceptor i and j NBO orbitals.
[c]Fock matrix element between i and j NBO orbitals.

Table 5.9 Important donor–accepter intermolecular interactions based on Second order perturbation theory analysis of Fock matrix in NBO basis for 3MA dimer and trimer at B3LYP/6–311G(d,p) level of theory.

Donor–acceptor intermolecular interaction	ED_i (*e*)	ED_j (*e*)	$E^{(2)a}$ (kcal/mol)	E(j)–E(i)[b] (a.u.)	F(i, j)[c] (a.u.)
from unit 1 to 2 (Dimer)					
n(LP_1N7) → σ*(N29–H35)	1.90259	0.04853	17.30	0.83	0.108
from unit 2 to 1 (Dimer)					
n(LP_1N22) → σ*(N11–H18)	1.88550	0.03297	10.93	0.80	0.085
from unit 1 to 2 (Trimer)					
n(LP_1N7) → σ*(N29–H35)	1.90499	0.04547	15.88	0.83	0.104
from unit 1 to 3 (Trimer)					
n(LP_1N4) → σ*(N47–H54)	1.88600	0.03195	10.10	0.80	0.082

Table 5.9 (*continued*)

from unit 2 to 1 (Trimer)					
$n(LP_iN22) \rightarrow \sigma^*(N11–H18)$	1.88565	0.03266	10.81	0.80	0.085
from unit 3 to 1 (Trimer)					
$n(LP_iN43) \rightarrow \sigma^*(N11–H17)$	1.90657	0.04442	15.04	0.83	0.101

Abbreviation used: ED_i – Electron density (e) for donor orbital, ED_j – Electron density (e) for acceptor orbital

[a]Energy of hyper conjugative interaction (stabilization energy).

[b]Energy difference between donor and acceptor i and j NBO orbitals.

[c]Fock matrix element between i and j NBO orbitals.

5.4.4 Frontier molecular orbitals

The highest occupied molecular orbital (HOMO) and lowest unoccupied molecular orbital (LUMO), called the frontier orbitals, play important role in chemical reactivity. The HOMO and LUMO energy eigenvalues are used to calculate various global reactivity descriptors and Fukui functions [108–114]. In this work, HOMO and LUMO energy eigenvalues, HOMO–LUMO energy gap and global reactivity descriptors such as electronic chemical potential (μ), the absolute chemical hardness (η), chemical softness (S) and the global electrophilicity (ω) are computed at DFT(B3LYP)/6–311++G(d,p) level of theory in gaseous and solution phase. The HOMO–LUMO energy gap is also approximated using excitation energy of HOMO–LUMO excitation at TD–B3LYP/6–311++G(d,p) level of theory. The details of chemical reactivity descriptors can be found in texts [111, 136] as well in section 2.2.7. The global electrophilicity index measures the tendency of chemical species to accept the electrons. Thus, the good electrophile and nucleophile can be characterized by low and high values of electrophilicity index respectively [136, 137]. The SCF energy, HOMO and LUMO energy eigenvalues, HOMO–LUMO energy gap and chemical reactivity descriptors are presented in Table 5.10. The HOMOs and LUMOs plot are shown in Fig. 5.11.

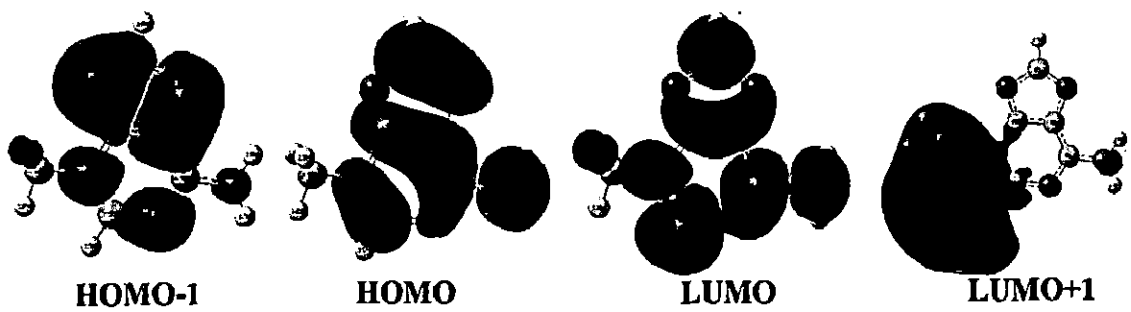

Fig. 5.11 Frontier molecular orbitals of 3MA in gas phase.

Table 5.10 Global parameters based on HOMO, LUMO energy eigenvalues for 3MA.

Parameters (a.u.)	B3LYP/6–311++G(d,p)			
	Gas	Water	Ethanol	DMSO
SCF Energy	−506.75982280	−506.78563524	−506.77609550	−506.78486596
Dipole moment (Debye)	4.1357	6.0693	5.8395	6.0282
ε_{HOMO} (−IP)	−0.22736	−0.23361	−0.23474	−0.23362
ε_{LUMO} (−EA)	−0.05464	−0.05472	−0.05614	−0.05486
Gap	0.17272	0.17889	0.17860	0.17876
(ε_{LUMO}- ε_{HOMO})	0.15880[a]	0.16510[a]	0.16450[a]	0.16450[a]
μ	−0.141	−0.144	−0.145	−0.144
X	0.141	0.144	0.145	0.144
H	0.08636	0.08944	0.08930	0.08938
S	5.78972	5.59033	5.59910	5.59409
Ω	0.11510	0.11592	0.11772	0.11600

Abbreviation used: IP– ionization potential, EA– electron affinity, μ–electronic chemical potential, χ–electronegativity, η–the absolute chemical hardness, S–chemical softness, ω–global electrophilicity.
[a]HOMO–LUMO excitation at TD-B3LYP/6–311++G(d,p)
Note: PCM model was used for solution phase calculations

5.4.5 Electrostatic potential, total electron density and molecular electrostatic potential

The electrostatic potential (ESP), total electron density (ED) and molecular electrostatic potential (MEP) of 3MA molecule in 3D plots at B3LYP/6–311G(d,p) level of theory are shown in Fig. 5.12 with colour range (in MEP) from −5.398E–2 (deepest red) to +5.398E–2 (deepest blue). The surfaces with blue, green and red colours indicate the positive, zero and negative values of the potential respectively. MEP map helps in the qualitative interpretation of the electrophilic and nucleophilic reactions for the study of biological recognition process and hydrogen bonding interactions [138]. In the present MEP plot, the surfaces over the N7 (−0.054 a.u.) and N9 (−0.052 a.u.) atoms are representing high negative electrostatic potential while the surfaces over the atoms H18 (0.040 a.u.), C5 (0.038 a.u.), H17 (0.047 a.u.), N4 (0.026 a.u.), H15 (0.035 a.u.) and N2 (0.042 a.u.) are showing high positive electrostatic potential. Thus, the high negative (red colour) and positive electrostatic potential surfaces (blue colour) are the sites for electrophilic and nucleophilic attack respectively. The knowledge of the molecular reactive site enables workers to predict how complex drugs interact with proteins.

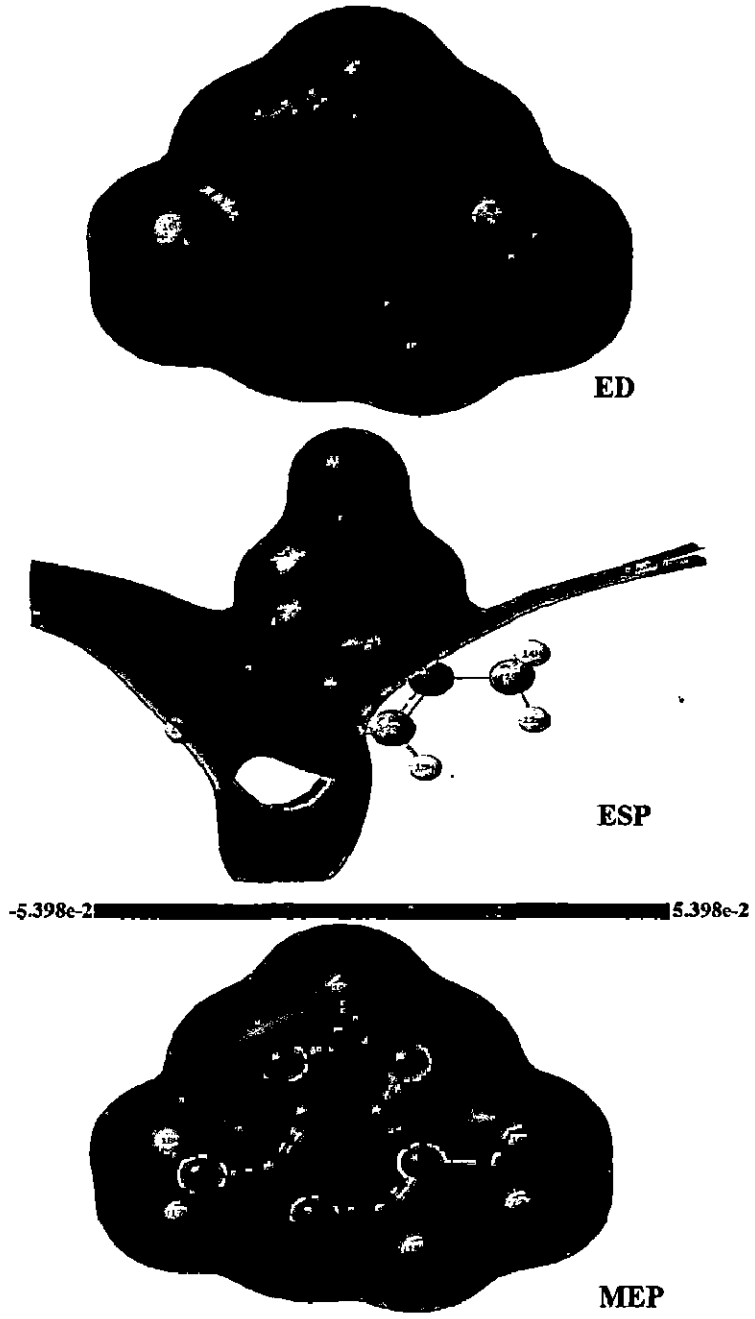

Fig. 5.12 Total electron density, electrostatic potential plots and molecular electrostatic potential map of 3MA molecule.

5.4.6 Other molecular properties

Atomic charges in a molecule are related to dipole moment, electronic structure, molecular polarizability and other properties of the molecule. In the present work, Mulliken and natural atomic charges on each atoms of 3MA molecule have been calculated at B3LYP, B3PW91, MP2 and HF theory with 6–311G(d,p) basis set and these are listed in Table 5.11. The H18 and H17 atoms have more positive charge among all other H atoms because electron density delocalizes toward electronegative nitrogen atom (N11). It is found that C5 and N11 accommodate higher positive and

negative charge respectively in comparison to other carbon and nitrogen atoms because charge displaces from C5 to N11 atom. The natural atomic charges for 3MA dimer and trimer are also depicted in Table 5.11. The comparisons of natural atomic charges for monomers, dimer and trimer are shown in Fig. 5.13. The hydrogen–bonded complexes have produced shift in natural atomic charges as compared to those of monomer. The atoms 7N, 4N, H18 and H17, which are involved in formation of intermolecular hydrogen bonded complexes, show significant changes in the charges. These changes strengthen the hydrogen bonds and stabilize dimeric and trimeric structures.

Table 5.11 Atomic charges (*e*) for 3MA monomer, dimer and trimer at different methods with 6–311G(d,p) basis set.

Atoms	Monomer								Dimer		Trimer		
	Natural				Mulliken				Natural		Natural		
	B3LYP	B3PW91	MP2	HF	B3LYP	B3PW91	MP2	HF	B3LYP		B3LYP		
									U1	U2	U1	U2	U3
C1	−0.343	−0.357	−0.247	−0.243	−0.147	−0.178	−0.058	−0.053	−0.343	−0.343	−0.343	−0.343	−0.343
N2	−0.375	−0.368	−0.466	−0.466	−0.397	−0.440	−0.555	−0.558	−0.377	−0.373	−0.376	−0.374	−0.377
C3	0.319	0.3122	0.461	0.469	0.208	0.226	0.338	0.348	0.324	0.323	0.327	0.3212	0.325
N4	−0.545	−0.542	−0.644	−0.644	−0.385	−0.428	−0.522	−0.532	−0.545	−0.595	−0.593	−0.591	−0.544
C5	0.439	0.4324	0.572	0.572	0.390	0.438	0.491	0.523	0.446	0.451	0.4548	0.4513	0.447
C6	−0.001	−0.005	−0.042	−0.070	−0.028	−0.017	0.042	0.021	0.008	−0.002	0.0086	−0.002	0.006
N7	−0.544	−0.541	−0.613	−0.595	−0.358	−0.394	−0.491	−0.477	−0.594	−0.54	−0.59	−0.542	−0.591
C8	0.246	0.2402	0.341	0.339	0.102	0.115	0.191	0.195	0.255	0.24	0.2491	0.2386	0.245
N9	−0.576	−0.572	−0.662	−0.665	−0.357	−0.389	−0.495	−0.497	−0.569	−0.576	−0.569	−0.578	−0.569
C10	0.349	0.3424	0.438	0.446	0.329	0.377	0.494	0.502	0.351	0.339	0.3413	0.3397	0.351
N11	−0.736	−0.737	−0.802	−0.790	−0.457	−0.490	−0.519	−0.550	−0.738	−0.736	−0.738	−0.737	−0.737
H12	0.193	0.1976	0.168	0.165	0.111	0.122	0.096	0.093	0.194	0.191	0.1922	0.1946	0.195
H13	0.211	0.2158	0.188	0.185	0.147	0.168	0.137	0.133	0.211	0.212	0.2122	0.2105	0.212
H14	0.211	0.2158	0.189	0.185	0.147	0.155	0.138	0.133	0.212	0.211	0.2115	0.2095	0.212
H15	0.181	0.1848	0.172	0.164	0.123	0.133	0.134	0.125	0.182	0.177	0.1784	0.184	0.183
H16	0.174	0.1773	0.16	0.155	0.088	0.098	0.093	0.084	0.177	0.173	0.1756	0.172	0.176
H17	0.394	0.3977	0.389	0.393	0.233	0.243	0.234	0.245	0.386	0.438	0.4325	0.4384	0.388
H18	0.402	0.4054	0.397	0.400	0.249	0.260	0.252	0.263	0.434	0.394	0.4281	0.3929	0.433

Dipole moments, zero point vibrational energy, rotational constants, rotational temperatures and several thermodynamic parameters such as enthalpy, heat capacity, free energy and entropy of 3MA have been computed at HF, MP2, B3PW91 and B3LYP methods utilizing 6–311G(d,p) basis set. These are tabulated in Table 5.12. The permanent electric dipole moment of a molecule is an important indicator of its behaviour in physical, chemical and biological process. It is measure of the charge density in a molecule. It is a reactivity index, which is important to define biological properties related to the interaction with active site of an enzyme [139]. The experimental determination of thermodynamic properties is not possible in some cases

[139]. Computational methods are valuable and sometimes indispensable tool in obtaining the thermodynamic quantities of molecules.

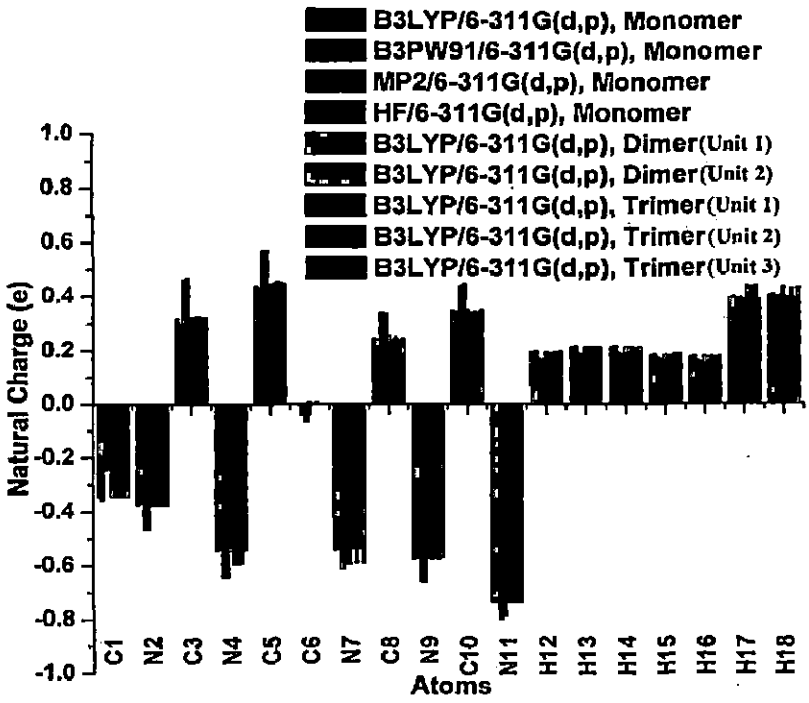

Fig. 5.13 Comparison of natural atomic charges for 3MA monomer, dimer and trimer.

Table 5.12 Theoretical computed zero point vibrational energy (kcal mol^{-1}), rotational constants (GHz), rotational temperature (Kelvin), thermal energy (kcal mol^{-1}), molar capacity at constant volume and at constant pressure (cal mol^{-1} K^{-1}), entropy (cal mol^{-1} K^{-1}), enthalpy (kcal mol^{-1}) and electric dipole moment (Debye) at STP.

Parameters	6-311G(d.p)			
	HF	MP2	B3PW91	B3LYP
Zero point vibrational energy	94.149 93.556[a]	88.374 87.352[a]	87.888 87.134[a]	87.432 86.972[a]
Rotational constants	1.644	1.623	1.626	1.618
	1.401	1.369	1.380	1.373
	0.760	0.746	0.750	0.746
Rotational temperatures	0.079	0.078	0.078	0.078
	0.067	0.066	0.066	0.066
	0.036	0.036	0.036	0.036
Energy				
Total	99.551 98.535[a]	93.967 93.069[a]	93.599 92.553[a]	93.180 92.101[a]
Translational	0.889	0.889	0.889	0.889
Rotational	0.889	0.889	0.889	0.889
Vibrational	97.773	92.189	91.822	91.402
Molar capacity at constant volume				
Total	31.778 31.248[a]	34.128 34.981[a]	34.135 33.721[a]	34.277 33.327[a]
Translational	2.981	2.981	2.981	2.981
Rotational	2.981	2.981	2.981	2.981
Vibrational	25.816	28.166	28.173	28.315
Molar capacity at constant pressure	33.764 33.234[a]	36.116 36.967[a]	36.121 35.707[a]	36.264 35.313[a]
Entropy				
Total	91.528 87.744[a]	92.455 92.722[a]	93.427 91.097[a]	93.805 88.236[a]
Translational	40.908	40.908	40.908	40.908
Rotational	29.598	29.651	29.636	29.651
Vibrational	21.022	21.896	22.884	23.246
Total Enthalpy	100.143 99.128[a]	94.560 93.662[a]	94.192 93.145[a]	93.772 92.694[a]
Dipole moment				
μ_x	1.114	1.571	−0.679	0.690
μ_y	−4.436	−4.404	−3.972	−3.955
μ_z	−0.00	0.750	0.226	0.226
μ_{total}	4.574	4.736	4.036	4.022

[a]anharmonic value

The non-linear optical properties of pi-conjugated organic molecules have drawn much attention because of their potential application in information technology, industries and generation of new light frequencies. Molecules having high hyperpolarizability and electron-donating strength of substituent groups show strong NLO responses and can be used for optoelectronics [140]. In this work, the first order static hyperpolarizability and related properties such as dipole moment, polarizability and anisotropy of the polarizability have been computed using HF, MP2 and DFT(B3LYP) methods with 6-311G(d,p) basis set for the ground state optimized

geometry of 3MA molecule. The results are presented in Table 5.13. The equations related to these parameters can be found in literatures [141, 142] as well in section 2.2.7. The high values of dipole moment and first order hyperpolarizability indicate the nonlinearity of 3MA molecule. The mean first hyperpolarizability of 3MA is 3.797 x 10^{-30} esu at MP2/6–311G(d,p) level of theory, which is about 10 times greater than those of urea (for urea β_0 is 0.3728 x 10^{-30} esu) [143]. Thus, the high value of dipole moment and first order hyperpolarizability show that 3MA might have the NLO properties.

Table 5.13 Calculated components of polarizability (a.u.) and first order hyperpolarizability (a.u.), mean polarizability ‹ α › (a.u.), anisotropy of the polarizability γ (a.u.) and the mean first order hyperpolarizability β_0 (esu, 1 a.u.=8.639 x 10^{-33} esu) of 3MA.

	6–311G(d,p)					
	HF	**MP2**	**B3LYP**	**HF**	**MP2**	**B3LYP**
α_{xx}	109.470	121.746	123.513	β_{xxx}	−283.568	365.651	−262.529
α_{xy}	−8.277	5.612	−6.063	β_{xxy}	15.527	85.295	0.973
α_{yy}	108.428	122.325	121.930	β_{xyy}	67.728	2.369	−2.668
α_{xz}	0.000	0.008	0.000	β_{yyy}	−251.544	−263.134	−273.978
α_{yz}	0.000	−0.005	0.000	β_{xxz}	−0.000	30.186	0.000
α_{zz}	45.445	46.760	46.988	β_{xyz}	0.000	9.066	−0.000
‹ α ›	87.781	96.944	97.477	β_{yyz}	0.000	6.151	0.000
γ	65.108	75.902	76.470	β_{xzz}	−34.502	34.515	−43.876
				β_{yzz}	9.621	5.698	8.396
				β_{zzz}	0.000	2.402	0.000
				β_0 (esu)	2.916 x 10^{-30}	3.797 x 10^{-30}	3.515 x 10^{-30}

5.5 Conclusion

FTIR and FT–Raman spectra of 3MA molecule have been investigated with the aid of quantum chemical calculations. The molecular geometry and vibrational spectra of the present molecule in gas phase isolated form have been computed using HF, MP2 and DFT (B3LYP and B3PW91) methods with 6–311G(d,p), 6–311++G(d,p) and cc–pVTZ basis sets. Most of the geometrical parameters calculated at HF level show good agreement with experiment. The anharmonic wavenumbers computed using PT2 and CC–VSCF theory within B3LYP framework give better results than VSCF as indicated by comparatively low values of RMS and MAD. Good agreements between the experimental and simulated anharmonic vibrational spectra have been achieved without any scaling. The anharmonic frequencies show large deviations from experiment for high and low frequency modes. This may be due to strong anharmonic

coupling of low and high frequency modes to others. The N–H stretching vibrational modes are found strongly coupled to mode 46. The high value of coupling strength is predicted between mode 47 to mode 46 and 48. The butterfly motion of purine ring is also showing strong coupling with mode 46. The differences between calculated anharmonic and experimental wavenumbers in some mid–frequency modes were also found large. Deviations may also be attributed to limitations of the calculations or neglect of higher order potential energy terms. The molecular structure, vibrational and NBO analysis have been also carried out for 3MA molecule in dimeric and trimeric form at B3LYP/6–311G(d,p) level of theory. The dimeric and trimeric parameters are well comparable with solid phase experimental data. The scaled harmonic frequencies of many vibrational modes of 3MA in intermolecular complexes have lower values than those of monomer and are close to corresponding experimental data, which reveal the existence of intermolecular hydrogen bonds. The NBO analysis has also shown the presence of intermolecular interactions, N···H–N–H. Vibrational assignments are made with great accuracy using anharmonic frequency, literatures, and animated modes. The high values of dipole moment and first order hyperpolarizability indicate the nonlinearity of 3MA molecule. Electrostatic potential map shows that negative regions are localized on surface around the N7 and N9 atoms while positive regions are confined over NH_2 and CH_3 group. The surface over the pyrimidine ring and H16 atom are neutral.

References

[1]. M. D. F. Kamenetskii, Physics Reports 288 (1997) 13–60.

[2]. M. D. Wyatt, J. M. Allan, Acbert Y. Lau, T. E. Ellenberger, L. D. Samson, Bio Essays 21 (1999) 686–676.

[3]. N. Vogt, O. V. Dorofeeva, V. A. Sipachev, A. N. Rykov, J. Phys. Chem. A 113 (2009) 13816–13823.

[4]. R. P. Lopes, R. Valero, J. Tomkinson, M. P. M. Marques, L. A. E. B. D. Carvalho, New J. Chem. 37 (2013) 2691–2699.

[5]. P. O. Seglen, P. B. Gordon, Proc. Natl. Acad. Sci. Cell Biology 79 (1982) 1889–1892.

[6]. S. Ito, N. Koshikawa, S. Mochizuki, K. Takenaga, Int. J. Oncol. 31 (2007) 261–268.

[7]. C. Takatsuka, Y. Inoue, K. Matsuoka, Y. Moriasu, Plant Cell Physiol. 45 (2004) 265–274.

[8]. B. Sedgwick, P. A. Bates, J. Paik, S. C. Jacobs, T. Lindahl, DNA Repair 6 (2007) 429–442.

[9]. E. B. Starikov, J. Photochem. Photobiol.: Photochem. Rev. 3 (2002) 147–167.

[10]. T. Rasheed, S. Ahmad, Vib. Spectrosc. 56 (2011) 51–59.

[11]. S. G. Stepanian, G. G. Sheina, E. D. Radchenko, Y. P. Blagoi, J. Mol. Struct. 131 (1985) 333–346.

[12]. M. J. Nowak, L. Lapinski, J. S. Kawiatkowski, J. Leszczynski, Spectrochim. Acta A 47 (1991) 87–103.

[13]. M. J. Nowak, H. Rostkowska, L. Lapinski, J. S. Kawiatkowski, J. Leszczynski, Spectrochim. Acta A 50 (1994) 1081–1094.

[14]. T. A. Mohamed, I. A. Shabaan, W. M. Zoghaib, J. Husband, R. S. Farag, A. El–Nasser, M. A. Alajhaz, J. Mol. Struct. 938 (2009) 263–276.

[15]. Y. Xue, D. Xie, G. Yan, Int. J. Quantum Chem. 76 (2000) 686–699.

[16]. M. J. Nowak, L. Lapinski, J. S. Kwiatkowski, J. Leszczynski, J. Phys. Chem. 100 (1996) 3527–3534.

[17]. Y. Yan, O. Khun, Phys. Chem. Chem. Phys. 12 (2010) 15695–15703.

[18]. J. Lin, C. Yu, S. Peng, I. Akiyama, K. Li, L. K. Lee, P. R. L. Breton, J. Am. Chem. Soc. 102 (1980) 4627–4631.

[19]. T. G. Burova, V. V. Ermolenkov, G. N. Ten, R. S. Shcherbakov, V. I. Baranov, I. K. Lednev, J. Phys. Chem. A 115 (2011) 10600–10609.

[20]. P. Colarusso, K. Zhang, B. Guo, P. F. Bernath, Chem. Phys. Lett. 269 (1997) 39–48.

[21]. R. Santamaria, E. Charro, A. Zacarias, M. Castro, J. Comput. Chem. 20 (1999) 511–530.

[22]. M. Mathlonthi, A. M. Senvre, Carbohydr. Res. 131 (1984) 1–15.

[23]. R. J. Bartlett, H. Weinstein, Chem. Phys. Lett. 30 (1975) 441–447.

[24]. A. Broo, A. Holmen, Chem. Phys. 211 (1996) 147–161.

[25]. I. Harada, R. C. Lord, Spectrochim. Acta A 26 (1970) 2305–2318.

[26]. A. Y. Hirakawa, H. Okada, S. Sasagawa, M. Tsuboi, Spectrochim. Acta A 41 (1985) 209–216.

[27]. M. Biczysko, P. Panek, V. Barone, Chem. Phys. Lett. 475 (2009) 105–110.

[28]. O. V. Shishkin, L. Gorb, J. Leszczynski, Chem. Phys. Lett. 330 (2000) 603–611.

[29]. H. Satzger, D. Townsend, A. Stolow, Chem. Phys. Lett. 430 (2006) 144–148.

[30]. T. Mineva, N. Russo, J. Mol. Struct. (Theochem) 943 (2010) 71–76.

[31]. G. N. Ten, V. V. Nechaev, V. I. Berezin, V. I. Baranov, J. Struct. Chem. 38 (1997) 262–267.
[32]. J. D. Gelder, K. D. Gussem, P. Vandenabeela, L. Moens, J. Raman Spectrosc. 38 (2007) 1133–1147.
[33]. S. Peng, A. Padva, P. R. Lebreton, Proc. Natl. Acad. Sci. 73 (1976) 2966–2968.
[34]. C. Plutzer, I. Hunig, K. Kleinermanns, Phys. Chem. Chem. Phys. 5 (2003) 1158–1163.
[35]. Y. Nosenko, M. Kunitski, C. Riehn, P. H. P. Harbach, A. Dreuw, B. Brutschy, Phys. Chem. Chem. Phys. 12 (2010) 863–870.
[36]. Z. Dhaouadi, M. Ghomi, J. C. Austin, R. B. Girling, R. E. Hester, P. Mojzes, L. Chinsky, P. Y. Turpin, C. Coulombeau, H. Jobic, J. Tomkinson, J. Phys. Chem. 97 (1993) 1074–1084.
[37]. L. B. Clark, J. Phys. Chem. 94 (1990) 2873–2879.
[38]. E. L. Stewart, C. K. Foley, N. L. Allinger, J. P. Bowen, J. Am. Chem. Soc. 116 (1994) 7282–7286.
[39]. J. W. Kuczera, M. Karplus, J. Am. Chem. Soc. 112 (1990) 5324–5340.
[40]. S. E. Lappi, W. Collier, S. Franzen, J. Phys. Chem. A 106 (2002) 11446–11455.
[41]. A. Dolgounitcheva, V. G. Zakrzewski, J. V. Ortiz, J. Phys. Chem. A 113 (2009) 14630–14635.
[42]. W. Zierkiewicz, L. Komorowski, D. Michalska, J. Cerny, P. Hobza, J. Phys. Chem. B 112 (2008) 16734–16740.
[43]. G. C. P. V. Zundert, S. Jaeqx, G. Berden, J. M. Bakker, K. Kleinermanns, J. Oomens, A. M. Rijs, Chem. Phys. Chem. 12 (2011) 1921–1927.
[44]. R. Savoie, D. Poirier, L. Prizant, A. L. Beauchamp, J. Raman Spectrosc. 11 (1981) 481–486.
[45]. K. Chmelova, J. Stepanek, J. Zachova, Vib. Spectosc. 19 (1999) 255–259.
[46]. S. I. Kawahara, T. Uchimaru, J. Mol. Struct. (Theochem) 588 (2002) 29–35.
[47]. D. C. Luhrs, J. Viallon, I. Fischer, Phys. Chem. Chem. Phys. 3 (2001) 1827–1831.
[48]. S. A. Oladepo, G. R. Loppnow, J. Phys. Chem. B 115 (2011) 6149–6156.
[49]. A. Terzis, N. Hadjiliadis, R. Rivest, T. Theophanides, Inorg. Chim. Acta 12 (1975) L5–L6.
[50]. C. S. Petersen, S. Furberg, Acta Chem. Scand. B 29 (1975) 37–40.
[51]. Y. Yamagata, K. I. Tomita, Acta Cryst. C 43 (1987) 1195–1197.
[52]. V. B. Pivovarov, S. G. Stepanian, I. D. Reva, G. G. Sheina, Y. P. Blagoi, Spectrochim. Acta A 51 (1995) 843–853.
[53]. G. Fogarasi, Spectrochim. Acta A 53 (1997) 1211–1224.
[54]. T. J. Kistenmacher, M. Rossi, Acta Cryst. 1333 (1977) 253–256.
[55]. R. F. Bryan, K. I. Tomita, Acta Cryst. 15 (1962) 1179–1182.
[56]. J. D. Orbell, C. Solorzano, L. G. Marzilli, T. J. Kistenmacher, Inorg. Chem. 21 (1982) 2630–2636.
[57]. E. S. Kryachko, G. Zundel, J. Mol. Struct. 446 (1998) 41–54.
[58]. K. S. Pandey, B. P. Asthana, P. C. Mishra, Spectrochim. Acta A 49 (1993) 53–72.
[59]. Y. Xue, D. Xu, D. Xie, G. Yan, Spectrochim. Acta A 56 (2000) 1929–1938.
[60]. M. A. Palafox, J. Talaya, A. G. Martinez, G. Tardajos, H. Kumar, J. K. Vats, V. K. Rastogi, Spect. Lett. 43 (2010) 51–59.
[61]. K. K. Irikura, R. D. Johnson, R. N. Kacker, J. Phys. Chem. A 109 (2005) 8430–8437.
[62]. M. A. Palafox, V. K. Rastogi, Spectrochim. Acta A 58 (2002) 411–440.

[63]. M. A. Palafox, M. Gill, N. J. Nunez, V. K. Rastogi, L. Mittal, R. Sharma, Int. J. Quantum Chem. 103 (2005) 394–421.
[64]. V. Barone, J. Chem. Phys. 122 (2005) 14108–14118.
[65]. R. Gerber, M. Ratner, Adv. Chem. Phys. 70 (1988) 97–132.
[66]. T. K. Roy, R. B. Gerber, Phys. Chem. Chem. Phys. 15 (2013) 9468–9492.
[67]. G. M. Chaban, J. O. Jung, R. B. Gerber, J. Chem. Phys. 111 (1999) 1823–1829.
[68]. Y. Miller, G. M. Chaban, R. B. Gerber, J. Phys. Chem. A 109 (2005) 6565–6574.
[69]. V. Barone, J. Chem. Phys. 101 (1994) 10666–10676.
[70]. C. Minichino, V. Barone, J. Chem. Phys. 100 (1994) 3717–3741.
[71]. V. Barone, C. Minichino, J. Mol. Struct. (Theochem) 330 (1995) 365–376.
[72]. V. Barone, M. Cossi, N. Rega, G. Scalmani, J. Comput. Chem. 24 (2003) 669–681.
[73]. V. Barone, J. Chem. Phys. 120 (2004) 3059–3065.
[74]. V. Parchansky, P. Bour, J. Chem. Phys. 133 (2010) 044117–044126.
[75]. J. Antony, G. V. Helden, G. Meijer, B. Schmidt, J. Chem. Phys. 123 (2005) 014305–014316.
[76]. A. Miani, E. Cane, P. Palmieri, A. Trombetti, N. C. Handy, J. Chem. Phys. 112 (2000) 248–259.
[77]. V. Barone, Chem. Phys. Lett. 383 (2004) 528–532.
[78]. G. C. Carney, L. L. Sprandel, C. W. Kern, Adv. Chem. Phys. 37 (1978) 305–379.
[79]. J. M. Bowman, J. Chem. Phys. 68 (1978) 608–610.
[80]. J. M. Bowman, Acc. Chem. Res. 19 (1986) 202–208.
[81]. P. Wojciechowski, K. Helios, D. Michalska, Vib. Spectrosc. 57 (2011) 126–134.
[82]. K. Ohno, S. Maeda, Chem. Phys. Lett. 503 (2011) 322–326.
[83]. C. Puzzarini, M. Biczysko, V. Barone, J. Chem. Theory Comput. 7 (2011) 3702–3710.
[84]. L. Pele, J. Sebek, E. O. Potma, R. B. Gerber, Chem. Phys. Lett. 515 (2011) 7–12.
[85]. P. Klaeboe, A. Horn, C. J. Nielsen, G. A. Guirgis, Vib. Spectrosc. 56 (2011) 136–145.
[86]. G. O. Ildiz, S. Akyuz, Vib. Spectrosc. 58 (2012) 12–18.
[87]. M. J. Alam, S. Ahmad, Spectrochim. Acta A 96 (2012) 992–1004.
[88]. M. J. Alam, S. Ahmad, J. Mol. Struct. 1059 (2014) 239–254.
[89]. M. J. Alam, S. Ahmad, Spectrochim. Acta A 128 (2014) 653–664.
[90]. M. J. Alam, S. Ahmad, Spectrochim. Acta A 136 (2015) 961–978.
[91]. J. Q. Jung, R. B. Gerber, J. Chem. Phys. 105 (1996) 10332–10349.
[92]. L. S. Norris, M. A. Ratner, A. E. Roitberg, R. B. Gerber, J. Chem. Phys. 105 (1996) 11261–11267.
[93]. P. Seidler, T. Kaga, K. Yagi, O. Christiansen, K. Hirao, Chem. Phys. Lett. 483 (2009) 138–142.
[94]. M. J. Frisch et al., Gaussian 09, Revision D.01, Gaussian Inc., Wallingford CT, 2009.
[95]. M. W. Schmidt, K. K. Baldridge, J. A. Boatz, S. T. Elbert, M. S. Gordon, J. H. Jensen, S. Koseki, N. Matsunaga, K. A. Nguyen, S. J. Su, T. L. Windus, M. Dupuis, J. A. Montgomery, J. Comput. Chem. 14 (1993) 1347–1363.
[96]. B. D. Becke, Phys. Rev. A 38 (1988) 3098–3100.
[97]. C. Lee, W. Yang, R. G. Parr, Phys. Rev. B 37 (1988) 785–789.
[98]. J. P. Perdew, J. A. Chevary, S. H. Vosko, K. A. Jackson, M. R. Pederson, D. J. Singh, C. Fiolhes, Phys. Rev. B 46 (1992) 6671–6687.

[99]. J. P. Perdew, J. A. Chevary, S. H. Vosko, K. A. Jackson, M. R. Pederson, D. J. Singh, C. Fiolhes, Phys. Rev. B 48 (1993) 4978–4978.
[100]. J. P. Perdew, K. Burke, Y. Wang, Phys. Rev. B 54 (1996) 16533–16539.
[101]. J. P. Perdew, K. Burke, Y. Wang, Phys. Rev. B 57 (1998) 14999–14999.
[102]. D. Michalska, R. Wysokiński, Chem. Phys. Lett. 403 (2005) 211–217.
[103]. NIST web, http://cccbdb.nist.gov/vibscale.asp.
[104]. GaussView, Version 5, Roy Dennington, Todd Keith, John Millam, Semichem Inc., Shawnee Mission KS, 2009.
[105]. K. Yagi, K. Hirao, T. Taketsugu, M. W. Schmidt, M. S. Gordon, J. Chem. Phys. 121 (2004) 1383–1389.
[106]. E. D. Glendening, A. E. Reed, J. E. Carpenter, F. Weinhold, NBO Version 3.1.
[107]. A. R. Allouche, J. Comp. Chem. 32 (2011) 174–182.
[108]. R. G. Parr, W. Yang, Density Functional Theory of Atoms and Molecules, Oxford University Press, New York, 1989.
[109]. R. G. Parr, W. T. Yang, Annu. Rev. Phys. Chem. 46 (1995) 701–728.
[110]. W. Kohn, A. D. Becke, R. G. Parr, J. Phys. Chem. 100 (1996) 12974–12980.
[111]. P. Geerlings, F. De Proft, W. Langenaeker, Chem. Rev. 103 (2003) 1793–1874.
[112]. P. Geerlings, F. De Proft, Phys. Chem. Chem. Phys. 10 (2008) 3028–3042.
[113]. P. W. Ayers, J. S. M. Anderson, L. J. Bartolotti, Int. J. Quantum Chem. 101 (2005) 520–534.
[114]. H. Chermette, J. Comput. Chem. 20 (1999) 129–154 and ref. cited therein.
[115]. R. E. Cassady, S. W. Hawkinson, Acta Cryst. B 38 (1982) 2206–2209.
[116]. K. Webar, T. B. Flanagan, J. Solid State Chem. 21 (1977) 105–115.
[117]. C. A. Morgado, P. Jurecka, D. Svozil, P. Hobza, J. Sponer, Phys. Chem. Chem. Phys. 12 (2010) 3522–3534.
[118]. P. Hobza, R. Zahradnik, Int. J. Quantum Chem. 42 (1992) 581–590.
[119]. J. Leszczynski, Handbook of Computational Chemistry, Springer, New York, 2012.
[120]. A. F. de C. Alcantara, A. F. Teixeira, I. F. da Silva, W. B. de Almeida, D. P. Veloso, Quim. Nova 27 (2004) 371–377.
[121]. A. T. Kowal, J. Mol. Struct. (Theochem) 625 (2003) 71–79.
[122]. G. Socrates, Infrared Characteristic Group Frequencies, 3rd edition, Wiley Interscience Publications, New York, 1980.
[123]. N. B. Colthup, L. H. Daly, S. E. Wiberley, Introduction to Infrared and Raman Spectroscopy, Academic Press, New York, 1990.
[124]. M. Govindarajan, M. Karabacak, S. Periandy, D. Tanuja, Spectrochim. Acta A 97 (2012) 231–245.
[125]. A. Toyama, H. Takeuchi, I. Harada, J. Mol. Struct. 242 (1991) 87–98.
[126]. P. B. Nagabalasubramanian, S. Periandy, Spectrochim. Acta A 77 (2010) 1099–1107.
[127]. Y. Kyogoku, S. Higuchi, M. Tsuboi, Spectrochim. Acta A 23 (1967) 969–983.
[128]. M. Boczar, L. Boda, M. J. Wojcik, J. Chem. Phys. 125 (2006) 84709–84722.
[129]. R. M. Lees, Z. D. Sun, B. E. Billinghurst, J. Chem. Phys. 135 (2011) 104306–104315.
[130]. M. Majoube, J. Mol. Struct. 143 (1986) 427–430.
[131]. Y. Miller, G. M. Chaban, R. B. Gerber, Chem. Phys. 313 (2005) 213–224.
[132]. J. Pesonen, J. Chem. Phys. 112 (2000) 3121–3132.
[133]. B. Njegic, M. S. Gordon, J. Chem. Phys. 129 (2008) 164107–164119.
[134]. A. E. Reed, L. A. Curtiss, F. Weinhold, Chem. Rev. 88 (1988) 899–926.

[135]. F. Weinhold, C. R. Landis, Chemistry Education: Research and Practice in Europe, 2 (2001) 91–104.
[136]. R. V. Reyes, F. N. Zarur, E. Martinez, Org. Elect. 9 (2008) 625–634 and ref. cited therein.
[137]. L. H. M. Huizar, C. H. R. Reyes, J. Mex. Chem. Soc. 55 (2011) 142–147.
[138]. B. Kosar, C. Albayrak, Spectrochim. Acta A 78 (2011) 160–167.
[139]. V. V. Speybroeck, R. Gani, R. J. Meier, Chem. Soc. Rev. 39 (2010) 1764–1779.
[140]. M. Amalanathan, I. H. Joe, I. Kostova, J. Raman Spectrosc. 41 (2010) 1076–1084.
[141]. J. Karpagam, N. Sundaraganesan, S. Sebastian, S. Manoharan, M. Kurt, J. Raman Spectrosc. 41 (2010) 53–62.
[142]. J. O. Verbal, L. P. Londono, J. Chem. Inf. Comput. Sci. 42 (2002) 1241–1246.
[143]. M. Arivazhagan, J. S. Kumar, Indian J Pure Appl. Phys. 50 (2012) 363–373.

Chapter 6

Structural and vibrational studies of allantoin molecule based on monomer and dimer calculations

6.1 Introduction

Allantoin molecule (5–ureidohydantoin) is a product of purine metabolism and it is present in many plants and bacteria. In most of the mammals, allantoin is formed from uric acid by the action of uricase [1–4]. It has a wide range of applications in cosmetic, antiperspirant and pharmaceutical products for skin softening, rapid generation of skin cells and treatment of skin diseases [5–10]. Due to its numerous applications, this molecule draws attention for the spectroscopic and quantum chemical investigations. Mootz [11] determined crystal structure of DL–allantoin by using XRD experiment. The optimized molecular geometries of different conformers of allantoin were computed using AM1 [12], HF/6–31+G(d,p) [4] and DFT/6–311G++(d,p) [13] levels of theory. For the study of binding of calcium ions with allantoin, the electrostatic potential map of allantoin was calculated using AM1 method [12]. Tuszkanow et al. [14] studied the silver complexes with allantoin using spectroscopic methods. The electronic transitions of allantoin were investigated using CNDO/S–CI method [12] and the UV spectra in aqueous as well as NaOH solutions [15]. Wang et al. have reported FT–Raman spectrum of allantoin molecule at different pH values [16]. The matrix isolation FTIR spectra of allantoin and FTIR of crystal RS–allantoin were recorded and investigated at DFT/6–311++G(d,p) level of theory in the harmonic approximation [13]. Kus et al. [13] have compared the IR spectra of allantoin with vibrational bands of urea [17]. Literature survey reveals that anharmonic computations of monomer, assignment of non–fundamental IR bands, harmonic calculations of dimers, anharmonic mode–mode coupling, NBO analysis, NLO properties, HOMO–LUMO analysis and reactivity descriptors of allantoin molecule have not been reported so far.

The vibrational studies in the harmonic approximation are of less computational cost and, sometime, important in the case of medium to large sized molecules but these are often not of sufficient accuracy. Therefore, various scaling procedures [18–21] have been used for compensating discrepancies. The vibrational modes of polyatomic molecules are anharmonic in nature. For the reliable assignments of vibrational frequencies, the anharmonic force field methods, Barone's PT2 [22, 23], VSCF and CC–VSCF (PT2–VSCF) [24–28] are used (section 2.2.6). These methods have drawn much attention in studying vibrational spectra of various polyatomic molecules [29–37]. In this work, the Barone's PT2 method as well as VSCF and CC–VSCF are tested for the isolated allantoin molecule. FTIR and FT–Raman spectra are recorded and investigated using quantum chemical calculations (HF, MP2 and DFT). The VSCF and CC–VSCF approaches based on quartic force field (QFF) potential function have also been utilized to compute anharmonic vibrational spectra at B3LYP/6–311G(d,p) level of theory, which are quite efficient for floppy molecules but demands high computational cost. Vibrational modes couple due to anharmonicity and coupling affects the frequencies of vibrational modes. In order to understand the coupling behaviour between pair of modes in isolated allantoin molecule, the mode–mode coupling strengths (CS) based on two mode coupling representation of the quartic force field (2MR–QFF) for the ground state were computed [38] and discussed in the section 6.4.2. The structural parameters and vibrational frequencies for four possible allantoin dimers have been calculated at B3LYP/6–311++G(d,p) level of theory to investigate the effect of the intermolecular interactions on the vibrational frequencies of the associated molecule by comparison of results of the monomer and dimers. Moreover, MEP mapping, HOMO–LUMO analysis and other molecular properties were also studied at same level of theory. The NBO analysis is carried out at B3LYP/6–311++G(d,p) level of theory for studying charge delocalization within the molecule and hydrogen bonded intermolecular interactions. The chemical reactivity descriptors are calculated for a better understanding of the chemical behaviour of allantoin.

6.2 Experimental details

The solid sample of allantoin compound was obtained from Sigma Aldrich Company, USA and it was used as such for spectral measurements. The FTIR spectrum of the

compound was recorded on Tensor 37 (Bruker) in the region 370–7500 cm^{-1} with 2 cm^{-1} spectral resolution using KBr pellet technique. To increase the signal–to–noise ratio, a minimum of 32 scans were accumulated. FT–Raman spectrum was recorded on Bruker RFS 27 Raman spectrometer in the region 50–4000 cm^{-1} with a spectral resolution of 2 cm^{-1}. The Nd:YAG laser (1064 nm, 100mW) was used as excitation source.

6.3 Computational details

The calculations on monomeric and dimeric structures of the allantoin molecule were performed by using Gaussian 09 software [39]. The ground state geometry of monomeric allantoin molecule was obtained by performing geometry optimization under tight convergence criterion using HF, MP2 and DFT calculations. The standard hybrid functional B3LYP was used for the DFT calculations [40, 41]. The standard basis sets, 6–311G(d,p), 6–311++G(d,p) and cc–pVTZ were adopted for the computations. The harmonic and anharmonic vibrational frequencies along with their intensities were evaluated at the ground state optimized geometry using same methods. All the real values of calculated frequencies confirm that the computed geometry corresponds to minima on the potential energy surface. Anharmonic corrections in vibrational frequencies were computed using Barone's PT2 with Gaussian 09 package as well as VSCF and CC–VSCF methods implemented into GAMESS–US package [42]. The PT2 method [22] was used within the HF, MP2 and DFT framework while VSCF and CC–VSCF approaches were applied only at B3LYP/6–311G(d,p) level of theory. In order to balance between accuracy and computational cost for the present monomeric simulation, the comparisons between PT2, VSCF and CC–VSCF have been made at B3LYP/6–311G(d,p) level of theory. Gaussian program provides Raman activities and does not calculate Raman intensities. Therefore, Raman intensities were computed using RAINT program [43]. The optimized molecular structure (under tight convergence criterion) and vibrational frequencies of four possible dimers of allantoin molecule (D1, D2, D3 and D4) were also calculated in the harmonic approximation at B3LYP/6–311++G(d,p) level of theory. In the case of dimers, the scaling factor of 0.983 and 0.958 were used to correct the overestimation of calculated harmonic frequencies above and below 1700 cm^{-1} respectively [44]. The modes at higher frequencies deviate more than those of

modes at lower frequencies. Therefore, different scaling factors for two different regions have been used to scale down the calculated frequencies for making them comparable to experiments. The vibrational assignments were made with high degree of accuracy using PED values calculated by VEDA4 program [45] and animated modes with the help of GaussView program [46]. The combination and overtone bands of FTIR spectra were also assigned with the help of anharmonic computations. The modes of large anharmonicity show larger mode–mode coupling strengths. In order to know the strength of the coupling between pair of modes, the magnitude of mode–mode coupling for the ground state has been estimated at B3LYP/6–311G(d,p) level of theory using 2MR–QFF potential energy function [38, 47]. The VSCF frequencies were used to calculate mode–mode coupling strengths. The natural bonding orbital (NBO) calculations [48] were performed at B3LYP/6–311++G(d,p) level of theory using NBO 3.1 program implemented in Gaussian 09 software [39]. The NBO analysis has been carried out to study the stability and charge delocalization in monomer and dimers. The Lorentzian band shape with FWHM of 5 cm^{-1} was used for the plot of simulated vibrational spectra [49]. The chemical behaviour of the allantoin was investigated on the basis of HOMO and LUMO energy eigenvalues computed at B3LYP/6–311++G(d,p) level of theory. These eigenvalues were used to calculate global reactivity descriptors such as chemical potential (μ), electronegativity (χ), chemical hardness (η), chemical softness (S) and electrophilicity index (ω) [50–56].

6.4 Results and discussion

6.4.1 Molecular geometry

Monomer form

The optimized geometry of isolated allantoin molecule with labelling of atoms has been illustrated in Fig. 6.1. Allantoin contains a ring and an ureidyl moiety. The minimum SCF energy values on the PES for allantoin molecule, obtained by different methods are shown in Table 6.1. The geometrical parameters of allantoin molecule were computed at different levels of theory and their comparisons with XRD data [11] are shown in Table 6.2 and 6.3. The calculated bond lengths and angles at HF/cc–pVTZ level are close to experiment as evident from RMS and MAD values. The comparisons between theoretical and experimental bond lengths and bond angles

for monomer have been shown in Fig. 6.2 and 6.3. The bond angles, C3–N6–H14 and H15–N7–H16 show large deviations from experiment in comparison to others. These deviations may be associated to intermolecular and intramolecular interactions in solid phase of allantoin. According to RMS and MAD values, the structural parameters predicted at B3LYP are comparable to those obtained at MP2 theory while DFT calculations are comparatively are of much less computations cost.

Dimer form

It is expected that the allantoin molecule form intermolecular complexes in solid phase which are stabilized by hydrogen bonding N–H···O=C. In this work, the four possible dimeric structures of allantoin, called dimers D1, D2, D3 and D4 were obtained in the ground state at B3LYP/6–311++G(d,p) level of theory. In fact, the compounds in solid phase exist with intermolecular interactions. In addition to other molecular properties, the molecular structure and vibrational spectra of molecules strongly depend on these interactions. The optimized geometries of dimers with intermolecular hydrogen bond description are given in Fig. 6.4. The dimers D1 and D2 belong to C_2 point group of symmetry while D3 and D4 fit in the point group C_1. The basis set superposition error (BSSE) corrected SCF energies are −1201.953723, −1201.957018, −1201.952944 and −1201.953181 a.u. for D1, D2, D3 and D4 dimers respectively at B3LYP/6–311++G(d,p) level of theory. The dimer D2 has lowest BSSE corrected SCF energy, therefore, it is most stable among all. The observed values for the length of intermolecular hydrogen bond (H···O) are 2.07, 1.87, 2.25 and 2.14Å and angles (N–H···O) are 159°, 173°, 172° and 167° in crystal structure [11]. These values are in good correlation with calculated values given in Table 6.2 and 6.3. The lengths of intermolecular hydrogen bonds are same for the dimers D1 and D2 while they differ from those of D3 and D4. The formation of non–covalent intermolecular bondings between carbonyl and amine group cause the present dimeric structure to be the stable. For the present case, the supermolecular method and the counterpoise procedure [57–59] were used to calculate the interaction energy of pair of interacting molecules. The BSSE corrected interaction energies of the formation of hydrogen bonded dimers D1, D2, D3 and D4 are −12.27, −14.30, −12.05 and −11.84 kcal/mole respectively computed at B3LYP/6–311++G(d,p) level of theory. For the present case, BSSE correction were found ca. 0.71, 0.73, 0.69 and 0.75 kcal/mole for D1, D2, D3 and D4 dimers respectively at same level of theory. The BSSEs are found

low (less than 1 kcal/mole) due to large basis set. In most stable dimer D2, the calculated bond length of N7–H15 is increased by 0.015 Å upon dimerization. The shortening of C3=O10 bond length by 0.015 Å upon dimerization is due to delocalization of the charges on electronegative atom, O10 [60]. Similarly, the predicted bond angles, C3–N7–H15 and 16H–N7–H15, are found larger than those of monomer by 3.8° and 2.8° respectively. By comparing the structural parameters of the monomer and dimers, it has been noted that intermolecular interactions through hydrogen bond change the molecular structure parameters of monomer and, therefore, the various molecular properties including vibrational spectra are affected [61]. The high value of dipole moment (6.399 Debye) of allantoin molecule favours the formation of dimers. The dipole moment for D1, D2, D3 and D4 dimers are 0.260, 2.067, 11.147 and 9.639 Debye respectively. The low values of dipole moment of D1 and D2 dimers are due to their centrosymmetric structure (C_2 point group) whereas larger dipole moments of the D3 and D4 dimers are associated to lack of molecular symmetry. The computed geometrical parameters of these dimers, presented in Table 6.2 and 6.3, are found in agreement with solid phase data. The intermolecular interaction between the σ* N–H orbitals and lone pair of the acceptor O atom is mainly responsible for the proton transfer. Therefore, the N–H···O and the O···H interactions may play important roles in the proton transfer reactions [61].

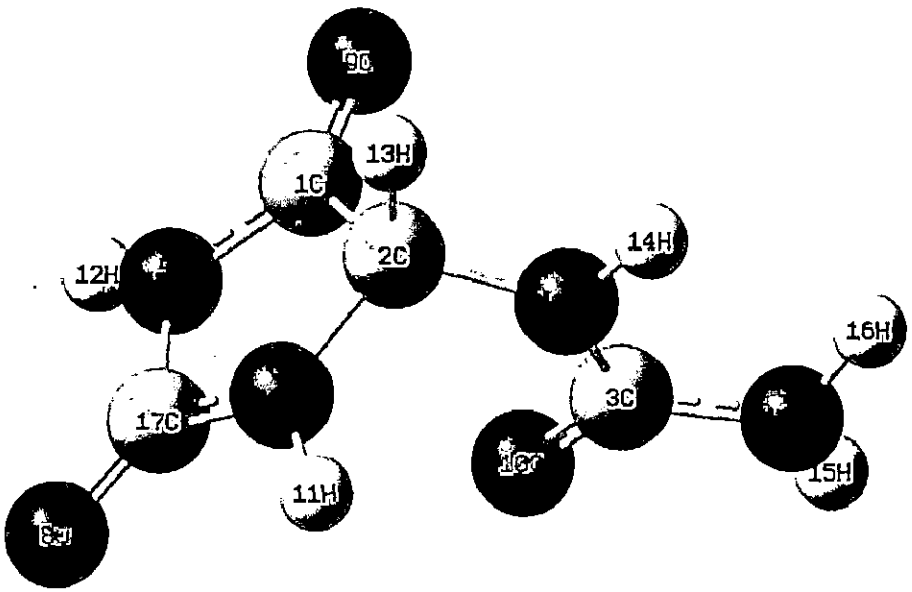

Fig. 6.1 The optimized structure of allantoin molecule with numbering scheme.

Table 6.1 Calculated minimum SCF energies (a. u.) of the allantoin monomer and dimers at different levels o

Basis Sets	Monomer			D1	D2	D3	
	B3LYP	MP2	HF	B3LYP	B3LYP	B3LYP	
6-311G(d,p)	-600.94845974	-599.39291092	-597.59029118	--	--	--	
6-311++G(d,p)	-600.96805371	-599.42469350	-597.60385430	-1201.953723	-1201.957018	-1201.952944	-1
cc-pVTZ	-601.01010058	--	-597.65936001	--	--	--	

Note: For the dimers, D1, D2, D3, D4, the basis set superposition error (BSSE) corrected SCF energies are presented

Table 6.2 Comparison of theoretical bond lengths of allantoin monomer and dimers with XRD.

Bond length (Å)	XRD[a]	Monomer								D1	D2	D3
		6-311G(d,p)			6-311++G(d,p)			cc-pVTZ		B3LYP/ 6-311++ G(d,p)	B3LYP/ 6-311++ G(d,p)	B3LYP/ 6-311 ++G(d,p)
		HF	MP2	B3LYP	HF	MP2	B3LYP	HF	B3LYP			
C1- C2	1.535	1.539	1.549	1.558	1.539	1.548	1.558	1.538	1.555	1.560	1.557	1.558, 1.553
C1-N5	1.362	1.361	1.376	1.373	1.361	1.375	1.372	1.358	1.369	1.372	1.374	1.376, 1.355
C1=O9	1.213	1.18	1.207	1.202	1.181	1.211	1.204	1.18	1.203	1.204	1.204	1.203, 1.218
C2-N4	1.461	1.441	1.452	1.454	1.441	1.449	1.453	1.437	1.45	1.453	1.452	1.452, 1.452
C2-N6	1.424	1.432	1.438	1.439	1.434	1.443	1.441	1.432	1.438	1.441	1.445	1.440, 1.441
C2-H13	1.070	1.083	1.095	1.094	1.083	1.095	1.094	1.082	1.092	1.094	1.094	1.095, 1.095
C3-N6	1.368	1.368	1.387	1.385	1.371	1.392	1.387	1.368	1.382	1.387	1.392	1.386, 1.385
C3-N7	1.335	1.367	1.388	1.383	1.364	1.382	1.379	1.362	1.379	1.382	1.353	1.384, 1.382
C3=O10	1.248	1.194	1.217	1.215	1.195	1.220	1.217	1.194	1.216	1.216	1.232	1.216, 1.216
N4-H11	0.890	0.993	1.009	1.007	0.994	1.011	1.008	0.991	1.005	1.008	1.008	1.021, 1.008
N4-C17	1.341	1.366	1.385	1.377	1.366	1.386	1.376	1.362	1.373	1.371	1.375	1.357, 1.380
N5-H12	0.960	0.994	1.010	1.009	0.995	1.011	1.010	0.992	1.007	1.027	1.009	1.009, 1.029
N5-C17	1.397	1.388	1.408	1.410	1.389	1.411	1.410	1.386	1.407	1.394	1.409	1.403, 1.413
N6-H14	1.010	0.991	1.008	1.006	0.992	1.010	1.007	0.989	1.004	1.007	1.008	1.008, 1.007
N7-H15	0.760	0.995	1.010	1.009	0.994	1.010	1.009	0.992	1.007	1.009	1.024	1.009, 1.009
N7-H16	0.900	0.994	1.010	1.009	0.993	1.009	1.008	0.991	1.006	1.009	1.007	1.009, 1.009
C17=O8	1.219	1.181	1.206	1.203	1.183	1.208	1.205	1.182	1.204	1.218	1.207	1.220, 1.204
RMS		0.073	0.076	0.076	0.070	0.076	0.075	0.069	0.074	0.076	0.077	0.076, 0.077
MAD		0.043	0.046	0.046	0.042	0.046	0.046	0.042	0.044	0.045	0.044	0.045, 0.047
Geometry of hydrogen bonds						H···O				1.864	1.871	1.866, 1.917
						N-H···O				165.0	173.1	164.3, 166.6
						C=O···H				127.4	124.7	122.1, 124.3

Ref. [11], *Abbreviation used:* RMS- Root Mean Square Error, MAD- Mean Absolute Deviation

Table 6.3 Comparison of theoretical bond angles of allantoin monomer and dimers with XRD.

Bond Angle (°)	XRD[a]	Monomer								D1	D2	D3	D4
		6-311G(d,p)			6-311++G(d,p)			cc-pVTZ		B3LYP/ 6-311++ G(d,p)	B3LYP/ 6-311++ G(d,p)	B3LYP/ 6-311++ G(d,p)	B3LYI 6-311+ G(d,p
		HF	MP2	B3LYP	HF	MP2	B3LYP	HF	B3LYP				
C2-C1-N5	106.9	105.7	105.3	105.4	105.8	105.6	105.5	105.8	105.5	105.9	105.5	105.2, 106.7	105.6, 1
C2-C1=O9	126.6	125.9	125.9	125.9	125.9	125.5	125.8	125.9	125.9	125.2	126.0	126.5, 124.6	125.7, 1
N5-C1=O9	126.5	128.4	128.7	128.7	128.3	128.9	128.6	128.2	128.5	128.8	128.4	128.2, 128.6	128.6, 1
C1-C2-N4	100.7	101.6	102.3	101.7	101.6	102.3	101.7	101.5	101.6	101.5	101.7	101.8, 101.2	101.7, 1
C1-C2-N6	114.1	113.5	111.1	113.1	114.2	113.4	114.1	114.2	113.9	114.6	115.1	113.0, 114.2	115.0, 1
C1-C2-H13	105.0	107.7	108.1	107.6	107.7	108.3	107.6	107.6	107.6	107.5	107.5.	107.6, 107.3	107.6, 1
N4-C2-N6	116.5	116.1	116.8	116.5	115.6	114.4	115.7	115.7	116.0	115.7	114.9	116.4, 116.4	115.0, 1
N4-C2-H13	113.0	111.1	111.4	111.2	111.1	111.3	111.1	111.2	111.2	111.0	111.2	111.2, 111.1	111.3, 1
N6-C2-H13	107.0	106.6	107.0	106.5	106.6	107.0	106.5	106.4	106.4	106.4	106.3	106.6, 106.3	106.2, 1
N6-C3-N7	116.8	114.8	113.3	114.3	115.2	114.6	114.9	115.1	114.7	114.7	116.0	114.4, 114.7	115.9, 1
N6-C3=O10	120.2	121.8	122.4	122.1	121.6	121.4	121.7	121.7	121.9	121.9	120.1	122.2, 121.9	120.3, 1
N7-C3=O10	122.9	123.4	124.3	123.5	123.2	123.8	123.3	123.1	123.3	123.3	123.8	123.4, 123.3	123.8, 1
C2-N4-H11	124.0	122.6	120.9	123.2	122.3	119.7	122.8	122.7	123.2	123.2	122.7	126.0, 123.2	123.1, 1
C2-N4-C17	112.7	112.6	112.0	113.1	112.5	111.7	113.0	112.6	113.1	112.3	113.0	113.0, 112.8	113.1, 1
H11-N4-C17	123.0	118.8	116.9	119.2	118.7	116.9	119.3	119.1	119.5	119.6	119.5	120.9, 119.4	119.7, 1
C1-N5-H12	127.0	123.5	122.4	123.5	123.6	122.6	123.7	123.8	123.8	125.8	123.8	124.0, 123.3	123.7, 1
C1-N5-C17	111.6	113.0	112.7	113.4	112.8	112.2	113.2	112.9	113.3	112.5	113.1	112.9, 112.7	113.1, 1
H12-N5-C17	120.0	121.6	120.6	121.4	121.6	120.4	121.4	121.8	121.5	121.0	121.5	122.0, 123.5	121.4, 1
C2-N6-C3	119.9	121.7	119.1	121.5	121.4	118.1	121.3	121.5	121.6	121.3	120.8	121.0, 121.9	120.7, 1
C2-N6-H14	113.0	118.0	117.4	118.0	117.2	116.0	117.3	117.0	117.5	117.1	115.7	117.4, 117.8	115.6, 1
C3-N6-H14	127.0	120.3	118.5	120.3	119.7	118.5	120.1	119.5	120.1	119.8	117.8	119.4, 120.3	117.7, 1
C3-N7-H15	113.0	113.7	111.6	112.9	114.5	113.0	113.9	114.4	113.3	113.5	117.7	113.3, 113.6	117.9, 1
C3-N7-H16	117.0	118.9	115.5	118.6	120.1	118.4	120.2	120.0	119.3	119.7	121.2	118.8, 119.7	121.3, 1
H15-N7-H16	124.0	115.1	113.1	114.5	115.9	114.6	115.5	115.9	114.9	115.1	118.3	114.7, 115.2	118.3, 1
N4-C17-N5	107.7	106.1	105.4	105.5	106.2	105.7	105.7	106.3	105.7	107.3	105.8	106.9, 105.9	105.8, 1
N4-C17=O8	127.7	127.9	128.1	128.4	127.9	128.2	128.3	127.9	128.3	126.6	128.3	128.4, 127.9	128.1, 1
N5-C17=O8	124.6	126.0	126.4	126.1	125.9	126.1	125.9	125.9	125.9	126.1	125.9	124.7, 126.2	126.1, 1
RMS		2.9	3.6	3.0	2.8	3.3	2.8	2.8	2.8	2.8	2.9	2.9, 2.9	2.9, 3.
MAD		2.0	2.6	2.1	2.0	2.3	2.1	2.0	2.0	1.9	2.1	1.9, 2.1	2.1, 2.

[a] Ref. [11], *Abbreviation used:* RMS- Root Mean Square Error, MAD- Mean Absolute Deviation

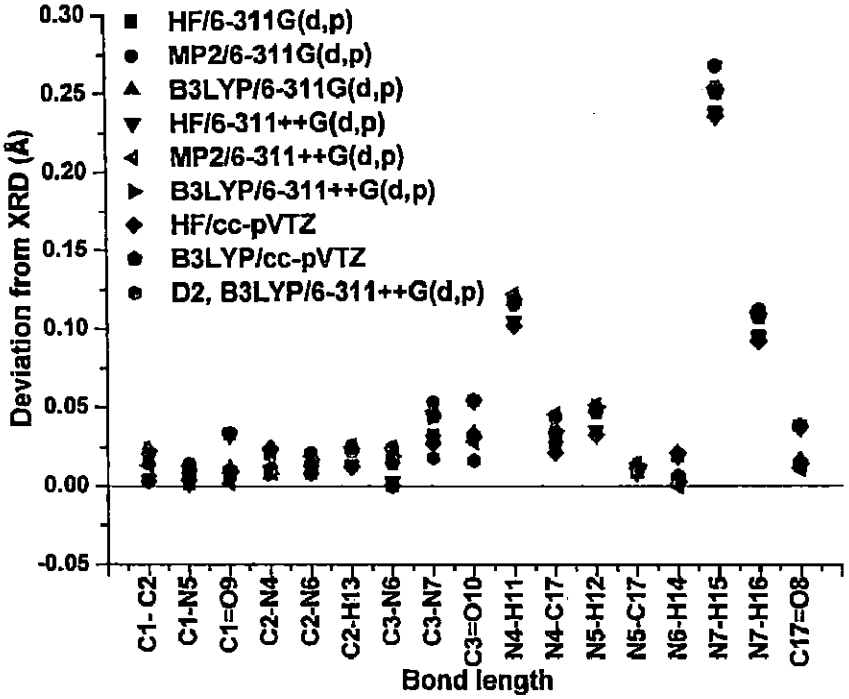

Fig. 6.2 Comparison of theoretical bond lengths with XRD data of allantoin.

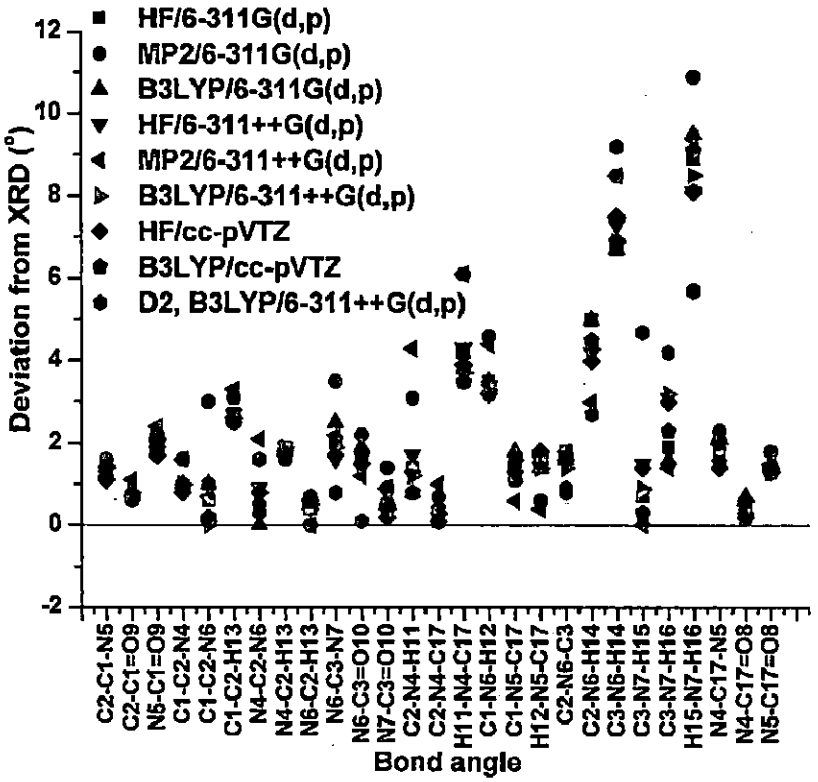

Fig. 6.3 Comparison of theoretical bond lengths with XRD data of allantoin.

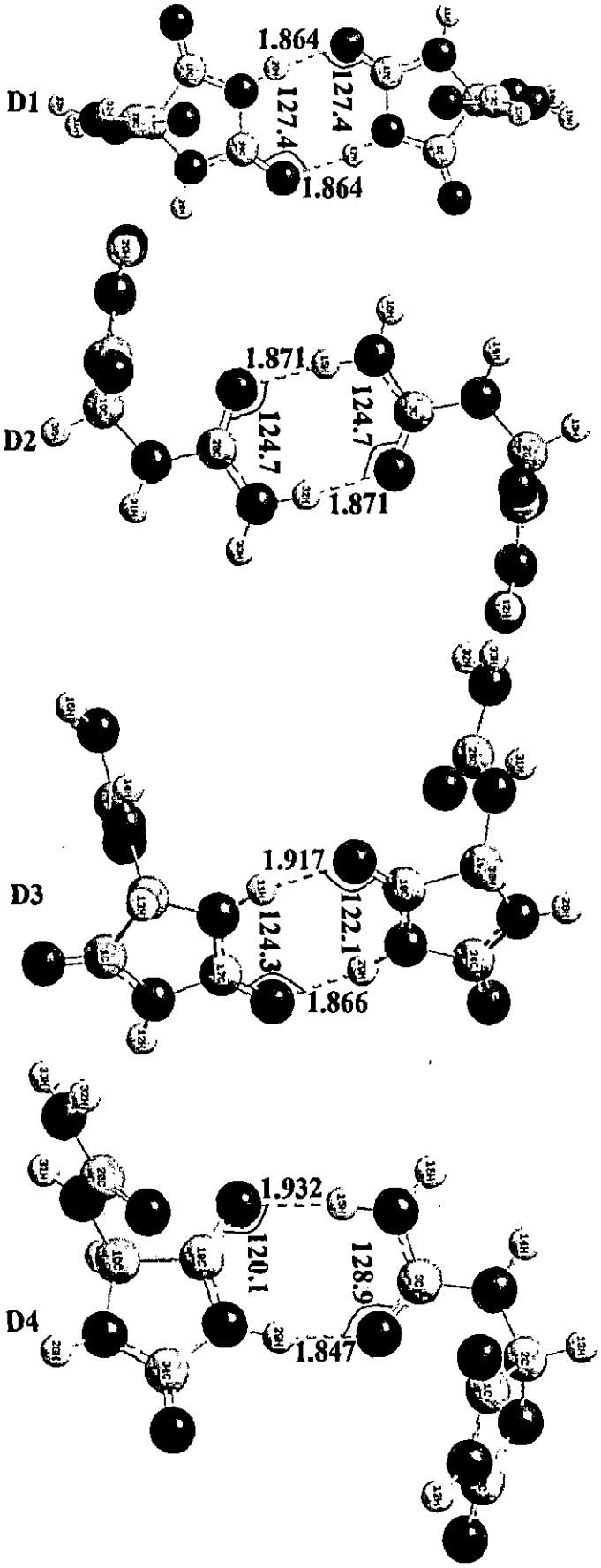

Fig. 6.4 Optimized dimeric structures of allantoin molecule with intermolecular hydrogen bonding descriptions.

6.4.2 Vibrational analysis

Allantoin molecule belongs to C_1 point group. Therefore, all the vibrational modes are active in both IR and Raman spectra. In the present work, the assignments are made for the fundamental, combination and overtone bands on the basis of anharmonic force field calculations. The vibrational frequencies along with their intensities and assignments are given in Table 6.4. The comparison among theoretical vibrational frequencies calculated at different levels of theory has been also presented in Table 6.5. The simulated and experimental vibrational spectra are shown in Fig. 6.5 and 6.6. The correlation plots between experimental and theoretical frequencies are presented in Fig. 6.7 and 6.8. The calculated anharmonic frequencies are found closer to matrix FTIR data [13]. The harmonic wavenumbers generally show overestimation due to neglect of anharmonic term in potential energy. The RMS and MAD values (Table 6.4) reveal that the remarkable accuracy is achieved in anharmonic computations. Moreover, the anharmonic DFT and MP2 computations have not shown significant difference between their RMS and MAD values. However, DFT has lesser computational cost than MP2 method. It can be concluded that both approaches show good performances and provide similar results with equal accuracy. The small differences between B3LYP and MP2 results reveal that each approach has its own pros and cons. Hence, none of them can be considered superior.

Allantoin molecule consists of NH_2, C=O and N–H groups which are also present in urea. The carbonyl group forms allantoin dimers by strong hydrogen bonding interaction with N–H/NH_2 group in solid phase. The intermolecular interactions can significantly affect the vibrational spectra. The calculation of vibrational frequencies for dimeric structures of allantoin show significant changes in frequencies of many vibrational modes. The comparisons of experimental frequencies with theoretical one, at B3LYP/6–311++G(d,p) level, for monomer and dimers are presented in Table 6.4. Assignments of vibrational modes of dimer were performed with help of visual inspection of the atomic displacements and through comparison with the assignments of the isolated molecule. It is interesting to note that the scaled frequencies of many vibrational modes of dimers are found more close to FTIR frequencies in solid phase in comparison to those of monomer. In this work, the molecular vibrations for C=O, N–H and NH_2 group in allantoin dimers are mainly discussed because these are involved in formation of hydrogen bonded dimers. The

mode-mode coupling strengths larger than of ca. 25 cm^{-1} for some important pairs of modes are presented graphically in Fig. 6.9. This plot shows that the high values of coupling strengths, greater than ca. 150 cm^{-1}, are found for the mode pairs (3, 34), (4, 39), (2, 31) and (1, 5). These modes involve mainly the displacement of nitrogen and hydrogen atoms. Anharmonic couplings between normal modes that involve the displacements of the same atoms are typically stronger [62]. This statement is confirmed for the present anharmonic mode–mode coupling calculations of allantoin. The anharmonic mode–mode coupling values greater than ca. 6 cm^{-1} for most of the mode pairs are also tabulated (Table 6.6). The pairs of modes that involve large amplitude of vibrations (i.e. large anharmonicity) possess high mode–mode coupling strength. The 3D graphical representation of mode–mode pair coupling strength in the 2–mode coupling representations of the quartic force field (2MR–QFF) calculated at B3LYP/6–311G(d,p) level for allantoin, is shown in Fig. 6.10. This figure indicates that most of the normal mode pairs have very low coupling strength in the 2MR–QFF except some pairs, which show the medium to high coupling strengths. The mode-mode couplings for important pairs of modes are discussed in the relevant sections. The frequencies (harmonic, Barone's PT2, diagonal, VSCF and CC–VSCF), contribution of intrinsic anharmonicity ($\Delta E_{diag.}$) and contribution of anharmonic mode-mode coupling ($\Delta E_{coupl.}$) to each mode calculated [63, 64] at B3LYP/6–311G(d,p) level of theory are given in Table 6.7. It is clear from Table 6.7 that the absolute values of ΔE_{coupl} are larger than the absolute values of $\Delta E_{diag.}$ for most of the modes. Therefore, it is worth to note that the contribution of anharmonic mode–mode coupling is larger than the intrinsic anharmonicity for the allantoin molecule. Thus, mode–mode coupling anharmonicity has been more important in the calculation of vibrational spectra of medium sized molecule. The combination and overtone bands in the FTIR spectra of allantoin are also assigned with the help of anharmonic computations (PT2). The experimental and calculated wavenumbers of non–fundamental bands are given in Table 6.8. Most of them are combination bands. The experimental and theoretical NIR spectra are shown in Fig. 6.11. The assignments of the fundamental normal modes of the molecule are discussed in the following sections.

NH_2 group vibrations

In allantoin, NH_2 group vibrations are very similar to the vibrations of this group in urea and other compounds containing amine group [13, 17, 65, 66]. There are six internal modes of vibration namely symmetric and asymmetric stretching, scissoring, rocking, wagging and twisting motions for NH_2 group. The bands due to NH_2 asymmetric and symmetric stretching vibrations usually occur in the regions 3550–3330 and 3450–3160 cm^{-1} respectively [66]. In the present FTIR/FT–Raman spectra, the bands at 3439/3438 and 3343/3341 cm^{-1} with medium to strong intensity are assigned to NH_2 asymmetric (Mode 1) and symmetric (Mode5) vibrations respectively. These assignments are in well agreement with earlier assignments [13, 17, 66]. These bands are pure stretching as evident from PED values. These vibrations are predicted at 3485 (Mode 1) and 3389 (Mode 5) cm^{-1} using CC–VSCF approach at B3LYP/6–311G(d,p) level of theory. The modes 1 and 5 are not accurately corrected using PT2 method. This may be due to strong anharmonicity associated with these modes or strong coupling between them or coupling with other modes of the molecules [37, 67]. It is predicted that mode 1 shows strong coupling with mode 5, 33 and 37 while weak coupling to other modes of allantoin molecule. The anharmonic frequencies calculated by CC–VSCF algorithm corresponding to these modes are closer to experiments than the harmonic and anharmonic values calculated by other approaches. The amine group shows medium to strong absorptions in the region 1650–1580 cm^{-1} due to scissoring motion [66]. In the case of urea, this vibration shows its presence in the region 1605–1515 cm^{-1} [13, 17, 66]. In the present work, the NH_2 scissoring vibration is observed at 1603 cm^{-1} in FTIR with medium intensity and at 1605 cm^{-1} in the Raman spectrum with very weak intensity. The mode 10 corresponds to scissoring vibration (89% PED) and it couples weakly to other modes [37]. In the present work, mode 10 couples to others with coupling strength less than ca. 25 cm^{-1} (relatively low value). Hence, the calculated anharmonic and harmonic wavenumbers are found very close to the experimental values. The NH_2 scissoring vibration is predicted at 1605 cm^{-1} using VSCF approach. The calculated anharmonic frequency for this vibration at MP2/6–311++G(d,p) level of theory is relatively more close to the experiment as compared to that of B3LYP/6–311++G(d,p). For the dimers, the scaled frequencies are found closer to the experiment. For the primary amines, the rocking vibration normally appears in the region 1150–900 cm^{-1} while

N–H out of plane bending vibration shows its presence in the region 850–500 cm^{-1} [66, 68–70]. The NH_2 rocking vibration was assigned at 1125/1101 cm^{-1} for allantoin crystal and at 1153 cm^{-1} in urea crystal [13, 17]. The FTIR band with weak intensity at 1079 cm^{-1} is attributed to NH_2 rocking vibration (27% PED in mode 20), which is mixed with C–NH_2 stretching (39% PED). These modes are coupled with mode 1 and 5 with coupling strength ca. 50 cm^{-1} (Table 6.6). It has also small contribution in modes 21 (12% PED) and 23 (11% PED). The anharmonic wavenumber for NH_2 rocking vibration is calculated at 1079 (PT2–B3LYP/6–311++G(d,p)) and 1099 (PT2–MP2/6–311++G(d,p)) cm^{-1}. It is well corrected using PT2 method. The N–H deformation vibrations of NH_2 group are mixed with other vibrations (Table 6.4). The N–H in plane bending vibrations of NH_2 group including scissoring and rocking vibrations have appeared in the region 1060–1605.The bands due to N–H out of plane bending vibrations of NH_2 group are appeared in the low wavenumber region (Table 6.4). These assignments are in accordance with literature [66]. The bands appeared with weak intensity at 500 cm^{-1} in the FT–Raman spectrum and with strong intensity at 453 cm^{-1} in the FTIR spectrum show main contribution of N–H out of plane bending vibrations of NH_2 group. The vibration appearing at 500 cm^{-1} is relatively pure (90% PED). According to animated modes and PED values, the NH_2 wagging vibration has shown its contribution in modes 34, 35 and 36 while the NH_2 torsion vibration is identified in mode 40.

C=O vibrations

A strong absorption band due to C=O stretching motion normally occurs in the region 1850–1550 cm^{-1}. This vibration is easily recognised in FTIR spectra because of its high intensity. In Raman spectra, it generally appears with weak intensity [66]. The stretching frequency of the group depends much on its environment and shifts due to intermolecular or intramolecular interactions [66]. In urea, this vibration appears in the region 1700–1650 cm^{-1} [66]. The C=O stretching bands were assigned at 1666/1663 cm^{-1} in allantoin crystal and at 1686 cm^{-1} in urea crystal [13]. In the present molecule, the C=O stretching vibrations, observed in both FTIR and FT–Raman spectra, are assigned to modes 7 to 9 which are in coherence with earlier reports [13, 35, 66]. The modes 7 and 8 have contributions from both the C=O groups attached to ring. The modes of C=O stretching vibrations are coupled weakly to other modes of allantoin as evident by low values of coupling strength (ca. 15 cm^{-1}). The

calculated anharmonic frequencies for these vibrations have relatively large deviations from solid phase FTIR as well as FT–Raman but they are close to matrix FTIR data. The reason for these deviations may be intermolecular and/or intramolecular interactions in solid phase. The contribution of intrinsic anharmonicity and mode–mode coupling anharmonicity are found relatively low for the C=C stretching vibrations. In solid phase, the carbonyl group form stable allantoin dimers by direct interaction with N–H or NH_2 group through hydrogen bonds. The intermolecular interaction affects the vibrational frequencies due to charge delocalization through hydrogen bonds (NBO analysis). In hydrogen bonded dimers the C=O stretching vibrations have lower frequencies than those of monomer due to the intermolecular interaction. The scaled vibrational frequencies of these vibrations in different allantoin dimers are close to the solid phase FTIR data. In the presen work, the C=O deformation (in plane as well as out of plane) vibrations of ring and ureidyl moiety are mixed with others (Table 6.4). In these modes, the displacement of O atoms seem to be very small due to their large masses as seen in animated mode by GaussView software [46]. The IR bands due to C=O out of plane bending vibrations were reported at 780 and 789 cm^{-1} in allantoin and urea respectively [13 17]. In the present case, these vibrations in the ureidyl moiety as well as in the ring are assigned respectively to modes 26 (75% PED) and 27 (87% PED). A strong band observed at 761 cm^{-1} in the FTIR spectrum is due to C=O out of plane bending vibration in the ring.

N–H and C–X vibrations

Normally, N–H stretching vibrations show their characteristic IR bands in the region 3500–3000 cm^{-1} [66, 71]. The bands appeared at 3218 and 3190 cm^{-1} in FTIR with medium intensities and at 3215 and 3190 cm^{-1} in FT–Raman spectra with weak intensities are allocated to these vibrations (mode 2 and 3). The modes 2, 3 and 4 are pure N–H stretching vibrations as evident from PED values. The scaled harmonic frequencies for N–H stretching vibrations in dimers are lower than corresponding anharmonic frequencies of monomer except that of mode 3. For the urazole anion N–H stretching vibrations are reported in solid phase FTIR and FT–Raman spectra at 3185 and 3210 cm^{-1} respectively [72]. In the present study of allantoin, the large deviations between experimental and theoretical wavenumbers (harmonic and anharmonic) of these modes may be associated to the strong anharmonicity c

inability of the theory to estimate the large amplitude vibrations, otherwise, these are due to intermolecular and intramolecular interactions in solid phase. The anharmonicity in stretching mode associated with heavy atoms is negligible due to their small amplitudes of vibrations. However, it is large for the mode associated to light atoms like H [73]. The very high values of coupling strengths are estimated for mode–mode pairs (2, 15), (2, 31), (2, 32), (3, 34) and (4, 39). For N–H stretching vibrations, the contribution of anharmonicity are found large (Table 6.7). The predicted intrinsic anharmonicities are larger than the mode–mode coupling anharmonicities for these vibrations. Many modes of the molecule have significant contributions of N–H in plane and out of plane bending vibrations (Table 6.4). According to PED calculations, the N–H in–plane bending vibrations have shown their significant contributions to the modes 11–18. The N–H out of plane bending vibrations are observed below the 580 cm^{-1} in the present vibrational spectra. The experimental wavenumbers of these vibrations are in well agreement with calculated anharmonic wavenumbers and are in accordance with literature [13, 66, 74].

The C–H stretching vibration (100% PED) is identified at 3059 and 3061 cm^{-1} in the FTIR and FT–Raman spectra respectively. The calculated harmonic frequencies for this vibration (mode 6) at different levels of theory are close to experiments. Kus et al. [13] have also reported this vibration at 2948 cm^{-1} for crystalline allantoin. The mode 6 is coupled with mode 13 and 19 (with moderate coupling strength of ca. 60 cm^{-1}) but it is weakly coupled to others. The C–H deformation vibration has been reported at 1385 cm^{-1} in the FTIR spectrum of allantoin crystal [13]. In this work, the C–H deformation vibrations with different phases have shown their contributions in modes 11–18. These are mixed with N–H deformation and/or N–C stretching vibrations. In modes 11 (64% PED), 12 (69% PED), 14 (55% PED) and 15 (58% PED), these vibrations are predicted with large PED contributions. The vibrational bands corresponding to these vibrations with different phases are observed with strong to medium intensity in the FTIR spectrum while with medium to weak intensity in the FT–Raman spectrum.

The C–NH_2 stretching vibration in aliphatic amine occurs in the region 1090–1020 cm^{-1} with weak intensity [13, 66, 69]. This vibration has shown its contribution to modes 16 (13% PED) and 20 (39% PED). It is observed with weak intensity at 1079 cm^{-1} (mode 20) in the FTIR spectrum.

The anharmonic frequencies of C–NH_2 stretching vibration (mode 20) are 1100 (CC–VSCF–B3LYP/6–311G(d,p)), 1079 (PT2–B3LYP/6–311++G(d,p)) and 1099 (PT2–MP2/6–311++G(d,p)) cm^{-1}. In the case of dimer D3, the calculated scaled frequency for this vibration is 1087 cm^{-1}. These values are close to present experiments and to that reported in the literatures [13, 66, 69].

Ring and some ureidyl moiety vibrations

Urea gives a strong characteristic band in the region 1300–1360 cm^{-1} due to stretching vibration of the N–C–N group [66]. The N–C–N asymmetric stretching vibration in ureidyl moiety, mixed with other vibration, is predicted at 1300 cm^{-1} (PT2–B3LYP/6–311++G(d,p)) which is close to the experiments. This vibration is assigned at 1301, 1284 and 1279 cm^{-1} in the matrix FTIR, solid phase FTIR and FT–Raman spectra respectively. It shows small contribution (13% PED) in mode 16. The bands due to N–C stretching vibrations of ring and ureidyl moiety have been observed with the mixing of other skeletal vibrations within the region as reported in literature [13]. The N–C stretching vibrations have shown their presence in the vibrational modes 11, 16, 19 and 20 in ureidyl moiety as well as in modes 11, 13–15 and 21–24 and 30 in ring. The C–N stretching vibrations are reported at 1326 and 870 in allantoin and at 1468 and 1005 cm^{-1} in urea molecule respectively [13, 17]. The C1–C2 stretching vibration in the ring has shown its contribution in mode 17, 23–25. The ring bending vibrations, predicted with mixing of others, are also assigned (Table 6.4). The ring bending vibrations are allocated to the modes 22 (11% PED), 28 (63% PED) and 30 (48% PED). In condensed phase FTIR spectrum, the bands observed at 1016, 707 and 632 cm^{-1} are assigned to ring bending vibrations.

experimental and theoretical vibrational frequencies (cm^{-1}) along with relative intensities, probable assignments and intoin.

rved mbers		Monomer								D1	D2	D3	D4	PED (≥1(
		B3LYP/ 6-311++G(d,p)				MP2/ 6-311++G(d,p)				B3LYP/ 6-311++ G(d,p)	B3LYP/ 6-311++ G(d,p)	B3LYP/ 6-311++ G(d,p)	B3LYP/ 6-311++ G(d,p)	
R	FT-Raman	ω_h	ω_{anh}	I_h	I^R	ω_h	ω_{anh}	I_h	I^R	ω_{scaled}	ω_{scaled}	ω_{scaled}	ω_{scaled}	
)s	3438vw	3696	3538	46	14	3738	3572	47	14	3536, 3536	3518, 3517	3536, 3531	3537, 3523	ν
m	3215w	3648	3497	50	28	3662	3509	34	28	3496, 3496	3495, 3495	3499, 3492	3499, 3499	ν
m	3190w	3643	3471	29	33	3658	3495	78	33	3489, 3489	3485, 3485	3489, 3482	3493, 3480	ν
		3637	3472	87	33	3657	3500	65	33	3429, 3429	3473, 3473	3429, 3425	3474, 3429	ν
vs	3341w	3583	3438	43	40	3614	3467	49	40	3208, 3181	3229, 3195	3273, 3170	3264, 3178	
m	3061w	3054	2908	18	60	3109	2977	16	60	2926, 2926	2924, 2924	2921, 2918	2922, 2918	ν
w		2777	2705			2789	2720							
s	1765s	1861	1825	172	76	1874	1839	297	76	1776, 1766	1781, 1781	1779, 1772	1784, 1776	ν_s[(C17=
vs	1718w	1823	1794	1067	5	1833	1797	820	5	1717, 1714	1745, 1745	1724, 1705	1746, 1714	ν_{as}[(C17=
vs	1655m	1774	1736	339	21	1801	1766	301	21	1704, 1702	1681, 1660	1703, 1700	1702, 1668	ν
m	1605vw	1634	1590	89	6	1644	1609	93	6	1607, 1566	1627, 1614	1605, 1604	1623, 1605	β
vs	1530vw	1542	1502	251	7	1547	1506	244	7	1516, 1476	1521, 1514	1519, 1517	1519, 1518	β [H14–N6–C ν[N6–
m		1413	1372	78	16	1431	1392	60	16	1411, 1375	1392, 1389	1445, 1413	1407, 1392	β [H11–N4–C
m	1392w	1407	1374	88	5	1413	1387	106	5	1400, 1362	1387, 1386	1402, 1392	1389, 1387	ν[N4–C17+ N5–C H18–N5–C17 + H
m	1359vw	1370	1338	61	15	1375	1345	46	15	1384, 1349	1352, 1349	1374, 1352	1375, 1354	β [H11–N4–C17+ β H14–N6–C2] (55)
m	1321w	1356	1318	63	9	1364	1326	71	9	1353, 1316	1346, 1341	1343, 1333	1349, 1341	β [H12–N5–C1+
m	1279w	1327	1300	183	8	1340	1307	151	8	1303, 1268	1331, 1329	1306, 1301	1330, 1302	β H–N1–C3 (22)+ β + ν_{as}N–C1(
		1273	1247	117	11	1300	1269	111	11	1254, 1218	1253, 1253	1271, 1255	1272, 1253	β H13–C2–(
ds	1189m	1193	1157	71	11	1212	1174	58	11	1187, 1155	1176, 1175	1182, 1174	1183, 1174	ν[R + N6–C2]
w		1164	1132	102	11	1191	1159	86	11	1148, 1118	1145, 1142	1150, 1148	1149, 1142	ν
w		1107	1079	14	26	1125	1099	1	26	1089, 1061	1113, 1108	1087, 1087	1106, 1088	νC–NH2
w	1067w	1084	1053	13	8	1109	1086	17	8	1067, 1038	1070, 1070	1077, 1070	1072, 1070	νN1–C
vw		1047	1009			1113	1024							
		1017	924			1070	967							
m	1019w	985	961	40	14	991	971	53	14	1007, 981	968, 968	986, 978	978, 967	ν_sN–C12(6
	871s	963	940	11	7	979	963	12	7	949, 923	958, 957	954, 950	957, 951	ν[C1–C2 + N–C2 + β [C2–N6
m	809m	853	836	4	79	865	845	3	79	841, 819	851, 850	842, 838	848, 842	Γ O5–C2–N5–C1(2 +
m	771vw	795	774	10	32	811	787	11	32	816, 774	787, 783	827, 790	827, 790	ν C1–C2 (35) + β
		774	753	14	5	777	762	17	5	784, 763	781, 763	781, 764	782, 763	Γ O10
s		760	748	17	10	755	736	23	10	761, 741	748, 748	762, 749	762, 749	Γ O6–
m	702vw	696	683	27	20	703	685	39	20	753, 734	740, 723	749, 696	747, 698	β [R +

nued)

!w	675vw	673	661	7	18	674	655	4	18	692, 672	687, 685	693, 668	693, 687	β [C_2–N_6–C_5 + + Γ C
!m	632m	637	622	25	70	651	627	36	70	665, 646	667, 665	662, 656	665, 659	β R (4
!m	577vw	589	578	27	19	590	572	30	19	627, 607	627, 627	629, 622	627, 623	β [C2–Cl= τ H_{12}–N_5–C_{17}–N
!s	517vw	561	539	161	4	567	532	145	4	583, 563	582, 580	583, 577	582, 577	τ H_{12}– β [C2–C1=
sh	485vw	512	492	14	20	558	446	330	20	509, 496	557, 556	535, 528	558, 513	β [N_7–C_5= + Γ C
	500vw	499	315	122	3	514	505	2	3	502, 489	514, 513	509, 499	509, 502	τ H_{12}
!s		428	365	127	8	480	407	133	8	438, 422	426, 426	490, 428	428, 423	τ (H_{16}–N_7–C_5– +
!w		410	397	111	26	462	398	34	26	420, 403	415, 409	420, 406	410, 406	β N_5–C=O (+ H_{14}
w	379vw	385	345	70	7	413	404	18	7	391, 379	392, 389	401, 368	376, 371	τ H_{11}
		359	359	6	39	364	364	2	39	359, 348	377, 366	368, 354	365, 355	β [N_4–C_2–I τ H_{11}
	309m	293	273	14	36	297	290	10	36	294, 286	298, 297	302, 300	301, 291	β [N_5–C_1=O_9 + (+τ [H_{14}–N_6 + H_{16}
	136s	203	135	12	6	279	165	11	6	226, 220	291, 283	275, 191	280, 207	β [C_1–C_2–N_6 + C_2–I + H_{14}–N_6–C_5–N τ [C_1–C_2–N_6 C_{17}–
	174sh	180	150	14	48	199	181	9	48	190, 183	212, 208	187, 181	195, 184	τ [H_{14}–N_6–C H_{16}–N_7–C_5=O_{10} C_2–N_4–C_{17}=O_1
	155sh	158	158	1	25	158	155	1	25	163, 156	158, 156	165, 161	165, 158	β [C_1–C_2– τ [C_1–N_5–C_1 C_1–N_5–C_{17}=O_9 + C + N_5–C_1–C_2–
	112s	98	100	2	81	116	109	1	81	132, 112	134, 126	122, 104	124, 118	τ [C_1–C_2–N C_{17}–I
	100sh	72	71	15	186	79	76	11	186	96, 81	120, 91	101, 82	108, 84	β [C_1–C_2– τ [(C_1–N_5–C_1 (C_2–
	79sh	61	64	5	412	67	65	4	412	78, 69	88, 77	79, 73	80, 75	τ [(C_{17}–N_4–C_2 (C_3–
S		148	100			161	106			72, 71	80, 78	79, 68	83, 69	
D		85	64			103	64			41, 41	48, 45	45, 37	49, 38	

M–mode no., ω_h–harmonic wavenumbers, ω_{anh} –Anharmonic wavenumbers, I_h– harmonic IR intensity (km/mole), I_{anh}– anhharmonic IR intensity (km/mole), I –plane bending, τ– torsional, r–rocking motion, β_{sci}.–scissoring; w–weak, m–medium strong, sh–shoulder, s–strong, vs–very strong. Γ ABCD: the angle betwee bered ring; RMS– Root Mean Square Error, MAD– Mean Absolute Deviation
ata from Ref. [13], The underline values are taken from Ref. [16]

Table 6.5 Theoretical harmonic and anharmonic vibrational frequencies (cm^{-1}) alongwith intensities for allantoin mono

#M	B3LYP								MP2				HF					
	6-311G(d,p)				cc-pVTZ				6-311G(d,p)				6-311G(d,p)			6-311+G(d,p)		
	ω_h	ω_{anh}	A	I^R	ω_h	ω_{anh}	A	I^R	ω_h	ω_{anh}	A	I^R	ω_h	ω_{anh}	A	ω_h	ω_{anh}	A	ω_h
1	3683	3519	35	18	3687	3522	39	16	3727	3561	37	14	3922	3796	56	3933	3795	63	3931
2	3653	3494	42	28	3651	3494	47	26	3679	3518	95	23	3898	3741	42	3892	3739	43	3892
3	3646	3463	34	25	3646	3472	26	30	3676	3523	70	23	3884	3743	54	3880	3739	58	3883
4	3644	3477	74	35	3639	3474	80	32	3674	3519	55	23	3877	3727	131	3873	3725	134	3874
5	3573	3417	34	39	3575	3425	38	39	3610	3461	41	32	3807	3695	56	3814	3693	64	3811
6	3052	2901	21	60	3047	2903	19	60	3114	2978	17	51	3233	3111	26	3235	3143	22	3218
7	1882	1854	172	43	1867	1833	154	49	1902	1875	274	62	2059	2018	142	2042	2007	145	2042
8	1846	1813	898	4	1830	1801	925	4	1863	1833	673	14	2015	1981	1360	1995	1955	1493	1996
9	1794	1758	301	15	1779	1744	296	16	1830	1796	256	14	1952	1914	431	1935	1899	453	1936
10	1636	1601	94	9	1634	1592	81	8	1644	1614	113	8	1784	1750	119	1781	1738	111	1781
11	1546	1503	248	7	1545	1501	235	6	1556	1517	225	6	1701	1657	299	1697	1660	297	1697
12	1412	1372	90	12	1413	1371	86	13	1430	1393	87	9	1576	1538	69	1575	1534	58	1573
13	1408	1378	94	6	1411	1379	81	5	1416	1387	122	8	1544	1523	169	1543	1518	157	1546
14	1368	1339	76	19	1372	1342	73	16	1373	1344	95	15	1507	1476	67	1506	1476	68	1501
15	1354	1317	72	7	1353	1310	54	8	1366	1331	74	7	1497	1472	80	1497	1470	67	1499
16	1330	1297	134	7	1331	1301	159	7	1347	1309	80	7	1454	1421	130	1449	1425	149	1451
17	1270	1237	103	11	1272	1239	106	9	1292	1265	90	10	1428	1403	187	1429	1406	212	1428
18	1189	1155	63	13	1195	1159	63	11	1207	1175	58	12	1315	1289	58	1318	1289	66	1319
19	1166	1135	100	8	1165	1131	97	7	1189	1159	85	8	1269	1243	101	1269	1236	98	1268
20	1110	1084	17	24	1110	1083	14	24	1127	1090	10	23	1214	1192	9	1211	1187	6	1211
21	1085	1056	17	6	1086	1054	14	6	1120	1086	17	5	1192	1163	20	1189	1163	19	1188
22	985	961	33	14	986	963	36	13	996	975	43	15	1076	1057	40	1075	1058	45	1074
23	969	940	8	9	966	935	8.7	8	990	970	6	8	1063	1040	6	1059	1047	7	1059
24	855	842	4	73	856	837	3.9	68	868	853	3	81	939	926	8	937	925	8	939
25	794	779	16	34	797	774	14	36	811	797	25	23	880	855	41	878	856	24	881
26	780	745	23	3	777	759	14	3	795	756	54	2	870	854	31	866	854	28	868
27	766	752	19	9	765	753	14	7	759	743	21	12	858	848	43	854	846	44	858
28	698	686	26	20	697	685	23	20	706	685	36	19	761	748	29	759	747	30	758
29	676	666	9	17	676	666	7	19	681	662	6	20	743	733	4	741	734	4	744
30	638	623	27	61	637	626	22	65	650	628	46	67	699	684	24	698	682	24	696
31	592	582	38	25	592	581	30	19	627	550	244	18	643	634	26	642	633	23	646
32	564	550	161	2	564	544	144	2	588	576	29	38	603	591	191	602	581	194	608

– Table 6.5 (*continued*)

33	546	374	199	27	522	354	164	25	563	540	154	12	569	330	210	554	548	2	556	548	3
34	514	503	1	20	512	482	16	9	517	511	3	24	556	549	1	529	347	108	534	375	97
35	426	380	46	14	431	400	87	15	447	374	56	17	460	446	13	459	428	24	462	384	778
36	411	384	88	48	411	386	78	34	430	385	94	54	447	411	186	452	403	265	451	418	228
37	384	368	70	16	377	343	67	15	411	395	14	5	430	384	74	430	370	111	419	358	81
38	362	354	9	51	359	353	6.6	42	381	324	52	19	391	384	8	390	389	6	389	385	7
39	303	245	16	44	297	280	13	35	361	308	46	47	324	297	12	319	301	13	319	301	14
40	231	1.24	52	32	201	230	26	13	291	276	16	32	216	182	67	228	184	5	233	156	9
41	186	176	6	11	186	187	8	30	204	190	7	20	205	100	43	195	166	20	202	173	15
42	156	158	0	33	159	161	1	26	153	153	1	52	169	175	1	170	170	1	172	170	1
43	101	95	1	99	98	96.6	2	80	111	108	1	96	108	107	2	107	109	3	107	104	2
44	73	55	15	221	71	82	14	221	86	80	11	147	77	75	11	78	78	16	77	73	18
45	58	48	8	423	59	79	7	407	66	63	3	369	53	112	22	67	75	8	69	69	5
RMS	120	82			119	80			136	90			224	178		222	175		222	175	
MAD	62	51			60	48			77	54			155	125		152	122		152	122	

Abbreviation used: M–mode no., ω_h–harmonic wavenumbers, ω_{anh} –Anharmonic wavenumbers, A– IR intensity (km/mole), I^R– Raman intensity (arb.unit), RMS–root mean square error, MAD–mean absolute deviation

Table 6.6 Anharmonic mode–mode coupling strength values (cm^{-1}) based on 2MR–QFF potential function at VSCF–B3LYP/6–311G(d,p) level of theory for allantoin molecule.

Mode Pairs	CS	Mode Pairs	CS	Mode Pairs	CS	Mode Pairs	CS
M(3, 34)	240.0	M(2, 23)	28.4	M(4, 43)	13.2	M(1, 43)	8.5
M(4, 39)	237.2	M(5, 39)	27.7	M(11, 16)	13.1	M(4, 22)	8.3
M(2, 31)	192.5	M(1, 45)	27.6	M(38, 40)	13.1	M(38, 41)	8.1
M(1, 5)	183.6	M(1, 39)	27.1	M(34, 41)	13.0	M(22, 33)	8.1
M(2, 32)	147.4	M(5, 45)	27.1	M(3, 42)	12.8	M(21, 34)	8.0
M(1, 33)	139.7	M(3, 17)	26.7	M(36, 40)	12.7	M(1, 25)	7.8
M(33, 34)	137.9	M(4, 45)	26.4	M(11, 38)	12.6	M(36, 43)	7.8
M(5, 33)	128.9	M(38, 45)	26.4	M(34, 42)	12.4	M(3, 38)	7.8
M(36, 37)	120.9	M(3, 35)	25.9	M(4, 37)	12.3	M(2, 16)	7.8
M(38, 39)	119.8	M(33, 35)	25.9	M(2, 42)	12.3	M(34, 45)	7.7
M(1, 37)	118.2	M(4, 40)	25.8	M(1, 32)	12.2	M(33, 44)	7.7
M(2, 15)	117	M(15, 31)	25.7	M(1, 35)	12.1	M(38, 43)	7.7
M(4, 38)	114.3	M(11, 39)	25.7	M(5, 32)	12.1	M(34, 36)	7.6
M(5, 37)	113.4	M(39, 40)	25.5	M(16, 39)	12.0	M(20, 38)	7.6
M(36, 39)	113.3	M(3, 21)	25.4	M(15, 23)	11.9	M(5, 25)	7.6
M(4, 11)	102.9	M(33, 36)	25.2	M(31, 43)	11.9	M(12, 17)	7.6
M(31, 32)	101.9	M(6, 16)	23.0	M(44, 45)	11.8	M(17, 34)	7.5
M(4, 36)	95.8	M(3, 13)	22.7	M(20, 36)	11.7	M(3, 27)	7.5
M(36, 38)	84.9	M(36, 44)	22.7	M(10, 38)	11.6	M(25, 45)	7.4
M(1, 10)	81.4	M(33, 45)	22.6	M(8, 42)	11.6	M(6, 35)	7.4
M(3, 33)	75.3	M(31, 34)	21.2	M(5, 35)	11.4	M(20, 39)	7.3
M(1, 36)	73.7	M(20, 33)	20.8	M(31, 33)	11.4	M(23, 31)	7.3
M(37, 38)	72.8	M(10, 37)	20.8	M(28, 34)	11.3	M(10, 36)	7.2
M(5, 36)	70.0	M(32, 34)	20.6	M(31, 42)	11.0	M(20, 34)	7.2
M(5, 10)	66.6	M(15, 32)	20.5	M(6, 41)	11.0	M(2, 19)	7.1
M(3, 12)	65.2	M(38, 44)	20.3	M(3, 41)	10.9	M(16, 38)	7.1
M(2, 35)	64.9	M(10, 20)	19.0	M(32, 43)	10.8	M(39, 42)	7.1
M(6, 19)	64.1	M(3, 31)	18.1	M(11, 36)	10.7	M(20, 22)	7.1
M(6, 13)	61.6	M(3, 14)	17.4	M(9, 25)	10.5	M(35, 42)	7.0
M(1, 38)	52.1	M(4, 33)	17.2	M(1, 16)	10.2	M(36, 41)	6.9
M(1, 20)	51.5	M(20, 37)	17.0	M(2, 27)	10.1	M(4, 42)	6.8
M(5, 38)	51.5	M(12, 34)	17.0	M(6, 21)	10.1	M(12, 19)	6.8
M(5, 20)	50.4	M(32, 33)	16.8	M(6, 28)	10.1	M(2, 33)	6.7
M(31, 35)	47.8	M(2, 43)	16.6	M(4, 17)	10.1	M(4, 28)	6.7
M(1, 34)	42.8	M(7, 8)	16.5	M(7, 26)	10.1	M(43, 44)	6.7
M(37, 39)	42.4	M(1, 22)	16.5	M(2, 29)	10.0	M(3, 37)	6.6
M(4, 16)	42.3	M(34, 37)	16.3	M(33, 41)	10.0	M(3, 22)	6.6
M(6, 17)	41.8	M(5, 22)	16.3	M(5, 16)	9.9	M(29, 33)	6.6
M(32, 35)	40.7	M(34, 38)	16.1	M(4, 18)	9.8	M(2, 28)	6.4
M(5, 34)	39.6	M(3, 16)	15.9	M(2, 34)	9.7	M(34, 39)	6.4
M(33, 38)	36.7	M(3, 28)	15.4	M(1, 44)	9.6	M(25, 34)	6.4
M(39, 44)	34.9	M(39, 41)	15.3	M(5, 44)	9.519	M(16, 33)	6.3
M(6, 12)	34.3	M(10, 33)	15.3	M(6, 11)	9.2	M(13, 34)	6.2
M(37, 45)	33.6	M(6, 14)	15.1	M(7, 42)	9.1	M(16, 34)	6.2
M(4, 44)	32.7	M(4, 41)	15.1	M(17, 19)	8.8	M(4, 35)	6.0
M(34, 35)	30.8	M(9, 45)	14.4	M(32, 42)	8.7	M(27, 34)	5.9
M(39, 45)	30.7	M(3, 32)	14.2	M(2, 17)	8.6	M(10, 34)	5.9
M(33, 39)	29.7	M(37, 44)	14.2	M(2, 14)	8.6	M(9, 44)	5.8
M(36, 45)	29.6	M(25, 33)	14.0	M(5, 43)	8.6	M(10, 22)	5.8
M(33, 37)	29.4	M(39, 43)	13.4	M(15, 35)	8.5	M(35, 43)	5.8

Abbreviation used: CS– Coupling Strength

Table 6.7 Comparison of vibrational frequencies (cm^{-1}) calculated at different algorithms within B3LYP/6−311G(d,p) level of theory, anharmonic IR intensities (km/mole), $\Delta E_{diag.}$ (cm^{-1}) and $\Delta E_{coupl.}$ (cm^{-1}) calculated for different modes.

#M	$\omega_{harm.}$	$\omega_{diagonal}$	ω_{VSCF}	$\omega_{CC-VSCF}$	$I_{anh.}$	ω_{PT2}	$\Delta E_{diag.}$	$\Delta E_{coupl.}$
1	3688	3770	3487	3485	34.4	3519	82	−285
2	3643	3528	3401	3429	73.2	3494	−115	−99
3	3633	3516	3380	3403	57.2	3463	−117	−113
4	3608	3489	3343	3376	19.1	3477	−119	−113
5	3575	3512	3404	3389	39.3	3417	−63	−123
6	3068	2961	2859	2875	10.7	2901	−107	−86
7	1872	1868	1850	1844	224	1854	−4	−24
8	1836	1841	1810	1807	813	1813	5	−34
9	1775	1771	1746	1744	337	1758	−4	−27
10	1630	1633	1605	1609	113	1601	3	−24
11	1529	1541	1505	1498	343	1503	12	−43
12	1415	1422	1400	1397	38.5	1372	7	−25
13	1405	1409	1380	1378	99.8	1378	4	−31
14	1375	1375	1354	1351	55.9	1339	0	−24
15	1354	1372	1341	1333	65.1	1317	18	−39
16	1305	1309	1296	1292	254	1297	4	−17
17	1267	1270	1253	1251	61.4	1237	3	−19
18	1186	1181	1161	1158	158	1155	−5	−23
19	1166	1173	1148	1144	76.8	1135	7	−29
20	1104	1113	1106	1100	17.6	1084	9	−13
21	1062	1061	1047	1044	16.8	1056	−1	−17
22	1002	1003	997	993	14.6	961	1	−10
23	976	976	964	961	27.5	940	0	−15
24	910	910	900	897	19	842	0	−13
25	778	779	779	788	42.5	779	1	9
26	766	767	761	761	19.9	745	1	−6
27	749	749	749	750	2.95	752	0	1
28	695	696	701	702	23.7	686	1	6
29	675	676	677	674	4.47	666	1	−2
30	627	627	623	622	21.1	623	0	−5
31	598	672	685	559	71.1	582	74	−113
32	579	627	656	593	124	550	48	−34
33	536	678	695	654	34.7	374	142	−24
34	529	661	688	667	166	503	132	6
35	502	515	553	520	19	380	13	5
36	437	513	577	416	67.6	384	76	−97
37	413	520	552	404	61.9	368	107	−116
38	381	438	521	412	53.4	354	57	−26
39	320	463	500	374	27.3	245	143	−89
40	247	250	267	262	0.91	1.25	3	12
41	185	189	212	208	9.37	176	4	19
42	137	148	165	160	1.49	158	11	12
43	100	109	135	131	6.31	95	9	22
44	62	80	115	107	7.8	55	18	27
45	20	69	109	97	9.07	48	49	28
RMS	144	133	104	87		82		
MAD	78	85	72	56		51		

Abbreviations used: M− mode no., $\omega_{harm.}$, $\omega_{diagonal}$, ω_{VSCF}, $\omega_{CC-VSCF}$, ω_{PT2}− frequencies using harmonic, diagonal, VSCF, CC−VSCF and PT2 approaches respectively, I_{anh}− anharmonic IR intensity using VSCF, $\Delta E_{diag.}$− contribution of intrinsic anharmonicity , $\Delta E_{coupl.}$− contribution of mode−mode coupling anharmonicity

Table 6.8 Assignments of non-fundamental vibrational bands appeared in FT-NIR.

Experimental Wavenumber (cm^{-1})	B3LYP/6-311++G(d,p)			MP2/6-311++G(d,p)			Assignment
	ω_h (cm^{-1})	ω_{anh} (cm^{-1})	I_{anh} (km /mole)	ω_h (cm^{-1})	ω_{anh} (cm^{-1})	I_{anh} (km /mole)	
6876	7392	6985	1.46	7475	7059	0.955	2 x 3439
6697	7296	6852	2.48	7323	6884	1.558	2 x 3343
5031	5330	5108	1.73	5382	5156	1.609	3439 + 1603
4947	5282	5088	0.001	5306	5113	0.013	3343 + 1603
4878	5190	4999	0.01	5208	5010	0.068	3343 + 1530
4811	5066	4876	0.001	5113	4916	0.005	3439 + 1361
4703	5018	4833	0.07	5037	4853	0.065	3343 + 1361
4544	4998	4791	0.04	5021	4810	0.995	3218 + 1326
4417	4755	4576	0.02	4787	4607	0.231	3343 + 1079
4312	4424	4245	0.17	4484	4318	0.168	2947 + 1361
4271	4410	4227	0.02	4472	4304	0.002	2947 + 1326
4098	4218	4041	0.001	4300	4136	0.011	2947+1136

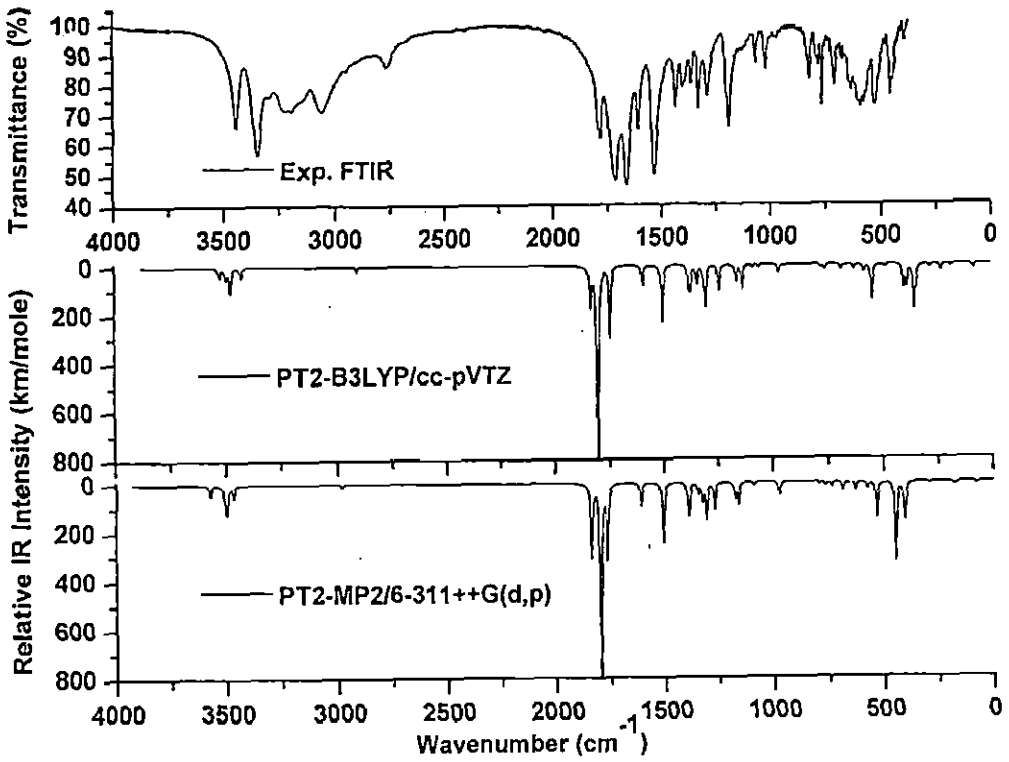

Fig. 6.5 Comparison of experimental and simulated IR spectra of allantoin.

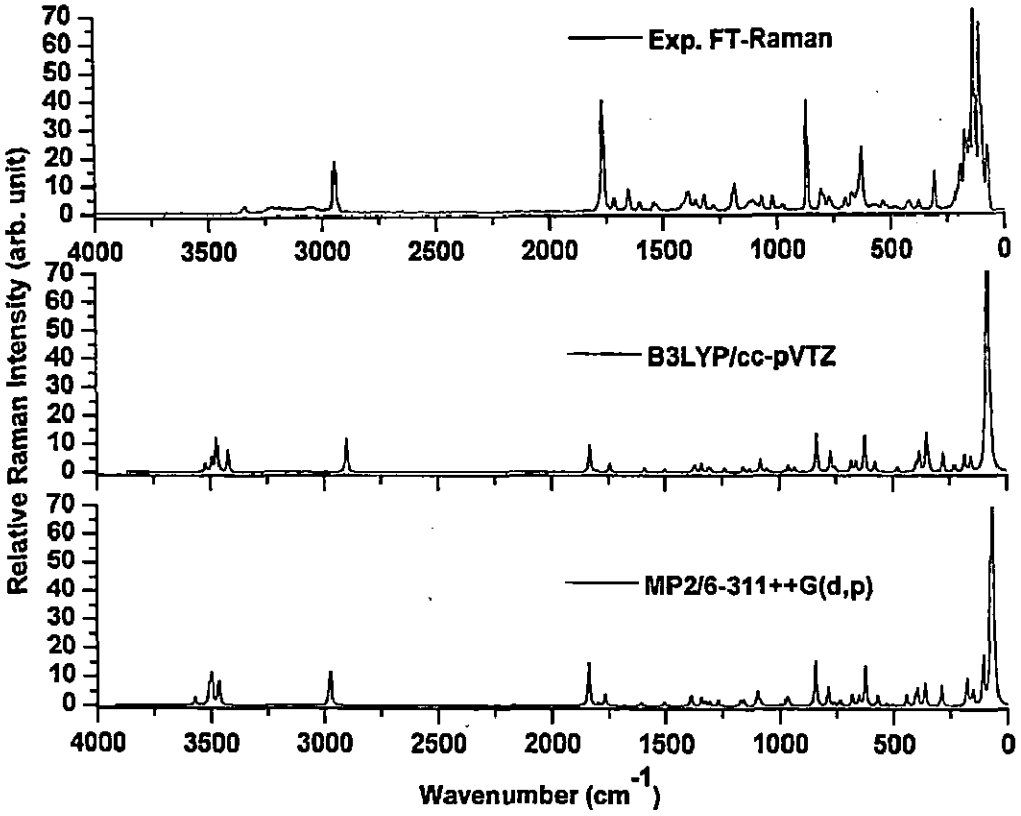

Fig. 6.6 Comparison of experimental and simulated Raman spectra of allantoin.

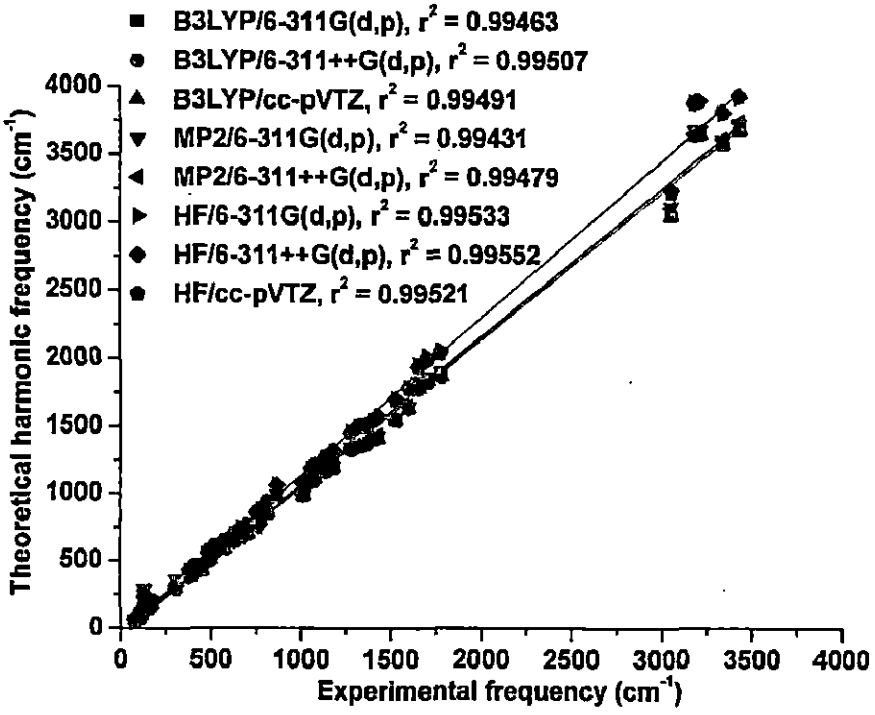

Fig. 6.7 Correlation plots between theoretical harmonic and experimental frequencies.

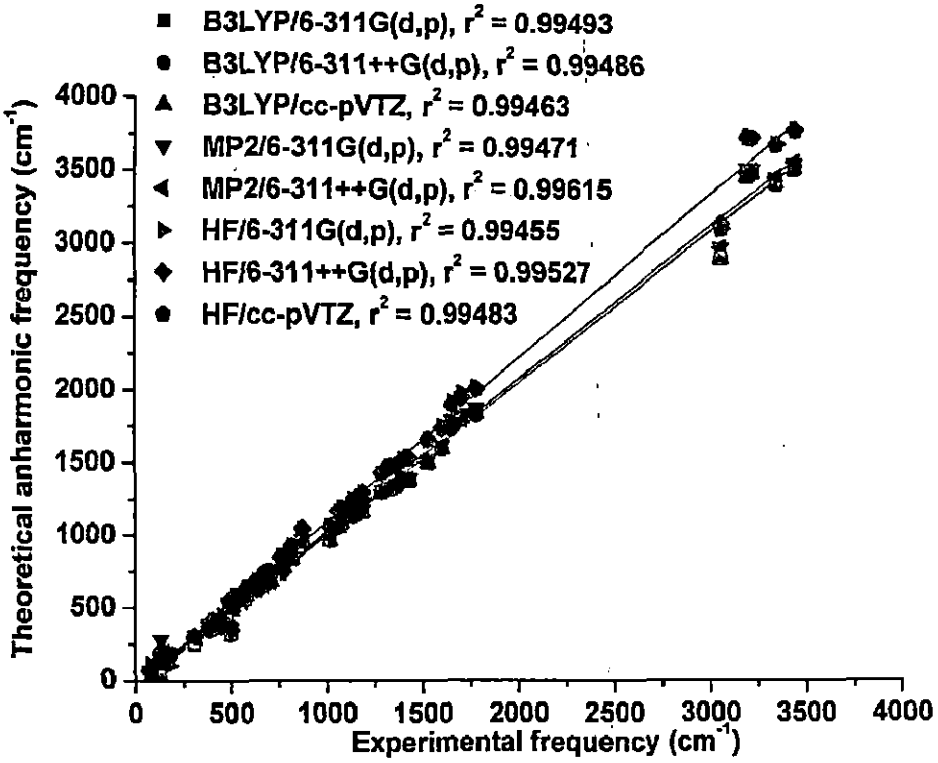

Fig. 6.8 Correlation plots between theoretical anharmonic and experimental frequencies.

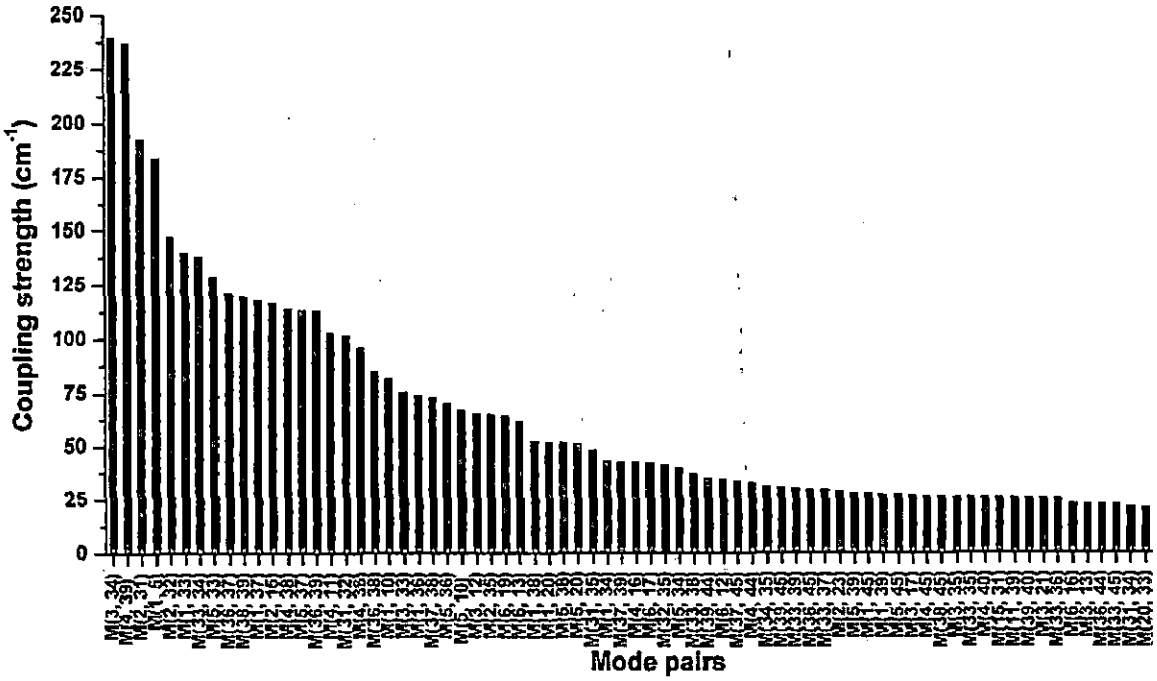

Fig. 6.9 Graphical representation of anharmonic mode–mode coupling strength values higher than 25 cm^{-1}.

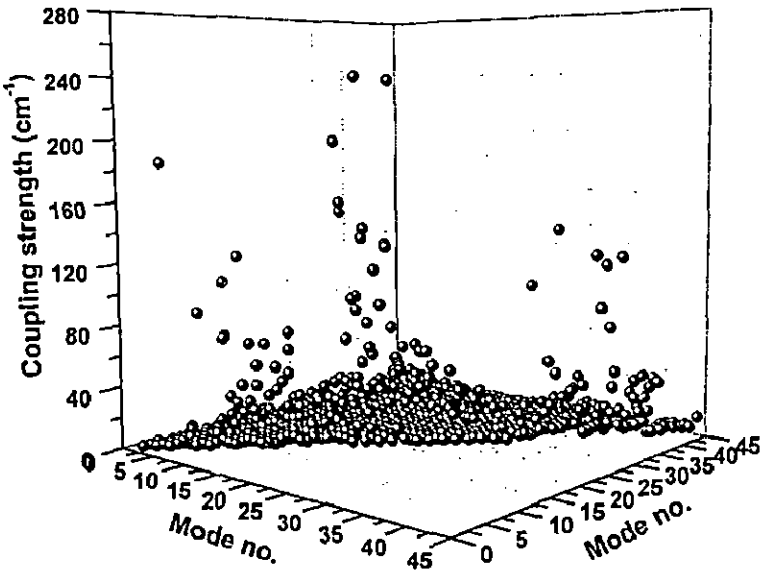

Fig. 6.10 Plot for the coupling strengths between all possible pairs of modes.

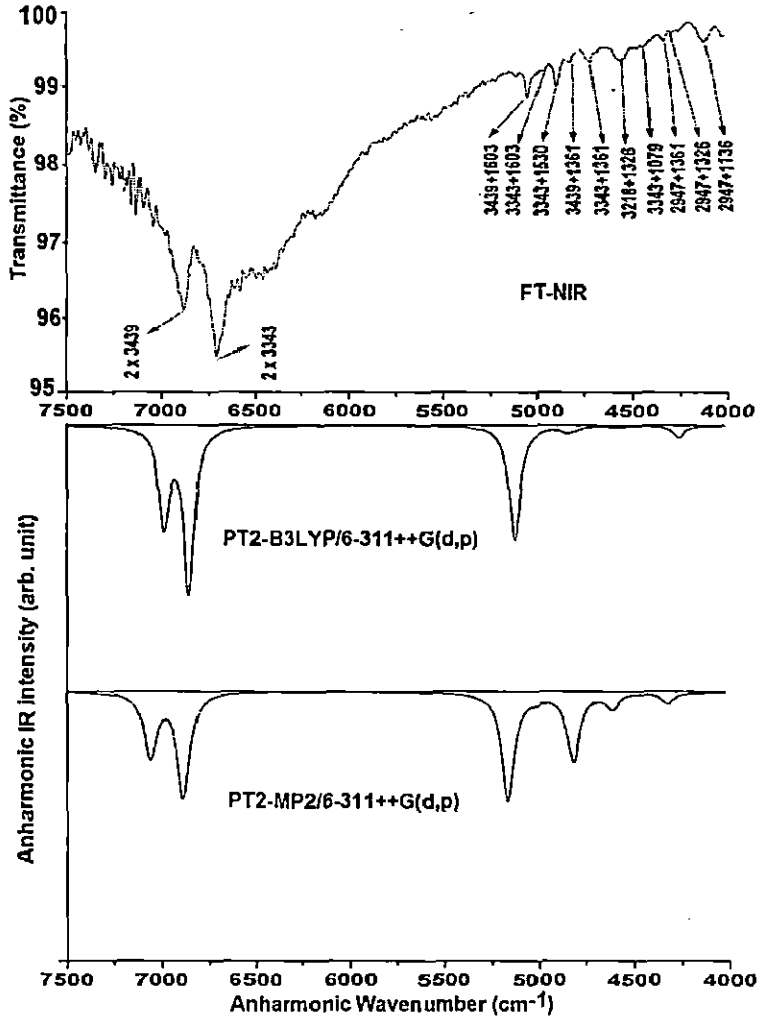

Fig. 6.11 Comparison of the experimental FT-NIR and theoretical anharmonic NIR spectra of allantoin molecule.

6.4.3 Natural bond orbital analysis

The natural bond orbital (NBO) analysis is very useful in understanding the hybridization, natural atomic charges, bond type, hydrogen bonded intermolecular or intramolecular interactions, donor–acceptor conjugative interactions or charge delocalization within molecule as well as Lewis and non–Lewis picture of the molecule [75, 76].

NBO analysis has been performed at B3LYP/6–311++G(d,p) level of theory using NBO 3.1 program [48] implemented in Gaussian 09 software [39]. Table 6.9 represents the bond type, its occupancy, electron densities of atoms involved in forming natural bonding and hybridization of filled orbitals of allantoin monomer. The high values of polarization coefficients [36] for oxygen and nitrogen atoms involved in bonding are predicted which show the high electronegativity of these atoms (Table 6.9). The atoms, attached to high electronegative atoms, show low values of polarization coefficient. From the NBO analysis (Table 6.9), the high occupancies are predicted for σ(C1–O9), σ(C3–N7), σ(C3–O10), σ(O8–C17) and π(O8–C17) bondings. On the basis of NBO analysis, the bonding, σ(C2–N6), between ring and ureidyl moiety is formed by sharing of 39.03% electron density of C2 atom and 60.97% of N6 atom. This NBO is formed by interaction of $sp^{2.85}$ (p–character: 73.91%) of carbon C2 and a $sp^{1.86}$ hybrid (p–character: 64.97%) of nitrogen N6. The hyper–conjugative interaction energies ($E^{(2)}$) between important donor and acceptor orbitals, determined by second order perturbation analysis of Fock matrix of allantoin monomer, are tabulated (Table 6.10). When the donor (filled) orbital interacts with acceptor (virtual) one, the energy and occupancy of donor orbital are lowered and delocalization of charge takes place. Thus, the occupied orbitals (Lewis type) are stabilized by overlapping with virtual orbitals (non–Lewis type) which may be one–centre Rydberg or two–centre anti–bonding NBO [77]. The larger value of stabilization energy, $E^{(2)}$, reflects the more intensive electron donor–acceptor interaction. The strong intermolecular hyper–conjugation interactions are found for $n(LP_1N4) \rightarrow \pi^*(O8–C17)$, $n(LP_1N5) \rightarrow \pi^*(C1–O9)$, $n(LP_1N5) \rightarrow \pi^*(O8–C17)$ and $\pi^*(C3–O10) \rightarrow \sigma^*(C3–O10)$ donor–acceptor interactions. The NBO analysis of allantoin dimers shows evidences of the formation of stabilized hydrogen bonded intermolecular interaction between LP (O) and σ* (N–H) orbitals at B3LYP/6–311++G(d,p) level of theory. Its existence is confirmed by the

intermolecular charge transfer due to n(LPO) → σ*(N–H) which causes the stabilization of dimers. The stabilization energies, $E^{(2)}$, between hydrogen bonded orbitals, n(LPO) ··· σ*(N–H) of allantoin dimers, are summerized in Table. 6.11. The stabilization energy measures the strength of the hydrogen bonding in dimers. The intermolecular hydrogen bonds are formed by overlapping between the orbitals n(LPO) and σ*(N–H) in dimers and hence it leads to increase the electron density of σ*(N–H) antibonding orbital. Moreover, it is predicted that the BSSE corrected SCF energy in the dimeric form (e.g. for D2, −1201.957018 a.u.) is more than twice of that energy of the monomer (−600.968054 a.u.) which shows that dimers are stable because of the existence of intermolecular hydrogen bonding.

Table 6.9 NBO analysis of allantoin at B3LYP/6–311++G(d,p) level of theory.

Bond (A–B)	Occupancy	ED_A %	ED_B %	NBO (% p character)
σ(C1–C2)	1.96845	47.45	52.55	$0.6889\ sp^{2.03}(66.96)_C + 0.7249\ sp^{2.86}(74.07)_C$
σ(C1–N5)	1.98852	37.29	62.71	$0.6107\ sp^{2.16}(68.27)_C + 0.7919\ sp^{1.81}(64.35)_N$
σ(C1–O9)	1.99583	35.38	64.62	$0.5948\ sp^{1.83}(64.62)_C + 0.8039\ sp^{1.39}(58.03)_O$
π(C1–O9)	1.98969	30.76	69.24	$0.5546\ sp^{99.99}(99.56)_C + 0.8321\ sp^{99.99}(99.80)_O$
σ(C2–N4)	1.98415	39.04	60.96	$0.6248\ sp^{3.12}(75.63)_C + 0.7808\ sp^{1.99}(66.48)_N$
σ(C2–N6)	1.98456	39.03	60.97	$0.6248\ sp^{2.83}(73.91)_C + 0.7808\ sp^{1.86}(64.97)_N$
σ(C1–H13)	1.96726	60.97	39.03	$0.7808\ sp^{3.16}(75.89)_C + 0.6247\ sp^{0.00}(0.04)_H$
σ(C3–N6)	1.98793	37.65	62.35	$0.6136\ sp^{2.11}(67.75)_C + 0.7896\ sp^{1.81}(64.33)_N$
σ(C3–N7)	1.99216	39.44	60.56	$0.6280\ sp^{2.03}(66.80)_C + 0.7782\ sp^{1.73}(63.39)_N$
σ(C3–O10)	1.99086	33.49	66.51	$0.5787\ sp^{3.22}(76.09)_C + 0.8155\ sp^{2.76}(73.32)_O$
π(C3–O10)	1.98705	30.85	69.15	$0.5554\ sp^{8.04}(88.59)_C + 0.8316\ sp^{6.74}(86.97)_O$
σ(N4–H11)	1.98600	70.93	29.07	$0.8422\ sp^{2.42}(70.70)_N + 0.5391\ sp^{0.00}(0.06)_H$
σ(N4–C17)	1.98683	61.83	38.17	$0.7863\ sp^{1.93}(65.78)_N + 0.6178\ sp^{2.05}(67.11)_C$
σ(N4–H12)	1.98579	71.64	28.36	$0.8464\ sp^{2.33}(69.93)_N + 0.5326\ sp^{0.00}(0.06)_H$
σ(N5–C17)	1.98372	62.86	37.14	$0.7929\ sp^{2.03}(67.00)_N + 0.6094\ sp^{2.28}(69.42)_C$
σ(N6–H14)	1.98551	69.96	30.04	$0.8364\ sp^{2.53}(71.62)_N + 0.5481\ sp^{0.00}(0.06)_H$
σ(N7–H15)	1.98766	70.16	29.84	$0.8376\ sp^{2.56}(71.84)_N + 0.5463\ sp^{0.00}(0.06)_H$
σ(N7–H16)	1.98687	69.14	30.86	$0.8315\ sp^{2.53}(71.63)_N + 0.5555\ sp^{0.00}(0.07)_H$
σ(O8–C17)	1.99493	63.83	36.17	$0.7989\ sp^{1.48}(59.63)_O + 0.6014\ sp^{1.74}(63.39)_C$
π(O8–C17)	1.99073	70.97	29.03	$0.8424\ sp^{99.99}(99.75)_O + 0.5388\ sp^{99.99}(99.99)_C$
Lone Pairs				
LP_1 N4	1.75824			$sp^{32.29}$ (96.97)
LP_1 N5	1.65872			$sp^{73.56}$ (98.64)
LP_1 N6	1.77098			$sp^{99.99}$ (99.02)
LP_1 N7	1.81458			$sp^{13.34}$ (93.00)
LP_1 O8	1.97871			$sp^{0.67}$ (40.24)
LP_2 O8	1.83343			$sp^{1.00}$ (99.91)
LP_1 O9	1.97827			$sp^{0.72}$ (41.83)
LP_2 O9	1.84404			$sp^{1.00}$ (99.92)
LP_1 O10	1.97750			$sp^{0.65}$ (39.45)
LP_2 O10	1.84458			$sp^{99.99}$ (99.87)

Abbreviation used: ED– Electron density

Table 6.10 Important donor–accepter interaction based on second order perturbation theory analysis of Fock matrix in NBO basis for allantoin monomer at B3LYP/6–311++G(d,p) level of theory.

Donor–acceptor interaction	ED[a] (*e*)	E[(2)b] (kcal/mol)	E(j)–E(i)[c] (a.u.)	F(i, j)[d] (a.u.)
n(LP$_1$N4) → σ*(C2–N6)	0.03440	7.04	0.62	0.062
n(LP$_1$N4) → σ*(C2–H13)	0.02724	6.59	0.65	0.062
n(LP$_1$N4) → π*(O8–C17)	0.31849	51.78	0.29	0.112
n(LP$_1$N5) → π*(C1–O9)	0.24279	54.75	0.29	0.115
n(LP$_1$N5) → π*(O8–C17)	0.31849	44.73	0.30	0.103
n(LP$_1$N6) → σ*(C1–C2)	0.09918	6.56	0.60	0.058
n(LP$_1$N6) → π*(C1–O9)	0.24279	0.59	0.29	0.012
n(LP$_1$N6) → σ*(C2–N4)	0.04324	10.16	0.61	0.074
n(LP$_1$N6) → σ*(C3–O10)	0.13281	6.79	0.69	0.063
n(LP$_1$N6) → π*(C3–O10)	0.23771	20.71	0.49	0.090
n(LP$_1$N7) → σ*(C3–O10)	0.13281	10.33	0.71	0.077
n(LP$_1$N7) → π*(C3–O10)	0.23771	13.91	0.51	0.076
n(LP$_1$O8) →RY*(1) C17	0.01570	18.79	1.84	0.166
n(LP$_1$O8) → σ*(N4–C17)	0.07837	2.38	1.12	0.047
n(LP$_1$O8) → σ*(N5–C17)	0.09106	2.03	1.07	0.042
n(LP$_2$O8) → σ*(N4–C17)	0.07837	25.39	0.68	0.120
n(LP$_2$O8) → σ*(N5–C17)	0.09106	28.34	0.64	0.122
n(LP$_1$O9) →RY*(1) C1	0.01663	18.44	1.66	0.156
n(LP$_1$O9) → σ*(C1–C2)	0.09918	2.04	1.01	0.041
n(LP$_1$O9) → σ*(C1–N5)	0.07953	2.06	1.13	0.044
n(LP$_2$O9) → σ*(C1–C2)	0.09918	24.27	0.58	0.107
n(LP$_2$O9) → σ*(C1–N5)	0.07953	26.57	0.70	0.125
n(LP$_1$O10) → RY*(1) C3	0.01639	17.64	1.76	0.158
n(LP$_1$O10) → σ*(C3–N6)	0.08044	1.78	1.11	0.040
n(LP$_1$O10) → σ*(C3–N7)	0.06665	1.81	1.11	0.041
n(LP$_2$O10) → π*(C1–O9)	0.24279	1.21	0.27	0.016
n(LP$_2$O10) → σ*(C3–N6)	0.08044	24.51	0.67	0.117
n(LP$_2$O10) → σ*(C3–N7)	0.06665	24.06	0.68	0.116
π*(C3–O10) → σ*(C3–O10)	0.13281	89.94	0.20	0.279

[a] Electron density (e) for acceptor orbital
[b] Energy of hyperconjugative interaction (stabilization energy)
[c] Energy difference between donor and acceptor i and j NBO orbitals
[d] Fock matrix element between i and j NBO orbitals

Table 6.11 Important donor–accepter intermolecular interactions based on second order perturbation theory analysis of Fock matrix in NBO basis for allantoin dimers at B3LYP/6–311++G(d,p) level of theory.

Donor–acceptor intermolecular interaction	ED$_i$ (*e*)	ED$_j$ (*e*)	E[(2)a] (kcal/mol)	E(j)–E(i)[b] (a.u.)	F(i, j)[c] (a.u.)
from unit 1 to 2 (dimer D1)					
n(LP$_1$O8) → σ*(N22–H29)	1.96507	0.04463	6.43	1.11	0.076
n(LP$_2$O8) → σ*(N22–H29)	1.84487	0.04463	8.54	0.69	0.071
from unit 2 to 1 (dimer D1)					
n(LP$_1$O25) → σ*(N5–H12)	1.96507	0.04463	6.43	1.11	0.076
n(LP$_2$O25) → σ*(N5–H12)	1.84487	0.04463	8.54	0.69	0.071
from unit 1 to 2 (dimer D2)					
n(LP$_1$O10) → σ*(N24–H32)	1.96507	0.03415	5.37	1.15	0.070
n(LP$_2$O10) → σ*(N24–H32)	1.85222	0.03415	8.58	0.72	0.072
from unit 2 to 1 (dimer D2)					
n(LP$_1$O27) → σ*(N7–H15)	1.96507	0.03415	5.37	1.15	0.070
n(LP$_2$O27) → σ*(N7–H15)	1.85222	0.03415	8.58	0.72	0.072
from unit 1 to 2 (dimer D3)					
n(LP$_1$O8) → σ*(N22–H29)	1.96576	0.04560	5.98	1.11	0.073

Table 6.11 (*continued*)

$n(LP_2O8) \rightarrow \sigma^*(N22-H29)$	1.84250	0.04560	9.30	0.69	0.073
from unit 2 to 1 (dimer D3)					
$n(LP_1O26) \rightarrow \sigma^*(N4-H11)$	1.96804	0.04098	4.57	1.13	0.064
$n(LP_2O26) \rightarrow \sigma^*(N4-H11)$	1.85270	0.04098	7.85	0.71	0.069
from unit 1 to 2 (dimer D4)					
$n(LP_1O10) \rightarrow \sigma^*(N22-H29)$	1.96267	0.04592	7.29	1.12	0.081
$n(LP_2O10) \rightarrow \sigma^*(N22-H29)$	1.85305	0.04592	8.41	0.69	0.070
from unit 2 to 1 (dimer D4)					
$n(LP_1O26) \rightarrow \sigma^*(N7-H15)$	1.97008	0.03002	3.49	1.14	0.056
$n(LP_2O26) \rightarrow \sigma^*(N7-H15)$	1.85159	0.03002	7.49	0.72	0.068

Abbreviation used: ED_i – Electron density (e) for donor orbital, ED_j – Electron density (e) for acceptor orbital
[a]Energy of hyperconjugative interaction (stabilization energy).
[b]Energy difference between donor and acceptor i and j NBO orbitals.
[c]Fock matrix element between i and j NBO orbitals.

6.4.4. Frontier molecular orbitals

The frontier molecular orbitals, HOMO and LUMO, play key role in predicting molecular properties as well as understanding process of interaction with other molecules and chemical activity of the molecules. The HOMO–LUMO gap provides the estimation of excitation energy and explains the charge transfer interaction within the molecule, which influences its biological activity [78]. The energy eigenvalues of HOMO and LUMO, which can easily loss or gain the electrons respectively, are used to calculate various chemical reactivity descriptors and Fukui functions [50–56]. The red and blue colours reflect numerically the negative and positive regions respectively in HOMO and LUMO plots (Fig. 6.12). In this work, the HOMO and LUMO energy eigenvalues, their gap and the chemical reactivity descriptors of allantoin molecule are computed at B3LYP/6–311++G(d,p) level of theory (Table 6.13). DFT calculations provide various energy derivatives and KS orbitals, which are of chemical significance. They define quantitatively the chemical reactivity such as chemical hardness, softness, chemical potential, electrophilicity, etc. The energy eigenvalues of highest occupied (HOMO) and lowest unoccupied (LUMO) KS orbitals for a molecule give the values of ionization potential and electron affinity respectively. The HOMO–LUMO energy gap is also approximated using excitation energy corresponding HOMO–LUMO excitation, H → L (59%), at TD–B3LYP/6–311++G(d,p) level of theory. It is clear from the plots of frontier orbitals, HOMOs are localized over the whole molecule. On the other hand, the LUMOs are over the ureidyl moiety and the positive charge is located over it. In LUMO +1 diagram, the most of the negative charge is spread over H16 atom.

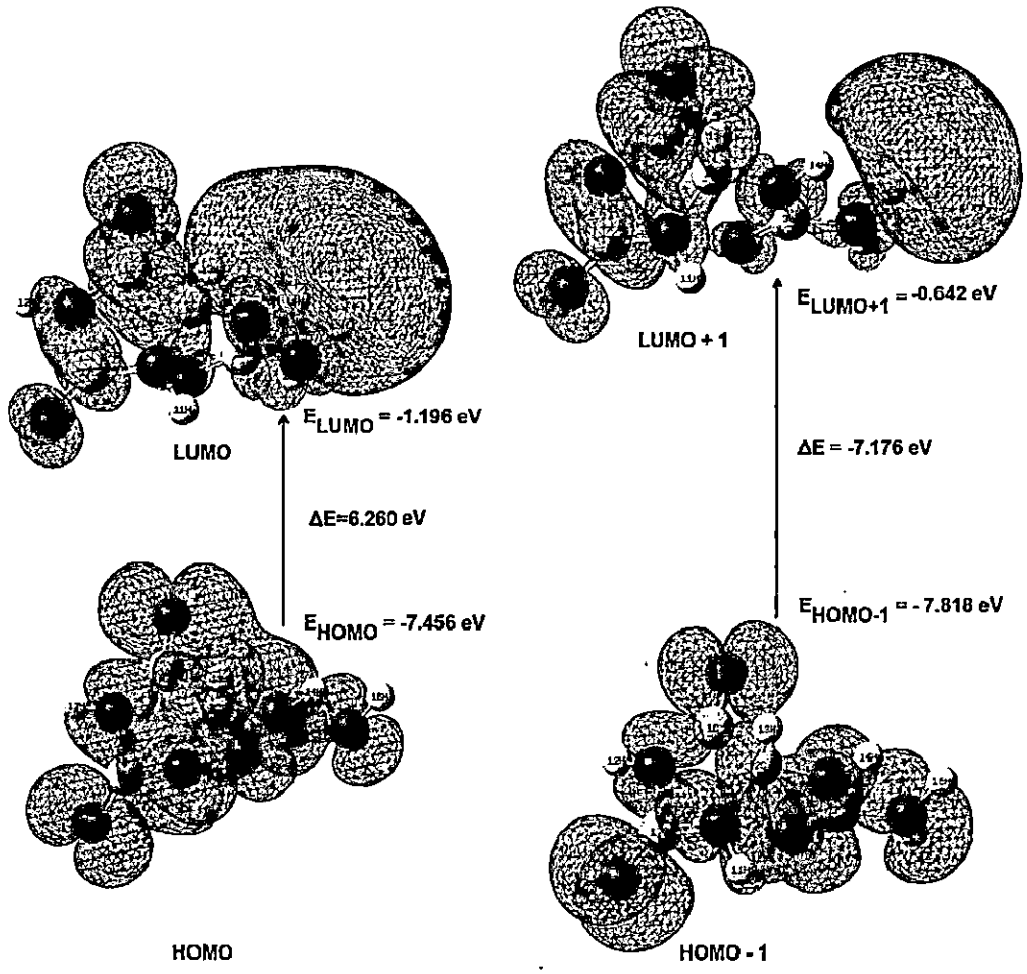

Fig. 6.12 Frontier molecular orbitals of allantoin molecule in gas phase.

6.4.5 Molecular electrostatic potential map

Molecular electrostatic potential (MEP) is a tool for understanding and predicting molecular interactions. This helps in elucidating and predicting the reactive behaviour of molecules with other chemical species. MEP also provides some quantitative measure of the chemical activities of various sites of the molecule [79]. It is computed at B3LYP/6−311++G(d,p) level of theory for allantoin. The MEP and contour diagram with colour range from −8.058E−2 (deepest red) to +8.058E−2 (deepest blue) are shown in Fig. 6.13. The electrostatic potential, represented by different colours, increases in the order red < yellow < green < blue. The regions of high and low potential are characterized by dominancy and deficiency of electrons respectively. The high positive potential regions of the MEP are the preferred sites of nucleophilic attack while the parts of high negative potential are the preferred sites of electrophilic attack. The regions over the electronegative atoms (O8, O9, O10) are at negative

potentials while those associated with hydrogen atoms are at positive potentials. The rest of region represents neutral potential and is shown in green colour.

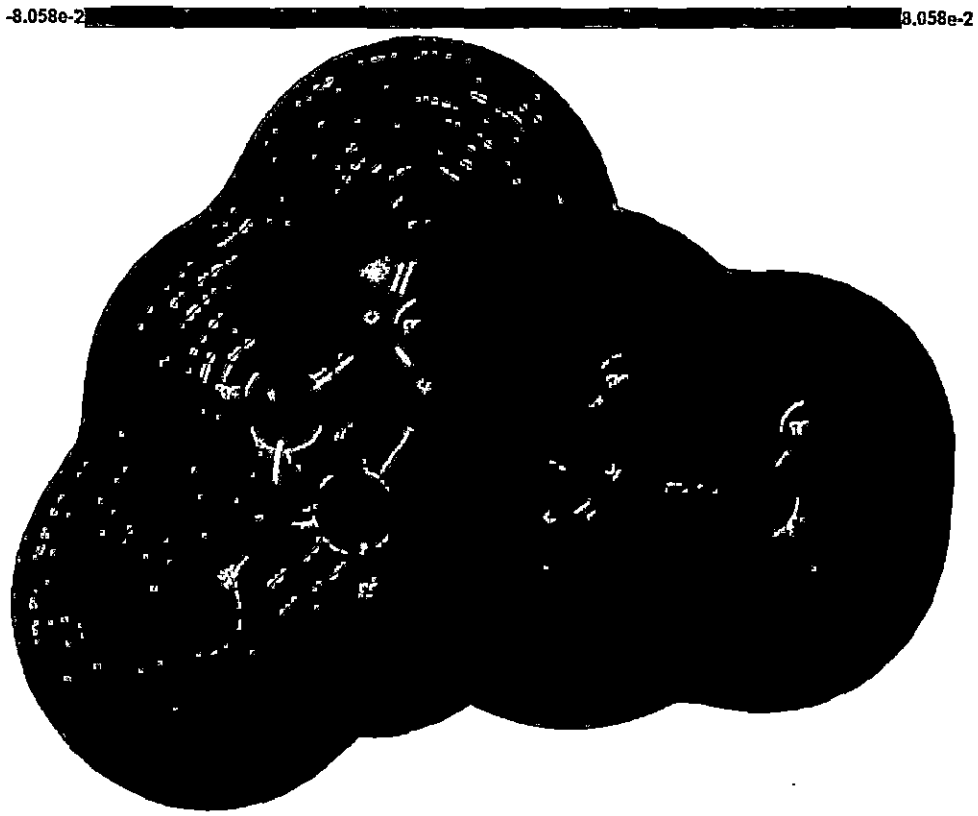

Fig. 6.13 Molecular electrostatic potential map for allantoin molecule.

6.4.6 Other molecular properties

The various molecular properties such as atomic charges, thermochemistry, dipole moment, non–linear optical properties (NLO), etc., are presented in Table 6.12, 6.13 and 6.14. The organic molecules, in which donor and acceptor groups are connected with pi–conjugated system e.g. aromatic ring, exhibit strong second order non–linearity (2^{nd} order molecular hyperpolarizabilty). This is because the system increases charge transfer through p–electron delocalization [80–82]. DFT calculations play a crucial role in designing NLO molecules and predicting their relevant properties like molecular dipole moments, polarizabilities and hyperpolarizabilities [83–87]. The total molecular dipole moment and mean first order hyperpolarizability of allantoin are 2.371 Debye and 1.333 x 10^{-30} esu respectively at B3LYP/6–311++G(d,p) level of theory (Table 6.14). The value of mean first order hyperpolarizability of allantoin is ca. 4 times greater than the value for urea

(β_0=0.3728 x 10^{-30} esu) [88]. The high value of first order hyperpolarizability of allantoin reflects its non–linear property. The natural atomic charges for monomer and dimers are depicted in Table 6.13. The positive charge on C2 and H13 atom among all the carbon and hydrogen atoms are found very low. This may be due to the attachment of high electronegative N6 atom in ureidyl moiety. The comparisons of natural atomic charges for monomer and dimers are shown in Fig. 6.14. The hydrogen–bonded dimers have produced shift in natural atomic charges upon dimerization. The atoms O8, O10, H11, H12 and H15, which are involved in formation of intermolecular hydrogen bonded dimers, show the significant changes in the charge values.

Table 6.12 Calculated SCF energy, zero point vibrational energy, thermodynamic quantities (at 298.15 K), rotational constants, rotational temperatures, energies of frontier molecular orbitals, global reactivity descriptors and dipole moment of allantoin.

Parameters	B3LYP/6–311++G(d,p)	MP2/6–311++G(d,p)
SCF Energy (a.u.)	−600.96805371 −600.99534493[b]	−599.42488419
Zero point vibrational energy (kcal mole^{-1})	77.961 76.868[a]	79.125 77.997[a]
Rotational constants (GHz)		
A	1.876	1.866
B	0.876	0.919
C	0.754	0.794
Rotational temperatures (K)	0.090	0.090
	0.042	0.044
	0.036	0.038
Total energy (thermal) (kcal mol^{-1})	84.462 83.736[a]	85.373 84.598[a]
Molar heat capacity at const. volume, C_v (cal mol^{-1} K^{-1})	37.756 39.132[a]	36.910 38.322[a]
Molar heat capacity at const. pressure, C_p (cal mol^{-1} K^{-1})	39.744 41.121[a]	38.896 40.311[a]
Total Entropy, S (cal mol^{-1} K^{-1})	100.186 102.751[a]	97.949 100.516[a]
Total Enthalpy, H (kcal mol^{-1})	85.055 84.326[a]	85.966 85.191[a]
Field independent dipole moment (Debye)		
μ_x	4.518	5.040
μ_y	0.624	1.145
μ_z	3.943	3.773
μ_{total}	6.028 8.562[b]	6.399
Frontier MO Energies (eV)		
E_{LUMO+1}	−0.642, −0.282[b]	
E_{LUMO}	−1.196, −1.018[b]	
E_{HOMO}	−7.456, −7.634[b]	
E_{HOMO-1}	−7.818, −7.821[b]	
$E_{LUMO} - E_{HOMO}$	6.260, 6.616[b] 5.126, 5.324[b]	
Global reactivity descriptors (eV)		
Ionization potential, *I*	7.456	
Electron affinity, *A*	1.196	
Electronegativity, χ	4.326	
Chemical potential, μ	−4.326	

Table 6.12 (*continued*)

Electrophilicity, ω	2.989
Hardness, η	3.130
Softness, S	0.160

[a]anharmonic value,
[b]values calculated in ethanol solution (PCM model)
Note: the underline value is approximated using TD–DFT calculations

Table 6.13 Natural atomic charges (e) on each atom of monomer and dimers of allantoin molecule.

Atoms	Monomer		D1	D2	D3	D4
	B3LYP/ 6–311++G(d,p)	MP2/ 6–311++G(d,p)	B3LYP/ 6–311++ G(d,p)	B3LYP/ 6–311++ G(d,p)	B3LYP/ 6–311++ G(d,p)	B3LYP/ 6–311++ G(d,p)
C1	0.692	0.843	0.694	0.691	0.698	0.692
C2	0.092	0.156	0.092	0.093	0.094	0.093
C3	0.801	0.983	0.800	0.813	0.805	0.815
N4	−0.663	−0.735	−0.652	−0.661	−0.675	−0.663
N5	−0.653	−0.744	−0.669	−0.655	−0.645	−0.653
N6	−0.669	−0.735	−0.669	−0.667	−0.663	−0.667
N7	−0.824	−0.861	−0.826	−0.817	−0.828	−0.818
O8	−0.599	−0.694	−0.654	−0.605	−0.657	−0.599
O9	−0.574	−0.677	−0.571	−0.571	−0.567	−0.571
O10	−0.642	−0.743	−0.637	−0.703	−0.637	−0.700
H11	0.408	0.410	0.409	0.408	0.445	0.408
H12	0.422	0.426	0.462	0.420	0.422	0.424
H13	0.214	0.194	0.213	0.214	0.216	0.212
H14	0.391	0.392	0.390	0.393	0.389	0.392
H15	0.401	0.400	0.400	0.443	0.398	0.437
H16	0.379	0.377	0.377	0.381	0.378	0.381
C17	0.824	1.008	0.841	0.824	0.833	0.824

Table 6.14 Calculated induced dipole moments, components of polarizability (a.u.) and first order hyperpolarizability (a.u.), mean polarizability ‹ α › (a.u.), anisotropy of the polarizability γ (a.u.) and the mean first order hyperpolarizability β_0 (esu, 1 a.u.=8.639 x 10^{-33} esu) of allantoin.

	MP2/ 6–311++G(d,p)	B3LYP/ 6–311++G(d,p)		MP2/ 6–311++G(d,p)	B3LYP/ 6–311++G(d,p)
μ_x	1.761	1.777	β_{xxx}	−27.208	−5.636
μ_y	0.430	0.245	β_{xxy}	95.572	105.609
μ_z	1.215	1.551	β_{xyy}	34.974	38.751
μ_{total}	2.182	2.371	β_{yyy}	−35.596	−53.951
α_{xx}	97.869	100.171	β_{xxz}	14.515	9.137
α_{xy}	10.392	9.028	β_{xyz}	45.125	57.791
α_{yy}	80.776	81.128	β_{yyz}	59.660	80.396
α_{xz}	7.965	8.295	β_{xzz}	21.512	29.640
α_{yz}	0.844	0.547	β_{yzz}	−10.766	1.329
α_{zz}	75.486	74.872	β_{zzz}	4.786	41.157
‹ α ›	84.710	85.390	β_0 (esu)	0.842 x 10^{-30}	1.333 x 10^{-30}
γ	30.447	31.189			

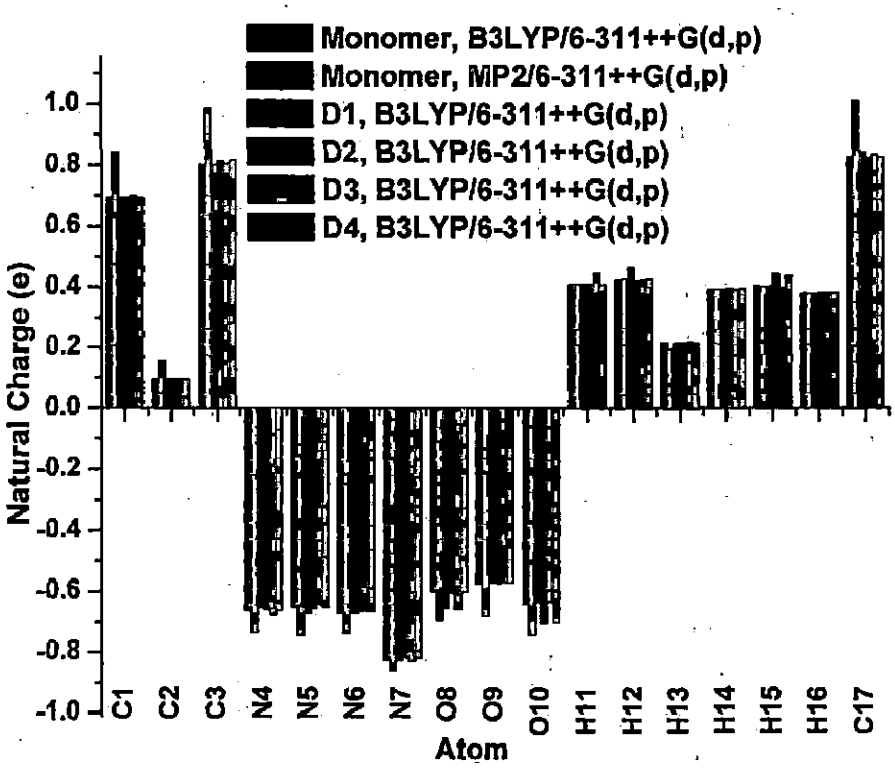

Fig. 6.14 The comparison of calculated natural charges for allantoin monomer and dimers.

6.5 Conclusion

The molecular structure and anharmonic vibrational spectra of isolated allantoin have been computed using the HF, B3LYP and MP2 methods with 6–311G(d,p), 6–311++G(d,p) and cc–pVTZ basis sets. The theoretical results are compared with experiments (XRD data, matrix FTIR, solid phase FTIR and FT–Raman spectra) and are found in good agreement. The RMS and MAD values at B3LYP and MP2 levels of theory for the calculations of structural parameters and vibrational frequencies show that the results are very similar but the B3LYP method is found more efficient than MP2 due to its lesser computational cost and similar accuracy. The anharmonic frequencies are computed using Barone's PT2 method as well as VSCF and CC–VSCF algorithms based on QFF potential function. The anharmonic wavenumbers for higher stretching modes have large deviation from experiments. This may be due to high anharmonicity associated with these modes or the neglect of higher order terms in potential expression in calculation. These modes are corrected well by VSCF and CC–VSCF approaches than Barone's PT2 algorithm. The anharmonic frequencies show large deviations from experiment for high and low frequency modes. This may be due to strong anharmonic coupling of low and high frequency modes with others and with themselves also. The N–H stretching

vibrational modes are found strongly coupled to mode 31, 32, 34 and 39. The high values of coupling strength are predicted for modes pairs, (3, 34), (4, 39), (2, 31) and (1, 5). It is predicted that the highest mode–mode couplings are involved among modes with large displacements of the same atoms. For the higher stretching modes (mode 1 to 9), the calculated harmonic frequencies show large deviations whereas the PT2 calculations demonstrate significantly better performance. For the anharmonic modes of higher and lower frequencies, which involve the large amplitude of vibrations, VSCF and CC–VSCF approaches have produced accurate result for allantoin. The NBO analysis has been performed at B3LYP/6–311++G(d,p) level of theory for studying hybridization of filled orbitals, natural atomic charges and intermolecular hyperconjugation interactions between donor and acceptor for allantoin molecule. The molecular structure, vibrational and NBO analyses have been also carried out for four possible dimers of the allantoin molecule at B3LYP/6–311++G(d,p) level of theory in harmonic approximation. The dimeric parameters are well comparable with solid phase experimental data. The scaled harmonic frequencies of many vibrational modes of dimeric structures have lower values and are more close to the experiments than those of monomer, which reveal the existence of intermolecular hydrogen bonds. The NBO analysis has also shown the presence of strong intermolecular interactions, C=O···H–N. The BSSE corrected interaction energies for complexes were obtained using counterpoise approach. The BSSE correction was found less than of 1 kcal/mol for the present case at B3LYP/6–311++G(d,p) level of theory. The vibrational modes of allantoin molecule have been assigned using PED values and animation of the modes. The non–fundamental bands in the NIR region are also assigned with the help of anharmonic force field calculations. The matrix FTIR bands are found very close to calculated anharmonic frequencies. The HOMO/ LUMO energy eigenvalues and related properties are also computed for understanding the chemical behaviour of the allantoin molecule.

References

[1]. H. Muratsubaki, K. Enomoto, A. Soejima, K. Satake, Anal. Biochem. 378 (2008) 65–70.

[2]. H. Muratsubaki, K. Satake, K. Enomoto, Anal. Biochem. 359 (2006) 161–166.

[3]. Y. C. Fu, L. H. A. Ferng, P. Y. Huang, Food Chem. 94 (2006) 541–549.

[4]. K. Kahn, P. A. Tipton, Bioorg. Chem. 28 (2000) 62–72.

[5]. L. B. Mendel, H. D. Dakin, J. Biol. Chem. 7 (1910) 153–156.

[6]. A. A. Christman, J. Biol. Chem. 70 (1926) 173–191.

[7]. A. V. Shestopalov, T. P. Shkurat, Z. I. Mikashinovich, I. O. Kryzhanovskaia, M. A. Bogacheva, S. V. Lomteva, V. P. Prokof'ev, E. P. Gus'kov, Izv. Akad. Nauk. Ser. Biol. 5 (2006) 541–545.

[8]. M. L. Schlossman, Chemistry and Manufacture of Cosmetics, 3rd edition, Allured Publishing Corporation, USA, 2002.

[9]. H. Eggensperger, Multiaktive Wirkstoffe für Kosmetika, Verlag Für Chemische Industrie, H. Ziolkowsky GmbH, Augsburg, 1995.

[10]. C. Thornfeldt, Dermat. Surg. 31 (2005) 873–880.

[11]. D. Mootz, Acta Crystallogr. 19 (1965) 726–734.

[12]. M. K. Shukla, P. C. Mishra, J. Mol. Struct. (Theochem) 285 (1993) 143–146.

[13]. N. Kus, S. H. Bayari, R. Fausto, Tetrahedron 65 (2009) 9719–9727, and ref. cited therein.

[14]. M. P. Tuszkanow, T. Grabowski, M. Daszkiewicz, J. Wietrzyk, B. Filip, G. Maciejewska, M. C. Golonka, J. Inorg. Biochem. 105 (2011) 17–22.

[15]. R. R. Braga, J. Sales, R. de C. E. E. Marins, G. M. D. Ortiz, S. Garcia, Spectrochim. Acta A 91 (2012) 389– 394.

[16]. C. H. Wang, M. J. Chen, C. Y. Tseng, K. M. Wei, W. Chen, Nat. Prod. Chem. Res. 1 (2013) 1–8.

[17]. J. E. Stewart, J. Chem. Phys. 26 (1957) 248–254.

[18]. M. A. Palafox, J. Talaya, A. G. Martinez, G. Tardajos, H. Kumar, J. K. Vats, V. K. Rastogi, Spect. Lett. 43 (2010) 51–59.

[19]. K. K. Irikura, R. D. Johnson, R. N. Kacker, J. Phys. Chem. A 109 (2005) 8430–8437.

[20]. M. A. Palafox, V. K. Rastogi, Spectrochim. Acta A 58 (2002) 411–440.

[21]. M. A. Palafox, M. Gill, N. J. Nunez, V. K. Rastogi, L. Mittal, R. Sharma, Int. J. Quantum Chem. 103 (2005) 394–421.

[22]. V. Barone, J. Chem. Phys. 122 (2005) 14108–14118.

[23]. V. Barone, Chem. Phys. Lett. 383 (2004) 528–532.

[24]. R. Gerber, M. Ratner, Adv. Chem. Phys. 70 (1988) 97–132.

[25]. T. K. Roy, R. B. Gerber, Phys. Chem. Chem. Phys. 15 (2013) 9468–9492.

[26]. G. C. Carney, L. L. Sprandel, C. W. Kern, Adv. Chem. Phys. 37 (1978) 305–379.

[27]. J. M. Bowman, J. Chem. Phys. 68 (1978) 608–610.

[28]. J. M. Bowman, Acc. Chem. Res. 19 (1986) 202–208.

[29]. P. Wojciechowski, K. Helios, D. Michalska, Vib. Spectrosc. 57 (2011) 126–134.

[30]. K. Ohno, S. Maeda, Chem. Phys. Lett. 503 (2011) 322–326.

[31]. C. Puzzarini, M. Biczysko, V. Barone, J. Chem. Theory Comput. 7 (2011) 3702–3710.

[32]. L. Pele, J. Sebek, E.O. Potma, R.B. Gerber, Chem. Phys. Lett. 515 (2011) 7–12.
[33]. P. Klaeboe, A. Horn, C. J. Nielsen, G. A. Guirgis, Vib. Spectrosc. 56 (2011) 136–145.
[34]. G. O. Ildiz, S. Akyuz, Vib. Spectrosc. 58 (2012) 12–18.
[35]. M. J. Alam, S. Ahmad, Spectrochim. Acta A 96 (2012) 992–1004.
[36]. M. J. Alam, S. Ahmad, J. Mol. Struct. 1059 (2014) 239–254.
[37]. M. J. Alam, S. Ahmad, Spectrochim. Acta A 128 (2014) 653–664.
[38]. P. Seidler, T. Kaga, K. Yagi, O. Christiansen, K. Hirao, Chem. Phys. Lett. 483 (2009) 138–142.
[39]. M. J. Frisch et al., Gaussian 09, Revision D.01, Gaussian Inc., Wallingford CT, 2009.
[40]. B. D. Becke, Phys. Rev. A 38 (1988) 3098–3100.
[41]. C. Lee, W. Yang, R. G. Parr, Phys. Rev. B 37 (1988) 785–789.
[42]. M. W. Schmidt, K. K. Baldridge, J. A. Boatz, S. T. Elbert, M. S. Gordon, J. H. Jensen, S. Koseki, N. Matsunaga, K. A. Nguyen, S. J. Su, T. L. Windus, M. Dupuis, J. A. Montgomery, J. Comput. Chem. 14 (1993) 1347–1363.
[43]. D. Michalska, R. Wysokiński, Chem. Phys. Lett. 403 (2005) 211–217.
[44]. M. Karabacak, L. Sinha, O. Prasad, A. M. Asiri, M. Cinar, V. K. Shukla, Spectrochim. Acta A 123 (2014) 352–362.
[45]. M. H. Jamroz, Vibrational Energy Distribution Analysis VEDA 4, Warsaw, 2004.
[46]. R. Dennington, T. Keith, J. Millam, GaussView, Ver. 5, Semichem Inc., Shawnee Mission KS, 2009.
[47]. K. Yagi, K. Hirao, T. Taketsugu, M. W. Schmidt, M. S. Gordon, J. Chem. Phys. 121 (2004) 1383–1389.
[48]. E. D. Glendening, A. E. Reed, J. E. Carpenter, F. Weinhold, NBO Version 3.1.
[49]. A. R. Allouche, J. Comp. Chem. 32 (2011) 174–182.
[50]. R. G. Parr, W. Yang, Density Functional Theory of Atoms and Molecules, Oxford University Press, New York, 1989.
[51]. R. G. Parr, W. T. Yang, Annu. Rev. Phys. Chem. 46 (1995) 701–728.
[52]. W. Kohn, A. D. Becke, R. G. Parr, J. Phys. Chem. 100 (1996) 12974–12980.
[53]. P. Geerlings, F. De Proft, W. Langenaeker, Chem. Rev. 103 (2003) 1793–1874.
[54]. P. Geerlings, F. De Proft, Phys. Chem. Chem. Phys. 10 (2008) 3028–3042.
[55]. P. W. Ayers, J. S. M. Anderson, L. J. Bartolotti, Int. J. Quantum Chem. 101 (2005) 520–534.
[56]. H. Chermette, J. Comput. Chem. 20 (1999) 129–154, and ref. cited therein.
[57]. C. A. Morgado, P. Jurecka, D. Svozil, P. Hobza, J. Sponer, Phys. Chem. Chem. Phys. 12 (2010) 3522–3534.
[58]. (a) P. Hobza, R. Zahradnik, Int. J. Quantum Chem. 42 (1992) 581–590.
(b) S. F. Boys, F. Bernardi, Mol. Phys. 19 (1970) 553–566.
[59]. J. Leszczynski, Handbook of Computational Chemistry, Springer, New York, 2012.
[60]. M. Karabacak, M. Cinar, Spectrochim. Acta A 86 (2012) 590– 599.
[61]. S. H. Kazemi, H. E. Hosseini, M. Mirzaei, Comput. Theor. Chem. 1004 (2013) 69–75.
[62]. M. Chaban, J. O. Jung, R. B. Gerber, J. Chem. Phys. 111 (1999) 1823–1829.
[63]. Y. Miller, G. M. Chaban, R. B. Gerber, J. Phys. Chem. A 109 (2005) 6565–6574.

[64]. T. Rasheed, S. Ahmad, Vib. Spectrosc. 56 (2011) 51–59.
[65]. J. C. Dobrowolski, R. Kołos, J. Sadlej, A. P. Mazurek, Vib. Spectrosc. 29 (2002) 261–282.
[66]. G. Socrates, Infrared Characteristic Group Frequencies, 3rd edition, Wiley Interscience Publications, New York, 1980.
[67]. A. T. Kowal, J. Mol. Struct. (Theochem) 625 (2003) 71–79.
[68]. N. P. G. Roges, A Guide to the Complete Interpretation of Infrared Spectra of Organic Structures, Wiley, New York, 1994.
[69]. N. B. Colthup, L. H. Daly, S. E. Wiberley, Introduction to Infrared and Raman Spectroscopy, Academic Press, New York, 1990.
[70]. M. Govindarajan, M. Karabacak, S. Periandy, D. Tanuja, Spectrochim. Acta A 97 (2012) 231–245.
[71]. V. Arjunan, A. Raj, P. Ravindran, S. Mohan, Spectrochim. Acta A 118 (2014) 951–965.
[72]. J. P. Ryall, T. J. Dines, B. Z. Chowdhry, S. A. Leharne, R. Withnall, Spectrochim. Acta A 78 (2011) 918–925.
[73]. http://dx.doi.org/10.1557/PROC–813–H3.6
[74]. M. A. Palafox, V. K. Rastogi, A. G. Martinez, G. Tardajos, J. Joe, J. K. vats, Vib. Spectrosc. 52 (2010) 108–121.
[75]. A. E. Reed, L. A. Curtiss, F. Weinhold, Chem. Rev. 88 (1988) 899–926.
[76]. F. Weinhold, C. R. Landis, Chemistry Education: Research and Practice in Europe 2 (2001) 91–104.
[77]. M. Amalanathan, V. K. Rastogi, I. H. Joe, M. A. Palafox, R. Tomar, Spectrochim. Acta A 78 (2011) 1437–1444.
[78]. M. Samsonwicz, Spectrochim. Acta A 118 (2014) 1086–1097.
[79]. A. M. Sapse, Molecular Orbital Calculations for Biological Systems, Oxford University Press, 1998.
[80]. B. L. Davydov, L. D. Derkacheva, V. V. Dunina, M. E. Zhabotinskii, V. F. Zolin, L. G. Koreneva, M. A. Samokhina, J. Exp. Theo. Phys. Lett. 12 (1970) 16–40.
[81]. S. J. Lalama, A. F. Garito, Phys. Rev. A 20 (1979) 1179–1194.
[82]. http://www.sigmaaldrich.com/materials–science/organic–electronics/photonic–optical–materials/tutorial/nlo–materials.html.
[83]. K. Wu, C. Liu, C. Mang, Opt. Mater. 29 (2007) 1129–1137.
[84]. T. M. Kolev, D. Y. Yancheva, B. A. Stamboliyska, M. D. Dimitrov, R. Wortmann, Chem. Phys. 348 (2008) 45–52.
[85]. I. M. Kenawi, A. H. Kamel, R. H. Hilal, J. Mol. Struct. (Theochem) 851 (2008) 46–53.
[86]. P. A. Fantin, P. L. Barbieri, A. C. Neto, F. E. Jorge, J. Mol. Struct. (Theochem) 810 (2007) 103–111.
[87]. M. Drozd, M. K. Marchewka, Spectrochim. Acta A 64 (2006) 6–23.
[88]. M. Arivazhagan, J. S. Kumar, Indian J. Pure Appl. Phys. 50 (2012) 363–373.

Chapter 7

Overall conclusion

The goal of the present work is studies of structure, vibrational spectra and various properties of the polyatomic molecules in their ground electronic state. The vibrational spectra of six polyatomic molecules have been recorded and fully analyzed using quantum chemical calculations (HF, MP2 and DFT) in the harmonic and anharmonic approximations. Some of experimental data like x–ray diffraction, electron diffraction, Raman, matrix FTIR spectra wherever is required for the present molecules have been taken from earlier works. The comparisons between experimental and theoretical molecular geometry and vibrational spectra have been made using root mean square, mean absolute deviations and correlation plots, which reveal the good agreement between theoretical and experimental results. The results obtained by Hartree–Fock calculations are found with large values of RMS error and MAD because of the ignorance of electron–electron correlations. The RMS and MAD values for the calculated structural parameters and vibrational frequencies at DFT and MP2 levels of theory show that the results of both the methods are very similar. The DFT method is found more efficient than MP2 due to its lesser computational cost. The SCF minimum energy of the investigated molecules shows that the stable structures have been found at B3LYP/cc–pVTZ level of theory. The anharmonic corrections in frequencies were computed using Barone's PT2, VSCF and CC–VSCF approaches that have yielded results, which are in remarkable agreement with experimental ones. The assignments of the experimental vibrational bands are proposed on the basis of anharmonic frequencies, relative intensities, PED values and animated modes. The present molecules have many torsional vibrations (anharmonic modes) that have appeared with mixing of others in lower modes. These modes normally damage the PED values due to its large anharmonicity. Therefore, such modes are assigned by visualizing the mode by arrow and animation. The vibrational

modes, in general, couple to others due to anharmonicity and, therefore, the vibrational energy flows from one mode to others. The mode–mode coupling behaviour are studied for the present molecules (L–aspartic acid, 3–methyladenine and allantoin) using coupling integral formula. The values of coupling integral have shown that the most of modes are coupled to others with low coupling strength except few modes which show medium to large coupling strength. The large values of coupling strengths of few modes show that these modes in the molecule have large anharmonicity that significantly affect the vibrational frequencies of coupled modes. In the present anharmonic mode–mode coupling calculations, it was noticed that the couplings between normal modes that involve the displacements of the same atoms are typically stronger. The contribution of anharmonicity in each mode due to intrinsic and mode–mode coupling are analysed. The present molecules consist of many anharmonic modes like freely rotating methyl groups modes, C–H and N–H stretching modes. In the present case, the contribution of anharmonicity due to mode–mode coupling is found larger than that of intrinsic anharmonicity in many modes of the presently investigated molecules (L–aspartic acid, 3–methyladenine and allantoin). The anharmonic methods fail to define hydrogenic stretching and soft torsional vibrations due to large perturbation because of their large amplitude of vibrations. The rectilinear coordinates are suitable to define small amplitude of vibrations but it fail to represent anharmonic modes that have large amplitudes of vibrations (floppy vibrations). Therefore, the large deviations are noticed in the experimental and calculated frequencies of such vibrations. In nature, the molecules exist with the intermolecular and intramolecular hydrogen bonding networks. The molecular simulations have also been carried out for intermolecular hydrogen bonded complexes of L–aspartic acid, 3–methyladenine and allantoin. According to RMS error and MAD values for intermolecular complexes, the structural parameters and vibrational frequencies are found close to solid phase data. Any further discrepancies, if found, may be due to the fact that the calculations have been carried out for the isolated molecule in gaseous phase while the experiments are performed in solid phase. Moreover, some molecular properties such as atomic charges, non–linear optical properties, thermodynamic quantities, chemical reactivity descriptors (global indices), molecular electrostatic potential mapping, natural bond orbital and HOMO–LUMO analysis have been carried out. The large values of mean first order hyperpolarizability of all investigated molecules are found higher than that of urea

molecule. Therefore, the present molecules have non–linear potential. The electrophilic and nucleophilic attacks on the sites of the present molecules are investigated with the help of molecular electrostatic potential map. The global chemical reactivity indices, obtained using DFT calculations, are presented to know the chemical behaviour of molecules. The HOMO–LUMO analysis of the present molecules has predicted that the HOMO→LUMO transitions show delocalization of electron density within molecules. The low value of the HOMO–LUMO gap explains the high reactivity and charge transfer interactions within the molecules.